ENGINEERING TOOLS FOR VARIABLE STIFFNESS VIBRATION SUPPRESSION AND ISOLATION

DISSERTATION

Michael F. Winthrop, Major, USAF

AFIT/DS/ENY/05-02

DEPARTMENT OF THE AIR FORCE

AIR UNIVERSITY

AIR FORCE INSTITUTE OF TECHNOLOGY

Wright Patterson Air Force Base, Ohio

The views expressed in this dissertation are those of the author and do not reflect the official policy or position of the United States Air Force, Department of Defense, or the United States Government.

AFIT/DS/ENY/05-02

ENGINEERING TOOLS FOR VARIABLE STIFFNESS VIBRATION SUPPRESSION AND ISOLATION

DISSERTATION

Presented to the Faculty

Graduate School of Engineering and Management

Air Force Institute of Technology

Air University

Air Education and Training Command

in Partial Fulfillment of the Requirements for the

Degree of Doctor of Philosophy

Michael F. Winthrop, B.S., M.S.

Major, USAF

December, 2004

AFIT/DS/ENY/05-02

ENGINEERING TOOLS FOR VARIABLE STIFFNESS VIBRATION SUPPRESSION AND ISOLATION

Michael F. Winthrop, B.S., M.S.

Major, USAF

Approved:

Richard G. Cobb (Chairman)	12/13/2004 Date
Donald L. Kunz (Dean's Representative)	12/13/2004 Date
Bradley S. Liebst (Member)	12/13/2004 Date
Gregory S. Agnes (Member)	12/13/2004 Date
William P. Baker (Member)	13 Dec 04 Date

Accepted:

Robert A. Calico, Jr
Dean, Graduate School of Engineering and Management

AFIT/DS/ENY/05-02

Abstract

With the advent of smart materials, the concept of semi-active control or dynamic control of stiffness and/or damping for vibration control of structures has become practical and has seen limited use. Semi-active control has advantages over active and passive control methods, since it provides almost as much capability as active control while requiring much less power. Its main disadvantage is its inherent nonlinearity, greatly complicating engineering design. The purpose of this research is to extend semi-active control vibration isolation tools and methods, considering applications for space launch and on-orbit systems.

After surveying the literature, variable stiffness using a general on-off control law with constant damping is examined in several contexts. First, the single degree of freedom problem is solved in exact form and approximated for the initial value problem. Results include development of an optimal control policy for all possible variable stiffness settings and a large range of viscous damping settings, guaranteed stability regions, and new possibilities for fast settling time even with an overdamped system. Second, the sinusoidally forced problem was approximated and a near optimal control policy was formulated. Third, the results of the initial value problem were extended to two multi-degree of freedom problems. The problems examined are representative of a cross section of a simple space telescope structure and of a variable stiffness beam. Besides providing new engineering design tools and insight into the nonlinear behavior of variable stiffness concepts, the results open several future research possibilities.

Acknowledgements

I am first grateful to the Lord Jesus Christ who is my savior. It would be impossible for me accomplish this work without him. Next, I would like to thank my family for their loving support and their willingness to let me spend the time it takes to do this kind of work. Finally, I would like to thank my advisor and committee members who have given their time so I could understand the concepts I have been working with and have given me new ideas that has resulted in this work.

Michael F. Winthrop

Table of Contents

List of Figures

List of Tables

List of Symbols

Symbol	Definition
a	Amplitude of response due to variable stiffness/damping action.
a_0	Initial conditions for Variation of Parameters Transformed Equation
a_p, a_m	Interval of amplitude in terms of phase angle ϕ ($p \Longrightarrow u = 1$, $m \Longrightarrow u = -1$)
α	Variable stiffness ratio of minimum to maximum stiffness
A^*	Variable A is a dimensional variable.
A	Variabe A is a nondimensional variable (Chapter 3-6).
β	Phase Shift of system
c, c_0, c_1	Damping Coefficients
$\tilde{c}$	$\tilde{c}\left(x, \dot{x}\right)$ Generic damping function of displacement and velocity with control law
$\left(C_p^s\right)_{total}$	Total capacitance for a piezoelectric device
ψ	Uncontrolled free vibration frequency of system
δ	$\delta\left(\psi, \varepsilon\right)$ Combined damping/variable stiffness constant
D	Electric Displacement for Piezoelectric
D_ϕ	Time to complete one period in phase
D_a	Amplitude change over one period in phase
ε, ε_k	Stiffness bandwidth or variation in variable stiffness
e	Exponential function
ε_c	Damping bandwidth
E	Electric strain for piezoelectrics or generic energy function
F	$F\left(t\right)$ Generic force
ϕ	Phase of response due to variable stiffness/damping action
ϕ_0	Initial conditions for Variation of Parameters Transformed Equation
ϕ_1, ϕ_2	Phase switching angles for variable stiffness device
ϕ_{crit}	Value of ϕ when $\dot{\phi} = 0$.
Γ_{ϕ_p}, Γ_{ϕ_m}	Interval of time in terms of phase angle ϕ ($p \Longrightarrow u = 1$, $m \Longrightarrow u = -1$)
j	Nonnegative integer
$J\left(u\left(\phi\right)\right)$	Function for identifying bifurcations due to variable stiffness, damping, and control
J_p	$J\left(\phi\right)$ when $u = 1$
J_m	$J\left(\phi\right)$ when $u = -1$
k, k_0, k_1	Stiffness Coefficients
k^{sc}, k^{oc}	Short circuit and open circuit stiffness for a piezoelectric

Symbol	Definition
$\tilde{k}$	$\tilde{k}(x, \dot{x})$ Generic stiffness function of displacement and velocity with control law
k	Also used as a dummy integer variable
L	Inductance
L^*	Dimensional length for scaling displacement
λ_1, λ_2	Tuning Parameters for Variable Stiffness Control Law
m	Mass in System
n	Nonnegative integer
μ	Nondimensional damping coefficient
μ_e	Equivalent damping coefficient for forced problem
μ_{crit}	Transition between underdamped and overdamped system behavior
n	The current period number
ν	Dummy change of variable used in integration
π	pi
P	Average Power for unforced problem
Q	$Q(t)$ Generic time varying forcing function
R	Resistance
σ_p, σ_m	$\sigma_p(\psi, \varepsilon)$, $\sigma_m(\psi, \varepsilon)$ Damping/variable stiffness constant. ($p \Longrightarrow u = 1$, $m \Longrightarrow u = -1$)
S	Mechanical strain
sgn	The sign or signum function
t	Time
t_{sw_k}	The k^{th} switching event in a time response
T	Mechanical Stress
u, u_k	Control Law for Variable Stiffness
u_c	Control Law for Variable Damping
V	Voltage
ω	Forcing frequency for
ω_0^*	Frequency for scaling time
ω_n, ω_e	Equivalent Natural Frequency for unforced and forced problems respectively
W_{in}, W_{out}	Work in and work out, respectively for unforced problem
x, $\dot{x}$, $\ddot{x}$	Displacement, Velocity and Acceleration using relative or absolute coordinates
x_0, $\dot{x}_0$	Initial conditions (displacement and velocity)
y, $\dot{y}$, $\ddot{y}$	Displacement, Velocity, and Acceleration using relative or absolute coordinates
z, $\dot{z}$, $\ddot{z}$	Displacement, Velocity, and Acceleration using relative or absolute coordinates
ζ	Equivalent Damping Ratio for unforced problem

List of Abbreviations

ENGINEERING TOOLS FOR VARIABLE STIFFNESS VIBRATION SUPPRESSION AND ISOLATION

1. Introduction

With the advent of smart materials, the concept of controlling stiffness and/or damping in a structure for vibration control of structures has become practical. These concepts together can be loosely called semi-active control methods. They are currently being researched by many industries including the automotive, building, and space industries. Some automotive applications are shock absorbers and engine mounts. Building industry applications include earthquake protection and damping of wind induced vibration. Space applications include isolation of payloads from rocket stages during launch and isolation of mirrors in space telescopes. These are just a few of the many possible applications.

Vibration control has typically been accomplished using passive, active or a combination of passive and active control systems (hybrid control). In the last 10 years, there has been much research on developing semi-active control, which performs better than passive control, but not as well as active control methods. In some situations, semi-active control might be a better choice than active control because it typically requires less energy than active or hybrid control. However, semi-active control is more complex to analyze than passive or active control methods. The complexity exists in part because the damping and stiffness characteristics of a vibrating structure are dynamically controlled using measurements of the structures' vibration, which is inherently nonlinear. The problem becomes even more complex because the smart devices that are capable of changing stiffness and/or damping exhibit nonlinear behavior as well. Hence, the well known linear techniques used to design many passive, active and hybrid control systems cannot be used or must be modified.

The purpose of this research is to extend semi-active control vibration isolation tools and methods considering space launch and on-orbit systems. After an extensive survey of the literature, the work begins with analysis of a single degree of freedom (SDOF) lumped

parameter model and eventually works up to multi-degree of freedom (MDOF) lumped parameter models, taking advantage of the knowledge gained from the SDOF problems. This work concentrates on dynamically controlling stiffness of a structure using a general control law and both confirms and extends previous work to include constant viscous damping. While the literature was reviewed to develop a link to real variable stiffness and variable damping devices, this work is restricted to analysis using a simplified abstract variable stiffness device. However, the results of this analysis could assist in choosing a real variable stiffness device to meet desired performance criteria. Because variable stiffness systems are nonlinear, the behavior from one disturbance type provides no information about how it will behave with another disturbance type. Hence, the initial value problem and the sinusoidally forced problem were examined separately, since they are representative of real disturbances such as those caused by shocks and rotating machinery.

Finally, various mathematical tools were used in the analysis. For the initial value SDOF problem, it was possible to solve the nonlinear equations exactly. However, the exact equations could not be written in an explicit closed form, so they were approximated with a linear equation. On the other hand, the exact solution for the sinusoidally forced SDOF problem could not be found, so a perturbation method and an ad hoc approach was used. For the MDOF problems considered, linear analysis methods could be used in conjunction with the SDOF approximation results because these results are linear. This allowed some insight to be developed into how these larger systems behave. In all cases, simulation was used to help validate the analytic and approximate results.

Chapter 2 begins with a survey of the literature. Vibration control, its application to space, and models of systems and smart materials are discussed. In the literature, much work was found using semi-active devices with vibration absorbers. Much less information was found that discussed vibration isolation. Further, almost all of the literature uses either variable stiffness devices or variable damping devices, rarely combining the two methods. This can be attributed to the difficulty in analyzing these kinds of systems. A survey of control laws used with variable stiffness and variable damping devices is also provided. The survey concludes by noting there is a need to better understand control schemes using nonlinear control devices.

Chapter 3 provides in depth analysis of an initial value SDOF system using a general on-off control law. The system contains both variable stiffness and constant viscous damping. The nonlinear equation of motion is solved implicitly in exact form for the first time. Because of the form of the nonlinear solution, an explicit solution could only be found in approximate form. An optimal control law was found and guaranteed stability for the system was found. It was discovered that the system can be switched between overdamped and underdamped states using the variable stiffness controller, creating fast settling behavior that cannot be achieved using a passively controlled system.

Chapter 4 provides analysis of a sinusoidally forced SDOF system using a general on-off control law. The system contains both variable stiffness and constant viscous damping. Since an exact solution could not be found, system behavior was approximated using an ad hoc direct method and by using a perturbation method. The results were compared with simulated results and much of the nonlinear system behavior was captured, though not all of it. The approximate solutions were then used to develop near optimal control laws.

Chapter 5 extends the work of Chapter 3 to MDOF problems. It shows that it is possible to take the SDOF approximate results and extend them to more complicated systems, with some restrictions. Two problems are considered. The first problem is a large mass with any number of equal masses attached in parallel with each other. Each attachment is assumed to consist of a variable stiffness element and a constant viscously damped element. The isolators are assumed to be the same for each attachment. This model could structurally represent a cross section of a space telescope. The other problem considered is a large number of equal masses connected in series with each other. This problem might be representative of a variable stiffness beam, if enough masses are provided. On the down side, the problem is difficult to solve analytically for systems with more than 3 degrees of freedom.

Chapter 6 ends this work by identifying major conclusions and identifying future research. As research is being carried out, new research opportunities are identified. It was found there are many directions for future research expanding on all of the previous

chapters. Besides providing some new engineering tools for semi-active systems, this work opens the door to several new research opportunities.

2. Background

2.1 Introduction

Research in removing unwanted vibration in applications is extensively documented in the literature. This chapter provides a broad and representative look at the state-of-the-art in vibration control, emphasizing semi-active control. The goal was to concentrate on vibration isolation problems, but other types of vibration control such as vibration absorption and vibration suppression are discussed, since these areas seem to have more extensive semi-active control documentation than vibration isolation does. Research was limited to those of space applications, though developments for other application areas are discussed where it appeared to be useful for future space applications research. This review expands on a recent review of current state of the art in vibration isolation technology by Winthrop and Cobb [1].

First, vibration control is defined. Using the literature, vibration absorption, vibration isolation, and vibration suppression, which are three well known types of vibration control are defined. Then, passive, active, hybrid, and semi-active control, which are four methods of achieving vibration control are discussed. This is followed by a review of vibration control in space applications, along with some information on how vibration control devices have been used. Next, some models used for vibration control are discussed as identified by the literature. The discussion continues with a look at semi-active devices, used to change either damping or stiffness of a system. Models of some of these devices are reviewed and some discussion of these models is provided. A discussion of isolation performance criteria is provided. Finally, semi-active control strategies are reviewed, concentrating most heavily on energy minimizing methods.

2.2 Vibration Control

Types of Vibration Control. Vibration control is an attempt to reduce unwanted oscillations in a structure [2]. Vibration isolation, one type of vibration control, occurs when compact, resilient connections are placed between a vibrating structure and a sensitive structure. If the connections are placed between a vibrating source and the surrounding

structure, it is called source isolation or force transmissibility. If the connections are placed between the vibration sensitive structure and the surrounding structure, then it is called receiver isolation or displacement transmissibility [2], [3].

Vibration absorption, also referred to as tuned mass damping, dynamic vibration absorption, vibration neutralization, or tuned vibration absorption, is another type of vibration control [4], [5]. A vibration absorber is a device added to a structure that minimizes vibrations to the host structure. It typically consists of a reaction mass, a spring element, and a damping element. It can be used both to control narrow-band or tonal vibrations and to control broadband vibrations [4].

A third kind of vibration control, vibration suppression, occurs when damping and stiffness of a system are changed, often through the use of feedback control or active control (which will be better defined in a following section). The goal of such control is to remove unwanted disturbances applied directly to the sensitive structure. This differs from vibration absorption since no device is being placed between the disturbance and the body to be kept quiet from vibration. Rather, actions are taken to damp out vibrations directly [6].

In Section 2.4, vibration suppression and vibration isolation models will be reviewed. Because this research focuses on suppression and isolation, vibration absorption will not be explicitly discussed. However, vibration absorption applications are referenced throughout this work since vibration absorption devices can also be used for vibration suppression and isolation applications.

Classifications of Vibration Control. Vibration control systems can be classified as passive, active, semi-active (adaptive-passive), or hybrid [7], [8]. A passive isolator is defined as a compact connection that receives no external energy or information [9], [7] and behaves like a low pass filter [10]. The compact connection consists of a resilient stiffness member and an energy dissipation or damping member that either absorbs vibrations or loads the vibrational path [3]. Advantages of passive systems are simplicity, guaranteed stability [11], reliability, and no required power [7]. However, passive control has many limitations for vibration isolation in space applications: 1) inability to practically achieve

isolation at very low frequencies, 2) trade-off between resonant peak and high-frequency attenuation, 3) trade-off between base motion isolation and disturbance rejection, 4) inability to adapt to changes in structural parameters over time resulting in reduced performance, 5) inability to optimize the design for varying excitation frequencies, 6) may amplify low frequency vibrations, and 7) may require structural off-load mechanisms to survive launch and ground tests [10], [3], [12].

Active control is a method of loading a vibrational path using force actuators that require external energy and information as inputs [8], [9]. Active isolation has many advantages over passive isolation: 1) it removes trade-offs between low-frequency amplification and high-frequency attenuation, 2) it removes the base motion isolation and disturbance rejection trade, 3) and allows intelligent and a fast response to disturbances [10], [7]. The disadvantages of active isolation are: 1) it requires relatively high power, 2) it can create instability in the system, 3) may require complex control laws and components, and 4) failure of the control system results in no isolation at all [7], [3], [12].

In practice, active isolation and passive isolation are combined into what is sometimes referred to as hybrid isolation. Advantages of hybrid isolation are it: 1) allows transmissions of static loads through the isolation system [9], 2) reduces the external power required in comparison to a purely active system by reducing the bandwidth needed by the active portion [3], [12], and 3) allows some vibration isolation if the active element fails [7]. Disadvantages are 1) a risk of instability created by the active element [7] and 2) a risk of degradation due to detuning of the passive element.

Semi-active control or adaptive passive control implements a tuning scheme to change tunable parameters of passive elements of stiffness and/or damping. Advantages of this method are: 1) it requires low external energy (or no external energy [13]), 2) cost less than active systems [3], 3) provides passive isolation if the semi-active portion fails, 4) can be nearly as effective as active systems [14], and 5) has guaranteed stability when just the damping element is varied [15]. It has been demonstrated however, that varying the stiffness element can cause instability in a system [16]. Physically, this is because changing the stiffness causes work to be performed on the system. The variable stiffness element can be visualized as a constant stiffness element and an active force element [17],

[4]. Hence, semi-active control differs from hybrid control in that hybrid control employs additional actuators to implement the active control and hybrid control does not attempt to change the passive portion of the control, once it is designed.

2.3 Space Applications of Vibration Control

Vibration control is being used or being considered for a variety of different space applications. Because of the nature of space systems, unique challenges exist which do not exist in other industries. For example, vibration control for payloads on launch vehicles must consider the effects of large changes in mass, since large amounts of burned propellant is expelled. Parts of satellites on orbital platforms may be constrained to displacements smaller than the wavelength of visible light. For all space systems, weight, cost, and power are critical constraints. Because of the importance of space to the United States, much research has been devoted to finding better ways of solving vibration problems.

The background that follows presents current capabilities and lists some relevant data that will be used in later Chapters to make assumptions and link existing systems to the results developed. Later chapters focus exclusively on constant mass problems. However, because of the importance of vibration control in variable mass system, it will be reviewed in some detail. In Chapter 6.3, which identifies proposed future research for variable mass problems, an approach for developing insight into vibration isolation of a simple variable mass system will be considered.

On-Orbit Applications. Spacecraft must deal with a variety of disturbances on orbit. For sensitive structures, failure to reduce the disturbances to a low enough level can either degrade or prevent mission completion. After introducing common types of disturbances that often occur in spacecraft, several vibration sensitive space applications are discussed.

Spacecraft Disturbances. Typical external disturbances to a spacecraft include solar radiation pressure, thermal effects, micro-meteorite impacts, atmospheric drag and gravity gradients [10], [18]. Internal disturbances in a spacecraft can include attitude

control components such as reaction wheels or control moment gyros, cryogenic coolers and solar array gimbals [12], [19], [20]. When the spacecraft is manned (such as the International Space Station), additional disturbances arise such as pumps, compressors, electric motors, fans, impacts, and astronaut motions [10]. There has been much effort to empirically model these disturbances. A standard reference [21] describing and providing data on many types of disturbances is available from the National Aeronautics and Space Administration (NASA). Some specific studies have examined reaction wheels [22] and cryocoolers [23]. For manned platforms, in depth models have been developed and are being improved for use in vibration environments [24], [10].

Space Telescopes. The current trend in space based telescopes is to build increasingly larger aperture mirrors, since larger apertures allow higher resolution in Earth observation applications and allows dimmer objects to be seen in astronomy. However, there are limits on aperture size due to difficulties in creating a single large optical surface and because of existing launch vehicle shroud volume constraints which limit aperture size to about 5 meters [25]. Larger aperture sizes also require more massive optics, requiring larger launch vehicles and increasing costs. Hence, one research trend is to create proportionally lighter optics. However, lighter optics are also less stiff than more massive ones, which increases susceptibility to lower frequency vibrational disturbances. This in turn, creates a trade-off of control architectures, where lighter structures require lower frequency active control than heavier ones [26].

A second research trend is in the development of space interferometers. The concept of interferometers in space, which typically consist of sparse aperture arrays, is a method of combining the light from two or more separated telescope apertures to create an image with the same resolution as a single aperture with a diameter equal to the separation distance between the smaller telescopes [27], [28]. This overcomes the volume constraints of launching the hardware, but requires more stringent six axis control. In fact, control must be sufficient to keep errors below nanometer and nanoradian levels for each mirror [29], [30]. For example, the HST has been compared to the NGST (now called the James Webb Space Telescope) [31]. Essentially, the HST is heavier and more rigid allowing

the entire satellite to be pointed at a target of interest. The NGST is lighter and more flexible and requires complex cascading control loops and the isolation corner frequencies are significantly lower than for HST.

Powers et. al. developed a preliminary design for a sparse aperture array telescope with six mirrors. Their design identifies a total mirror mass with support structure of 883. 4 kg while the mass of the rest of the satellite is 2533 kg. Hence, one mirror with support structure would have a mass of about 147 kg [29]. More recently, the Air Force Research Laboratory has developed a ground based sparse array space telescope testbed for demonstrating key technologies such as control nanometer control of the primary mirrors [32]. Using system identification methods, a model of the different modes found in the three mirrored system was developed. A multi objective MDOF control system was successfully developed and demonstrated to isolate the mirrors, reject disturbances, and properly point the mirrors [30].

A third trend in space telescope research is investigation of the supporting structure for the telescopes. Due to launch vehicle constraints, large optics must be deployable. However, due to low vibration tolerances, the support structure must be stiff [33]. As a result, small, otherwise unnoticed nonlinearities (called microdynamics) of the structure become large problems. One important nonlinearity called microlurch has been identified and is believed to be caused by a sudden release of strain energy built up due to frictional effects in joints and latches of a structure. The latches and joints are traditionally used to make the structure deployable. A microlurch tends to excite high frequency vibrations that fall well outside the bandwidth of typical active control systems [34].

There seem to be two novel approaches for developing better support structure for deployable telescopes. One approach is to create much stiffer joints, for example, using a stiff folding composite. Some testing has been performed on this concept showing deployability similar to conventional joints though with some apparently, manageable nonlinearities [35]. The other novel approach is to almost completely mechanically decouple satellite deployable telescope (payload module) from the rest of the satellite (support module). In this concept, the payload module is controlled by reacting on the support module with noncontact actuators and sensors. The support module uses external actuators to

react against the surroundings to control the spacecraft [36]. Hence, the entire range of structural stiffness possibilities are under consideration.

Microgravity Research on the International Space Station. The ISS represents one platform for performing microgravity research. The purpose of microgravity research is to perform basic research to better understand the phenomenon in the areas of fluid physics, combustion, fundamental physics, material science, biotechnology and other areas [37]. Study of some phenomena is greatly improved when studied in an environment nearly free of gravity. Vibrations also can damage these experiments and much effort is being devoted to vibration minimization. An excellent survey of this work was written by Grodsinsky and Whorton [10]. A rack isolation system for experiments known as the ARIS is being developed, capable of providing isolation to multiple experiments. Risk reduction flights for the technology have been made [38]. Other efforts are being made to isolate individual experiments from the ISS [39], [40], [41], [42].

Precision Pointing. A goal of commercial communications is the capability of transmitting information to any location on the Earth. An ideal way of accomplishing this is to create a satellite communications network where information is retransmitted between several satellites before being transmitted to the ground. One way to accomplish this goal is to use optical intersatellite links, which has been surveyed by Arnon [43]. Another use for precision pointing is on the SBL. SBL is expected to require approximately a 10 m diameter mirror and to be able to reduce vibration by approximately 80 dB [44]. Issues with deploying optics larger than 5 m have already been discussed in terms of space telescopes. Further, the laser has attributes similar to a rocket engine, such as combustion induced vibration, and will create disturbances on the precision optics [45]. Riker provides an overview of the risk reduction Integrated Flight Experiment to demonstrate SBL technologies [46].

Launch Vehicle.

Shock and Isolation. The goal of launch isolation is to prevent damage to the payload by removing unwanted structural and acoustical vibrations. Disturbances for

launch vehicles include vibrational/acoustic loads and aerodynamic loads [47]. In small launch vehicles, the sound level can exceed 130 dB and can cause payload damage [48]. Methods of overcoming acoustical noise damage to the payload are not reviewed here, but this area is well documented [49] and is an active research area.

The purposes of launch isolation are to allow 1) more sensitive equipment to be launched, 2) reduced risk of equipment failures, and 3) reduced spacecraft bus mass with design considerations to minimize impacts on payload and launch hardware/software [50]. Passive launch isolation has been successfully used and designed for many payloads for specific launch events. It has been used for Hubble Space Telescope servicing missions in the space shuttle, achieving attenuation above 8 Hz for the solar array resupply mission [51] and has achieved attenuation above 30 Hz on a mission to replace various modules [52]. The passive interface between the space shuttle and the payloads has been analyzed and methods to decrease transmissibility to the payload have been suggested [53].

More recently, for small launch vehicles, two types of passive launch protection devices are being pursued: 1) whole spacecraft isolation [54] and 2) shock isolation [55]. Launch isolation has been applied both to axial (thrust axis) and to multiaxial (thrust axis and lateral axis) cases and has flown successfully a minimum of five times making this a mature technology [19]. Shock isolation is also being developed. Vibration isolation has been designed to attenuate frequencies above 30 Hz, while shock isolation has been designed to attenuate frequencies above 100 Hz. Vibration isolation can isolate vibrations at lower frequencies than shock isolation, but can also couple with the guidance, navigation and control system of the launch vehicle requiring more complex analysis to allow a successful flight, where as shock isolation does not have this problem [50]. A more generic vibration system for the Evolved Expendable Launch Vehicle is being developed, which would isolate one large payload and up to six smaller payloads on the medium lift vehicle [56], [57], [58]. The concept is also being developed for Minotaur and the Space Shuttle [59]. A generic, adaptive passive, multi-axis launch isolation system has been proposed for Delta II, capable of compensating for the time varying static loads the launch vehicle applies to a payload and is envisioned for all launch vehicles [13].

Active and passive isolators have been studied, showing the improved performance of active isolation over passive [60]. Hybrid launch isolation has been proposed and designed, providing large improvements over purely passive isolation [53], [61], [62], [63]. Further, adaptive control combined with passive control has been studied resulting in additional improvements over active control with passive [64]. Finally, Honeywell has bridged a gap between launch isolation and on-orbit isolation using a single isolation system capable of doing both jobs [65].

Typical Payloads to be Isolated. Sutton provides a table of typical launch vehicle masses at launch along with payload weights to 100 nautical mile orbit and to geosynchronous orbit. Table 2.1 provides the results of calculating the payload fraction for payloads launched into a LEO of 100 nautical miles and into GEO at the instant the launch vehicle is launched. These launch vehicles are older vehicles and have two or more stages. Appendix A provides a more detailed comparison of payload and mass fractions for various launch vehicles. The payload fraction ranges between 0.002 and 0.153 while the mass fraction ranges between 0.847 to 0.998 at the instant of launch.

Table 2.1 Payload Fraction for Some American Launch Systems

Launch Vehicle	**Launch Mass (metric tons)**	**LEO Payload (lb)**	**GEO Payload (lb)**	**LEO Mass Fraction**	**GEO Mass Fraction**
Titan 34D	1,091	30,000	1,820	0.012	$1.663 * 10^{-3}$
Delta II 6925	132	5,600	1,454	0.019	0.011
Atlas Centaur	141	6,100	1,545	0.02	0.011
Scout	21.5	500	45	0.011	$2.109 * 10^{-3}$

Isakowitz et. al. provides a more in depth summary of launch vehicle performance [66]. The authors provide weights for various stages in a vehicle, nominal staging events and weights for both dry and fully loaded stages. Enough information is available to create an approximate model of how the mass of a launch vehicle decreases as a payload is launched into an orbit [64]. A challenge to the designer is to create an isolation system that operates optimally over this entire range.

MDOF Vibration Control. Vibration control devices for space applications and for ground testing are typically MDOF. Launch devices have already been discussed, so only on-orbit devices will be briefly mentioned. For a recent review of such devices, see Thayer et. al. [67] and Cobb et. al. [68]. Almost all devices being considered are designed as hexapods or Stewart platforms (see Geng and Haynes for a discussion on Stewart platforms [69]) and have been designed as hybrid, purely active, or purely passive systems. Thayer et. al. provides an interesting summary of current hexapod devices where comparisons were made of actuator stroke lengths, passive damping capabilities and corner frequencies, provision for gravity off-load devices, and active bandwidth requirements. It was noted earlier that passive damping and active control trade-off with each other [26] and Cobb et. al. has noted that high actuator stroke lengths allow hexapod devices to be used to steer payloads while low stroke lengths limit the system just to vibration control. Further, hexapods have been used for vibration isolation, vibration absorption and steering simultaneously. In closing, future research in hexapods seems to be working towards increasing isolation capability of control systems [67] and towards miniaturizing of hexapod hardware [20]. As already noted earlier, novel methods of multidegree control are also being considered in the idea of contactless sensors and actuators between payload and satellite, with a goal of substantially increasing isolation performance [36].

2.4 Modeling Vibration Control Problems (System Models)

Many simplified models of real applications have been considered in the literature. Simple models have the benefit of being more understandable and can be analyzed relatively easily. Unfortunately, they may not represent the real systems very accurately. More complex models can be more representative of real systems, but the complexity makes them more difficult or impossible to analyze. The existing models found in the literature serve as a reference and starting point for the analysis presented later. Both linear and nonlinear models are considered.

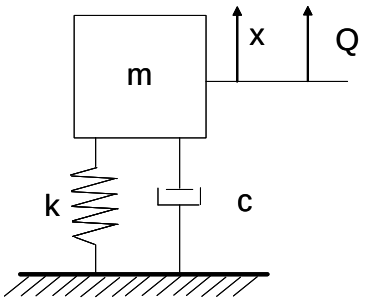

Figure 2.1 SDOF Suppression Problem with Constant Parameters

Equations of Motion for Constant Parameter Systems.

SDOF Models. Vibration control problems have been modeled in many ways in the literature. The simplest model is the SDOF system (Figure 2.1), which is well documented for constant parameters of mass, damping and stiffness [70], [71]. This system has been called source isolation [2] and vibration suppression. The equation of motion is

$$m\ddot{x} + c\dot{x} + kx = Q, \tag{2.1}$$

where m is the mass of the system, c is the damping coefficient, and k is the stiffness coefficient.

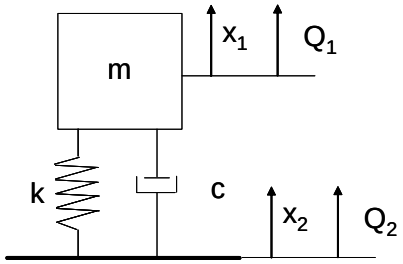

Figure 2.2 SDOF Constant Parameter Isolation Problem

Alternatively, the vibration isolation problem or receiver isolation problem [2] is shown in Figure 2.2 when $Q_1 = 0$. It is assumed that either Q_2 or x_2 is prescribed and vibration of m is to be minimized. The equations of motion (assuming x_2 is prescribed) are [72]

$$m\ddot{x}_1 + c\dot{x}_1 + kx_1 = c\dot{x}_2 + kx_2 \tag{2.2}$$

and Q_2 is

$$Q_2 = k\left(x_2 - x_1\right) + c\left(\dot{x}_2 - \dot{x}_1\right). \tag{2.3}$$

However, if Q_2 is prescribed, then by substituting Equation 2.3 into Equation 2.2 results in

$$m\ddot{x}_1 = Q_2 \tag{2.4}$$

and displacement x_2 is found by substituting the results of Equation 2.4 into Equation 2.3.

2 Degree of Freedom Models. The 2 degree of freedom (DOF) model is considered to be better for analyzing vibration isolation and has also been extensively analyzed [2], [73] again with constant parameters. Typically, such systems in the literature assume a fixed or moving support attached to the model with a spring and/or damper. Since there are no fixed supports in space or in a launch application, a free-free type model is considered.

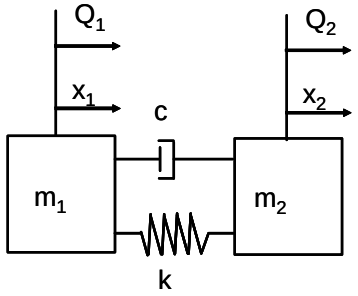

Figure 2.3 2 DOF Isolation/Suppression Problem with Constant Parameters

Figure 2.3 shows the 2 DOF system located in space. If we assume m_2 is to have vibrations minimized, then if $Q_1 \neq 0$ and $Q_2 = 0$, the isolation problem is being considered. When $Q_1 = 0$ and $Q_2 \neq 0$, the suppression problem is under consideration. Of course, both problems could be examined simultaneously. The equations of motion are

$$m_1\ddot{x}_1 - g\left(x_1, x_2, \dot{x}_1, \dot{x}_2\right) = Q_1 \tag{2.5}$$

and

$$m_2\ddot{x}_2 + g\left(x_1, x_2, \dot{x}_1, \dot{x}_2\right) = Q_2 \tag{2.6}$$

where

$$g\left(x_1, x_2, \dot{x}_1, \dot{x}_2\right) = c\left(\dot{x}_2 - \dot{x}_1\right) + k\left(x_2 - x_1\right). \tag{2.7}$$

MDOF Models. A general series MDOF model has been considered by Meiriovitch [71]. He considers a linear series system with p masses connected by $p+1$ springs and dampers with fixed connections on either side of the system. Each mass has a force Q_i operating on it where $i = 1, 2, ...p$. The general equations of motion are

$$\sum_{j=1}^{p} \left[m_{ij}x_j + c_{ij}\dot{x}_{ij}\dot{x}_j + k_{ij}x_{ij}\right] = Q_i \tag{2.8}$$

where

$$\begin{array}{lll} m_{ij} = \delta_{ij}m_i & & \\ c_{ij} = 0 & k_{ij} = 0 & j = 1, 2, ..., i-2, i+2, ..., n \\ c_{ij} = -c_i & k_{ij} = -k_i & j = i-1 \\ c_{ij} = c_i + c_{i+1} & k_{ij} = k_i + k_{i+1} & j = i \\ c_{ij} = -c_{i+1} & k_{ij} = -c_{i+1} & j = i+1 \end{array} \tag{2.9}$$

and δ is the Kronecker delta function

$$\delta_{ij} = \begin{cases} 1 & \text{if } i = j \\ 0 & otherwise \end{cases}. \tag{2.10}$$

The equations can be written in matrix form as

$$[m]\left\{\ddot{x}\left(t\right)\right\} + [c]\left\{\dot{x}\left(t\right)\right\} + [k]\left\{x\left(t\right)\right\} = \left\{Q\left(t\right)\right\} \tag{2.11}$$

In general, Equation 2.11 is very difficult to solve analytically except in special cases. Solving these equations exactly requires the the matrices $[m]$, $[c]$, and $[k]$ be simultaneously diagonalizable. These matrices can be diagonalized if and only if

$$\begin{array}{l} [c][m] = [m][c] \\ [m][k] = [k][m] \\ [c][k] = [k][c]. \end{array} \tag{2.12}$$

That is, any two matrices of Equation 2.11 must commute in multiplication [74], [75], [76]. If the system is diagonalizable, then modal analysis can be used to solve the equations of motion [71].

Equations of Motion for Variable Parameter Systems. When stiffness and/or the damping of a system can be controlled, the system is considered to have tunable parameters [3] or is semi-active. Extensive literature exists on attenuating harmonic excitations through the use of vibration absorbers and is surveyed by Sun et. al. [4]. Vibration absorbers are widely used to attenuate unwanted narrow-band disturbances, but can also be used for broadband applications [4], [3].

Vibration isolation and vibration suppression will be considered in the following sections. Equations of motion in the literature for varying parameter systems are surveyed. The goal is to review how vibration control problems allowing variable stiffness, variable damping, and/or variable mass have been mathematically modelled in the literature.

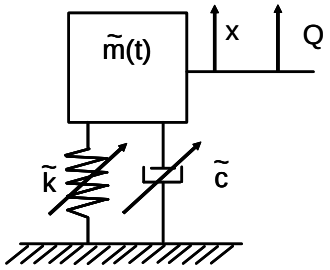

Figure 2.4 1 DOF Suppression Problem

SDOF Models. Leitmann studies the SDOF suppression problem (see Figure 2.4) and develops control laws for variable damping, variable stiffness and constant mass ($m(t) = m$). Note, that Leitmann concludes variable damping should always be maximum, so varying damping is not very useful in this problem. The equation of motion he considers is

$$m\ddot{x} + c(u_c)\,\dot{x} + k(u_k)\,x = Q, \tag{2.13}$$

where u_c and u_k are control parameters that instantaneously change the damping and stiffness of the system. The functions c and k are damping and stiffness, respectively

while Q is the disturbance function. Leitmann considers a case where u_c and u_k can be controlled independently and a case where $u_c = u_k = u$ where the damping and stiffness can not be changed independently [77]. The problem of only varying stiffness was also studied earlier [78].

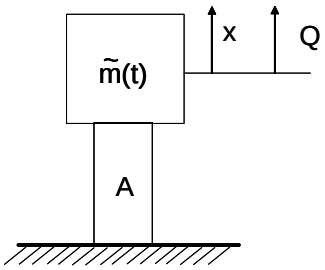

Figure 2.5 1DOF General Suppression Problem

Clark analyzes the system of Figure 2.5 where element A is a piezoelectric hollow cylinder. His analysis is similar to Leitmann's, except by changing the type of shunt attached to the piezoelectric, Clark is able to change the characteristics of element A, causing it to have damping characteristics or both damping and stiffness characteristics. Clark's equations of motion are

$$m\ddot{x} + g\left(x, \dot{x}\right) = Q, \tag{2.14}$$

where $g\left(x, \dot{x}\right)$ is the force generated by element A (piezoelectric element) [79].

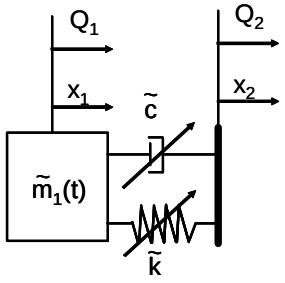

Figure 2.6 1 DOF Isolation Problem with Explicit Varying Mass Representation

The SDOF isolation problem is shown in Figure 2.6. Variants of this problem have been studied, typically with $m_1\left(t\right) = m_1$ where m_1 is constant. For example, Karnopp uses this type of model with constant stiffness and a variable damper to isolate m_1 from a

disturbance Q_2. The equation of motion used is

$$m_1\ddot{x} + g\left(x, \dot{x}\right) = Q, \tag{2.15}$$

where

$$x = x_2 - x_1 \tag{2.16}$$

and

$$g\left(x, \dot{x}\right) = \tilde{c}\dot{x} + \tilde{k}x \tag{2.17}$$

is the the combined isolation device and control law [80], [15].

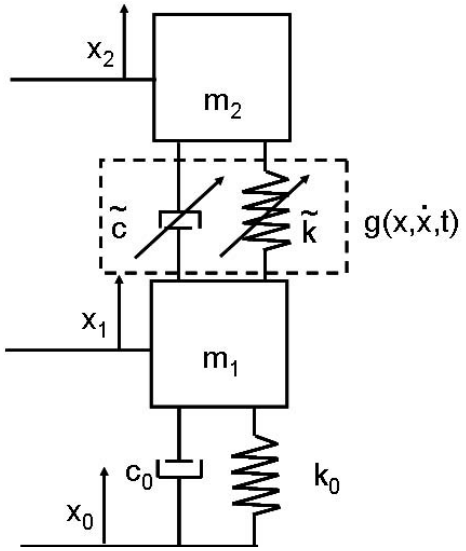

Figure 2.7 Quarter-Car Model

2 DOF Models. A commonly used model in the automotive industry called the quarter-car model is shown in Figure 2.7. Mass m_2 is often called the sprung mass (representing the mass of an automobile) while mass m_1 is called the unsprung mass (representing the mass of a tire). A prescribed displacement at x_0 represents the disturbance of the system (road noise). Equations of motion for this system are

$$m_1\ddot{x}_1 - g\left(x, \dot{x}, t\right) + c_0\left(\dot{x}_1 - \dot{x}_0\right) + k_0\left(x_1 - x_0\right) = 0 \tag{2.18}$$

and

$$m_2\ddot{x}_2 + g\left(x, \dot{x}, t\right) = 0 \tag{2.19}$$

where $g\left(x_1, x_2, \dot{x}_1, \dot{x}_2\right)$ is the the combined isolation device and control law. This type of model has been studied by many authors using variable damping devices [14], [81], [82], [83].

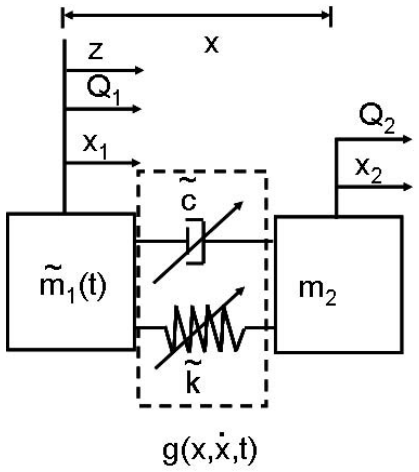

Figure 2.8 2 DOF System with an Inertial and a Relative Coordinate

Balandin et. al. has considered a different derivation of the 2 DOF problem [84]. They use one inertial coordinate and one relative coordinate using the transformations

$$z = x_1 \tag{2.20}$$

and

$$x_2 = x + z, \tag{2.21}$$

where x is the relative displacement between x_2 and x_1. They define the isolator as simply $g\left(x, \dot{x}, t\right)$ as shown in Figure 2.8. Further, they consider $m_1\left(t\right) = m_1$ to be constant and $Q_2 = 0$. The equations of motion are

$$m_1\ddot{z} + m_2\left(\ddot{x} + \ddot{z}\right) = Q_1\left(t\right) \tag{2.22}$$

and

$$m_2 (\ddot{x} + \ddot{z}) = g (x, \dot{x}, t) . \tag{2.23}$$

By solving Equation 2.23 for $\ddot{z}$ and substituting into Equation 2.22, the uncoupled second order equation

$$\ddot{x} - \frac{g (x, \dot{x}, t)}{\mu} = \frac{Q_1}{m_1} \tag{2.24}$$

is derived, where $\mu = \frac{m_1 m_2}{m_1 + m_2}$ is called the reduced mass. Equation 2.24 is a SDOF equation describing the isolation of the system [84], [85]. Note that Equations 2.20 and 2.21 is simply a transformation of the 2 DOF problem from inertial to modal coordinates.

2.5 Semi-Active Control Devices (Device Models)

Constant stiffness elements and damping elements are well understood and examples of elegant designs of isolation struts for use in space have existed for many years [86]. For an overview of passive damping design (viscoelastic materials, viscous fluids, magnetic and passive piezoelectrics), see Johnson [87]. Much effort is now going into smart materials allowing stiffness and/or damping to be varied during operation of vibration control systems. For damping elements, research lines have considered MRFs, ERFs, piezoelectrics, and hydraulic concepts [88]. Variable stiffness elements are also being examined, though these technologies appear to be newer and less mature than variable damping devices. Devices being considered for variable stiffness include SMA, MREs, piezoelectrics and others. Each of these will be briefly reviewed and their corresponding mathematical models will be presented.

Variable Damping.

ERF/MRF Dampers. MRF dampers are well developed devices currently in use in the automotive industry [89], while ERF dampers are in a prototype stage of being studied [90], [91]. These dampers have the ability to change their damping characteristics by application of an electric field for ERFs or by applying a magnetic field for MRFs. When these fields are applied, micro size particles distributed in the fluid form chains. Field strength can be increased to the point where the chains solidify resulting in a high yield

stress and an increase in damping for MRF or ERF dampers. Removal of the field results in the fluid returning to its original state. Changes in state occur within milliseconds [90], [92], [93], [94].

ERFs can be easily manufactured (silicon oil and cornstarch will work) [90], but MRFs have several advantages over ERFs. MRFs generate higher yield stresses than ERFs, allowing MRF dampers to provide a wider range of variable damping than an ERF damper. Additionally, MRFs can use low voltage while ERFs tend to require high voltage. MRF dampers are insensitive to impurities in the fluid allowing less stringent manufacturing requirements. Further, a larger number of additives can be used with MRFs simplifying design for seals and minimization of wear [94].

There are many studies that model ERF dampers and MRF dampers that trade accuracy for complexity. Typically, the damper is tested and increasingly complex non-linear models are applied. Testing usually entails measuring force, displacement and velocity generated by the damper for an input signal (random or sinusoidal) [14], [95], [7] over a range of input currents. Models follow a hierarchy of roughly increasing order of complexity and accuracy, are mostly nonlinear, and are not always continuous functions.

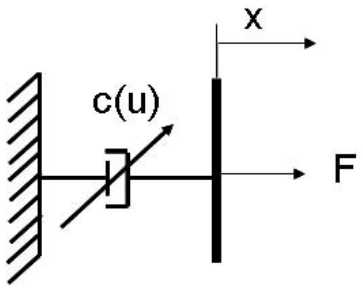

Figure 2.9 Equivalent Viscous Damping Model

The equivalent viscous damping method (a linearization) equates energy dissipation with that of an equivalent damper, making damping a function of input current and displacement amplitude [95], [96], [7]. This type of model has been analyzed by Leitmann (see Figure 2.9) in the form

$$F = c\,(u)\,\dot{x}, \tag{2.25}$$

where $u \in [-1, 1]$ and

$$c(u) = \frac{1}{2}\left[(c_0 + c_1) + (c_1 - c_0)\, u\right] \qquad \ni c_1 > c_0 > 0. \tag{2.26}$$

The complex stiffness method (another linearization) calculates storage stiffness and loss stiffness in the form of a complex number, which will be a function of the excitation frequency [95].

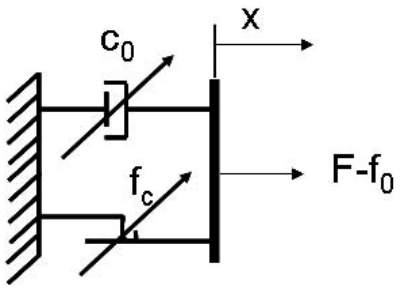

Figure 2.10 Bingham Viscoplastic Model

The Bingham viscoplastic model adds the yield stress of the fluid (often modelled as a frictional element), but has limitations that make its use as a control model debatable [97], [95], [94]. Figure 2.10 shows the model. The equations of motion are

$$F = f_c \,\mathrm{signum}\,(\dot{x}) + c_0 \dot{x} + f_0. \tag{2.27}$$

Here, f_c is a frictional force related to the yield stress of the fluid inside the damper. The coefficient c_0 is the damping coefficient and f_0 can be used to account for the nonzero mean observed in variable dampers containing a pressurized tank used to prevent fluid cavitation. Pan et. al. has proposed that f_c and c_0 vary approximately linearly as

$$f_c = f_a + f_b V \tag{2.28}$$

and

$$c_0 = c_a + c_b V, \tag{2.29}$$

where f_a, f_b, c_a, and c_b are constants and V is the input voltage to the damper [98].

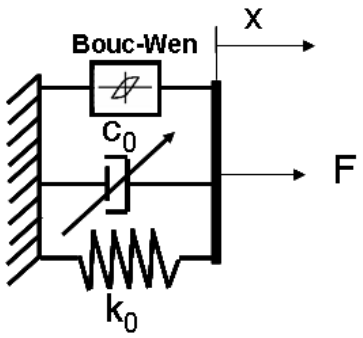

Figure 2.11 Bouc-Wen Model

The Bouc-Wen model, shown in Figure 2.11, adds a hysteresis element, but has some of the same limitations as the Bingham model. It has been used in vibration isolation applications [94], [14]. The equations of motion for the Bouc-Wen model are

$$F = c_0\dot{x} + k_0\left(x - x_0\right) + \alpha z \tag{2.30}$$

and

$$\dot{z} = -\gamma\left|\dot{x}\right| z\left|z\right|^{n-1} - \beta\dot{x}\left|z\right|^{n} + A\dot{x}. \tag{2.31}$$

The parameters α, β, and γ control the scale and shape of the hysteresis curve, n controls sharpness of the curve as it transitions from one region to another, c_0 is the damping coefficient, and k_0 is the stiffness coefficient [99]. Pan et. al. has approximated c_0 and α linearly as

$$c_0 = c_a + c_b V \tag{2.32}$$

$$\alpha = \alpha_a + \alpha_b V \tag{2.33}$$

where c_a, c_b, α_a, and α_b are constants and V is the input voltage to the damper. The variable x_0 physically corresponds to an initial displacement of the damper due to a pressurized gas filled accumulator in the damper used to prevent cavitation of the fluid.

Spencer et. al. has proposed a modified Bouc-Wen model shown in Figure 2.12, which is able to account for fluctuating magnetic fields being applied to the MRF damper.

The equations of motion for this system are

$$F = c_1\dot{y} + k_1\left(x - x_0\right), \tag{2.34}$$

$$\dot{z} = -\gamma\left|\dot{x} - \dot{y}\right| z\left|z\right|^{n-1} - \beta\left(\dot{x} - \dot{y}\right)\left|z\right|^{n} + A\left(\dot{x} - \dot{y}\right), \tag{2.35}$$

$$\dot{y} = \frac{1}{c_0 + c_1}\left\{\alpha z + c_0\dot{x} + k_0\left(x - y\right)\right\}, \tag{2.36}$$

$$\alpha = \alpha_a + \alpha_b u, \tag{2.37}$$

$$c_1 = c_{1a} + c_{1b}u, \tag{2.38}$$

$$c_0 = c_{0a} + c_{0b}u, \tag{2.39}$$

and

$$\dot{u} = \eta\left(u - V\right), \tag{2.40}$$

where the parameters c_{0a} ,c_{0b}, k_0, c_{1a}, c_{1b}, k_1, x_0, α_a, α_b, γ, β, n, η, and A (fourteen total parameters) are determined in a nonlinear optimization problem. The variable V is the voltage being supplied to the damper and is assumed to cause α, c_1, and c_0 to vary linearly. The variable u is used to describe dynamics of the MRF achieving rheological equilibrium [94].

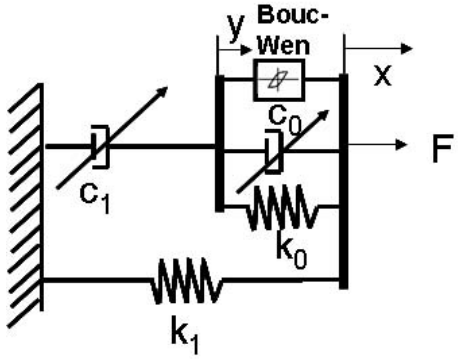

Figure 2.12 Modified Bouc-Wen Model

As can be seen, many models have been proposed to represent MR and ER damping devices. The choice of which model to use depends on the desired accuracy in solving a

problem. Unfortunately, the price for accuracy is much more complexity, which can limit the insight to be gained in analysis.

Damping with Piezoelectrics. Use of piezoelectrics for damping vibrations in a structure has been extensively reviewed in the literature. Hagood and von Flotow created the analytical foundation for understanding how piezoelectrics can be used for damping. When piezoelectrics are combined with a resistor, they create damping analogous to viscoelastic damping. The piezoelectric combined with the resistor electrically creates an RC shunt network, since the piezoelectric acts like a capacitor [100]. Maximum damping has a stronger frequency dependence than viscoelastic materials and occurs at a point related to the inverse of the RC time constant for the shunt circuit [101]. Tang, Liu and, Wang reviewed semi-active damping and hybrid damping methods. The hybrid method can be divided into active and passive damping abilities of the piezoelectric itself and active damping with the piezoelectric combined with traditional passive damping materials [11].

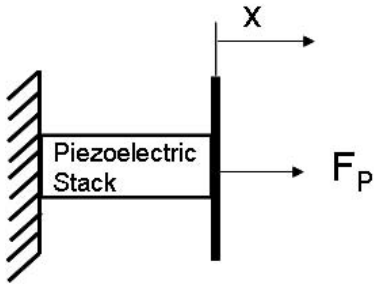

Figure 2.13 Piezoelectric Damping

Corr and Clark derive the damping force of a piezoelectric stack using linear theory and the following derivation comes directly from their article [102]. Refer to Figure 2.13. They consider the piezoelectric stack as N identical layers bonded together and wired in parallel. They begin with the one dimensional, uniaxial loading constitutive equations [103]

$$\begin{bmatrix} D \\ S \end{bmatrix} = \begin{bmatrix} \varepsilon_3^T & d_{33} \\ d_{33} & s_{33}^E \end{bmatrix} \begin{bmatrix} E \\ T \end{bmatrix}, \tag{2.41}$$

where D is electrical displacement (charge/area), S is mechanical strain, E is the electric field (volts/meter), T is mechanical stress (force/area), ε_3^T is the dielectric constant, d_{33} is the piezoelectric constant, and s_{33}^E is the piezoelectric compliance. The superscripts T and E indicate the parameters were measured at constant stress or electric field, respectively. The subscript 3 represents the orientation of the piezoelectric being modelled. Making the substitutions

$$V = L_p E, \tag{2.42}$$

$$q_1 = AD, \tag{2.43}$$

$$S = \frac{x}{L_p}, \tag{2.44}$$

and

$$T = \frac{F_p}{A}, \tag{2.45}$$

where L_p is the thickness of the piezoelectric layer, q_1 is the generated charge for one piezoelectric layer, and A is the cross sectional area results in

$$\begin{bmatrix} F_p \\ q_1 \end{bmatrix} = \begin{bmatrix} k^{sc} & -k^{sc} d_{33} \\ k^{sc} d_{33} & C_p^s \end{bmatrix} \begin{bmatrix} x \\ V \end{bmatrix}, \tag{2.46}$$

where

$$k^{sc} = \frac{A}{s_{33}^E L_p}, \tag{2.47}$$

$$C_p^T = \frac{A\varepsilon_3^T}{L_p}, \tag{2.48}$$

$$C_p^S = C_p^T \left(1 - k_{33}^2\right), \tag{2.49}$$

and

$$k_{33} = \sqrt{\frac{d_{33}^2}{s_{33}^E \varepsilon_3^T}}. \tag{2.50}$$

For N piezoelectric layers,

$$\begin{bmatrix} F_p \\ q_N \end{bmatrix} = \begin{bmatrix} k_{eq}^{sc} & -k^{sc} d_{33} \\ k^{sc} d_{33} & \left(C_p^s\right)_{total} \end{bmatrix} \begin{bmatrix} x \\ V \end{bmatrix}, \tag{2.51}$$

where k_{eq}^{sc} is the equivalent short circuit stiffness for springs in series while $\left(C_p^s\right)_{total}$ is the equivalent capacitance for each piezoelectric layer in parallel. By solving the second of Equation 2.51 for V and substituting into the first equation of Equation 2.51, and letting $Q^{app} = q_n$ (applied charge) results in the equation of motion

$$F_p = \left(k_{eq}^{sc} + \frac{\left(k^{sc} d_{33}\right)^2}{\left(C_p^s\right)_{total}} \right) x - \frac{\left(k^{sc} d_{33}\right)}{\left(C_p^s\right)_{total}} Q^{app}. \tag{2.52}$$

Typically, some type of shunt circuit is added to the piezoelectric device which changes the electrical charge Q^{app}. One type of shunt circuit discussed by Corr and Clark is

$$L\ddot{Q}^{app} + R\dot{Q}^{app} + \frac{1}{\left(C_p^s\right)_{total}} Q^{app} = \frac{k^{sc} d_{33}}{\left(C_p^s\right)_{total}} x, \tag{2.53}$$

where R is the resistance of the shunt circuit and L is the inductance of the shunt circuit [17]. Lesieutre classifies different types of shunt circuits and their effect on a mechanical system. When $L = 0$, the shunt circuit converts electrical energy to heat, dispersing it from the system. Hence, mechanical energy is converted to electrical energy by the piezoelectric which is then converted to heat by the resistive shunt. By varying the resistance of the shunt circuit using a control law, it is possible to vary the amount of energy damped out by a piezoelectric. When $L \neq 0$, the shunt circuit is analogous to a vibration absorber [101]. Energy is most efficiently dissipated when the impedance of the resister in the shunt circuit matches the impedance of the piezoelectric [104].

Corr and Clark considered changing the damping of a piezoelectric by alternately connecting and disconnecting an RL shunt circuit to the piezoelectric. In tests, they were able to attenuate the third mode of a clamped-clamped beam [102]. In another approach, Wang et. al. researched semi-active damping with piezoelectric patches attached to a cantilever beam. One piezoelectric patch is used to create a disturbance to the beam, while the other is used to damp out the disturbance. They formulated the equations of motion for a cantilever beam and for the piezoelectric with a variable resistance-inductance shunt circuit. They note that a variable resister can be created using a digital potentiometer and variable inductors can be emulated using an OP amp circuit [105].

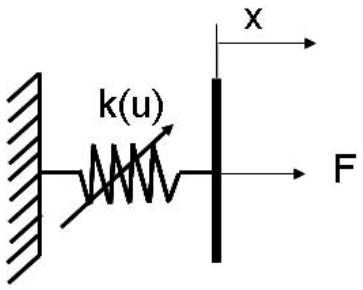

Figure 2.14 Equivalent Stiffness Element

Variable Stiffness. The simplest model of a variable stiffness element is shown in Figure 2.14. The stiffness is

$$F = k\left(u\right)x, \tag{2.54}$$

where $u \in [-1, 1]$,

$$k\left(u\right) = \frac{\left(k_0 + k_1\right)}{2}\left[1 + \varepsilon u\right] \ \ni k_1 > k_0 > 0, \tag{2.55}$$

$$\varepsilon = \frac{k_1 - k_0}{k_1 + k_0}, \tag{2.56}$$

k_0 is the smallest stiffness the variable stiffness device can achieve, and k_1 is the largest stiffness the variable stiffness device can achieve. The variable u is an input variable for controlling the stiffness device while ε is a measure of the maximum variation of a variable stiffness device. While real devices do not behave as this simplistic model suggests, it does allow for analysis and hence is often used in the literature.

In the literature, researchers often document maximum and minimum natural frequencies achieved using a device or they report the maximum and minimum stiffness achieved by a device. Since actuating a variable stiffness device does not change the mass of the system, a characterization parameter α can be defined as

$$\alpha = \left(\frac{\omega_{\min}}{\omega_{\max}}\right)^2 = \frac{k_0}{k_1}. \tag{2.57}$$

where α is the variable stiffness ratio of a variable stiffness device, $\omega_{\min}$ is the minimum natural frequency of a system with a variable stiffness device, and $\omega_{\max}$ is the maximum natural frequency of a system with a variable stiffness device. The relationship between

α and ε is

$$\varepsilon = \frac{1-\alpha}{1+\alpha}. \tag{2.58}$$

These parameters will be used to develop physical insight into the capabilities of different variable stiffness devices when such data is available.

Shape Memory Alloy Models. SMAs are metal alloys that recover otherwise permanent strains when heated. Stable phases of SMAs include a low temperature phase called martensite and a high temperature phase called austenite. SMAs have two properties which are exploited for use in vibration control called the SME and the PE. The SME occurs when a SMA in martensitic form is deformed by a load and then heated to austenitic form where it recovers its original shape. The PE occurs when a load is applied to a SMA in austenitic form, which under proper conditions, can induce a phase change to martensitic form. When the load is released, the material is transformed back to austenitic form and recovers its original shape [106]. Detailed discussion of SMA mechanisms are available [107]. In addition to discussing SMA mechanisms, models describing both SME and PE in SMAs has been extensively reviewed [108].

The SME has been used to create semi-active absorbers and isolators. In one article, Williams et. al. used three SMAs and steel wires configured as cantilever beams with a concentrated mass at the end to create a vibration absorber. The reported change in natural frequency was $\frac{\omega_{\min}}{\omega_{\max}} = \frac{1}{1.73}$ resulting in $\alpha = 0.33$ [109].

In another case, a novel actuator was created using a weave of SMA wires surrounding disks with passive springs in between [110]. The actuator uses mechanical advantage to increase stroke length and has millisecond response rates. The actuator has been used for semi-active control and successfully damped out impulse disturbances in 360 msec. The problem with all of these SME concepts is the time required for SMAs to cool off, which can be mitigated by clever design, but not completely eliminated [111].

Another example is an aircraft wing spar strut concept with an internal piston and multiple preloaded standard and SMA springs on either side of the piston. The SMA springs are inactive while in martensitic phase. Since the standard springs are stiffer than

the SMA springs, stop spacers are used to prevent preloading of the SMA springs. When heated, the SMA changes to austenitic phase, increases in stiffness, and becomes able to support the preload. The result is a decrease in overall stiffness in the strut, due to clever design [112].

The PE of SMAs has been proposed for use in place of softening springs for passive isolation of large loads. Typically, a soft spring is desired for isolation, but a stiff spring is needed to prevent large displacements. A softening spring can be used, but it lowers isolator resonance frequencies and damping must be added. This in turn, degrades higher frequency isolation. Use of SMAs might remove this trade-off. Recent work has looked at building simplified models for SMAs [113] and has been studied for use in passive isolation [113], [114].

Magnetorheological Elastomers. MREs are solid polymers with dispersed micron-sized magnetizable particles. The elastomer is cured in a magnetic field causing the magnetic particles to align in chains and remain aligned after the magnetic field is removed. Application of a magnetic field changes the stiffness of the elastomer [115]. The Ford Motor Company has been researching MREs for use as variable stiffness elements for control-arm bushings and engine mounts in automobiles. They have studied and modelled the MRE phenomena [116], [117] and are developing tunable vibration absorbers. MRE absorbers have been fabricated and both stiffness and damping were observed to increase with increasing magnetic fields [118]. Additionally, resonant frequency was found to decrease with increasing input acceleration amplitude attributed to strain-softening behavior of the elastomer [119], making this variable spring non-linear.

Zhou notes that a primary difference between MRFs and MREs is that MRFs operate in post yield conditions while MREs operate in preyield conditions. As a result, an MRE should be used in a structure to change its natural frequency. Changing the natural frequency can prevent resonance response or other coupled behavior in a structure. Zhou studies a device made of silicone rubber and carbonyl iron particles. Zhou models the

MRE in a SDOF system as

$$m\ddot{x} = -\frac{G\left(B_{MRE}\right)S}{h}x - \beta_m\left(B_{MRE}\right)\left(\sqrt{\frac{G\left(B_{MRE}\right)S}{h}m}\right)\dot{x}, \tag{2.59}$$

where $G\left(B_{MRE}\right)$ is the shear modulus of elasticity for the MRE, B_{MRE} is the magnetic induction or magnetic flux density, S is the surface area of the MRE, h is the thickness of the MRE, $\beta_m\left(B_{MRE}\right)$ is a damping factor and m is the mass of a covering plate attached to the MRE. Note that G and β_m are functions of B_{MRE}. Zhou determined G and β_m experimentally by fitting experimental data to Equation 2.59. The author concludes that $G\left(B_{MRE}\right)$ is a linear function and $\beta_m\left(B_{MRE}\right)$ is a constant. Zhou found he could vary the natural frequency of his system from 1397.6 to 1773.5 radians/second [120] or $\alpha = 0.62$.

In another experiment, Albanese and Cunefare tested silicone mixed with several different percentages of iron particle concentrations. They concluded that at 35% iron content, as much as a 400% change in frequency could be made by applying a magnetic field. In their conference briefing, they concluded 30% iron content could cause a nearly 900% change in frequency. Their results are reported in terms of $\alpha^{-\frac{1}{2}}$ or equivalently, they tested several devices in the range $0.11 \leq \alpha \leq 0.91$ [121], [122].

Piezoelectric Models. Stiffness of piezoelectrics can be varied by connecting them to a capacitive shunt circuit. This and other methods of shunting piezoelectrics for vibration control was reviewed by Lesieutre [101]. A simple method of varying stiffness of piezoelectric devices is to switch it between open and closed circuit conditions. This has the effect of changing the electrical capacitance of the piezoelectric device and varies the stiffness between its highest and lowest stiffness values. The equation of motion for a SDOF problem discussed by Kurdila et. al. is

$$m\ddot{x} + \left(k^{sc} + \frac{\left(k^{sc}d_{33}\right)^2}{C_P^S}\left(1-\Delta\right)\right)x - \frac{\left(k^{sc}d_{33}\right)^2}{C_P^S}\left(1-\Delta\right)x_0 = F\left(t\right), \tag{2.60}$$

where k^{sc} is the short circuit stiffness of the piezoelectric, d_{33} is the piezoelectric constant, C_P^S is the constant strain piezoceramic capacitance, m is a vibrating mass, x_0 is the displacement of the actuator at the instant the piezoelectric is switched to an open circuit

condition, and Δ is either 0 or 1. Setting the control parameter Δ to 1 sets the piezoelectric to its lowest stiffness while setting Δ to 0 maximizes the stiffness. The authors observe that selecting a control law making $x_0 \neq 0$ introduces a step function into the system. They eventually conclude switching should only occur when $x\dot{x} = 0$ to make $x_0 = 0$ [123]. Richard et. al. experimented with this method and found superior performance as compared to a resistively shunted nonswitching system [124].

Corr and Clark have also experimented with this concept. For their setup, they concluded this method provided only small changes in stiffness and was not as effective as other shunt circuits with associated control laws. Other shunt circuits experimented with include pure resistor and resistor/inductor shunt circuits [17], [102].

In an earlier paper, Clark analyzed effective beam stiffness in the case of a piezoelectric bonded to a cantilever. As the ratio of beam to piezoelectric patch thickness decreased, the open circuit to short circuit stiffness ratio or α^{-1} was found to increase to a maximum value approaching 2.0. That is, $\alpha \rightarrow \frac{1}{2}$. [125]

Varying stiffness has been used to tune vibration absorbers when the resonant frequency varies. Davis and Lesieutre created and demonstrated a tunable vibration absorber that tracked a disturbance frequency. The piezoelectric stiffness element was actively tuned using a shunt circuit ladder of capacitors allowing various discrete levels of capacitance to be chosen. Davis and Lesieutre were able to vary the natural frequency of their system by almost 7.5% over a range of 313 Hz to 338 Hz [126]. This translates to an α of 0.86.

More recently, Ramaratnam et. al. propose using piezoelectrics for robotic applications. They simulated both open and closed switching and the use of capacitive shunt circuits to minimize tip deflection of a translational flexible beam. Both methods achieved similar results. The capacitive shunt method allowed a more gradual change in stiffness than the open/closed switching method. Their predicted equivalent stiffness for the capacitive method translates to an α of approximately 0.045. Future experimental work is planned [127].

Other Devices. Other methods of varying stiffness have been explored. One approach is to place a MRF damper in series with a spring, which is then placed in parallel

with another spring, creating a three parameter isolator. Varying the MRF damping then changes the apparent stiffness of the isolator [128], [7].

Two mechanical concepts for varying stiffness have been discussed in the literature. One concept is a vibration absorber that consists of a mass attached to helical spring with a spring collar dividing the spring into two parts. The spring collar isolates part of the spring from the rest of the absorber and the number of coils used in the absorber can be changed by rotating the spring [8]. Another concept is to connect two leaf springs in opposition to each other and use a stepper motor to increase the separation distance between the two springs. In this concept, the authors report a change of stiffness of $\alpha^{-1} = 62$ in a nonlinear range and $\alpha^{-1} = 45$ in an approximately linear range. The linear range where $\alpha = \frac{1}{45} = 0.02$ corresponds to a value for ε very close to its largest possible value [129].

Summary. Table 2.2 summarizes the results of these calculations for some proposed hardware values for ε and α found in the literature in order of reported ability to change stiffness from highest to lowest. These devices offer a wide range of choices for the control system designer, with a potential wide range of achievable performance.

2.6 Semi-Active Control Strategies

It is clear from the previous discussion that passive and hybrid control concepts have often been used operationally in space applications and are well documented. On the other hand, no examples of semi-active control have been found operationally in space applications, though numerous studies (both space and non-space) on the subject exist. Further, most studies concentrate on vibration absorption and suppression problems with very little found on vibration isolation. Studies can be divided up into studies using only variable stiffness, using only variable damping, and using both variable stiffness and variable damping.

Sun et. al. provides a review of ATVAs through 1995. Tuned vibration absorbers only function for set conditions which may vary with time. ATVAs overcome this by using a control system to tune them automatically as conditions vary [4]. Manual tuning of a

Table 2.2 Parameter Values for Proposed Variable Stiffness Devices in the Literature

Source	Year	Device	α	ε
Albanese and Cuefare [122]	2003	MRE 30% Fe	0.01	0.98
Walsh and Lamancusa [129]	1992	Leaf Spring	0.02	0.96
Albanese and Cuefare [121], [122]	2003	MRE 35% Fe	0.05	0.91
Albanese and Cuefare [121], [122]	2003	MRE 25% Fe	0.11	0.80
Albanese and Cuefare [121], [122]	2003	MRE 40% Fe	0.19	0.68
Albanese and Cuefare [121], [122]	2003	MRE 10% Fe	0.31	0.53
Williams, Chiu, and Bernhard [109]	2002	SMA	0.33	0.50
Albanese and Cuefare [121], [122]	2003	MRE 50% Fe	0.35	0.49
Clark [125]	2000	Piezoelectric Patch on Cantilever (On-Off)	0.50	0.33
Zhou [120]	2003	MRE 27% Fe	0.62	0.23
Albanese and Cuefare [121], [122]	2003	MRE 0% Fe	0.83	0.10
Ramaratnam, Jalili, and Grier [127]	2003	Piezoelectric (Capactive Shunt)	0.91	0.05
Davis and Lesieutre [126]	2000	Piezoelectric (Capactive Shunt)	0.93	0.04

vibration absorber with a large tuning range (1375-2010 Hz) was demonstrated using a magnetostrictive device [130]. Davis and Lesieutre were able to automatically tune an ATVA in discrete steps using a capacitive shunt piezoelectric device [126]. Franchek et. al. has also designed a tuning scheme, which was experimentally verified on a subscale building [8].

The control law idea of maximizing or minimizing an element has also been used in variable damping devices. For example, Yao et. al. designed this type of controller for an automotive shock absorber [14] and used a nonlinear function of velocity to switch the damping. The control law used is called the skyhook damper and will be discussed further below.

However, study is not limited to this type of control law. Spencer et. al.'s development of better MR damping models opens the possibility of improved vibration control [94]. Oh, Onoda, and Minesugi simulated an improved control as compared to on-off damping with an ERF damper used to isolate reaction wheel disturbances. While the improved control law used on-off control, the damping was not always maximized or minimized at

all frequencies tested, which decreased the effects of harmonics created by instantaneous on-off switching [131], [132].

Wang and many associates have examined several different kinds of semi-active control laws. Sliding mode control has been studied in depth with multiple semi-active dampers to remove vibrations of a simply supported beam [133], [93], [134]. Wang et. al. have also considered using energy based control laws similar to those described in the next section. They mounted two piezoelectric patches to a cantilever beam near the fixed support and used one to disturb the beam while using the other to damp out disturbances. The piezoelectric damping out disturbances was connected to a shunt circuit with a variable inductor and variable resistor. An energy based control law was created to vary the resistance, inductance and the rate of change of the inductance in the shunt circuit. The system was simulated and disturbances to the beam were attenuated [105].

Almost no results were found on semi-active control where both stiffness and damping are varied. Kidner and Brennan used a fuzzy controller to vary both stiffness and damping of a vibration absorber, allowing both improved performance and tuning of the absorber [135]. Kimbrough discusses bilinear systems and develops a method for controlling stiffness, damping or both. The method results in a nonlinear control system and was applied to variable damping suspension systems for automobiles [136]. Jalili explored a combined semi-active/active combination where the semi-active system is tuned, the active system is changed adaptively, or both systems are changed together [137]. Finally, Jalili has also considered semi-active control for vibration isolation for a SDOF system [3]. He reviews the possibility of tuning a vibration isolation system by varying the natural frequency of a system [138].

Minimizing Energy Change through Variable Stiffness. Vibrations in a structure can be damped out by varying stiffness in the absence of damping and has been developed for suppression problems. Leitmann formulates a simple though not necessarily optimal on-off control law considering both variable damping and variable stiffness for the SDOF suppression problem and finds that setting damping as high as possible removes the most energy from the system [77]. This variable stiffness control law has also been considered

by others, and is briefly discussed, though this control law is not necessarily an optimal law [78], [139]. Rearranging and multiplying Equation 2.13 through by $\dot{x}$ and then making use of Equations 2.26 and 2.55, the change in energy, the rate of work, or the power of the system is found by taking

$$\dot{E}\left(u_c, u_k\right) = m\ddot{x}\dot{x} = -c\left(u_c\right)\dot{x}^2 - k\left(u_k\right)x\dot{x} + Q\dot{x}. \tag{2.61}$$

To make $\dot{E}\left(u_c, u_k\right)$ as negative as possible, it is clear that $c\left(u_c\right)$ should be maximized $\left(c\left(u_c\right) = c_{\max}\right)$ and

$$k\left(u_k\right) = \begin{cases} k\left(-1\right) = k_{\min} \text{ if } x\dot{x} < 0 \\ k\left(1\right) = k_{\max} \text{ if } x\dot{x} > 0 \end{cases} \tag{2.62}$$

where $k_{\max}$ is the maximum stiffness the variable stiffness device can create while $k_{\min}$ is the lowest stiffness the variable stiffness device can create. The energy of the system can be found by integrating $\dot{E}\left(u_c, u_k\right)$ over time resulting in

$$E\left(u_c, u_k\right) = \frac{mx^2}{2} = -\frac{k\left(u_k\right)x^2}{2} + \int_0^t \left(-c\left(u_c\right)\dot{x}^2 + Q\dot{x}\right) d\tau. \tag{2.63}$$

Hence, $E\left(u_c, u_k\right)$ represents the kinetic energy of the system due to the motion of the mass.

Douay and Hagood developed optimal control laws for the variable stiffness problem with no damping. They conclude the optimal control delays switching time, having the effect of increasing equivalent natural frequency while decreasing equivalent damping ratio of the system. The control law increases energy dissipation more than the simple control law. An explicit form for the control law is not developed, but is shown graphically from numerical simulation [139].

Kobs and Sun developed optimal control laws for the variable stiffness problem also, but realized that real systems cannot switch instantly, as assumed by on-off type control laws. They created a continuous control law that accounts for both tuning range and rate of change for a variable stiffness device. They showed the continuous control law dissipated less energy than a on-off control law, but conclude a continuous control law is more representative of reality [140].

Crespo and Sun also developed optimal control laws for both the variable stiffness problem and the variable stiffness problem with constant damping. They used a numerical method called simple cell mapping to develop solutions to these problems. Their method allowed them to graphically present an optimal on-off control law of the form

$$u_k = sgn\left[\left(\lambda_1 x + \dot{x}\right)\left(\lambda_2 \dot{x} + x\right)\right], \tag{2.64}$$

where λ_1 and λ_2 are parameters implicitly chosen by their optimization method. This control law seems to have first been proposed by Onoda, who found the optimal settings for λ_1 and λ_2 for a SDOF suppression problem with no viscous damping [141]. Crespo and Sun observe that "analytic" solutions in the form of numerical simulations exist in the literature to the variable stiffness with no damping SDOF problem. They further note that neither analytic nor numeric solutions to the variable stiffness constant damping problem appear in the literature [142], [143].

Minimizing Energy Change through Variable Damping. A review of the literature credits Karnopp et. al. with first discussing the concept of the skyhook damper and the following discussion is derived from their article [80]. Consider a free-free 2 DOF system (see Figure 2.3) with spring constant k and a viscous damper with damping coefficient c isolating the two degrees from each other. The isolator can be described as

$$g\left(x, \dot{x}\right) = c\left(\dot{x}_2 - \dot{x}_1\right) + k\left(x_2 - x_1\right). \tag{2.65}$$

This is a typical passive system with many limitations already discussed in section 2.3. Karnopp et. al. cites linear optimal control theory to conclude that the ideal isolator is

$$g\left(x, \dot{x}\right) = c\dot{x}_2 + k\left(x_2 - x_1\right). \tag{2.66}$$

Physically, to realize this ideal control law, the damper must be connected to an inertial reference. This is impossible for many systems, so the idea of a skyhook damper is to create the same forces a damper connected to an inertial reference would create. This can be accomplished through active control and can be partially created through

semi-active control. The force of a damper F_d will dissipate energy only when

$$F_d \left(\dot{x}_2 - \dot{x}_1 \right) \geq 0. \tag{2.67}$$

The nonlinear control law for the force of the semi-active damper is

$$F_d = c\dot{x}_2, \quad \text{if } \dot{x}_2 \left(\dot{x}_2 - \dot{x}_1 \right) > 0. \tag{2.68}$$

A damper cannot create a negative damping force when

$$F_d \left(\dot{x}_2 - \dot{x}_1 \right) < 0 \tag{2.69}$$

since the damper has no capability to add energy to the system. Active control has this capability. To most closely approximate an active system, the force of the damper is set as low as possible, or ideally,

$$F_d = 0 \quad \text{if } \dot{x}_2 \left(\dot{x}_2 - \dot{x}_1 \right) < 0. \tag{2.70}$$

Karnopp discusses two special cases when $\dot{x}_2 \left(\dot{x}_2 - \dot{x}_1 \right) = 0$. If $\dot{x}_2 = 0$, the $F_d = 0$. When $\left(\dot{x}_2 - \dot{x}_1 \right) = 0$, the semi-active damper can "lock up" the system. These cases happen rarely, and usually for a finite amount of time before the system returns to another condition.

2.7 Some Conclusions on State of the Art

A review of some of the space applications for vibration control technologies shows immense challenges. Some of these challenges are being met today using passive, active, and hybrid control concepts. However, these technologies may not be able to achieve all future challenges identified in their current forms. While many of these technologies are mature, much opportunity for research exists in semi-active control, though it is not clear if these technologies can meet all of the future challenges. The literature shows that smart materials have been and are being developed that make semi-active control concepts

physically viable. Research opportunities exists in the realm of smart materials in creating better analytical models for use in vibration control applications. Much work has been found showing how smart materials can be applied to the vibration absorption problem, and this area is clearly an area rich in research opportunities. It also appears gaps exist in the literature in that limited information was found on semi-active vibration isolation as opposed to vibration absorption where much more exists. Hence, semi-active vibration isolation may have even more opportunities for research than vibration absorption.

A review of semi-active vibration control literature shows semi-active control problems are inherently nonlinear. Several authors have identified the need to gain a better understanding of control schemes using nonlinear control devices [3], [11]. Unfortunately, the nonlinearity makes analysis both difficult and time consuming. Because of the nonlinearity of variable damping and variable stiffness devices, analysis is even more difficult.

In order to begin developing new insights and engineering tools for this challenging field, a model that could be analyzed and provides some insights into how a real system would behave was needed. It was decided to begin where the literature stops by choosing a relatively simple problem, which provides some knowledge of real systems. One such model is Equation 2.13. Since varying damping greatly complicates the analysis and is not as helpful as using constant damping for initial value vibration suppression SDOF problems (see Section 2.4), damping was made constant. Hence, the equation of motion considered is

$$m\ddot{x}(t) + c\dot{x}(t) + \frac{1}{2}\left[(k_1 + k_0) + (k_1 - k_0)\, u(\lambda_1, \lambda_2)\right] x(t) = Q(t) \tag{2.71}$$

where

$$u(\lambda_1, \lambda_2) = sgn\left[(\lambda_1 x + \dot{x})(\lambda_2 \dot{x} + x)\right] \tag{2.72}$$

Understanding Equation 2.71 represents an incremental improvement over the current state of the art since past analysis has considered problems with no damping. Further, while past analysis has made use of the proposed two parameter control, the analysis is somewhat incomplete. In practice, it moves analytic understanding of semi-active control

problems closer to experimental real world research which has been going on over the last decade.

Hence, in Chapter 3, the initial value problem with $Q(t) = 0$ is solved for the first time exactly. An approximate solution linked to the exact solution is then developed and both solutions are used to develop new insights. In Chapter 4, the sinusoidally forced problem is approximated and some new insights are developed. Interestingly, the approximate solutions that were developed in both chapters are linear. Hence, Chapter 5 demonstrates some instances where the linear approximations of Chapters 3 and 4 can be used to gain insights into MDOF problems, which begin to approximate the expected behavior of real space system structures.

3. Initial Value Variable Stiffness with Constant Damping SDOF Problem

3.1 Introduction

An exact and approximate solution to Equation 2.71, an initial value SDOF variable stiffness suppression ordinary nonlinear differential equation (ODE) with constant damping will be developed. Winthrop et. al. recently solved this problem for the case of no viscous damping using a simpler control law than the one that will be used here [144]. Equation 2.71 was selected to be approximately representative of a true variable stiffness system which can be analyzed. The purpose of this analysis is to 1) determine the optimal control of the system using a general on-off control law, 2) determine system stability, and 3) develop an approximate explicit solution to the exact implicit solution to develop insight into what variable stiffness contributes. Equation 2.71 is immediately nondimensionalized since nondimesionalizing the ODE greatly simplifies it and allows generalization of the results to any dimensional problem.

Next, the nondimensional second order ODE is transformed to two first order ODE's which are related to the phase angle and amplitude of a trajectory in the phase plane. The first order ODE's are simpler to solve than the untransformed second order ODE. The ODE's were solved implicitly, treating time as though it was a dependent variable, rather than an independent variable. In the process, different types of behavior for the system are identified and the exact switching times for the system are found analytically.

The resulting solution to the two ODE's was complicated and resulted in a transcendental equation that cannot be solved explicitly. Hence an explicit approximate solution was developed to better explore system behavior. The explicit solution has the same form as a linear viscously damped oscillator, so equivalent damping ratio, natural frequency, and damped natural frequency was found. Using the approximate and exact solutions, an expression for guaranteed system stability and an approximate optimal control of the system were found. Afterward, examples showing how the system behaves are provided. Following the examples, the energy use of the stiffness device is explored. The analysis is concluded by identifying design metrics that can be used to understand variable stiffness devices.

3.2 Nondimensional Equations

From the literature [77], the initial value variable stiffness vibration suppression problem

$$m^*\ddot{x}^* + c^*\dot{x}^* + \frac{1}{2}\left[(k_1^* + k_0^*) + (k_1^* - k_0^*)\,u\right]x^* = 0, \tag{3.1}$$

was selected for study where m is the mass of the system, c is the damping coefficient, k_0 is the smallest value the stiffness can be, k_1 is the largest value stiffness can be, x is a reference displacement, and u is a control law to be specified later such that $-1 \leq u \leq 1$. The "*" superscript designates a variable as a dimensional variable, while variables without the "*" superscript are nondimensional variables. The initial conditions considered herein are either for initial displacement or initial velocity defined as

$$x^*(0) = x_0^*, \quad \dot{x}^*(0) = 0 \tag{3.2}$$

or

$$x^*(0) = 0, \quad \dot{x}^*(0) = \dot{x}_0^*, \tag{3.3}$$

respectively. Equation 3.1 can be nondimensionalized by defining the uncontrolled natural frequency ($u = 0$)

$$\omega_0^* = \sqrt{\frac{k_0^* + k_1^*}{2m^*}}, \tag{3.4}$$

and by defining a reference length L^*, such that the nonzero initial condition is unity. For the initial conditions of Equation 3.2 use

$$L^* = x_0^*, \tag{3.5}$$

while for the initial conditions of Equation 3.3 use

$$L^* = \frac{\dot{x}_0^*}{\omega_0^*}. \tag{3.6}$$

Nondimensional time can be scaled to be

$$t = t^*\omega_0^* \tag{3.7}$$

and the displacement can be scaled to be

$$x = \frac{x^*}{L^*}. \tag{3.8}$$

When $L^* = 0$, Equation 3.8 becomes invalid. However, $L^* = 0$ implies no initial disturbance to the system, resulting in the trivial solution for Equation 3.1. Equation 3.1 can then be rewritten in nondimensional form as

$$\ddot{x} + 2\mu\dot{x} + (1 + \varepsilon u)\, x = 0, \tag{3.9}$$

where

$$\mu = \frac{c^*}{\sqrt{2m^* \left(k_0^* + k_1^*\right)}} \tag{3.10}$$

and

$$\varepsilon = \frac{k_1^* - k_0^*}{k_1^* + k_0^*} \tag{3.11}$$

Note that $0 \leq \varepsilon < 1$. Further, μ will be restricted such that $0 \leq \mu < 1$. This was done to allow selection of an oscillatory solution form, though it restricts the solution range of validity. When $\varepsilon = 0$ and $\mu < 1$ Equation 3.9 is an underdamped system with an oscillatory solution.[71]

A two parameter on-off control law is used given by

$$u\left(x, \dot{x}\right) = sgn\left[\left(\lambda_1 x + \dot{x}\right)\left(\lambda_2 \dot{x} + x\right)\right] \tag{3.12}$$

where

$$sgn\left(z\right) = \begin{cases} 1 & \text{if } z > 0 \\ 0 & \text{if } z = 0 \\ -1 & \text{if } z < 0 \end{cases}, \tag{3.13}$$

and λ_1 and λ_2 are real valued design parameters of the controller. In the special case when $\lambda_1 = \lambda_2 = 0$, Equation 3.12 becomes the simple though not necessarily optimal control law discussed by several authors [77], [78], [139]. With a proper transformation and when $c^* = 0$, Equation 3.1 can be used to model a SDOF variable stiffness system

with a piezoelectric actuator using a short circuit/open circuit switching device, modeled by Kurdila et. al. The SDOF piezoelectric model used is

$$m^*\ddot{x}^* + \left(k^{sc^*} + \frac{\left(k^{sc^*} d_{33}^*\right)^2}{C_P^{S^*}} (1 - \Delta) \right) x^* = 0 \tag{3.14}$$

where k^{sc^*} is the short circuit stiffness of the piezoelectric, d_{33}^* is the piezoelectric constant, $C_P^{S^*}$ is the constant strain piezoceramic capacitance, m^* is a vibrating mass and Δ is either 0 or 1 [123]. Letting

$$k_0^* = k^{sc^*} \tag{3.15}$$

and

$$k_1^* = k^{sc^*} + \frac{\left(k^{sc^*} d_{33}^*\right)^2}{C_P^{S^*}} \tag{3.16}$$

transforms 3.14 to Equation 3.1.

Equation 3.12 was proposed by Onoda et. al. [141] and is implied by Crespo and Sun [142] from an applied optimal control method. This control law assumes instantaneous changes in stiffness, which is not realistic [140]. However, when the variable stiffness device time constant is much shorter than the time constant of the actual system, Equation 3.12 is expected to be a reasonable approximation of reality. One way to verify this is to measure the switching time of a variable stiffness device and compare it to the reciprocal of ω_0^* calculated by Equation 3.4. In section 3.13, a more accurate system time constant will be derived that can be used to validate the instantaneous change in stiffness control law. Equation 3.12 was chosen because it is general enough to consider nearly any switching policy and makes use of physical quantities that are easy to measure in real physical systems.

3.3 Transformed Equations by Method of Variation of Parameters

Equations 3.9 and 3.12 can be transformed into two first order differential equations using the method of variation of parameters as shown in Appendix B. The solution to Equation 3.9 is of the form

$$x = ae^{-\mu t} \cos \phi \tag{3.17}$$

and the velocity is of the form

$$\dot{x} = -ae^{-\mu t}\left[\mu\cos\phi + \psi\sin\phi\right] = -x\left[\mu + \psi\tan\phi\right] \tag{3.18}$$

where a and ϕ are functions of time. Using Equations 3.17 and 3.18, the control law can be transformed into

$$u\left(\phi\right) = sgn\left(\left[\lambda_1 - \left(\mu + \psi\tan\phi\right)\right]\left[1 - \lambda_2\left(\mu + \psi\tan\phi\right)\right]\right). \tag{3.19}$$

where

$$\psi = \sqrt{1-\mu^2}. \tag{3.20}$$

The functions a and ϕ satisfy the differential equations

$$\dot{\phi} = \frac{\psi u}{2\delta}\left[J\left(\phi\right) + \cos\left(2\phi\right)\right] = \psi\left(\frac{u}{\delta}\cos^2\phi + 1\right) \tag{3.21}$$

and

$$\frac{\dot{a}}{a} = \frac{\psi u}{2\delta}\sin\left(2\phi\right) \tag{3.22}$$

where

$$J\left(u\left(\phi\right)\right) = J\left(\phi\right) = \frac{2\delta}{u} + 1 \tag{3.23}$$

and

$$\delta = \frac{\psi^2}{\varepsilon}. \tag{3.24}$$

Because $0 \leq \mu < 1$, $0 < \psi \leq 1$ implies $\delta > 0$. For the initial displacement problem, the initial conditions are

$$\phi_0 = -\tan^{-1}\frac{\mu}{\psi},\ a_0 = \frac{1}{\psi}. \tag{3.25}$$

For the initial velocity problem, the initial conditions are

$$\phi_0 = -\frac{\pi}{2},\ a_0 = \frac{1}{\psi}. \tag{3.26}$$

Both versions of the initial conditions are derived in Appendix B. Note that $\phi_0 \neq 0$ in the initial displacement problem since $\psi \neq 0$. In Equation 3.24 $\varepsilon \to 0$ implies $\delta \to \infty$, and Equations 3.21 and 3.22 simplify to $\dot{\phi} = \psi$ and $\frac{\dot{a}}{a} = 0$. These equations have solutions $\phi = \psi t + \phi_0$ and $a = a_0$, which when substituted into Equation 3.17 yields the simple linear underdamped oscillator

$$x = a_0 e^{-\mu t} \cos(\psi t + \phi_0). \tag{3.27}$$

Hence, ψ represents the damped natural frequency of the uncontrolled system ($u = 0$). The parameters J and δ have no physical meaning when $\varepsilon = 0$. However, when $\varepsilon > 0$, these parameters will later be shown to define if the system is underdamped, critically damped, or overdamped in the classical sense.

Another way to interpret Equations 3.17 and 3.18 is to put them in polar form as

$$\frac{\dot{x}}{x} = -[\mu + \psi \tan\phi] = \tan\Phi \tag{3.28}$$

and

$$r = \frac{a e^{-\mu t} \psi \sqrt{1 + \tan^2\Phi}}{\sqrt{1 + 2\mu \tan\Phi + \tan^2\Phi}} \tag{3.29}$$

where Φ is an angle of rotation of a trajectory in phase space or phase angle while r is the distance from the origin of a trajectory in phase space. When $\mu = 0$, Equations 3.28 and 3.29 simplify to the standard polar coordinates transformation. Equation 3.28 is an affine transformation for phase. Therefore, both ϕ and Φ will be called the phase of the system.

3.4 Solution Strategy

Equations 3.21 and 3.22 will be solved implicitly using the method of separation of variables. Equations 3.21 and 3.22 can be rewritten as

$$dt = \frac{2\delta d\phi}{\psi u(\phi)\left[J(\phi) + \cos(2\phi)\right]} \tag{3.30}$$

and

$$\frac{da}{a} = \frac{\psi u(\phi)}{2\delta} \sin(2\phi)\, dt = \frac{\sin(2\phi)\, d\phi}{J(\phi) + \cos(2\phi)}. \tag{3.31}$$

Next, it is tempting to immediately integrate both equations as

$$\int_0^t d\tau = \frac{2\delta}{\psi} \int_{\phi_0}^{\phi} \frac{d\Phi}{u(\Phi)\left[J(\Phi) + \cos(2\Phi)\right]} \tag{3.32}$$

and

$$\int_{a_0}^{a} \frac{dA}{A} = \int_{\phi_0}^{\phi} \frac{\sin(2\Phi)\, d\Phi}{J(\Phi) + \cos(2\Phi)} \tag{3.33}$$

where A, Φ, and τ are dummy variables of integration. Unfortunately, the integrals on the right hand side of Equations 3.32 and 3.33 can have discontinuous integrands and also have different solution forms depending on the values of J. To evaluate Equations 3.32 and 3.33, the right hand side must be broken up into sums of integrals over the intervals of continuity and the effect of varying J (Equation 3.23) must be understood.

3.5 Bifurcations and Solution Region Definitions

Applying the control law of Equation 3.12 in Equation 3.9 demonstrates a number of behavioral changes or bifurcations by varying the parameters ε, μ, λ_1, and λ_2. These changes result in rich behavior for Equation 3.9, which is common in nonlinear equations. This behavior creates different solution regions which can be identified in the ε and μ plane and in the λ_1 and λ_2 plane. The next sections will derive and identify these solution regions.

Bifurcations due to Varying Stiffness Using an On-Off Control Law. Equations 3.32 and 3.33 have two different forms due to how J (defined by Equation 3.23) depending on $u = \pm 1$. This bifurcation is a direct result of varying the stiffness of the system using the on-off control law of Equation 3.19. Since $J(\phi)$ is constant for a particular u, two new constants will be defined. When $u = +1$, define

$$J(\phi) = J_p \triangleq 1 + 2\delta \tag{3.34}$$

and when $u = -1$, define

$$J(\phi) = J_m \triangleq 1 - 2\delta. \tag{3.35}$$

The subscript p corresponds to $u = 1$ and can be thought of as an abbreviation for "plus." Similarly, the subscript m corresponds to $u = -1$ and can be thought of as an abbreviation for "minus."

Phase Switching Angles. Next, it must be determined when a switching events occur, in terms of the phase ϕ. The phase ϕ will switch to a different function whenever $u = 0$. Applying Equation 3.19, switching occurs when

$$\tan\phi = \frac{\lambda_1 - \mu}{\psi} \tag{3.36}$$

or

$$\tan\phi = \frac{1 - \lambda_2\mu}{\lambda_2\psi}. \tag{3.37}$$

For convenience, the angles

$$\phi_1 = \tan^{-1}\left(\frac{\lambda_1 - \mu}{\psi}\right) \tag{3.38}$$

and

$$\phi_2 = \tan^{-1}\left(\frac{1 - \lambda_2\mu}{\lambda_2\psi}\right) \tag{3.39}$$

are defined where ϕ_1 and ϕ_2 are the principle values of the $\tan^{-1}$ function (i.e. $-\frac{\pi}{2} < \phi_1, \phi_2 < \frac{\pi}{2}$). Then the behavior of the phase angle ϕ will change when

$$\phi = \phi_1, \phi_1 + \pi, \phi_1 + 2\pi, ... \tag{3.40}$$

or

$$\phi = \phi_2, \phi_2 + \pi, \phi_2 + 2\pi, ... \tag{3.41}$$

The Control Law Parameters λ_1 and λ_2. The parameters λ_1 and λ_2 can be physically interpreted using Equation 3.12 in phase space as shown in Figure 3.1. When a trajectory of the system is in the shaded area, $u = 1$. Otherwise, $u = -1$. The settings for λ_1 and λ_2 change where control switching occurs, which changes the system performance

(as will be shown). The phase angles Φ_1 and Φ_2 can be calculated using Equations 3.28, 3.38, and 3.39.

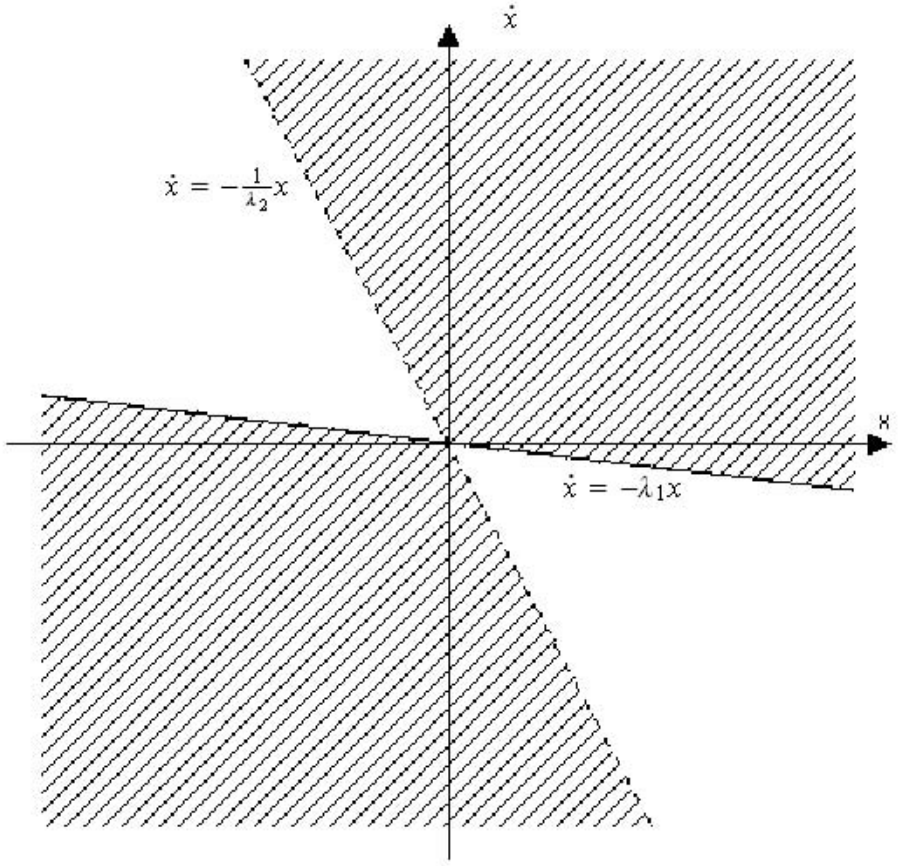

Figure 3.1 u in Phase Space (Shaded area $u = 1$, Unshaded area $u = -1$)

Depending on the values of λ_1 and λ_2, and considering Equations 3.38 and 3.39, three cases arise. Either $\phi_1 < \phi_2$, $\phi_1 = \phi_2$, or $\phi_1 > \phi_2$. The case where $\phi_1 = \phi_2$ implies

$$\lambda_1 \lambda_2 = 1, \tag{3.42}$$

making the two switching lines of Figure 3.1 collinear. The result is no switching can occur. This is easily seen by substituting Equation 3.42 into Equation 3.12 resulting in:

$$u(x, \dot{x}) = sgn\left[\lambda_2 (\lambda_2 \dot{x} + x)^2\right] = sgn(\lambda_2). \tag{3.43}$$

This case is not considered further.

The other two cases present possible switching control laws for Equation 3.12. When $\phi_1 < \phi_2$ or $\lambda_1 < \frac{1}{\lambda_2}$, Equations 3.40 and 3.41 can be combined in order of smallest to highest switching angles as

$$\phi = \phi_1, \phi_2, \phi_1 + \pi, \phi_2 + \pi, ... \tag{3.44}$$

Similarly, when $\phi_1 > \phi_2$ or $\lambda_1 > \frac{1}{\lambda_2}$ order of switching angles becomes

$$\phi = \phi_2, \phi_1, \phi_2 + \pi, \phi_1 + \pi, ... \tag{3.45}$$

Figure 3.2 shows settings for λ_1 and λ_2 where this bifurcation in the solutions occurs. The unshaded areas represent the regions where Equation 3.44 applies while the shaded areas represent the regions where Equation 3.45 applies. It is immediately apparent from Equations 3.44 and 3.45 that ϕ is periodic and has period π.

Continuous Intervals for ϕ and a Bifurcation in λ_2. Equation 3.44 and 3.45 define phase angles where a switch in u occurs. Between these switching angles are continuous intervals where no switching occurs and $u = \pm 1$. In this section, the settings for λ_1 and λ_2 for a particular value of u in a continuous interval are determined. In the process, a bifurcation due to the parameter λ_2 is identified.

When $\lambda_2 \neq 0$ Equation 3.19 can be rewritten as

$$u(\phi) = sgn\left(\frac{\lambda_1 - \mu}{\psi} - \tan\phi\right) sgn(\lambda_2)\, sgn\left(\frac{1 - \lambda_2\mu}{\lambda_2\psi} - \tan\phi\right) \tag{3.46}$$

or recalling Equations 3.38 and 3.39,

$$u(\phi) = sgn(\lambda_2)\, sgn(\tan\phi_1 - \tan\phi)\, sgn(\tan\phi_2 - \tan\phi). \tag{3.47}$$

When $\lambda_2 = 0$,

$$u(\phi) = sgn(\tan\phi_1 - \tan\phi). \tag{3.48}$$

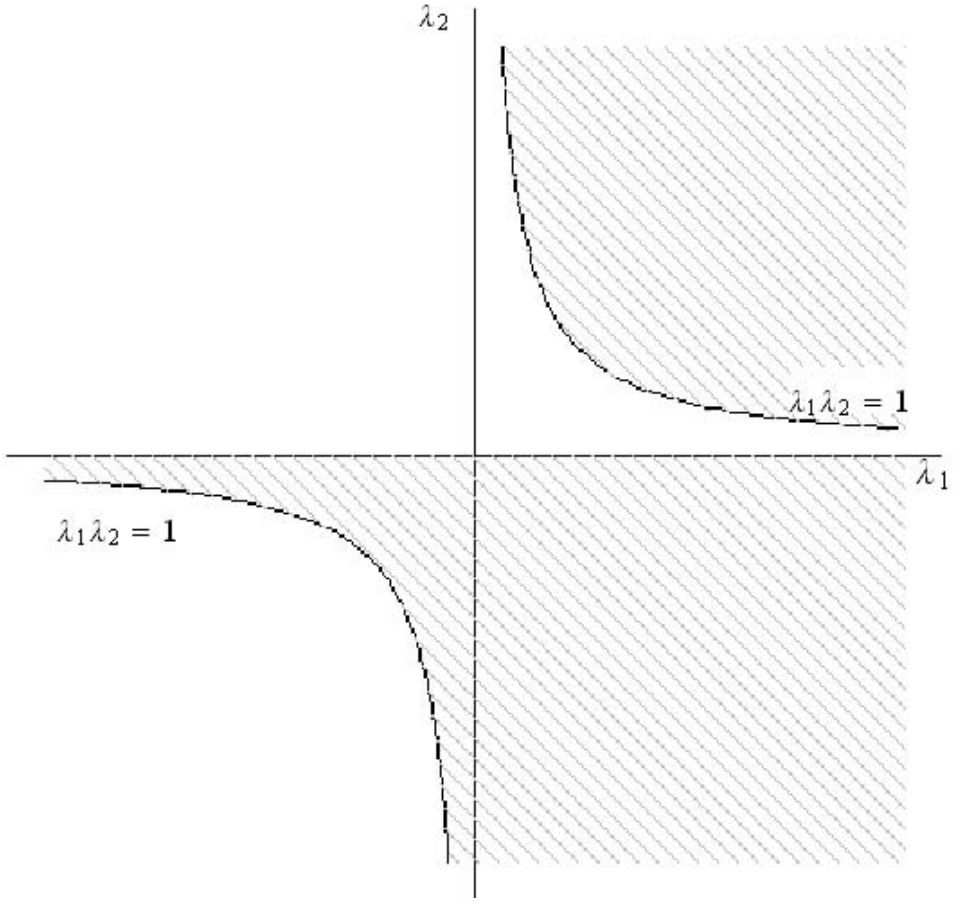

Figure 3.2 Bifurcation due to Varying $\phi_1(\lambda_1)$ and $\phi_2(\lambda_2)$. ($\lambda_1 < \frac{1}{\lambda_2}$ Unshaded Area, $\lambda_1 > \frac{1}{\lambda_2}$ Shaded Area)

A bifurcation point exists at $\lambda_2 = 0$ because changing $\lambda_2 < 0$ or $\lambda_2 > 0$ immediately changes the sign of $u(\phi)$. Suppose $\phi_1 < \phi_2$ and $\phi \in (\phi_1 + n\pi, \phi_2 + n\pi)$, where $n = 0, 1, 2, ...$ When $\lambda_2 \geq 0$, $u = -1$. When $\lambda_2 < 0$, $u = 1$. Now, suppose $\phi_1 > \phi_2$ and $\phi \in (\phi_2 + n\pi, \phi_1 + n\pi)$. When $\lambda_2 > 0$, $u = -1$. When $\lambda_2 < 0$, $u = 1$. Notice it is impossible for $\lambda_2 = 0$ and $\phi_1 > \phi_2$ since it requires $\lambda_1 \to \infty$, which will at best, make $\phi_1 = \phi_2$. Besides being unrealistic to implement with real hardware, $\phi_1 = \phi_2$ implies $\lambda_1\lambda_2 = 1$, which creates a nonswitching variable stiffness system. As previously discussed, the solution to the nonswitching variable stiffness system is a simple viscously damped linear oscillator, which is already well understood.

Bifurcations due to Damping and Variable Stiffness Strength: Underdamped, Critically Damped, or Overdamped. For ease of analysis, the properties of J_m^2 and J_p^2 are examined in preparation for solving Equation 3.21. These parameters mathematically define what the solution form will be for Equation 3.21. By examining the original differential equation of the system (Equation 3.9) for a value of u, it is possible to label in a classical sense whether the system is underdamped, critically damped, or overdamped. Correlating physical insight with the solution form for Equation 3.21 defines what type of system is being analyzed.

When $u = 1$, Equation 3.34 is valid and it is clear that $J_p > 1$ since $\delta > 0$. The characteristic values of Equation 3.9 are $s = -\mu \pm i\sqrt{1 + \varepsilon - \mu^2}$, which are always oscillatory for $0 < \varepsilon < 1$ and $0 \leq \mu < 1$. Therefore, the system is always underdamped when $u = 1$ and no bifurcation exists.

When $u = -1$, Equation 3.35 is valid and it is possible for $J_m^2 < 1$, $J_m^2 = 1$, and $J_m^2 > 1$. Depending on the value for J_m, the system will either be underdamped, critically damped, or overdamped. Table 3.1 summarizes how J_m varies for settings of μ and ε. The characteristic value of Equation 3.9 was correlated with the possible values for J_m to develop physical meaning. Figure 3.3 graphically depicts the three different regions of Table 3.1 where

$$\mu_{crit} = \sqrt{1 - \varepsilon} \tag{3.49}$$

is defined as the transition between regions and defines when the system is critically damped. When $\varepsilon = 0$, the system is underdamped for $\mu < 1$. This is the behavior of a simple linear oscillator with viscous damping. When $\varepsilon = 1$, the system can never be underdamped.

Since the system switches between $u = \pm 1$, it is possible for it to switch between two underdamped systems, an underdamped and critically damped system, or an underdamped and an overdamped system. For convenience, a system that switches between an underdamped and a critically damped system will simply be called a critically damped system. Similarly, one that switches between underdamped and overdamped will be called an overdamped system. With these definitions, it will be seen later that it is possible to

Table 3.1 Variable Stiffness Constant Damping Problem Conditions for Underdamped, Critically Damped, or Overdamped System

J_m^2 **Value**	**Damping/Stiffness Relation**	**Eigenvalues**	**System Property**
$J_m^2 < 1$	$\mu_{crit} < \mu < 1$	$s = -\mu \pm \sqrt{\mu^2 - \mu_{crit}^2}$	Overdamped
$J_m^2 = 1$	$\mu = \mu_{crit}$	$s = -\mu$	Critically Damped
$J_m^2 > 1$	$0 \leq \mu < \mu_{crit}$	$s = -\mu \pm i\sqrt{\mu_{crit}^2 - \mu^2}$	Underdamped

have an oscillatory response for underdamped, critically damped, and overdamped systems, with the proper settings of the control law u.

Solution Forms for Phase and Amplitude. Equations 3.32 and 3.33 are rewritten as

$$\int_{t_L}^{t_U} d\tau = t_U - t_L = \frac{2\delta}{\psi} \int_{\phi_L}^{\phi_U} \frac{d\Phi}{u\left(J + \cos\left(2\Phi\right)\right)} \tag{3.50}$$

and

$$\int_{a_L}^{a_U} \frac{dA}{A} = \ln\left(a_u\right) - \ln\left(a_L\right) = \int_{\phi_L}^{\phi_U} \frac{\sin\left(2\Phi\right) d\Phi}{J + \cos\left(2\Phi\right)} \tag{3.51}$$

where the intervals (ϕ_U, ϕ_L), (t_U, t_L), and (a_U, a_L) are continuous intervals. From the previous discussion on bifurcations, the intervals of integration and the solution to Equations 3.50 and 3.51 varies by changing λ_1, λ_2, μ, and ε. The solution to 3.21 and 3.22 will be a summation of these continuous intervals identified by the phase switching angles. The solutions to all of the integrals in this section were found using standard integral tables.[145] To simplify writing the exact solution, the actual bounds of integration will be considered later. Only the solution form is studied here.

Solution Forms for Phase. The right hand side of Equation 3.50 has four solutions, depending on whether $u = \pm 1$ and the settings for μ and ε. The following solutions make use of Equations 3.34 and 3.35. Additionally, the constants

$$\sigma_p = \sqrt{\psi^2 + \varepsilon} \tag{3.52}$$

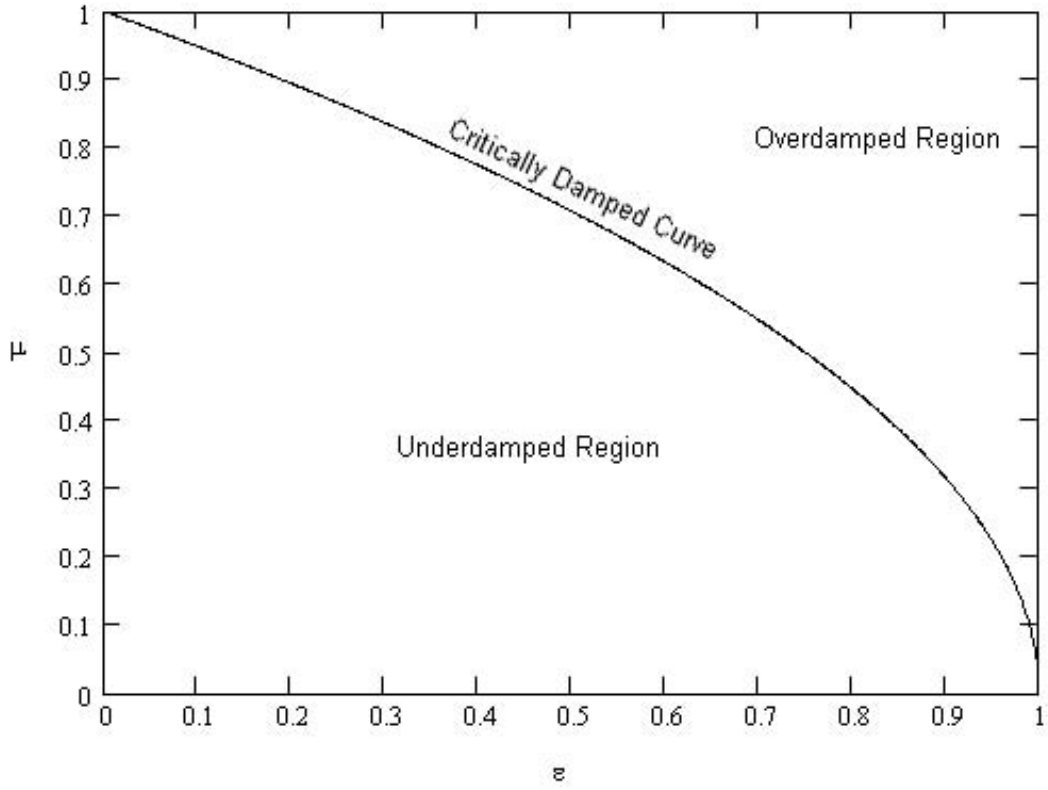

Figure 3.3 Overdamped and Underdamped Regions

and

$$\sigma_m = \begin{cases} \sqrt{\psi^2 - \varepsilon} & \text{if} \quad 0 \le \mu < \mu_{crit} \\ 0 & \text{if} \quad \mu = \mu_{crit} \\ \sqrt{\varepsilon - \psi^2} & \text{if} \quad \mu_{crit} < \mu < 1 \end{cases} = \sqrt{\left|\psi^2 - \varepsilon\right|} \tag{3.53}$$

are defined to simplify the solutions. When $u = 1$, the solution is

$$\Gamma_{\phi_p}(\phi_L, \phi_U) = \frac{2\delta}{\psi} \int_{\phi_L}^{\phi_U} \frac{d\Phi}{J_p + \cos 2\Phi} = \frac{1}{\sigma_p} \left[\tan^{-1}\left(\frac{\psi}{\sigma_p} \tan \phi_U \right) - \tan^{-1}\left(\frac{\psi}{\sigma_p} \tan \phi_L \right) \right]. \tag{3.54}$$

When $u = -1$, the solution is

$$\Gamma_{\phi_m}(\phi_L, \phi_U) = \frac{2\delta}{\psi} \int_{\phi_L}^{\phi_U} \frac{d\Phi}{J_m + \cos 2\Phi} \tag{3.55a}$$

$$= \begin{cases} \frac{1}{\sigma_m} \left[\begin{array}{l} \tan^{-1}\left(\frac{\psi}{\sigma_m} \tan\phi_U\right) \\ -\tan^{-1}\left(\frac{\psi}{\sigma_m} \tan\phi_L\right) \end{array} \right] & \text{if} \quad 0 \le \mu < \mu_{crit} \\ -\frac{1}{\psi}\left[\cot\phi_U - \cot\phi_L\right] & \text{if} \quad \mu = \mu_{crit} \\ -\frac{1}{2\sigma_m} \ln\left[\left(\frac{\psi\tan\phi_U + \sigma_m}{\psi\tan\phi_U - \sigma_m}\right)\left(\frac{\psi\tan\phi_L - \sigma_m}{\psi\tan\phi_L + \sigma_m}\right)\right] & \text{if} \quad \mu_{crit} < \mu < 1, \end{cases} \tag{3.55b}$$

which accounts for the three possible damping conditions of Table 3.1 when $u = -1$. Note that all forms of Equations 3.54 and 3.55b use the tangent function which has the identity $\tan(\phi) = \tan(\phi + n\pi)$ where $n = 0, 1, 2, \ldots$. This result is used later to simplify answers. Additionally, in using Equations 3.54 and 3.55b, care must be used when calculating the arctangent function to make sure the value returned is in the correct quadrant. For Equations 3.54 and 3.55b to evaluate correctly, they must always return a nonnegative real value, to be physically realistic. One way to force this to happen is to add $\frac{\pi}{\sigma_p}$ or $\frac{\pi}{\sigma_m}$ to the results of Equations 3.54 and 3.55b, respectively, whenever the function evaluates to something less than 0. This is only done for the functions that use the arctangent function.

Solution Forms for Amplitude. The right hand side of Equation 3.51 has two solutions, depending only on $u = \pm 1$. The following solutions again make use of Equations 3.34 and 3.35. When $u = 1$, the solution is

$$\Gamma_{a_p}(\phi_L, \phi_U) = \int_{\phi_L}^{\phi_U} \frac{\sin(2\Phi)\, d\Phi}{J_p + \cos(2\Phi)} = \ln\sqrt{\frac{\delta + \cos^2\phi_L}{\delta + \cos^2\phi_U}} = \ln\sqrt{\frac{\psi^2 + \varepsilon\cos^2\phi_L}{\psi^2 + \varepsilon\cos^2\phi_U}}. \tag{3.56}$$

When $u = -1$, the damping conditions of Table 3.1 have no effect on the solution. The solution is

$$\Gamma_{a_m}(\phi_L, \phi_U) = \int_{\phi_L}^{\phi_U} \frac{\sin(2\Phi)\, d\Phi}{J_m + \cos(2\Phi)} = \ln\sqrt{\frac{\delta - \cos^2\phi_L}{\delta - \cos^2\phi_U}} = \ln\sqrt{\frac{\psi^2 - \varepsilon\cos^2\phi_L}{\psi^2 - \varepsilon\cos^2\phi_U}}. \tag{3.57}$$

Considering Equations 3.56 and 3.57, Equation 3.51 can be simplified since it is written in terms of the natural log function on both sides of the equation. Depending on whether $u = \pm 1$, Equations 3.51 , 3.56, and 3.57 can be rewritten as

$$\frac{a_U}{a_L} = a_p\left(\phi_L, \phi_U\right) = \sqrt{\frac{\delta + \cos^2\phi_L}{\delta + \cos^2\phi_U}} = \sqrt{\frac{\psi^2 + \varepsilon\cos^2\phi_L}{\psi^2 + \varepsilon\cos^2\phi_U}} \tag{3.58}$$

or

$$\frac{a_U}{a_L} = a_m\left(\phi_L, \phi_U\right) = \sqrt{\frac{\delta - \cos^2\phi_L}{\delta - \cos^2\phi_U}} = \sqrt{\frac{\psi^2 - \varepsilon\cos^2\phi_L}{\psi^2 - \varepsilon\cos^2\phi_U}}. \tag{3.59}$$

Both Equations 3.58 and 3.59 use the square of the cosine function which has the identity $\cos^2(\phi + n\pi) = \cos^2(\phi)$ for $n = 0, 1, 2, \ldots$. This result is used later to simplify answers.

3.6 The Range of the Phase Angle

The range of ϕ can be found by studying Equation 3.21. The purpose of understanding the phase is to determine when ϕ increases without bound or when it is bounded by a constant. This is important to allow better understanding of the solutions of Equation 3.21. When ϕ is bounded, the control law of the system (Equation 3.19) may not switch at all. Without switching, the system behaves like a simple damped linear oscillator, which defeats the purpose of using variable stiffness. Hence, it is important to understand where no switching occurs, to properly design a control law.

Critical or Stationary Points. When $\dot{\phi} = 0$ in Equation 3.21, ϕ becomes constant and the control law is no longer switching. Hence, ϕ_{crit} will be defined such that $\dot{\phi} = 0$. From Equation 3.21, ϕ_{crit} exists only when $u = -1$ and implies

$$\cos^2\phi_{crit} = \delta \tag{3.60}$$

or

$$\tan\phi_{crit} = \pm\frac{\sigma_m}{\psi}, \tag{3.61}$$

where only the principle values of the tangent function are used to define ϕ_{crit}. Notice $-\frac{\pi}{2} < \phi_{crit} < \frac{\pi}{2}$ and $\phi_{crit} \neq \pm\frac{\pi}{2}$ since $\delta > 0$. The only time ϕ_{crit} can exist is when

$0 < \delta \leq 1$. It was previously shown that when $0 < \delta < 1$, the system is overdamped and when $\delta = 1$, the system is critically damped. Since ϕ_{crit} does not exist when $\delta > 1$, settings making the system underdamped implies Equation 3.19 will always switch at regular intervals.

Critical Points for Phase Angle. Next, it will be proven that when ϕ_{crit} exists, $\phi_0 < \phi_{crit}$. Recall that ϕ_0 is the phase of the system at time $t = 0$ and is defined by Equation 3.25 or 3.26. To prove $\phi_0 < \phi_{crit}$, the following Lemma is required.

Lemma 1 *When ϕ_{crit} exists, $\mu - \sigma_m > 0$.*

Proof. By definition, $0 \leq \varepsilon < 1$ which implies

$$1 - \varepsilon > 0. \tag{3.62}$$

Adding and subtracting μ^2 on the left side of Equation 3.62 and recalling Equations 3.20 and 3.53 results in

$$\mu^2 - \varepsilon + 1 - \mu^2 = \mu^2 - \left(\varepsilon - \psi^2\right) = \mu^2 - \sigma_m^2 > 0 \tag{3.63}$$

Note that since ϕ_{crit} exists, then by Equation 3.53, $\sigma_m^2 = 0$ when the system is critically damped and $\sigma_m^2 = \varepsilon - \psi^2$ when the system is overdamped. Factoring Equation 3.63 results in

$$(\mu + \sigma_m)(\mu - \sigma_m) > 0. \tag{3.64}$$

Since $\mu + \sigma_m > 0$, $\mu - \sigma_m > 0$. ■

Now it can be proven $\phi_0 < \phi_{crit}$. The proof is given for the initial displacement problem and the initial velocity problem.

Theorem 2 *When ϕ_{crit} exists, $\phi_0 < \phi_{crit}$.*

Proof. Because $\mu \pm \sigma_m > 0$ when ϕ_{crit} exists,

$$-\frac{\mu}{\psi} < \pm\frac{\sigma_m}{\psi} \tag{3.65}$$

which implies

$$-\frac{\pi}{2} < -\tan^{-1}\frac{\mu}{\psi} < \pm\tan^{-1}\frac{\sigma_m}{\psi} = \phi_{crit} \tag{3.66}$$

Note that $-\frac{\pi}{2} < -\tan^{-1}\frac{\mu}{\psi}$ is true because $0 < \psi \leq 1$ and $\mu < 1$. The two terms on the left hand side of Equation 3.66 are definitions of ϕ_0 for the initial velocity and initial displacement problem (Equations 3.26 and 3.25, respectively). Then $\phi_0 < \phi_{crit}$. ■

Effects of Control Law Tuning.

Boundedness and Increasing/Decreasing Criteria for Phase. Substituting ϕ_{crit} into Equation 3.19 when $u = -1$ implies

$$[\lambda_1 - (\mu + \psi\tan\phi_{crit})]\,[1 - \lambda_2\,(\mu + \psi\tan\phi_{crit})] < 0. \tag{3.67}$$

Substituting Equation 3.61 results in

$$[\lambda_1 - (\mu \pm \sigma_m)]\,[1 - \lambda_2\,(\mu \pm \sigma_m)] < 0. \tag{3.68}$$

Solving Equation 3.68 results in

$$\lambda_1 > \mu - \sigma_m \quad \text{and} \quad \lambda_2 > \frac{1}{\mu + \sigma_m} \tag{3.69}$$

or

$$\lambda_1 < \mu + \sigma_m \quad \text{and} \quad \lambda_2 < \frac{1}{\mu - \sigma_m}. \tag{3.70}$$

The shaded areas of Figure 3.4 illustrates the regions where ϕ_{crit} exists in the λ_1 and λ_2 plane. It will be shown that in the regions where ϕ_{crit} exists (shaded regions), ϕ is bounded and where ϕ_{crit} does not exist (unshaded regions) ϕ is not bounded. The fact that there are regions where ϕ_{crit} does not exist means it is possible to design a system that switches between underdamped and overdamped or underdamped and critically damped states. This result will be examined in more detail, later.

First, the criteria when $\dot{\phi}$ is an increasing function and when it is a decreasing function will be identified. Understanding the behavior of $\dot{\phi}$ will make it possible to understand

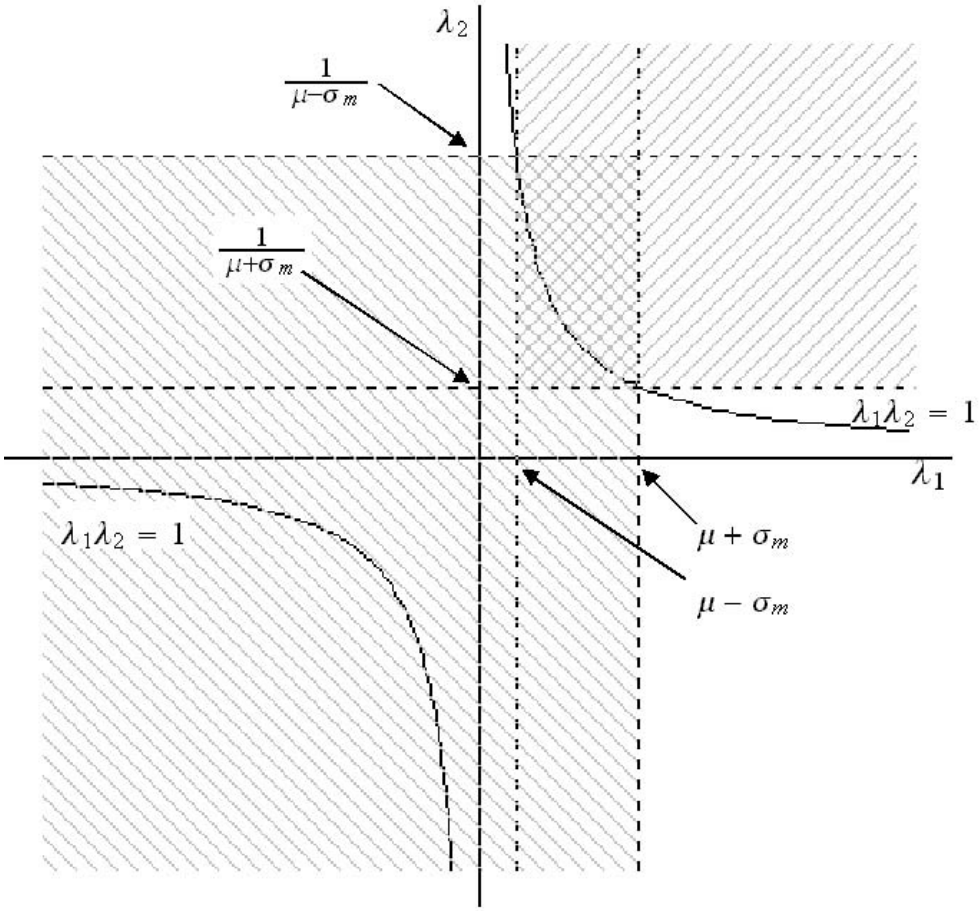

Figure 3.4 Regions where ϕ_{crit} Exists (Shaded Area)

what ϕ is bounded by. Letting $u = 1$ in Equation 3.21 results in $\dot{\phi} = \psi\left(\frac{1}{\delta}\cos^2\phi + 1\right) > 0$ since both $\psi > 0$ and $\delta > 0$. Hence, when $u = 1$, $\dot{\phi} > 0$.

In the case when $u = -1$, it is possible for $\dot{\phi} > 0$ and $\dot{\phi} < 0$. Substituting $u = -1$ into Equation 3.21 results in $\dot{\phi} = \psi\left(-\frac{1}{\delta}\cos^2\phi + 1\right)$. Then, $\dot{\phi} > 0$ when

$$\cos^2\phi < \delta \tag{3.71}$$

and $\dot{\phi} < 0$ when

$$\cos^2\phi > \delta. \tag{3.72}$$

Regions where Variable Stiffness Switching Stops. Regions in Figure 3.4 where ϕ is bounded by ϕ_{crit} will be identified. When ϕ reaches ϕ_{crit}, ϕ no longer changes since $\dot{\phi} = 0$. Variable stiffness switching stops because ϕ never increases enough to reach the next switching phase angle. The next theorem identifies the regions where ϕ approaches ϕ_{crit} for $\phi_1 < \phi_2$. Although not shown, when $\phi_1 > \phi_2$ such that $\lambda_1 > \mu - \sigma_m$ and $\lambda_2 > \frac{1}{\mu - \sigma_m}$, then ϕ will also approach ϕ_{crit}. This proof is omitted since it is similar to the case where $\phi_1 < \phi_2$.

Theorem 3 *The conditions $u = -1$, ϕ_{crit} exists, and $\phi_1 \leq \phi < \phi_{crit} < \phi_2$ implies $\lambda_1 < \mu - \sigma_m$ and $\lambda_2 < \frac{1}{\mu - \sigma_m}$. Further ϕ is an increasing function.*

Proof. Substituting Equations 3.38, 3.39, and 3.61 into the inequality $\phi_1 \leq \phi < \phi_{crit} < \phi_2$ results in

$$\tan^{-1}\left(\frac{\lambda_1 - \mu}{\psi}\right) \leq \phi < -\tan^{-1}\frac{\sigma_m}{\psi} < \tan^{-1}\left(\frac{1 - \lambda_2\mu}{\lambda_2\psi}\right). \tag{3.73}$$

Simplifying results in

$$\lambda_1 \leq \psi\tan\phi + \mu < \mu - \sigma_m < \frac{1}{\lambda_2}.$$

Then

$$\lambda_1 < \mu - \sigma_m \tag{3.74}$$

and

$$\lambda_2 < \frac{1}{\mu - \sigma_m}. \tag{3.75}$$

Now it is shown that ϕ is an increasing function. It is sufficient to show Equation 3.71 is true when $\phi = \phi_1$. Since Equation 3.74 is true,

$$\lambda_1 < \mu + \sigma_m \tag{3.76}$$

is also true since $\sigma_m \geq 0$. Then

$$(\lambda_1 - \mu + \sigma_m)(\lambda_1 - \mu - \sigma_m) > 0 \tag{3.77}$$

or

$$\lambda_1^2 - 2\lambda_1\mu + \mu^2 - \sigma_m^2 > 0. \tag{3.78}$$

Recalling Equation 3.53 and because ϕ_{crit} exists implies $\mu_{crit} \leq \mu < 1$ or $\sigma_m^2 = \varepsilon - \psi^2$,

$$\lambda_1^2 - 2\lambda_1\mu + 1 - \varepsilon > 0 \tag{3.79}$$

since $\mu^2 + \psi^2 = 1$ by Equation 3.20. Rearranging and multiplying through by ψ^2,

$$\frac{\psi^2}{\varepsilon} > \frac{\psi^2}{\lambda_1^2 - 2\lambda_1\mu + 1}. \tag{3.80}$$

Recalling Equations 3.24 and 3.38 results in

$$\delta > \cos^2\phi_1. \tag{3.81}$$

■

Figure 3.5 summarizes the regions where $\phi \to \phi_{crit}$, when ϕ_{crit} exists.

Corridors of Rapid Variable Stiffness Switching or Chattering. Next when $u = -1$, values of λ_1 and λ_2 where $\dot{\phi}$ can be negative are determined. Rewriting the definitions of ϕ_1 and ϕ_2 (Equations 3.38 and 3.39) in terms of cosine functions and substituting into Equation 3.72 results in

$$\cos^2\phi_1 = \frac{\psi^2}{\lambda_1^2 - 2\lambda_1\mu + 1} > \frac{\psi^2}{\varepsilon} \tag{3.82}$$

and

$$\cos^2\phi_2 = \frac{\psi^2\lambda_2^2}{\lambda_2^2 - 2\lambda_2\mu + 1} > \frac{\psi^2}{\varepsilon}. \tag{3.83}$$

Solving for λ_1 and λ_2 results in

$$\mu - \sigma_m < \lambda_1 < \mu + \sigma_m \tag{3.84}$$

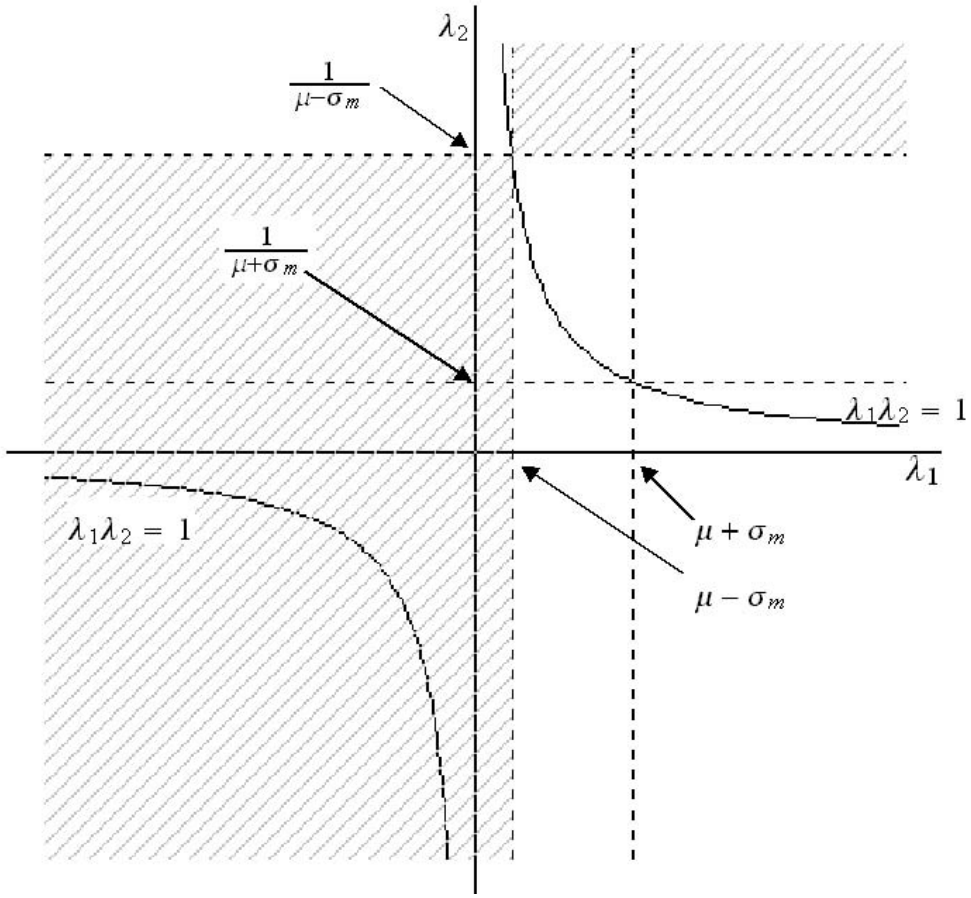

Figure 3.5 Regions (shaded) where $\phi \to \phi_{crit}$ when ϕ_{crit} exists

and

$$\frac{\mu - \sigma_m}{1 - \varepsilon} < \lambda_2 < \frac{\mu + \sigma_m}{1 - \varepsilon}. \tag{3.85}$$

The fractions in Equation 3.85 can be reduced to a more recognizable form by multiplying the left fraction by $\frac{\mu+\sigma_m}{\mu+\sigma_m}$ and the right fraction by $\frac{\mu-\sigma_m}{\mu-\sigma_m}$. Then, by recognizing $\mu^2 - \sigma_m^2 = \mu^2 - \varepsilon + \psi^2 = 1 - \varepsilon$, (which is true only when ϕ_{crit} exits), Equation 3.85 can be rewritten as

$$\frac{1}{\mu + \sigma_m} < \lambda_2 < \frac{1}{\mu - \sigma_m}. \tag{3.86}$$

Equations 3.84 and 3.86 define the two "corridors" seen in Figure 3.4. When $\phi_1 < \phi_2$ and Equation 3.84 holds, letting $\phi = \phi_1$ in Equation 3.21 makes $\dot{\phi}$ negative. The same result applies for Equation 3.86 when $\phi_1 > \phi_2$ and $\phi = \phi_2$. In the previous section, regions

were defined where $\phi \rightarrow \phi_{crit}$. Some of these regions overlap the "corridors" defined by Equations 3.84 and 3.86. In these overlapping regions, ϕ cannot reach ϕ_1 when $\phi_1 < \phi_2$ or reach ϕ_2 when $\phi_1 > \phi_2$ since ϕ must cross through $\phi = \phi_{crit}$ to do so. At this point, $\dot{\phi} = 0$ and ϕ becomes constant. Hence, $\dot{\phi} < 0$ for Equation 3.84 only when $\lambda_1\lambda_2 < 1$. Similarly, $\dot{\phi} < 0$ for Equation 3.86 only when $\lambda_1\lambda_2 > 1$. The shaded areas of Figure 3.6 show the regions where $\dot{\phi} < 0$ occurs.

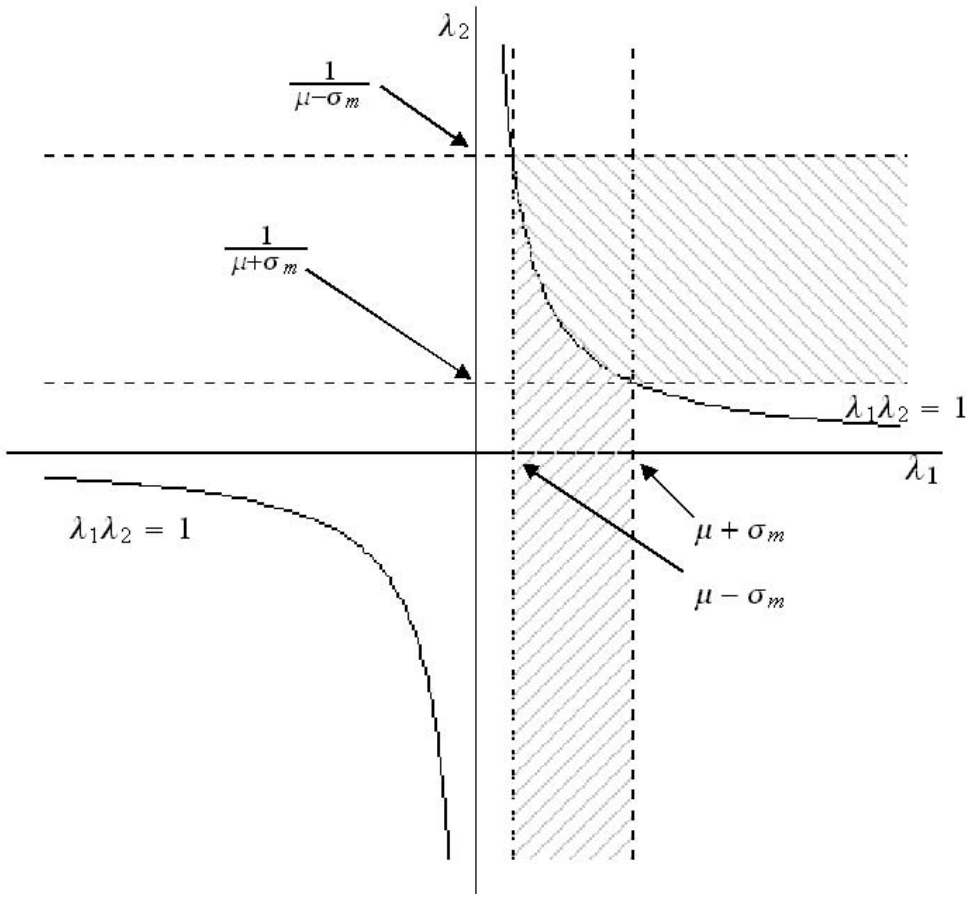

Figure 3.6 Rapid Switching or Chattering Corridors

The result of being in one of the regions is ϕ increases until it reaches either ϕ_1 or ϕ_2, depending on which region. When $\phi = \phi_1$ or $\phi = \phi_2$, $\dot{\phi}$ becomes negative, causing ϕ to decrease. Since ϕ_1 and ϕ_2 are switching angles, the control law switches when ϕ decreases until it is less than ϕ_1 or ϕ_2. At this point, $\dot{\phi} > 0$ and ϕ increases again. This switching cycle repeats endlessly, resulting in rapid switching or chattering of the variable switching

device. In running simulations, the switching time is extremely rapid, but the number of switches is finite. For example, there can be as many as 5 switches in 0.1 nondimensional time units. From a practical standpoint, real hardware can only switch at a finite rate and a finite number of times before the hardware fails. Further, examples of slightly better performance was found by moving away from this region. Hence, it would seem desirable to select λ_1 and λ_2 to prevent $\dot{\phi} < 0$ and risk possible premature hardware failure.

3.7 Solution to Initial Displacement Problem

The previous two sections discussing bifurcations due to the parameters λ_1, λ_2, μ, and ε and identifying the range of ϕ were critical to understanding how to write the solution to Equations 3.32 and 3.33. Understanding the bifurcations not only provides physical insight into different system behaviors, but mathematically determines how to break up the integrals of Equations 3.32 and 3.33. Understanding the range of ϕ for any particular parameter setting identifies where the solutions to Equations 3.32 and 3.33 are valid.

It is now possible to write the solution to Equations 3.21 and 3.22. The solution to Equation 3.21 is in the form

$$t(\phi) = t_b(\phi) + t_{mi}(\phi) + t_e(\phi) \tag{3.87}$$

and the solution to Equation 3.22 is in the form

$$a(\phi) = a_0 a_b(\phi)\, a_{mi}(\phi)\, a_e(\phi) \tag{3.88}$$

where the subscripts b, mi, and e are abbreviations for beginning, middle, and ending intervals, respectively. The beginning interval provides a solution from the initial condition to the first switching time. The middle interval provides a solution for any number of complete switching phase angle periods which occurs in π intervals. Finally, the ending interval provides a solution when between switching events, but not in the beginning interval. The following sections define the terms in Equations 3.87 and 3.88.

Implicit Solution for Phase in terms of time.

Solution for Phase from Initial Condition to First Switching Angle. Recalling Equation 3.30, the goal is to define $t(\phi)$ with initial condition ϕ_0 defined by Equation 3.25. Depending on settings for λ_1 and λ_2, six possible solution regions exist when integrating Equation 3.30 from ϕ_0 to the first switching angle. Table 3.2 details the six initial starting conditions and identifies the six different possible regions. For convenience, a new variable Reg_r is defined where the subscript $r = 1, 2, ..6$ identifies the region of interest. Figure 3.7 depicts the regions where each condition occurs.

Table 3.2 Variable Stiffness Controller Solution Regions

Region	**Condition**	λ_1, λ_2 **Settings**	**Interval**	u
1	$\phi_0 \leq \phi_1 < \phi_2$	$0 \leq \lambda_1 < \frac{1}{\lambda_2}$	Reg_1	$+1$
2	$\phi_1 \leq \phi_0 < \phi_2$	$\lambda_1 < 0 < \frac{1}{\lambda_2}$	Reg_2	-1
3	$\phi_1 < \phi_2 < \phi_0$	$\lambda_1 < \frac{1}{\lambda_2} < 0$	Reg_3	-1
4	$\phi_0 < \phi_2 < \phi_1$	$0 < \frac{1}{\lambda_2} < \lambda_1$	Reg_4	$+1$
5	$\phi_2 < \phi_0 \leq \phi_1$	$\frac{1}{\lambda_2} < 0 \leq \lambda_1$	Reg_5	$+1$
6	$\phi_2 < \phi_1 < \phi_0$	$\frac{1}{\lambda_2} < \lambda_1 < 0$	Reg_6	-1

Then

$$t_b(\phi) = \begin{cases} \Gamma_{\phi_p}(\phi_0, \phi) & \text{if } Reg_1 \wedge \phi < \phi_1 \\ \Gamma_{\phi_m}(\phi_0, \phi) & \text{if } Reg_2 \wedge \phi < \phi_2 \\ \Gamma_{\phi_m}(\phi_0, \phi) & \text{if } Reg_3 \wedge \phi < \phi_1 + \pi \\ \Gamma_{\phi_p}(\phi_0, \phi) & \text{if } Reg_4 \wedge \phi < \phi_2 \\ \Gamma_{\phi_p}(\phi_0, \phi) & \text{if } Reg_5 \wedge \phi < \phi_1 \\ \Gamma_{\phi_m}(\phi_0, \phi) & \text{if } Reg_6 \wedge \phi < \phi_2 + \pi \\ t_{sw_0} & otherwise \end{cases} \tag{3.89}$$

is the solution to Equation 3.30 until the first switching angle is reached. The first six entries represent time as ϕ increases, until reaching the first switching angle. After the first switching angle is reached, $t_b = t_{sw_0}$ where t_{sw_0} is the first time the variable stiffness device switches. It is possible that the first switching angle is never reached as ϕ may be

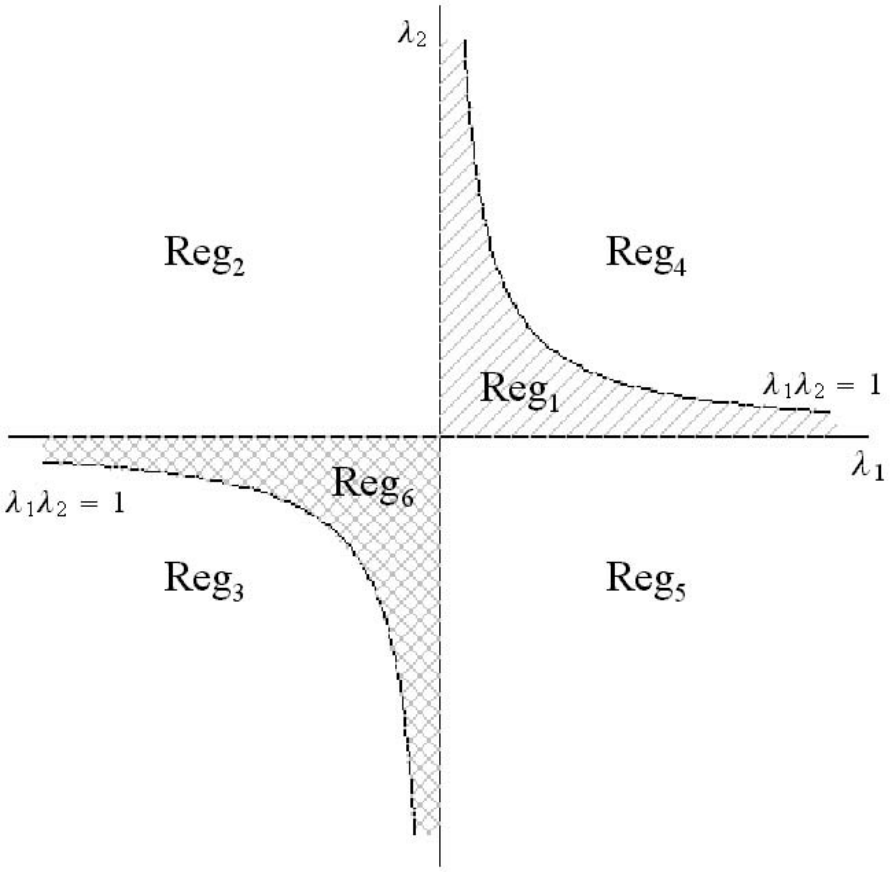

Figure 3.7 Solution Regions for Variable Stiffness Constant Damping Initial Displacement Problem

bounded as was discussed previously. Equation 3.89 can be simplified somewhat as

$$t_b(\phi) = \begin{cases} \Gamma_{\phi_p}(\phi_0, \phi) & \text{if } [\phi < \phi_1 \wedge (Reg_1 \vee Reg_5)] \vee [\phi < \phi_2 \wedge Reg_4] \\ \Gamma_{\phi_m}(\phi_0, \phi) & \text{if } [\phi < \phi_2 \wedge Reg_2] \vee [\phi < \phi_1 + \pi \wedge Reg_3] \vee [\phi < \phi_2 + \pi \wedge Reg_6] \\ t_{sw_0} & otherwise \end{cases} . \tag{3.90}$$

where "$\vee$" is the boolean symbol for "or" and "$\wedge$" is the boolean symbol for "and." Because the form of solutions for Γ_{ϕ_p} and Γ_{ϕ_m} have a period of π, Cases 1 and 5 and Cases 2 and

6 of Table 3.2 are the same upon passing the first switching angle. That is

$$t_{sw_0} = \begin{cases} \Gamma_{\phi_p}(\phi_0, \phi_1) & \text{if } Reg_1 \vee Reg_5 \\ \Gamma_{\phi_m}(\phi_0, \phi_2) & \text{if } Reg_2 \vee Reg_6 \\ \Gamma_{\phi_p}(\phi_0, \phi_1) & \text{if } Reg_3 \\ \Gamma_{\phi_m}(\phi_0, \phi_2) & \text{if } Reg_4 \end{cases}. \tag{3.91}$$

where t_{sw_0} is the first switching time for the variable stiffness device.

Implicit Solution for Full Period Switching. Since ϕ is periodic, it is possible to find $t(\phi)$ for ϕ having passed through an entire period. Recalling Equation 3.91, a period begins at t_{sw_0} and u switches from either negative to positive or positive to negative, depending on what it was initially as defined in Table 3.2. An entire period is completed when u has switched twice. Then,

$$t_{mi}(\phi) = \begin{cases} \sum_{k=0}^{n-1}\left[\Gamma_{\phi_m}(\phi_1 + k\pi, \phi_2 + k\pi) + \Gamma_{\phi_p}(\phi_1 + k\pi, \phi_2 + k\pi)\right] & \text{if } Reg_1 \\ \sum_{k=0}^{n-1}\left[\Gamma_{\phi_p}(\phi_2 + k\pi, \phi_1 + k_1\pi) + \Gamma_{\phi_m}(\phi_1 + k_1\pi, \phi_2 + k_1\pi)\right] & \text{if } Reg_2 \\ \sum_{k=0}^{n-1}\left[\Gamma_{\phi_p}(\phi_1 + k_1\pi, \phi_2 + k_1\pi) + \Gamma_{\phi_m}(\phi_2 + k_1\pi, \phi_1 + k_2\pi)\right] & \text{if } Reg_3 \\ \sum_{k=0}^{n-1}\left[\Gamma_{\phi_m}(\phi_2 + k\pi, \phi_1 + k\pi) + \Gamma_{\phi_p}(\phi_1 + k\pi, \phi_2 + k_1\pi)\right] & \text{if } Reg_4 \\ \sum_{k=0}^{n-1}\left[\Gamma_{\phi_m}(\phi_1 + k\pi, \phi_2 + k_1\pi) + \Gamma_{\phi_p}(\phi_2 + k_1\pi, \phi_2 + k_1\pi)\right] & \text{if } Reg_5 \\ \sum_{k=0}^{n-1}\left[\Gamma_{\phi_p}(\phi_2 + k_1\pi, \phi_1 + k_1\pi) + \Gamma_{\phi_m}(\phi_1 + k_1\pi, \phi_2 + k_2\pi)\right] & \text{if } Reg_6 \end{cases} \tag{3.92}$$

is the time for an entire period of ϕ, where $n(\phi)$ is the number of complete periods ϕ has passed through, $k_1 = k+1$, and $k_2 = k+2$. Since Γ_{ϕ_m} and Γ_{ϕ_p} are π periodic, the periodic constants added to ϕ_1 and ϕ_2 can be dropped. This allows considerable simplification of Equation 3.92 to

$$t_{mi}(\phi) = n(\phi) D_\phi \tag{3.93}$$

where

$$D_\phi = \begin{cases} \Gamma_{\phi_m}(\phi_1, \phi_2) + \Gamma_{\phi_p}(\phi_2, \phi_1) & \text{if } Reg_1 \vee Reg_2 \vee Reg_5 \vee Reg_6 \\ \Gamma_{\phi_p}(\phi_1, \phi_2) + \Gamma_{\phi_m}(\phi_2, \phi_1) & \text{if } Reg_3 \vee Reg_4 \end{cases} \tag{3.94}$$

and

$$n(\phi) = \begin{cases} floor\left(\frac{\phi-\phi_1}{\pi}\right) & \text{if } Reg_1 \vee Reg_5 \\ floor\left(\frac{\phi-\phi_2}{\pi}\right) & \text{if } Reg_2 \vee Reg_4 \\ floor\left(\frac{\phi-\phi_1-\pi}{\pi}\right) & \text{if } Reg_3 \\ floor\left(\frac{\phi-\phi_2-\pi}{\pi}\right) & \text{if } Reg_6 \end{cases}, n \geq 0. \tag{3.95}$$

Alternatively,

$$n(\phi) = floor\left(\frac{\phi}{\pi} - \theta_e\right), n \geq 0 \tag{3.96}$$

where

$$\theta_e = \frac{1}{\pi} \begin{cases} \phi_1 & \text{if } Reg_1 \vee Reg_5 \\ \phi_2 & \text{if } Reg_2 \vee Reg_4 \\ \phi_1 + \pi & \text{if } Reg_3 \\ \phi_2 + \pi & \text{if } Reg_6 \end{cases} \tag{3.97}$$

Solution for Partial Periods. Finally, the solution when ϕ falls between periods is found that occurs after the first switching angle. A partial period could begin at the first switching angle or some multiple of π of the first switching angle. Again Table 3.2 can be used and once again, u switches from either negative to positive or positive to negative at the first switching angle or at multiples of π of the first switching angle. The

solution looks like

$$t_e(\phi,k)=\begin{cases}\Gamma_{\phi_m}(\phi_1,\phi) & \text{if } Reg_1\wedge\phi_1+k\pi<\phi<\phi_2+k\pi\\ \Gamma_{\phi_m}(\phi_1,\phi_2)+\Gamma_{\phi_p}(\phi_2,\phi) & \text{if } Reg_1\wedge\phi_2+k\pi<\phi<\phi_1+k_1\pi\\ \Gamma_{\phi_p}(\phi_2,\phi) & \text{if } Reg_2\wedge\phi_2+k\pi<\phi<\phi_1+k_1\pi\\ \Gamma_{\phi_p}(\phi_2,\phi_1)+\Gamma_{\phi_m}(\phi_1,\phi) & \text{if } Reg_2\wedge\phi_1+k_1\pi<\phi<\phi_2+k_1\pi\\ \Gamma_{\phi_p}(\phi_1,\phi) & \text{if } Reg_3\wedge\phi_1+k_1\pi<\phi<\phi_2+k_1\pi\\ \Gamma_{\phi_p}(\phi_1,\phi_2)+\Gamma_{\phi_m}(\phi_2,\phi) & \text{if } Reg_3\wedge\phi_2+k_1\pi<\phi<\phi_1+k_2\pi\\ \Gamma_{\phi_m}(\phi_2,\phi) & \text{if } Reg_4\wedge\phi_2+k\pi<\phi<\phi_1+k\pi\\ \Gamma_{\phi_m}(\phi_2,\phi_1)+\Gamma_{\phi_p}(\phi_1,\phi) & \text{if } Reg_4\wedge\phi_1+k\pi<\phi<\phi_2+k_1\pi\\ \Gamma_{\phi_m}(\phi_1,\phi) & \text{if } Reg_5\wedge\phi_1+k\pi<\phi<\phi_2+k_1\pi\\ \Gamma_{\phi_m}(\phi_1,\phi_2)+\Gamma_{\phi_p}(\phi_2,\phi) & \text{if } Reg_5\wedge\phi_2+k_1\pi<\phi<\phi_1+k_1\pi\\ \Gamma_{\phi_p}(\phi_2,\phi) & \text{if } Reg_6\wedge\phi_2+k_1\pi<\phi<\phi_1+k_1\pi\\ \Gamma_{\phi_p}(\phi_2,\phi_1)+\Gamma_{\phi_m}(\phi_1,\phi) & \text{if } Reg_6\wedge\phi_1+k_1\pi<\phi<\phi_2+k_2\pi,\end{cases}\tag{3.98}$$

where the periodic constant has been omitted from Γ_{ϕ_m} and Γ_{ϕ_p}. Although not shown, Equation 3.98 can be simplified slightly since Regions 1 and 5 and Regions 2 and 6 are similar, except for the conditions of when they apply.

Switching Times. When switching occurs, the exact switching times can be identified, using Equation 3.87. As was discussed previously, switching occurs at π multiples of ϕ_1 and ϕ_2. The first switching time is defined by Equation 3.91. Switching occurs when

$$t_{swe}(n)=t_{sw_0}+nD_\phi\tag{3.99}$$

or

$$t_{swo}(n)=t_{sw_0}+nD_\phi+\begin{cases}\Gamma_{\phi_m}(\phi_1,\phi_2) & \text{if } Reg_1\vee Reg_5\\ \Gamma_{\phi_p}(\phi_2,\phi_1) & \text{if } Reg_2\vee Reg_6\\ \Gamma_{\phi_p}(\phi_1,\phi_2) & \text{if } Reg_3\\ \Gamma_{\phi_m}(\phi_2,\phi_1) & \text{if } Reg_4\end{cases}\tag{3.100}$$

where t_{swe} is defined as an even number switching time, t_{swo} is defined as an odd number switching time, and $n=0,1,2,....$ Using Equations 3.99 and 3.100, the switching time for

even and odd times can be combined to create one equation defining all switching times in the order they occur as

$$t_{sw_k} = \frac{1}{2}\left(\left[1+(-1)^k\right] t_{swe}\left(\frac{k}{2}\right) + \left[1-(-1)^k\right] t_{swo}\left(\frac{k-1}{2}\right)\right) \tag{3.101}$$

where $k = 0, 1, 2, ...$ is the k^{th} time the stiffness device has switched since time 0.

Solution for Amplitude. Development of the solution for the amplitude of the system is simpler than the development of the solution for phase ϕ. The solution uses the same boundaries of integration as the solution for ϕ, but amplitude is only affected by the change in variable stiffness (Equations 3.58 and 3.59). Since development of the solution for amplitude follows the same logic as the solution for ϕ, the solution is stated without discussion.

$$a_b(\phi) = a_0 \begin{cases} a_p(\phi_0, \phi) & \text{if } [\phi < \phi_1 \wedge (Reg_1 \vee Reg_5)] \vee [\phi < \phi_2 \wedge Reg_4] \\ a_m(\phi_0, \phi) & \text{if } [\phi < \phi_2 \wedge Reg_2] \vee [\phi < \phi_1 + \pi \wedge Reg_3] \vee [\phi < \phi_2 + \pi \wedge Reg_6] \\ a_{sw_0} & otherwise \end{cases} . \tag{3.102}$$

$$a_{sw_0} = a_0 \begin{cases} a_p(\phi_0, \phi_1) & \text{if } Reg_1 \vee Reg_5 \\ a_m(\phi_0, \phi_2) & \text{if } Reg_2 \vee Reg_6 \\ a_p(\phi_0, \phi_1) & \text{if } Reg_3 \\ a_m(\phi_0, \phi_2) & \text{if } Reg_4 \end{cases} . \tag{3.103}$$

$$a_{mi}(\phi) = D_a^{n(\phi)} \tag{3.104}$$

$$D_a = \begin{cases} a_m(\phi_1, \phi_2)\, a_p(\phi_2, \phi_1) & \text{if } Reg_1 \vee Reg_2 \vee Reg_5 \vee Reg_6 \\ a_p(\phi_1, \phi_2)\, a_m(\phi_2, \phi_1) & \text{if } Reg_3 \vee Reg_4 \end{cases} . \tag{3.105a}$$

$$= \begin{cases} \sqrt{\frac{\left(\psi^2 - \varepsilon\cos^2\phi_1\right)\left(\psi^2 + \varepsilon\cos^2\phi_2\right)}{\left(\psi^2 - \varepsilon\cos^2\phi_2\right)\left(\psi^2 + \varepsilon\cos^2\phi_1\right)}} & \text{if } Reg_1 \vee Reg_2 \vee Reg_5 \vee Reg_6 \\ \sqrt{\frac{\left(\psi^2 + \varepsilon\cos^2\phi_1\right)\left(\psi^2 - \varepsilon\cos^2\phi_2\right)}{\left(\psi^2 + \varepsilon\cos^2\phi_2\right)\left(\psi^2 - \varepsilon\cos^2\phi_1\right)}} & \text{if } Reg_3 \vee Reg_4 \end{cases} . \tag{3.105b}$$

$$a_e(\phi,k)=\begin{cases} a_m(\phi_1,\phi) & \text{if } Reg_1 \wedge \phi_1+k\pi<\phi<\phi_2+k\pi \\ a_m(\phi_1,\phi_2)\,a_p(\phi_2,\phi) & \text{if } Reg_1 \wedge \phi_2+k\pi<\phi<\phi_1+k_1\pi \\ a_p(\phi_2,\phi) & \text{if } Reg_2 \wedge \phi_2+k\pi<\phi<\phi_1+k_1\pi \\ a_p(\phi_2,\phi_1)\,a_m(\phi_1,\phi) & \text{if } Reg_2 \wedge \phi_1+k_1\pi<\phi<\phi_2+k_1\pi \\ a_m(\phi_1,\phi) & \text{if } Reg_3 \wedge \phi_1+k_1\pi<\phi<\phi_2+k_1\pi \\ a_m(\phi_1,\phi_2)\,a_p(\phi_2,\phi) & \text{if } Reg_3 \wedge \phi_2+k_1\pi<\phi<\phi_1+k_2\pi \\ a_m(\phi_2,\phi) & \text{if } Reg_4 \wedge \phi_2+k\pi<\phi<\phi_1+k\pi \\ a_m(\phi_2,\phi_1)\,a_p(\phi_1,\phi) & \text{if } Reg_4 \wedge \phi_1+k\pi<\phi<\phi_2+k_1\pi \\ a_m(\phi_1,\phi) & \text{if } Reg_5 \wedge \phi_1+k\pi<\phi<\phi_2+k_1\pi \\ a_m(\phi_1,\phi_2)\,a_p(\phi_2,\phi) & \text{if } Reg_5 \wedge \phi_2+k_1\pi<\phi<\phi_1+k_1\pi \\ a_m(\phi_2,\phi) & \text{if } Reg_6 \wedge \phi_2+k_1\pi<\phi<\phi_1+k_1\pi \\ a_m(\phi_2,\phi_1)\,a_p(\phi_1,\phi) & \text{if } Reg_6 \wedge \phi_1+k_1\pi<\phi<\phi_2+k_2\pi \end{cases}. \tag{3.106}$$

3.8 Solution for Initial Velocity Problem

Implicit Solution for Phase in Terms of Time. The solution form for the initial velocity problem is the same as the initial displacement problem (Equations 3.87 and 3.88). Recalling Equation 3.30, the goal is to define $t(\phi)$ with initial condition ϕ_0 defined by Equation 3.26. Depending on settings for λ_1 and λ_2, four possible solution regions exist when integrating Equation 3.30 from ϕ_0 to the first switching angle. Table 3.3 details the six initial starting conditions and identifies the six different possible regions. Again for convenience, the variable Reg_r is defined where the subscript $r = 1, 2, ..4$ identifies the region of interest. Figure 3.8 depicts the regions where each condition occurs.

Table 3.3 Variable Stiffness Controller Solution Regions (Initial Velocity Problem)

Region	**Condition**	λ_1, λ_2 **Settings**	**Interval**	u
1	$\phi_1 < \phi_2$	$\lambda_1 < \frac{1}{\lambda_2} \wedge \lambda_2 \geq 0$	Reg_1	$+1$
2	$\phi_2 < \phi_1$	$\frac{1}{\lambda_2} < \lambda_1 \wedge \lambda_2 \geq 0$	Reg_2	$+1$
3	$\phi_1 < \phi_2$	$\lambda_1 < \frac{1}{\lambda_2} \wedge \lambda_2 < 0$	Reg_3	-1
4	$\phi_2 < \phi_1$	$\frac{1}{\lambda_2} < \lambda_1 \wedge \lambda_2 < 0$	Reg_4	-1

Development of the solution is the same as for the initial displacement problem, the solution is presented with little discussion. The solution form is simpler than for the

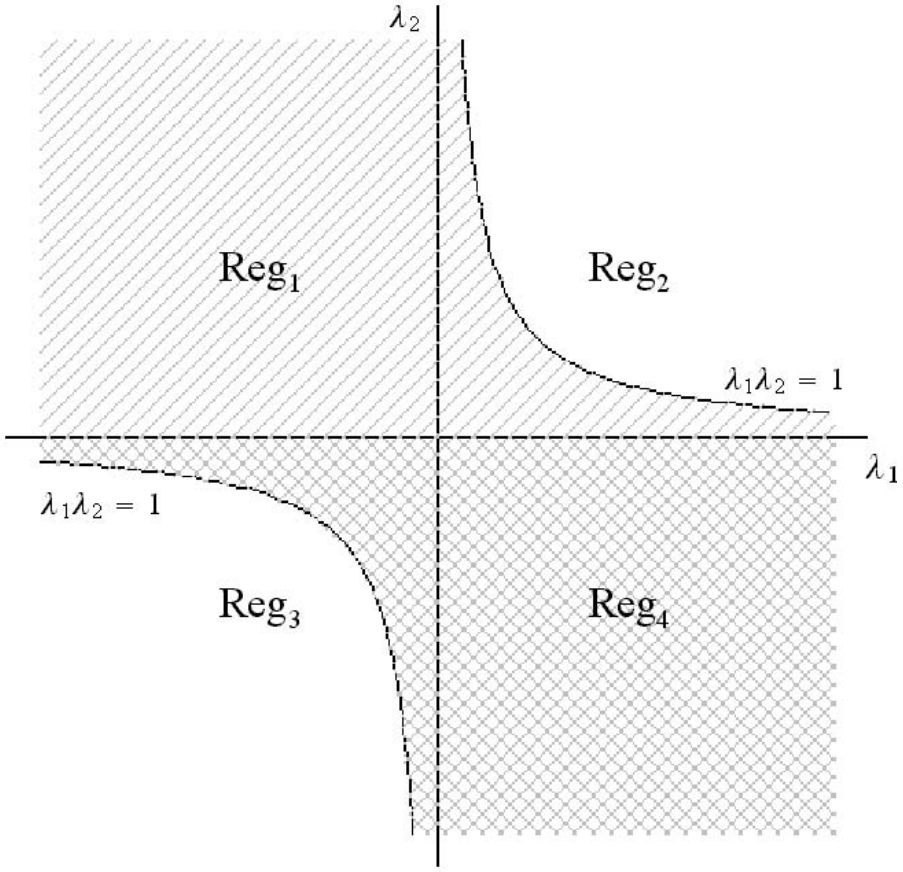

Figure 3.8 Solution Regions for Variable Stiffness Constant Damping Initial Velocity Problem

initial displacement problem since $\phi_0 = -\frac{\pi}{2}$ and does not change as a function of μ as in the initial displacement problem. The solution for the beginning portion of the solution is

$$t_b(\phi) = \begin{cases} \Gamma_{\phi_p}\left(-\frac{\pi}{2}, \phi\right) & \text{if } Reg_1 \wedge \phi < \phi_1 \vee Reg_2 \wedge \phi < \phi_2 \\ \Gamma_{\phi_m}\left(-\frac{\pi}{2}, \phi\right) & \text{if } Reg_3 \wedge \phi < \phi_1 \vee Reg_4 \wedge \phi < \phi_2 \\ t_{sw_0} & otherwise \end{cases} \tag{3.107}$$

where

$$t_{sw_0} = \begin{cases} \Gamma_{\phi_p}\left(-\frac{\pi}{2}, \phi_1\right) & \text{if } Reg_1 \\ \Gamma_{\phi_p}\left(-\frac{\pi}{2}, \phi_2\right) & \text{if } Reg_2 \\ \Gamma_{\phi_m}\left(-\frac{\pi}{2}, \phi_1\right) & \text{if } Reg_3 \\ \Gamma_{\phi_m}\left(-\frac{\pi}{2}, \phi_2\right) & \text{if } Reg_4 \end{cases}. \tag{3.108}$$

is the first switching time for the variable stiffness device.

Similar to the initial displacement problem,

$$D_\phi = \begin{cases} \Gamma_{\phi_m}(\phi_1, \phi_2) + \Gamma_{\phi_p}(\phi_2, \phi_1) & \text{if } Reg_1 \vee Reg_4 \\ \Gamma_{\phi_p}(\phi_1, \phi_2) + \Gamma_{\phi_m}(\phi_2, \phi_1) & \text{if } Reg_2 \vee Reg_3 \end{cases} \tag{3.109}$$

and

$$n(\phi) = \begin{cases} floor\left(\frac{\phi-\phi_1}{\pi}\right) & \text{if } Reg_1 \vee Reg_3 \\ floor\left(\frac{\phi-\phi_2}{\pi}\right) & \text{if } Reg_2 \vee Reg_4 \end{cases}, n \geq 0. \tag{3.110}$$

Alternatively,

$$n(\phi) = floor\left(\frac{\phi}{\pi} - \theta_e\right), n \geq 0 \tag{3.111}$$

where

$$\theta_e = \frac{1}{\pi} \begin{cases} \phi_1 & \text{if } Reg_1 \vee Reg_3 \\ \phi_2 & \text{if } Reg_2 \vee Reg_4 \end{cases}. \tag{3.112}$$

Equation 3.111 is the same as Equation 3.96, but θ_e is defined differently.

The solution for a partial period is

$$t_e(\phi, k) = \begin{cases} \Gamma_{\phi_m}(\phi_1, \phi) & \text{if } Reg_1 \wedge \phi_1 + k\pi < \phi < \phi_2 + k\pi \\ \Gamma_{\phi_m}(\phi_1, \phi_2) + \Gamma_{\phi_p}(\phi_2, \phi) & \text{if } Reg_1 \wedge \phi_2 + k\pi < \phi < \phi_1 + k_1\pi \\ \Gamma_{\phi_m}(\phi_2, \phi) & \text{if } Reg_2 \wedge \phi_2 + k\pi < \phi < \phi_1 + k\pi \\ \Gamma_{\phi_m}(\phi_2, \phi_1) + \Gamma_{\phi_p}(\phi_1, \phi) & \text{if } Reg_2 \wedge \phi_1 + k\pi < \phi < \phi_2 + k_1\pi \\ \Gamma_{\phi_p}(\phi_1, \phi) & \text{if } Reg_3 \wedge \phi_1 + k\pi < \phi < \phi_2 + k\pi \\ \Gamma_{\phi_p}(\phi_1, \phi_2) + \Gamma_{\phi_m}(\phi_2, \phi) & \text{if } Reg_3 \wedge \phi_2 + k\pi < \phi < \phi_1 + k_1\pi \\ \Gamma_{\phi_p}(\phi_2, \phi) & \text{if } Reg_4 \wedge \phi_2 + k\pi < \phi < \phi_1 + k\pi \\ \Gamma_{\phi_p}(\phi_2, \phi_1) + \Gamma_{\phi_m}(\phi_1, \phi) & \text{if } Reg_4 \wedge \phi_1 + k\pi < \phi < \phi_2 + k_1\pi, \end{cases} \tag{3.113}$$

where $k_1 = k + 1$.

Switching Times. Switching times are defined the same as for the initial displacement problem except

$$t_{swo}(n) = t_{sw_0} + nD_\phi + \begin{cases} \Gamma_{\phi_m}(\phi_1, \phi_2) & \text{if } Reg_1 \\ \Gamma_{\phi_m}(\phi_2, \phi_1) & \text{if } Reg_2 \\ \Gamma_{\phi_p}(\phi_1, \phi_2) & \text{if } Reg_3 \\ \Gamma_{\phi_p}(\phi_2, \phi_1) & \text{if } Reg_4 \end{cases} \tag{3.114}$$

where t_{swe} is defined as an even number switching time, t_{swo} is defined as an odd number switching time, D_ϕ is defined using Equation 3.109, and $n = 0, 1, 2, ...$ Switching times in the order they occur are defined using Equation 3.101.

Solution for Amplitude. The solution for the amplitude is similar to the initial displacement problem and is given without discussion.

$$a_b(\phi) = \begin{cases} a_p\left(-\frac{\pi}{2}, \phi\right) & \text{if } Reg_1 \wedge \phi < \phi_1 \vee Reg_2 \wedge \phi < \phi_2 \\ a_m\left(-\frac{\pi}{2}, \phi\right) & \text{if } Reg_3 \wedge \phi < \phi_1 \vee Reg_4 \wedge \phi < \phi_2 \\ t_{sw_0} & otherwise \end{cases} \tag{3.115}$$

where

$$a_{sw_0} = \begin{cases} a_p\left(-\frac{\pi}{2}, \phi_1\right) & \text{if } Reg_1 \\ a_p\left(-\frac{\pi}{2}, \phi_2\right) & \text{if } Reg_2 \\ a_m\left(-\frac{\pi}{2}, \phi_1\right) & \text{if } Reg_3 \\ a_m\left(-\frac{\pi}{2}, \phi_2\right) & \text{if } Reg_4 \end{cases} . \tag{3.116}$$

$$a_{mi}(\phi) = D_a^{n(\phi)} \tag{3.117}$$

$$D_a = \begin{cases} a_m(\phi_1, \phi_2)\, a_p(\phi_2, \phi_1) & \text{if } Reg_1 \vee Reg_4 \\ a_p(\phi_1, \phi_2)\, a_m(\phi_2, \phi_1) & \text{if } Reg_2 \vee Reg_3 \end{cases} \tag{3.118a}$$

$$= \begin{cases} \sqrt{\frac{\left(\psi^2 - \varepsilon\cos^2\phi_1\right)\left(\psi^2 + \varepsilon\cos^2\phi_2\right)}{\left(\psi^2 - \varepsilon\cos^2\phi_2\right)\left(\psi^2 + \varepsilon\cos^2\phi_1\right)}} & \text{if } Reg_1 \vee Reg_4 \\ \sqrt{\frac{\left(\psi^2 + \varepsilon\cos^2\phi_1\right)\left(\psi^2 - \varepsilon\cos^2\phi_2\right)}{\left(\psi^2 + \varepsilon\cos^2\phi_2\right)\left(\psi^2 - \varepsilon\cos^2\phi_1\right)}} & \text{if } Reg_2 \vee Reg_3 \end{cases} \tag{3.118b}$$

$$a_e(\phi,k)=\begin{cases} a_m(\phi_1,\phi) & \text{if } Reg_1 \wedge \phi_1+k\pi<\phi<\phi_2+k\pi \\ a_m(\phi_1,\phi_2)\,a_p(\phi_2,\phi) & \text{if } Reg_1 \wedge \phi_2+k\pi<\phi<\phi_1+k_1\pi \\ a_m(\phi_2,\phi) & \text{if } Reg_2 \wedge \phi_2+k\pi<\phi<\phi_1+k\pi \\ a_m(\phi_2,\phi_1)\,a_p(\phi_1,\phi) & \text{if } Reg_2 \wedge \phi_1+k\pi<\phi<\phi_2+k_1\pi \\ a_p(\phi_1,\phi) & \text{if } Reg_3 \wedge \phi_1+k\pi<\phi<\phi_2+k\pi \\ a_p(\phi_1,\phi_2)\,a_m(\phi_2,\phi) & \text{if } Reg_3 \wedge \phi_2+k\pi<\phi<\phi_1+k_1\pi \\ a_p(\phi_2,\phi) & \text{if } Reg_4 \wedge \phi_2+k\pi<\phi<\phi_1+k\pi \\ a_p(\phi_2,\phi_1)\,a_m(\phi_1,\phi) & \text{if } Reg_4 \wedge \phi_1+k\pi<\phi<\phi_2+k_1\pi \end{cases}. \tag{3.119}$$

3.9 Approximate Explicit Solution

Unfortunately Equation 3.87 is a transcendental equation which cannot be solved explicitly for ϕ. The system can be solved exactly between switching events explicitly, but this type of solution is both tedious to develop and not useful since it is too complicated to allow adequate understanding of the behavior of the system. However, an approximate solution can be written by considering the long time behavior of the system. The long term approximate behavior of the system will then be used to gain insight into the performance of the system for use in engineering design. The approximate solution can always be checked against the exact solution, if desired.

The long term behavior for the system can be approximated for both ϕ and amplitude of the system. First, an approximate solution for ϕ is found using Equations 3.87 and 3.96 or 3.111. When u is switching, ϕ will increase without bound. One way to approximate $\phi(t)$ is as a straight line. This can be done by neglecting t_e by assuming t_{mi} dominates the solution in the long term in Equation 3.87 and approximating n as

$$n(\phi)=floor\left(\frac{\phi}{\pi}-\theta_e\right)\approx\frac{\phi}{\pi}-\theta_e. \tag{3.120}$$

Equation 3.120 is exact at even switching times. Combining Equations 3.87 and 3.120 results in

$$t\approx t_b+t_{mi}=t_b+nD_\phi\approx t_b+\left(\frac{\phi}{\pi}-\theta_e\right)D_\phi \tag{3.121}$$

where t_b is constant since the long term behavior of the system is being considered. Equation 3.121 can be solved for ϕ resulting in

$$\phi \approx \frac{\pi}{D_\phi} t + C \tag{3.122}$$

where C absorbs all of the constants of Equation 3.121. Selecting $C = \phi_0$ is convenient in Equation 3.122 since it forces the approximate solution to pass through ϕ_0 when $t = 0$. Hence, an approximation for ϕ is

$$\phi \approx \frac{\pi}{D_\phi} t + \phi_0 \tag{3.123}$$

where D_ϕ is defined by either Equations 3.94 or 3.109.

Using the same approach, Equation 3.88 can be approximated. Assuming a_e is close to unity results in

$$a \approx a_0 a_{sw_0} a_{mi} = a_0 a_{sw_0} D_a^n \approx a_0 a_{sw_0} D_a^{\frac{t}{D_\phi}+C} \tag{3.124}$$

where various constants are absorbed into C. Selecting $C = -\frac{\ln a_{sw_0}}{\ln D_a}$ will cause Equation 3.124 to pass through a_0 when $t = 0$. The approximate solution is

$$a \approx a_0 a_{sw_0} D_a^{\frac{t}{D_\phi} - \frac{\ln a_{sw_0}}{\ln D_a}} = a_0 a_{sw_0} e^{\left(\frac{t}{D_\phi} - \frac{\ln a_{sw_0}}{\ln D_a}\right) \ln D_a} = a_0 e^{\frac{\ln D_a}{D_\phi} t}. \tag{3.125}$$

where D_a is defined using either Equations 3.105a or 3.118a and a_{sw_0} is defined using Equations 3.103 or 3.116.

Finally, substituting Equations 3.123 and 3.125 into Equations 3.17 and 3.18 results in an approximate explicit solution for displacement and velocity. The equations are

$$x = a_0 e^{\left(\frac{\ln D_a}{D_\phi} - \mu\right) t} \cos\left(\frac{\pi}{D_\phi} t + \phi_0\right) \tag{3.126}$$

and

$$\dot{x} = -a_0 e^{\left(\frac{\ln D_a}{D_\phi} - \mu\right) t} \left[\mu \cos\left(\frac{\pi}{D_\phi} t + \phi_0\right) + \psi \sin\left(\frac{\pi}{D_\phi} t + \phi_0\right)\right]. \tag{3.127}$$

3.10 Mapping Phase to Time

With the exact solutions known and an understanding of the range of ϕ, it is now possible to understand the effects on time t. When ϕ_{crit} does not exist, continuous switching occurs and ϕ is unbounded. When $\phi \to \infty$, $t \to \infty$. The reason this is true can be found in Equation 3.87. When $\phi \to \infty$, $t_b(\phi)$ is constant and $t_e(\phi)$ does not exist since no finite value for ϕ is ever reached. This is another way of stating that $t_{mi}(\phi)$ dominates all other terms. Realistically, a stable real system will not switch for all time since the displacement and velocity of the system will become too small to be sensed by real hardware. At this point, the displacement and velocity has effectively been damped out and switching is expected to cease.

Next, consider when ϕ is bounded by ϕ_{crit}. This only occurs in the regions shown in Figure 3.5 and only applies for the critically damped or overdamped situations. Further, ϕ_{crit} was found to exist only when $u = -1$. Since ϕ is bounded by ϕ_{crit}, $t_{mi}(\phi) = 0$. Then all that is left is

$$t(\phi) = t_b(\phi) + t_e(\phi). \tag{3.128}$$

Recalling Equation 3.55b, consider $\phi_U \to \phi_{crit}$ for the critically damped case. The result is

$$\lim_{\phi_U \to \phi_{crit}} \Gamma_{\phi_m}(\phi_L, \phi_U) = -\frac{1}{\psi}\left[\cot\phi_{crit} - \cot\phi_L\right] = -\frac{1}{\psi}\left[\pm\frac{\psi}{\sigma_m} - \cot\phi_L\right] = \pm\infty \tag{3.129}$$

since $\sigma_m = 0$ when the system is critically damped. Since time cannot be negative, the system must reach $\phi_{crit} = -\tan^{-1}\left(\frac{\psi}{\sigma_m}\right)$ and it takes an infinite amount of time to do so. Similarly, when the system is overdamped, the result is

$$\begin{aligned}\lim_{\phi_U \to \phi_{crit}} \Gamma_{\phi_m}(\phi_L, \phi_U) &= \frac{-1}{2\sigma_m}\ln\left[\left(\frac{\psi\tan\phi_{crit} + \sigma_m}{\psi\tan\phi_{crit} - \sigma_m}\right)\left(\frac{\psi\tan\phi_L - \sigma_m}{\psi\tan\phi_L + \sigma_m}\right)\right] \\ &= \frac{-1}{2\sigma_m}\ln\left[\left(\frac{\pm\sigma_m + \sigma_m}{\pm\sigma_m - \sigma_m}\right)\left(\frac{\psi\tan\phi_L - \sigma_m}{\psi\tan\phi_L + \sigma_m}\right)\right] = \pm\infty.\end{aligned} \tag{3.130}$$

Again, the conclusion is the system takes an infinite amount of time to reach $\phi_{crit} = -\tan^{-1}\left(\frac{\psi}{\sigma_m}\right)$, since negative time is impossible.

3.11 System Stability

Corless and Leitmann demonstrated at least one on-off control law exists that can make a variable stiffness system with viscous damping unstable [16]. Kurdila et. al. proved Equation 3.1 is stable when $c^* = 0$, $\lambda_1 = 0$, and $\lambda_2 = 0$ [123]. With the exact solution available for a damped variable stiffness system, it is now possible to provide more insight into the stability of a more general type of system than shown in the literature. The parameters λ_1 and λ_2 for particular ε and μ that make the system stable can be found by solving

$$\lim_{t\to\infty} x(t) = 0 \tag{3.131}$$

for λ_1 and λ_2. Substituting Equation 3.17 into Equation 3.131 results in

$$\lim_{t\to\infty} a(\phi(t))\, e^{-\mu t} \cos\phi(t) = 0. \tag{3.132}$$

Since in general, $\cos\phi(t) \neq 0$ for all t, only the amplitude functions determine system stability. Then

$$\lim_{t\to\infty} a(\phi(t))\, e^{-\mu t} = 0. \tag{3.133}$$

Next, consider only the systems with oscillatory response or systems where ϕ_{crit} does not exist. The systems where the variable stiffness device does not switch are simple linear oscillators with well known stability characteristics. When ϕ_{crit} does not exist, $t \to \infty$ implies $\phi \to \infty$. Hence

$$\lim_{\phi\to\infty} a(\phi)\, e^{-\mu t(\phi)} = 0. \tag{3.134}$$

Substituting Equations 3.87 and 3.88 into Equation 3.134 and realizing that the terms $t_e(\phi)$ and $a_e(\phi)$ do not exist since they can never be reached results in

$$\lim_{\phi\to\infty} a_b(\phi)\, a_{mi}(\phi)\, e^{-\mu[t_b(\phi)+t_{mi}(\phi)]} = 0 \tag{3.135}$$

for stability. Recognizing $a_b(\phi)$ and $t_b(\phi)$ are constant as $\phi \to \infty$, Equation 3.135 can be simplified as

$$\lim_{\phi\to\infty} a_{mi}(\phi)\, e^{-\mu t_{mi}(\phi)} = \lim_{\phi\to\infty} D_a^{n(\phi)} e^{-\mu n(\phi) D_\phi} \tag{3.136a}$$

$$= \lim_{\phi\to\infty} e^{n(\phi)\ln D_a} e^{-\mu n(\phi) D_\phi} \tag{3.136b}$$

$$= \lim_{\phi\to\infty} e^{n(\phi)\left[\ln D_a - \mu D_\phi\right]} = 0 \tag{3.136c}$$

Then the system is stable when

$$\ln D_a - \mu D_\phi < 0. \tag{3.137}$$

By similar reasoning, the system is marginally stable when

$$\ln D_a - \mu D_\phi = 0 \tag{3.138}$$

and is unstable when

$$\ln D_a - \mu D_\phi > 0. \tag{3.139}$$

Incidentally, analysis of stability for the approximate solution (Equation 3.126) has precisely the same stability behavior as the exact solution. Equation 3.138 is transcendental in λ_1 and λ_2, but can be solved numerically for specific settings of μ and ε. Figure 3.9 shows some marginal stability curves when $\varepsilon = 0.8$. When λ_1 and λ_2 are tuned to fall on a marginal stability curve, the variable stiffness device is adding the same amount of energy the viscous damper is dissipating from the system. Depending on the strength of μ and ε, it is possible to identify marginally stable and unstable systems even for some overdamped oscillatory variable stiffness system.

Equation 3.137 will always be satisfied or the system is guaranteed stable when

$$\ln D_a < 0, \tag{3.140}$$

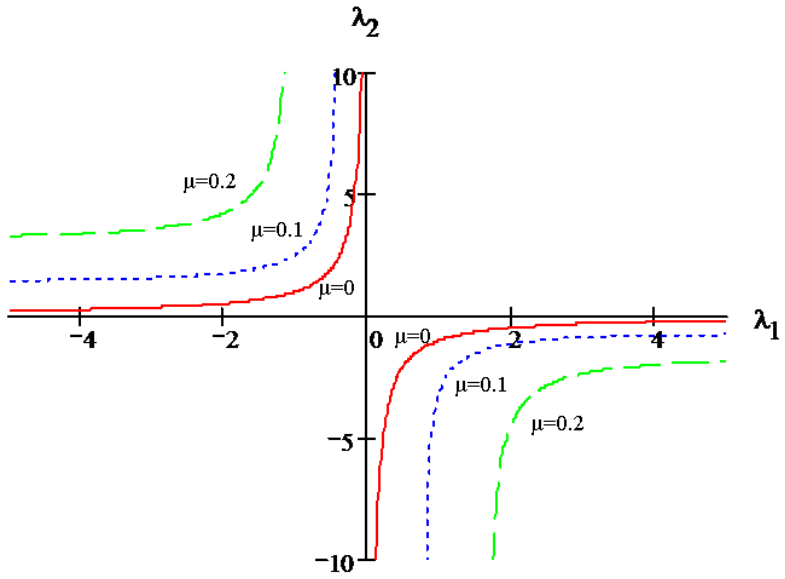

Figure 3.9 Marginal Stability Control Law Tuning when $\varepsilon = 0.8$

since $D_\phi \geq 0$. This is because $D_\phi < 0$ implies negative time in Equation 3.87 which is impossible. Considering Equation 3.137, the SDOF system can be stable when $\ln D_a > 0$, since the viscous damping is dissipating energy and might dissipate more energy than the variable stiffness device is adding to the system. In effect, the variable stiffness device is fighting or conflicting with the viscous damper. However, it makes no sense to use the variable stiffness device to add energy to the system when the goal is to dissipate as much energy as possible. Therefore, in practice, it is preferable to restrict the control law using Equation 3.140 rather than Equation 3.137.

Equation 3.140 is solved by first solving

$$\ln D_a = 0, \tag{3.141}$$

which defines when the variable stiffness device is neither dissipating nor adding energy to the system. When $\mu = 0$ and $\varepsilon \neq 0$, Equation 3.141 also defines when the undamped variable stiffness system is marginally stable. Hence, Equation 3.141 will be called the zero-energy boundary of the variable stiffness device. Regardless of initial conditions and regions (i.e. applying Equation 3.140 or Equation 3.118a) and applying Equations 3.105a,

3.58, and 3.59 results in

$$\cos^2\phi_1 = \cos^2\phi_2 \tag{3.142}$$

or

$$\frac{\psi^2}{\lambda_1^2 - 2\lambda_1\mu + 1} = \frac{\lambda_2^2\psi^2}{\lambda_2^2 - 2\lambda_2\mu + 1}. \tag{3.143}$$

Solving for λ_1 results in

$$\lambda_1 = \frac{2\mu\lambda_2 - 1}{\lambda_2} \text{ or } \lambda_1 = \frac{1}{\lambda_2}. \tag{3.144}$$

The case $\lambda_1 = \frac{1}{\lambda_2}$ is a nonswitching case and is stable. However, the other case is the settings for the controller where the variable stiffness device does no work on the system. Equivalently,

$$\lambda_1\lambda_2 - 2\mu\lambda_2 + 1 = 0. \tag{3.145}$$

Thus, the system is guaranteed to be stable or the variable stiffness device is removing energy from the system when

$$\lambda_1\lambda_2 - 2\mu\lambda_2 + 1 > 0 \tag{3.146}$$

and the variable stiffness device is adding energy to the system when

$$\lambda_1\lambda_2 - 2\mu\lambda_2 + 1 < 0. \tag{3.147}$$

Figure 3.10 identifies guaranteed stability regions for the variable stiffness system and identifies the regions where the system is either conflicted or unstable. A conflicted variable stiffness system will be defined as one where the variable stiffness device is adding energy to the system which is still stable due to dissipation from the viscous damper. Interestingly, the dynamic capability of the variable stiffness device (the range of ε) has no effect on the guaranteed stability region.

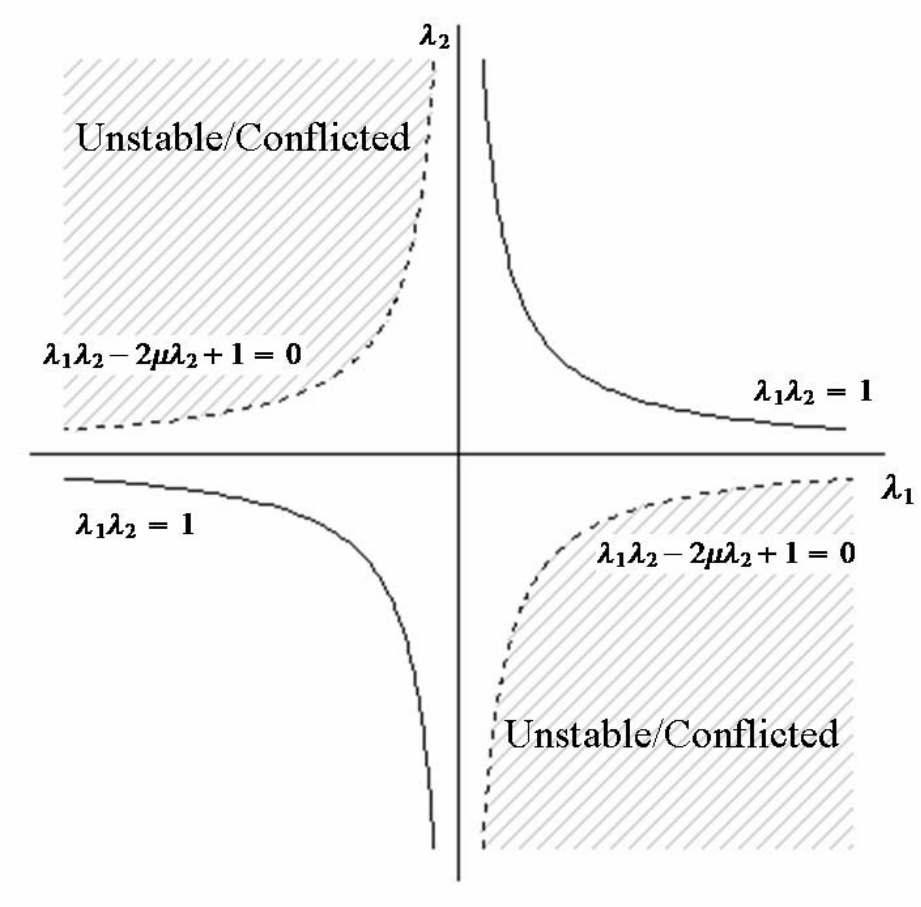

Figure 3.10 Regions where the Variable Stiffness System is Guarranteed Stable

3.12 Optimal Control Law

To maximize damping of the system, it is desired to select λ_1 and λ_2 for any fixed values of μ and ε such that Equation 3.137 is as small as possible. This is found by finding

$$\min_{\lambda_1,\lambda_2} \left(\ln D_a - \mu D_\phi\right) \tag{3.148}$$

which can be found by solving

$$\nabla \left(a\left(\phi\right) e^{-\mu t}\right) = \underline{0} \tag{3.149}$$

where $a\left(\phi\right)$ is defined by Equation 3.88 and ∇ defines the gradient operator with respect to the parameters λ_1 and λ_2. Equation 3.150 is transcendental in λ_1, λ_2 and ϕ requiring it be solved numerically. Additionally, in $\nabla \left(a\left(\phi\right) e^{-\mu t}\right)$ the parameters λ_1 and λ_2 cannot

be separated from ϕ making λ_1 and λ_2 functions of ϕ. However, the approximate solution (Equation 3.126) can be used to estimate an optimal control where λ_1 and λ_2 are constants. Considering only the amplitude term of Equation 3.126, the estimated optimal control should minimize the argument of the exponential function. Since time can be separated from the rest of the argument, the optimal control law need only satisfy the equation

$$\nabla \left(\frac{\ln D_a}{D_\phi} - \mu \right) = \underline{0} \tag{3.150}$$

where ∇ defines the gradient operator with respect to λ_1 and λ_2. Further, the solution to Equation 3.150 is constrained to only those choices of λ_1 and λ_2 where the system is stable and where the system produces oscillatory responses (i.e. the variable stiffness device mathematically switches an infinite number of times as $t \to \infty$).

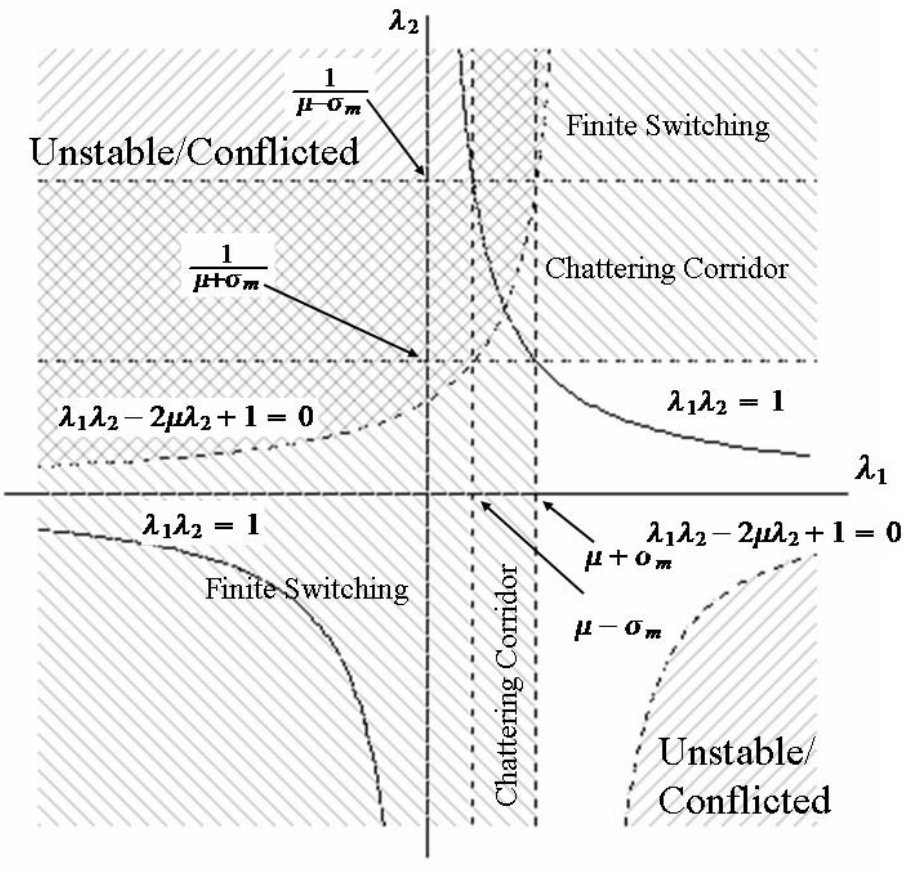

Figure 3.11 Variable Stiffness Constant Damping Candidate (Unshaded) and Non-Candidate (Shaded) Optimal Control Regions

The unstable and conflicted regions of Figure 3.10 are not candidate regions for optimal control for underdamped, critically damped, or overdamped systems. Further, in the critically damped and overdamped case, additional regions can be ruled out as candidate regions. In the "finite switching" region, the system demonstrates classical overdamped behavior after switching possibly only one time resulting in slow settling time. In the "Chattering Corridor" the system switches extremely fast, resulting in possible premature hardware failure. Figure 3.11 depicts a combination of unstable regions and overlays Figure 3.4 showing the regions where the number of switching events is finite or extremely fast. Hence, only the unshaded areas of Figures 3.10 and 3.11 are considered to be candidate regions for optimal control in the critically damped or overdamped systems.

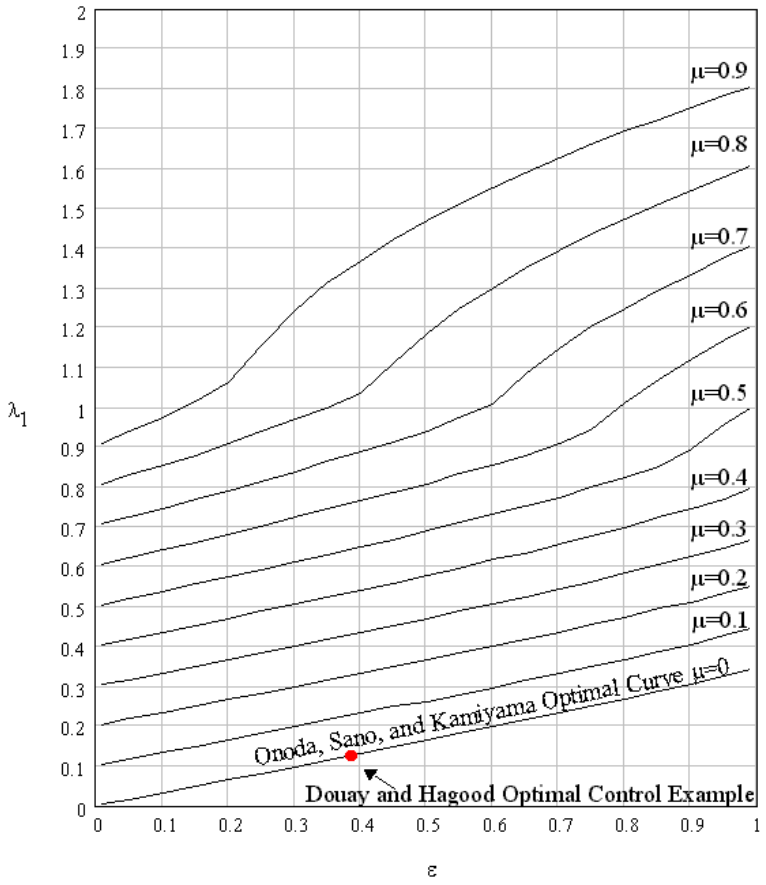

Figure 3.12 Variable Stiffness Constant Damping Optimal Control Policy ($\lambda_2 = 0$)

Equation 3.150 was solved numerically and graphed in Figure 3.12. In all cases, $\lambda_2 = 0$ while λ_1 varied with respect to μ and ε. The same result was found by Onoda et. al. for the case $\mu = 0$.[141] Attempts to find solutions where $\lambda_2 \neq 0$ resulted in a control law that can be transformed back to the case where $\lambda_2 = 0$ and λ_1 varies. Hence, it appears the control law of Equation 3.12 can be simplified. It should be noted that, because these results were developed using numerical simulation, it can only be strictly concluded that Figure 3.12 represents a local minima.

The solutions in Figure 3.12 are linear for small values of μ. For larger values of μ, the values are linear for small ε, but the optimal solution changes form for ε near 1, creating curvature. The change occurs because λ_1 cannot be set any lower without entering the chattering corridors. Hence, $\lambda_1 = \mu + \sigma_m$ in these regions. In practice, to prevent chattering of the variable stiffness controller, set $\lambda_1 > \mu + \sigma_m$.

The curve found for $\mu = 0$ appears to exactly match the optimal control curve found by Onoda et. al. [141] The point highlighted in Figure 3.12 is the same optimal control policy used by Douay and Hagood [139], found using optimal control theory. By selecting $\lambda_1 = 0.124$, $\varepsilon = 0.386$, and $\mu = 0$, a sample result reported by Douay and Hagood can be recreated. It has been noted in the literature that past work has considered control laws that are either "nonintuitive" and optimal such as the one reported by Douay and Hagood or has considered control laws that are intuitive and difficult to prove to be optimal in a conventional optimal control formulation.[140] While this difficulty still remains, the fact that Douay and Hagood's example matches the control law proposed by Onoda, Sano, and Kamiyama (Equation 3.12) suggests the two methods are equivalent.

Figure 3.13 shows the optimal exponential decay coefficient for the approximate solution. To maximize system damping, high values of μ and ε should be selected. Of particular note is the decay coefficient can be less than -1. In a passive system, setting the decay coefficient less than -1 results in a classical overdamped response. However, the benefit of variable stiffness is overdamped behavior is changed and the system no longer provides the slow settling time behavior of the classical overdamped problem. Now, it creates an oscillatory response which is much faster than the classical overdamped behavior.

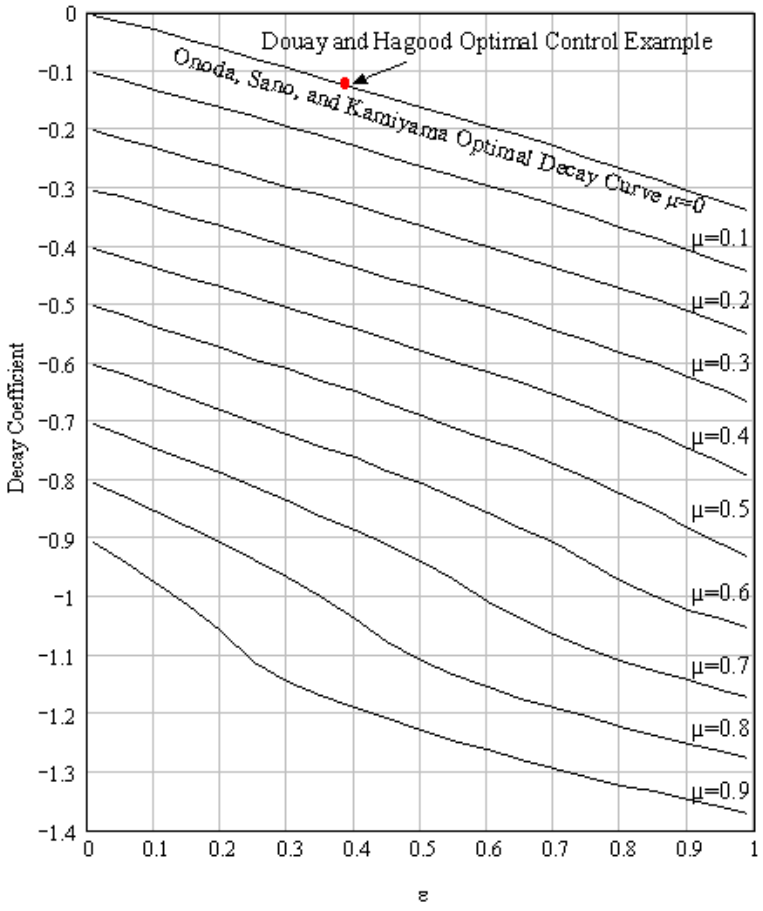

Figure 3.13 Variable Stiffness Constant Damping Optimal Exponential Decay Coefficient

3.13 Approximate Equivalent Viscously Damped System

The classical second order viscously damped system

$$\ddot{x} + 2\zeta\omega_n\dot{x} + \omega_n^2 x = 0 \tag{3.151}$$

where ζ is the damping ratio, and ω_n is the natural frequency of the system. With initial conditions $x(0) = d_0$ and $\dot{x}(0) = v_0$, this system has the following solution for the underdamped case

$$x(t) = a_0 e^{-\zeta\omega_n t}\cos[\omega_d t + \theta_0] \tag{3.152}$$

where

$$a_0 = \frac{\sqrt{d_0^2\omega_d^2 + (\dot{x}_0 + \zeta\omega_n x_0)^2}}{\omega_d}, \tag{3.153}$$

$$\theta_0 = -\tan^{-1}\left(\frac{v_0 + d_0\zeta\omega_n}{d_0\omega_d}\right), \tag{3.154}$$

and

$$\omega_d = \omega_n\sqrt{1-\zeta^2}, \tag{3.155}$$

which is called the damped natural frequency. Comparing Equation 3.152 with Equation 3.126 allows the long term behavior or an averaged equivalent natural frequency and equivalent damping ratio of the variable stiffness system to be estimated using the equations

$$-\zeta\omega_n = \left(\frac{\ln D_a}{D_\phi} - \mu\right) \tag{3.156}$$

and

$$\omega_d = \frac{\pi}{D_\phi}. \tag{3.157}$$

Solving the two equations for ζ and ω_n results in

$$\zeta = -\frac{(\ln D_a - D_\phi\mu)}{\sqrt{\pi^2 + (\ln D_a - D_\phi\mu)^2}}. \tag{3.158}$$

and

$$\omega_n = \frac{\sqrt{\pi^2 + (\ln D_a - D_\phi\mu)^2}}{D_\phi} \tag{3.159}$$

Equation 3.158 matches the theoretical damping ratio found by Douay and Hagood calculated using an energy method when $\lambda_1 = \lambda_2 = \mu = 0$.

Comparing Equations 3.151 and 3.9 suggests that

$$1 + \varepsilon u \backsim \omega_n^2 \tag{3.160}$$

and

$$\mu \backsim \zeta\omega_n. \tag{3.161}$$

The " $\backsim$ " is used to mean the quantity on the left hand side of the relationship is replaced by the quantity on the right hand side. The quantities of the relationship are not equal. In fact, since the variable stiffness device does work on the system, the quantity on the right hand side of Equation 3.161 is a combination of the equivalent damping due to this work and the viscous damping. Solving Equation 3.10 for c^* and applying approximate Equations 3.160 and 3.161 to Equation 3.1 suggests the original dimensional differential equation can be approximated as

$$m^*\ddot{x}^* + c^*_{eq}\dot{x}^* + k^*_{eq}x^* = 0, \tag{3.162}$$

where

$$c^*_{eq} = 2\zeta\omega_n\sqrt{m^*k^*}, \tag{3.163}$$

and

$$k^*_{eq} = k^*\omega_n^2 \tag{3.164}$$

with

$$k^* = \frac{k^*_1 + k^*_0}{2}. \tag{3.165}$$

Equations 3.163 and 3.164 define an approximate equivalent damping coefficient and stiffness coefficient, respectively, for the variable stiffness constantly damped SDOF problem. It is only valid for the initial value problem.

The coefficients of Equation 3.162 can be used to define two time constants. One time constant is based on the natural frequency of the approximate system which is

$$T^*_n = \sqrt{\frac{m^*}{k^*_{eq}}} = \frac{1}{\omega_n}\sqrt{\frac{m^*}{k^*}}. \tag{3.166}$$

The other is based on the damped natural frequency of the approximate system and can be calculated to be

$$T^*_d = \frac{1}{\omega_n}\sqrt{\frac{m^*}{k^*}}\frac{1}{\sqrt{1-\zeta^2}}. \tag{3.167}$$

Equation 3.167 represents the period of the approximate system with viscous damping. Equation 3.167 can be compared with the time needed to switch between stiffness states

of a variable stiffness device. If the time to switch between stiffness states is much faster than T_d^*, then the on-off control law assumption made at the beginning of this analysis should be valid. If the two time constants are close to each other, the assumption of instantaneous stiffness changes will not be valid.

Because of Equation 3.162, it is also possible to find an approximate switching control law. Since u in Equation 3.160 is an exact switching control law and ω_n^2 is an approximate natural frequency, replacing u with u_{eq} allows Equation 3.160 to be solved to determine an averaged switching law. The solution is

$$u_{eq} = \frac{\omega_n^2 - 1}{\varepsilon}. \tag{3.168}$$

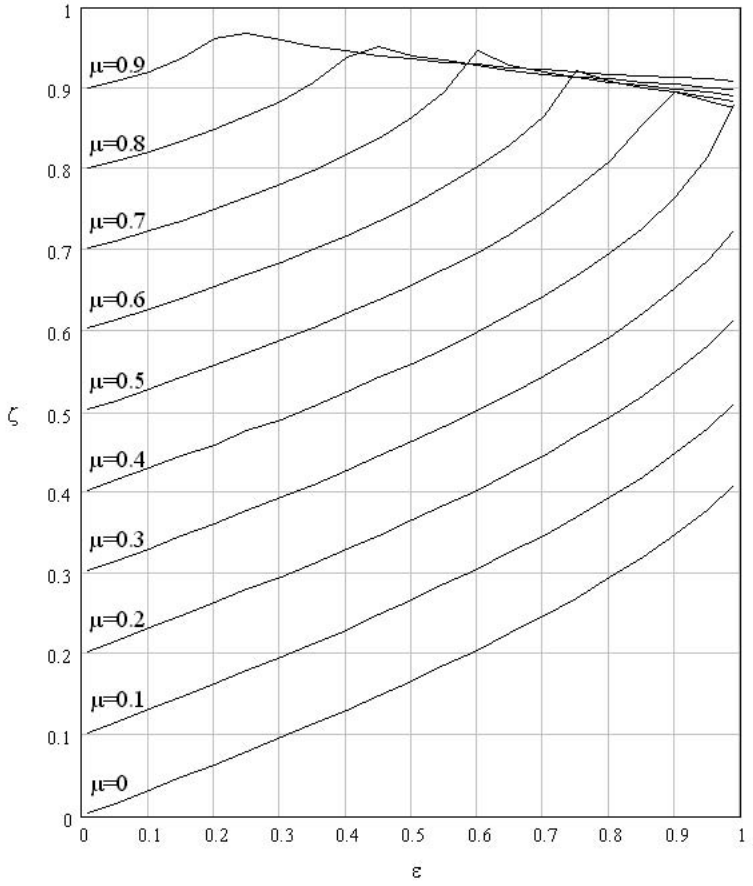

Figure 3.14 Variable Stiffness Constant Damping Optimal Equivalent Damping Ratio

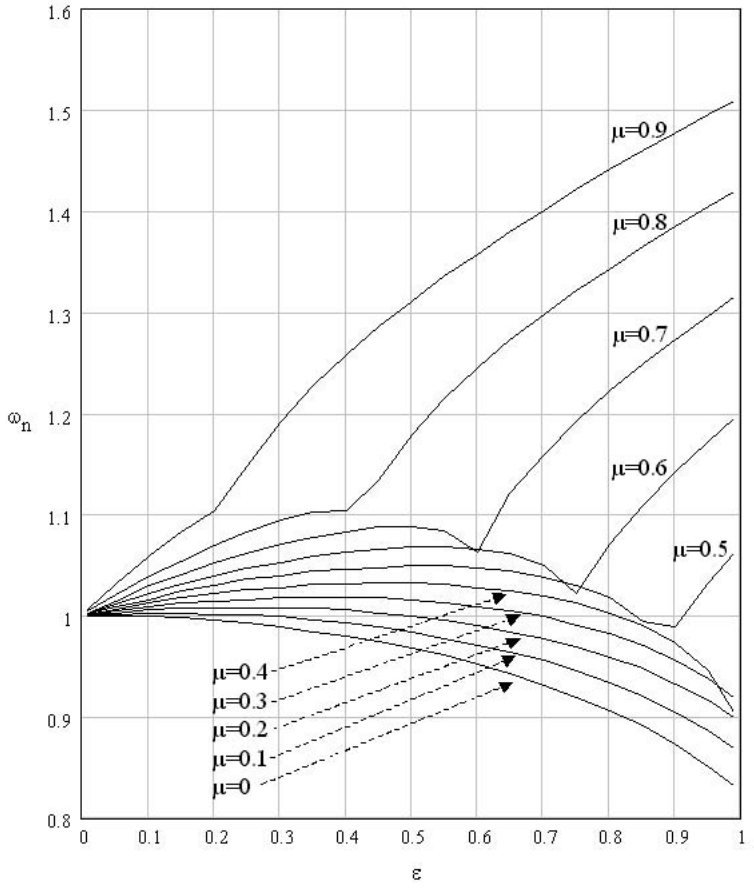

Figure 3.15 Variable Stiffness Constant Damping Optimal Equivalent Natural Frequency

Figures 3.14, 3.15, and 3.16 are graphs of Equations 3.158, 3.159 and 3.157, respectively. All graphs were created for optimal settings of λ_1 and λ_2. Figure 3.14 shows the equivalent damping ratio increases with increasing ε for low values of μ. The damping ratio seems to nearly match the optimal damping ratio found by Douay and Hagood [139]. For high values of μ, the damping ratio reaches a maximum and then slowly decreases. Because this problem is a nonlinear problem, the natural frequency of the system also varies as μ and ε vary.

Figure 3.15 shows the equivalent natural frequency always decreases when $\mu = 0$ for increasing ε. When $\mu > 0$, the natural frequency can increase to a maximum then decrease, at least for $\mu \leq 0.4$. For high values of μ, the natural frequency increases to a maximum, decreases to a local minimum, and then increases again. Comparing Figures

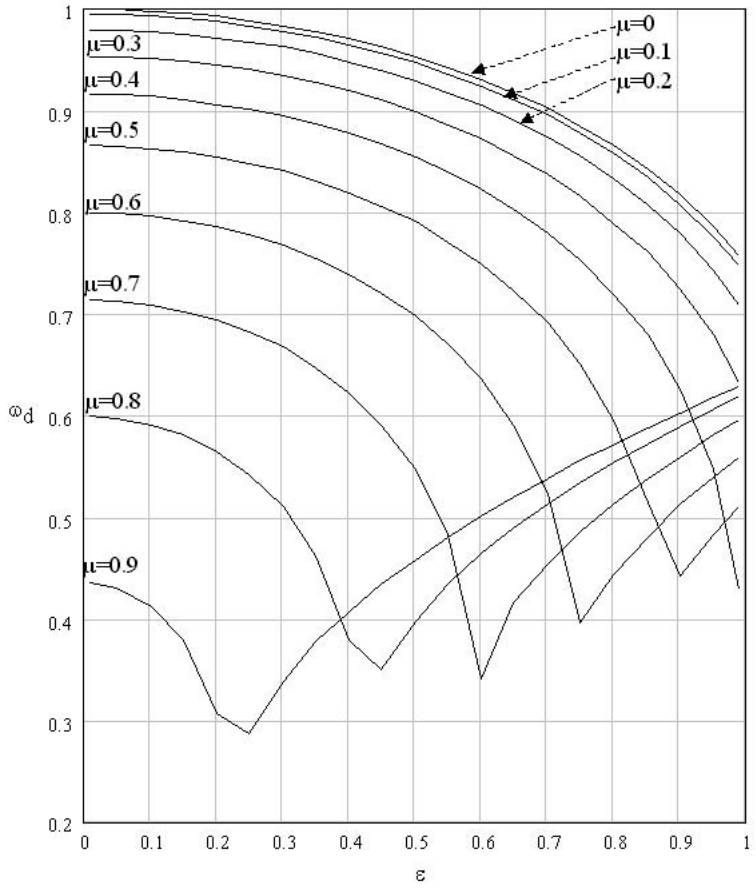

Figure 3.16 Variable Stiffness Constant Damping Optimal Equivalent Damped Natural Frequency

3.14 and 3.15 with Figure 3.13 shows a trade-off between equivalent damping ratio and natural frequency. For low values of μ, the variable stiffness device behaves more like a viscous damper, since most damping is due to an increasing damping ratio. However, for high values of μ, both damping ratio and increasing natural frequency are working synergistically to increase damping of the system. In fact, the damping ratio begins to change very little as ε changes, but the natural frequency increases dramatically. This effect is perhaps more clearly observed by considering the damped natural frequency of Figure 3.16. For low values of μ, ω_d decreases as ε increases. However, for higher values of μ, ω_d reaches a minimum and then increases.

3.14 Control Law Effects

The effect of varying λ_1 on system performance will be considered. Since the optimal control policy always makes $\lambda_2 = 0$, only varying λ_1 was considered. Figure 3.17 shows the effects of varying λ_1 for equivalent natural frequency, damping ratio, damped natural frequency, and damping coefficient. For damping ratio and damped natural frequency, increasing λ_1 increases the frequency, though the effect is bounded. On the other hand, the damping ratio is maximum when $\lambda_1 = 0$. Because frequency is shifted by changing stiffness, the optimal damping coefficient occurs when $\lambda_1 > 0$, which confirms previous discussion. Although not shown, the same basic trends were found as μ was increased. However, as μ is increased, λ_1 is restricted since setting it too low results in the variable stiffness chattering or non-switching conditions discussed earlier.

3.15 Sample Results and Validation

Sample results (found on pages 3-55 through 3-61) for the variable stiffness constant damping initial velocity problem will be presented to demonstrate the behavior of the system and to validate the analytical and approximate solutions. Although not shown, the same types of plots can be made for the initial displacement problem. For each result, graphic representation of the control law is provided followed by time response plots of the phase angle ϕ, the amplitude of the system, and the displacement. Simulated, exact, approximate solutions, and switching times are shown on these plots. The displacement plots also show a settling time envelope ($d = 0.05$) to make comparing plots simpler. Some of the time response plots show the same system with no variable stiffness ($\varepsilon = 0$) showing the effects of the variable stiffness device. Additionally, the system is shown in phase space along with switching lines calculated using Equations 3.28, 3.38, and 3.39. For some plots, an additional line is added representing ϕ_{crit} (when it exists) which is calculated using Equations 3.28 and 3.61. In all cases, the exact and simulated solutions were found to match. The simulated solution was calculated using the standard adaptive Runge-Kutta routine in Mathcad version 11. The exact and approximate solutions use the various equations discussed earlier in this chapter. The approximate solution is only valid when the system is switching. When the system is not switching it is a simple viscously damped

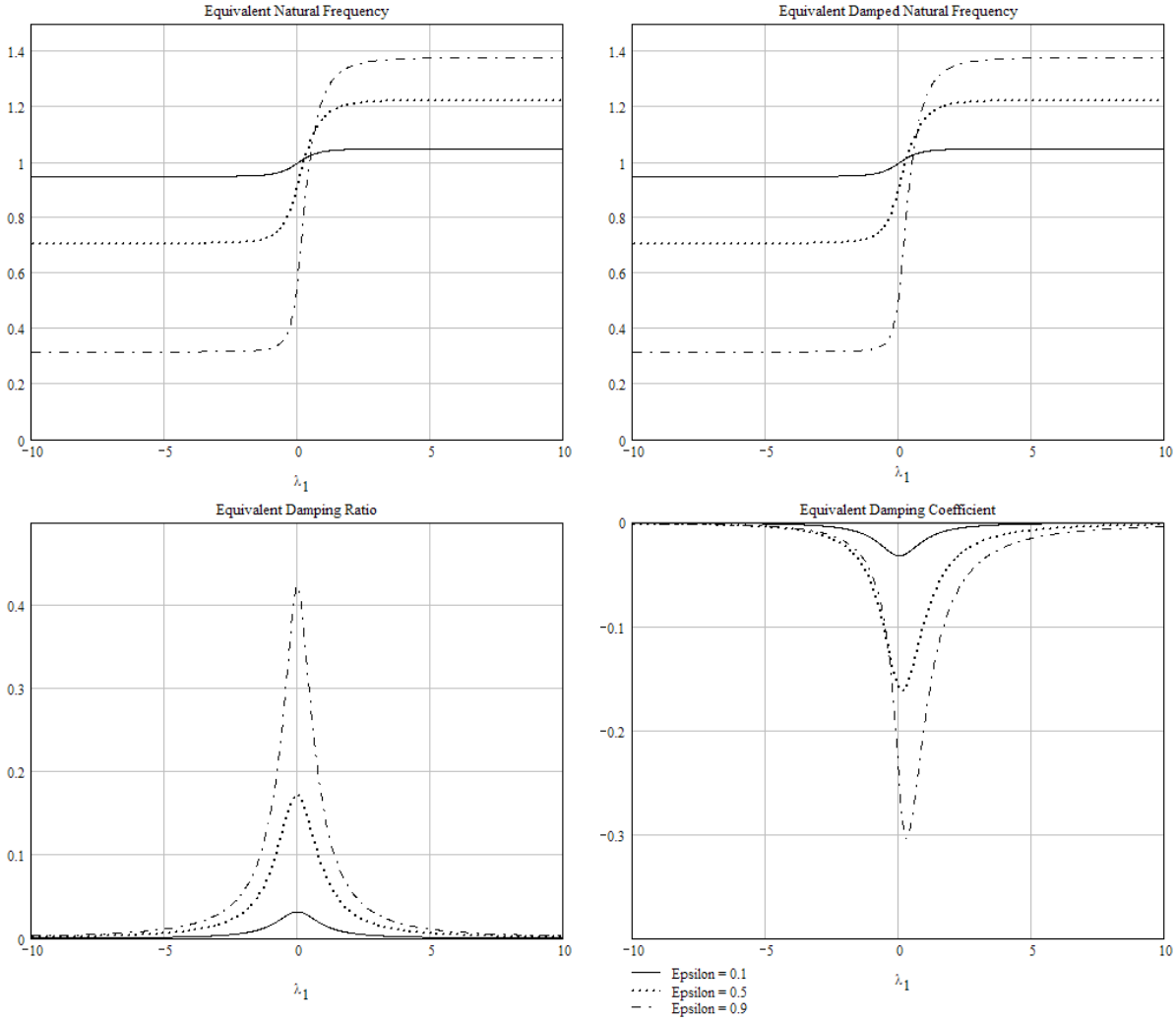

Figure 3.17 System Effects of Varying λ_1 for $\mu = 0$

system and no approximate solution is needed since it can be found using standard linear theory.

Figure 3.18 shows several response plots of an optimally controlled underdamped system with no viscous damping. The plot of the λ_1 and λ_2 plane graphically marks the tuning of the control law on a plot similar to Figure 3.10. As previously demonstrated in the literature, the variable stiffness device is effectively suppressing vibration. Both the phase ϕ and amplitude of the system have oscillatory behavior. The scale for the phase ϕ was divided by π making it easy to see the length of a period is π. The approximate solution

predicts first order behavior for phase and amplitude, but is missing the oscillatory behavior of the true solution. For long time behavior, however, the error between approximate and exact solutions gets progressively smaller, as demonstrated by the amplitude, time response, and phase plane plots.

Figure 3.19 shows a sample underdamped system with viscous damping. The same basic trends can be seen showing the oscillatory behavior in all plots and showing the approximate solution becoming more accurate for the long time behavior of the system. Clearly, the variable stiffness device has increased the damping of the system, since it performs much better than the equivalent system with no variable stiffness. As expected, the settling time for Figure 3.19 is lower than the settling time for Figure 3.18.

Figure 3.20 shows the slow behavior of a suboptimal overdamped system. In the λ_1 and λ_2 plane plot, boundaries lines that are functions of σ_m and μ are graphed. These boundaries were also graphed in Figure 3.11 and make it easy to identify which region. The controller was tuned so that ϕ_{crit} exists and ϕ asymptotically approaches this boundary. In this case, the controller switched the stiffness device one time and then never switched again. The phase plot shows the trajectory following the line defined by the angle ϕ_{crit}. A viscously damped system has much better behavior than this system does using the variable stiffness device. Designing the system with this type of controller would result in undesirable response and should be avoided. The exact solution is not completely plotted as compared to the simulated solution since it requires selecting successive values of ϕ closer and closer to ϕ_{crit} to solve for larger time values, since ϕ asymptotically approaches ϕ_{crit}. While this could be done using an appropriate function, it provides no new information and was not done.

Figure 3.21 shows another suboptimal overdamped system. The variable stiffness controller begins in a stable configuration and then switches. After that, it switches very rapidly and never slows down. Despite the controller instability, the system itself is stable. In this case, ϕ oscillates about ϕ_1 at a very rapid rate and the oscillations are very small. The switching was omitted from the displacement plot because it would have blotted out the other plots. The behavior of the system is much better than in Figure 3.20, but the

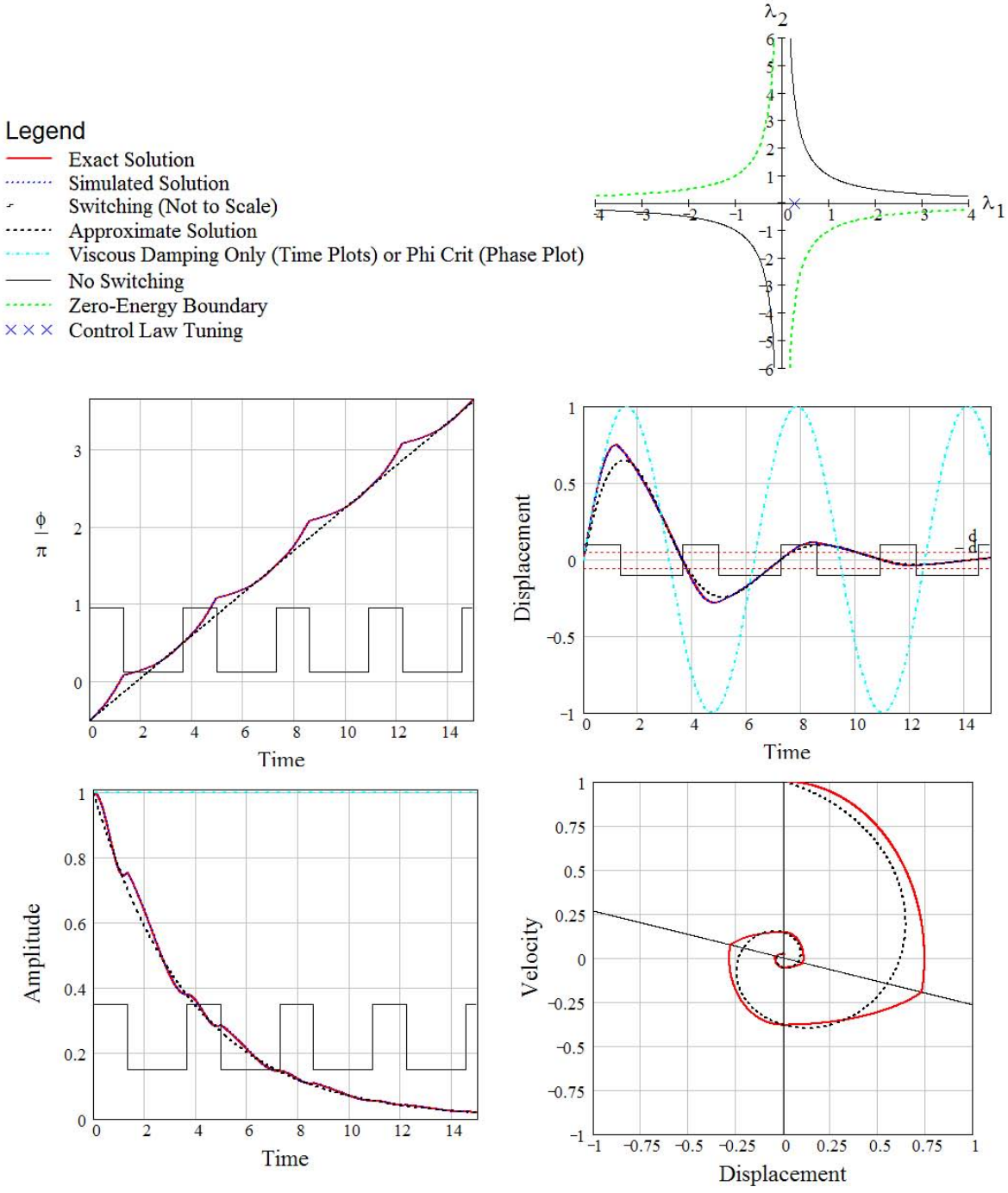

Figure 3.18 Sample Optimal Underdamped System with no Viscous Damping ($\lambda_1 = .266$, $\lambda_2 = 0$, $\mu = 0$, $\varepsilon = 0.8$)

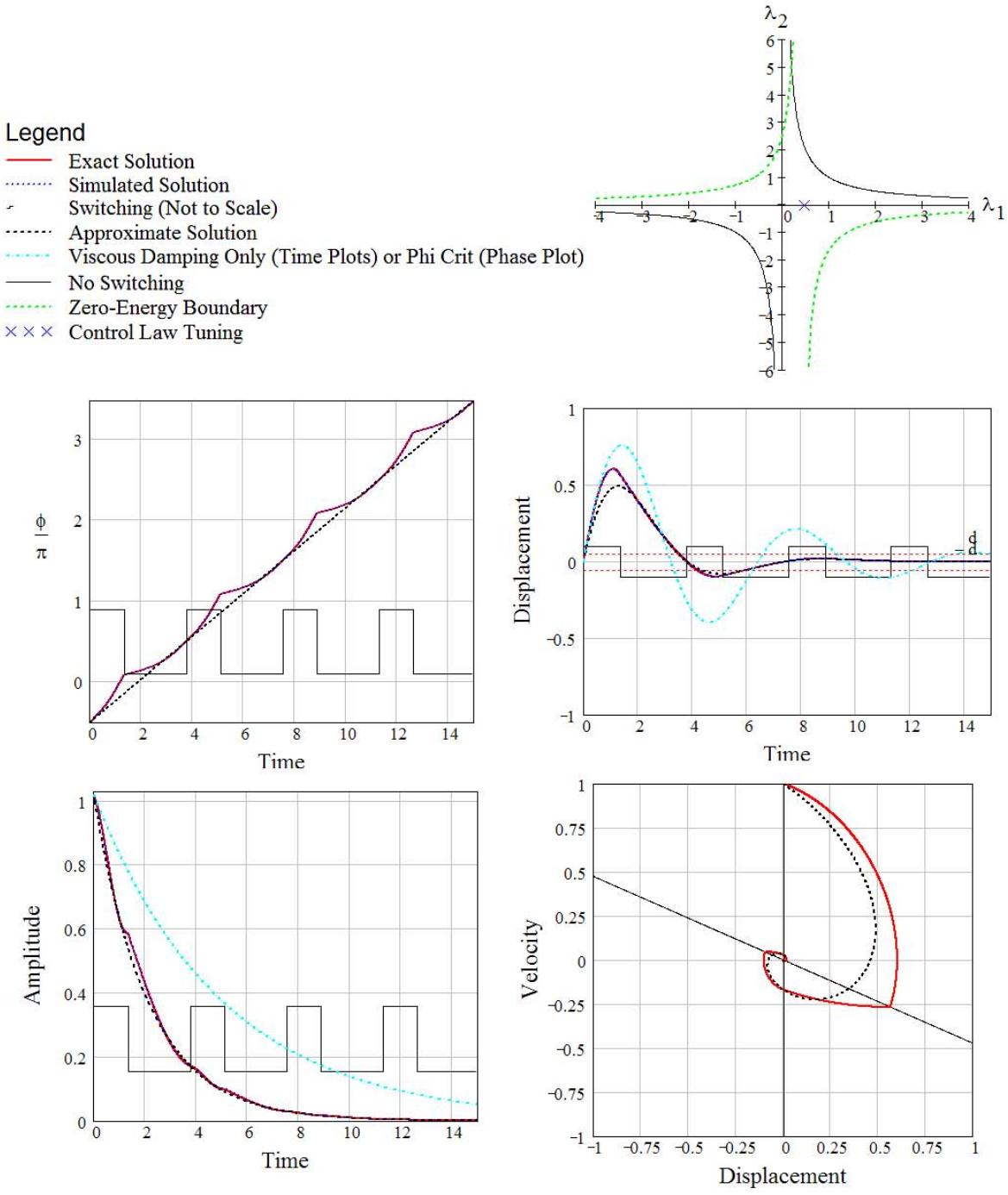

Figure 3.19 Sample Optimal Underdamped System with Viscous Damping ($\lambda_1 = .473$, $\lambda_2 = 0$, $\mu = 0.2$, $\varepsilon = 0.8$)

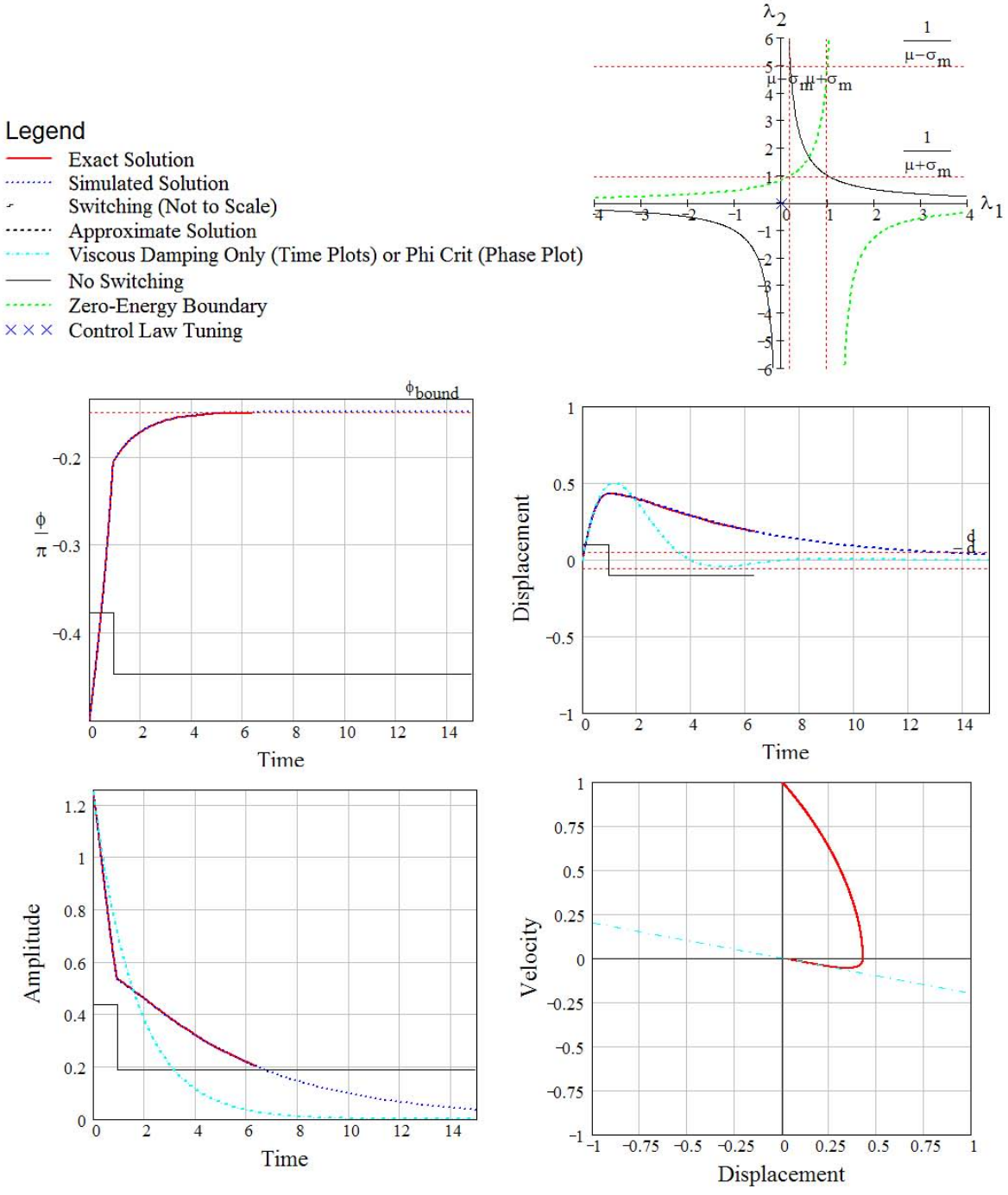

Figure 3.20 Sample SubOptimal Overdamped System ($\lambda_1 = 0$, $\lambda_2 = 0$, $\mu = 0.6$, $\varepsilon = 0.8$)

controller chattering has the potential of damaging hardware. Therefore, this tuning of the controller should be avoided.

Figure 3.22 shows an optimal overdamped system. The setting for λ_1 is only slightly beyond the region where the controller becomes unstable, resulting in a response like Figure 3.21. To be safe, λ_1 may need to be increased more to account for modelling uncertainty. The response of this optimal system shows good settling time and has avoided the controller instability. The phase plot of this system is very similar to Figure 3.21, but it does not have the oscillatory switching behavior.

Figure 3.23 shows the results of selecting the controller to make the system marginally stable in a classical sense. For a system with no damping, the settings for λ_1 and λ_2 that create a marginally stable system can be found exactly using Equation 3.145. With damping added, finding the point of marginal stability requires solving Equation 3.138 using numerical methods. Essentially, this is one point on the curve $\mu = 0.2$ of Figure 3.9 where the energy the variable stiffness device is adding to the system is equal to the amount of energy the viscous damper is dissipating. As expected, a viscously damped system with no variable stiffness will behave much better than a marginally stable system since the variable stiffness device is cancelling out the viscous damper. Finally, the phase plane shows the orbit trajectory the system follows. The approximate solution provides an excellent first order approximation of the orbit by creating an ellipse.

3.16 Energy Usage

From the literature, changing the stiffness of the system does work on the system [4]. Switching the variable stiffness device requires energy and is the system input that can cause marginal stability or instability. Because the exact switching times for the variable stiffness device are known, it is possible to calculate the exact work going into the variable stiffness device used to suppress vibration. Theoretically, it is also possible to calculate the work the variable stiffness device is applying to the system. Finally, with expressions for work out and work in, one could be divided by the other to create an efficiency factor. In practice the actual analytic calculations are too complex to provide much insight. Hence,

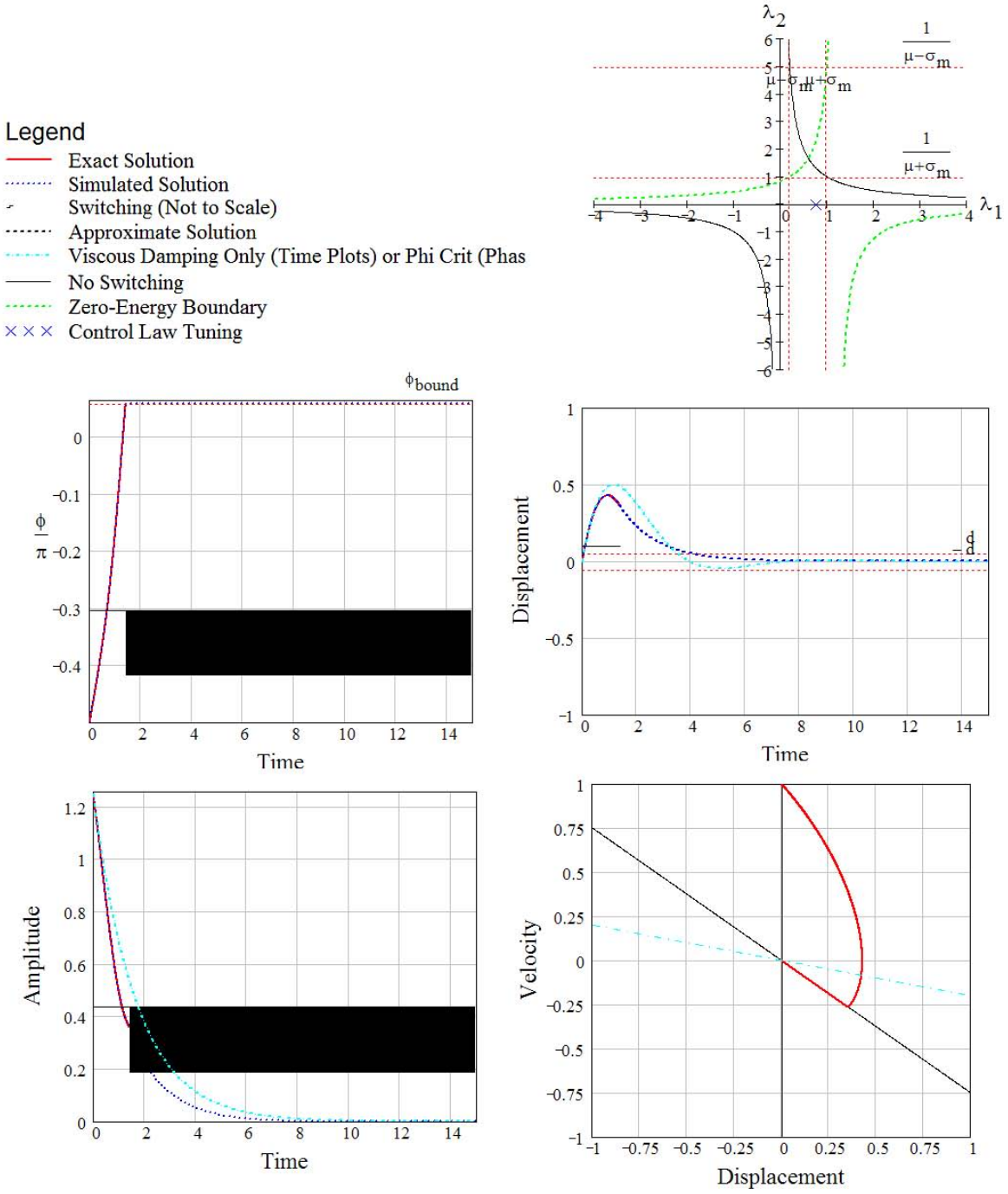

Figure 3.21 Sample SubOptimal Overdamped System Controller Instability ($\lambda_1 = 0.75$, $\lambda_2 = 0$, $\mu = 0.6$, $\varepsilon = 0.8$)

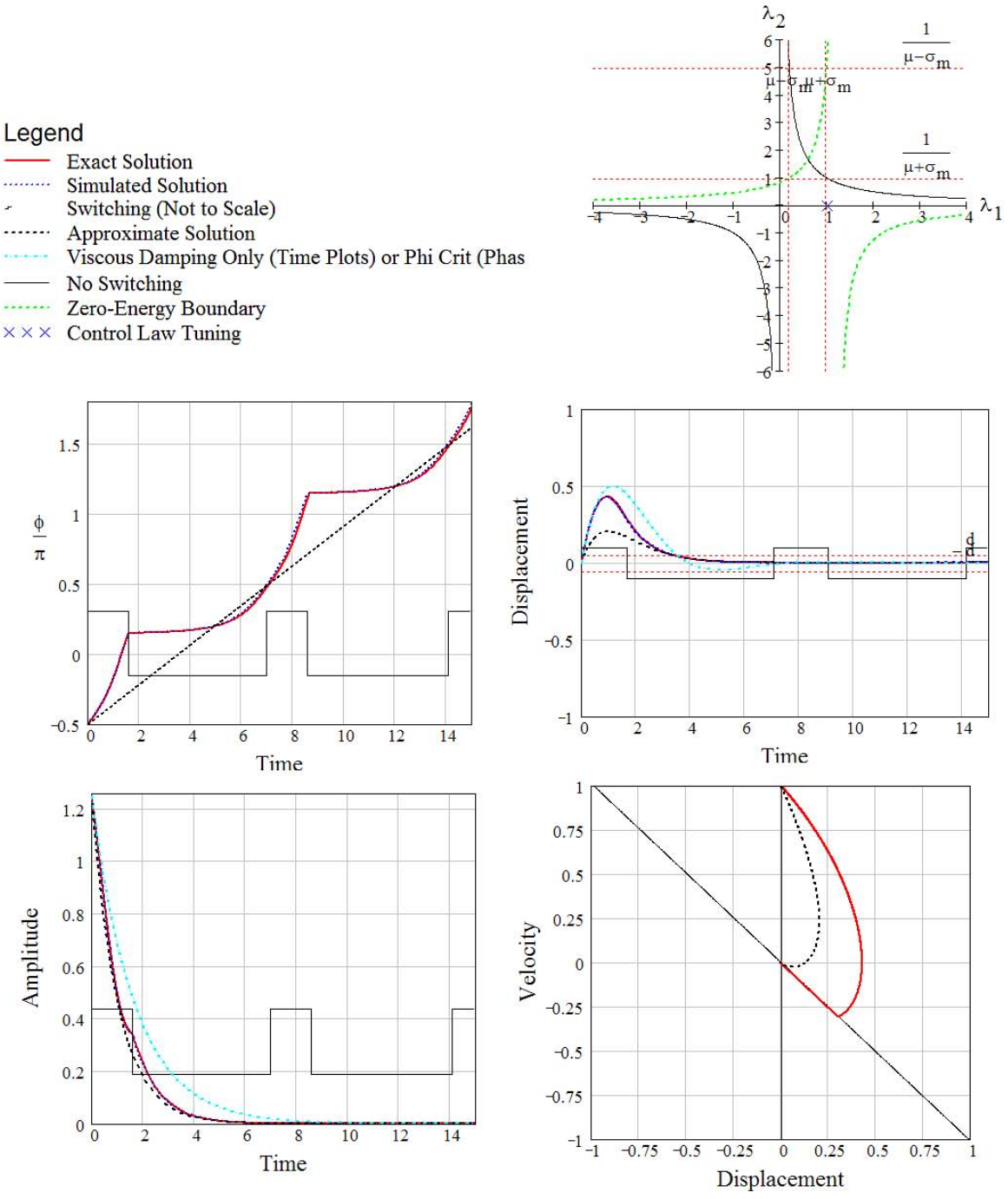

Figure 3.22 Sample Optimal Overdamped System ($\lambda_1 = 1.01$, $\lambda_2 = 0$, $\mu = 0.6$, $\varepsilon = 0.8$)

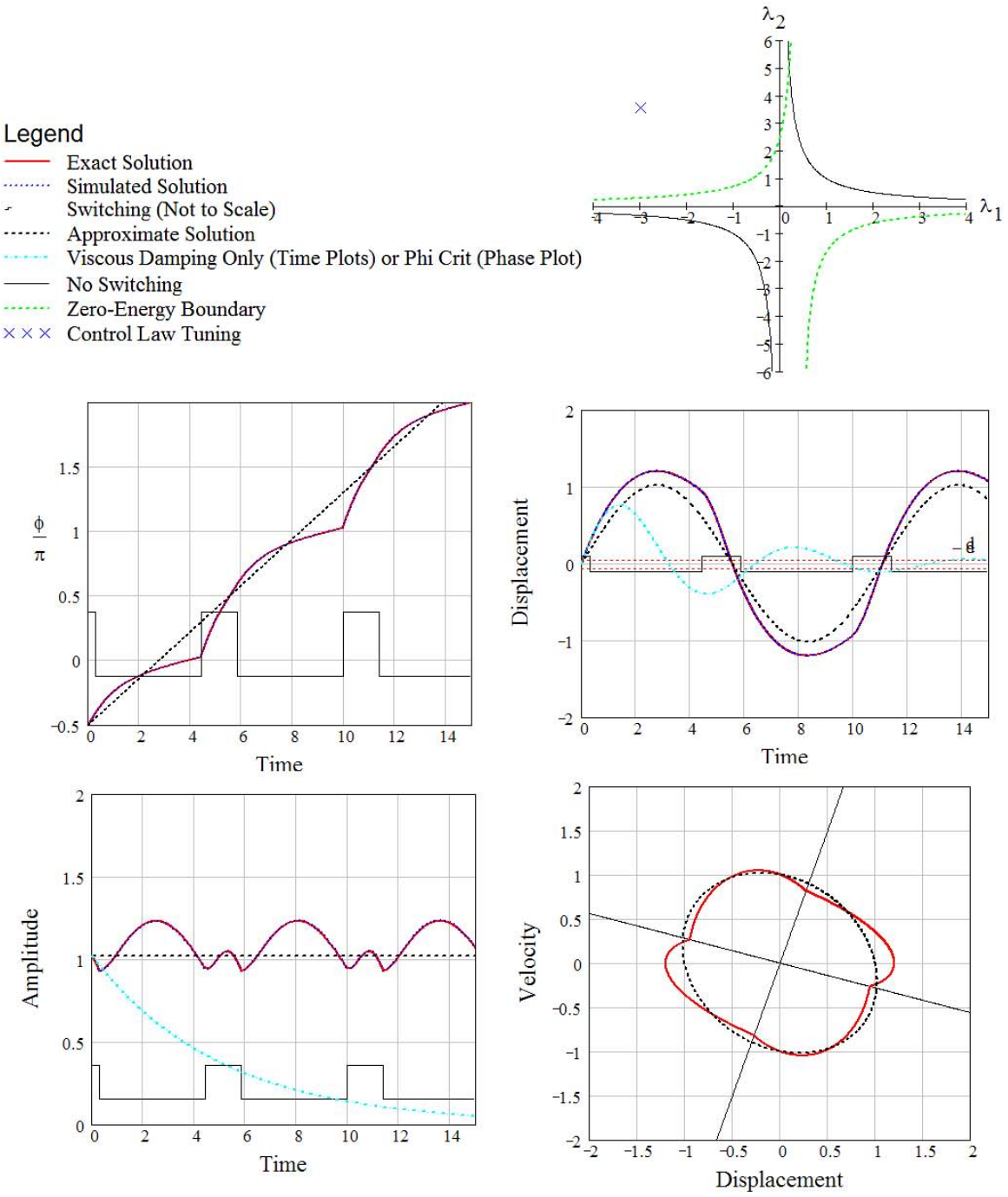

Figure 3.23 Sample Orbit in an Underdamped System ($\lambda_1 = -3$, $\lambda_2 = 3.566$, $\mu = 0.2$, $\varepsilon_k = 0.8$)

this efficiency factor is probably best calculated numerically for specific systems. The following discussion provides detail of how to calculate both types of work.

Work In. Work is defined as

$$W_{in} = Pt \tag{3.169}$$

where W is the work done by the variable stiffness device, P is the average power expended by the variable stiffness device during time t, and t is the time the device uses power. Since the variable stiffness device switches between two states, the power needed for each state must be known and the time spent in each state must be calculated. The power to switch the variable stiffness device can be found by measuring the energy input to the variable stiffness device and has been done on various devices in the literature. Determining the time spent in each stiffness setting requires making use of the exact switching times (Equations 3.99, 3.91, 3.100, 3.108 and 3.114 depending on initial conditions). Only the energy used for the initial velocity problem will be discussed, since the initial displacement problem is similar. Further, only the long term behavior will be considered. That is, the work for a partial period of ϕ will be ignored.

To begin, define P_p as the power used by the variable stiffness device when $u = 1$ and P_m as the power used when $u = -1$. It is likely that $P_m = 0$, but this is not required. Next, the interval of time where $u = 1$ is defined as

$$t_p = \begin{cases} D_\phi - \Gamma_{\phi_m}(\phi_1, \phi_2) & \text{if } Reg_1 \\ D_\phi - \Gamma_{\phi_m}(\phi_2, \phi_1) & \text{if } Reg_2 \\ \Gamma_{\phi_p}(\phi_1, \phi_2) & \text{if } Reg_3 \\ \Gamma_{\phi_p}(\phi_2, \phi_1) & \text{if } Reg_4 \end{cases} \tag{3.170}$$

and the interval of time where $u = -1$ is defined as

$$t_m = \begin{cases} \Gamma_{\phi_m}(\phi_1, \phi_2) & \text{if } Reg_1 \\ \Gamma_{\phi_m}(\phi_2, \phi_1) & \text{if } Reg_2 \\ D_\phi - \Gamma_{\phi_p}(\phi_1, \phi_2) & \text{if } Reg_3 \\ D_\phi - \Gamma_{\phi_p}(\phi_2, \phi_1) & \text{if } Reg_4 \end{cases}. \tag{3.171}$$

Because initial conditions make it possible to start in the middle of a switching cycle, the initial time is

$$t_{p0} = \begin{cases} \Gamma_{\phi_p}(\phi_0, \phi_1) & \text{if } Reg_1 \\ \Gamma_{\phi_p}(\phi_0, \phi_2) & \text{if } Reg_2 \\ 0 & otherwise \end{cases} \tag{3.172}$$

when $u = 1$ and

$$t_{p0} = \begin{cases} \Gamma_{\phi_m}(\phi_0, \phi_1) & \text{if } Reg_3 \\ \Gamma_{\phi_m}(\phi_0, \phi_2) & \text{if } Reg_4 \\ 0 & otherwise \end{cases} \tag{3.173}$$

where $u = -1$. The total work done on the system due to the variable stiffness device is

$$W_{in} = (W_p + W_m)\, n + W_{p0} + W_{m0} \tag{3.174}$$

where $W_p = P_p t_p$, $W_m = P_m t_m$, $W_{p0} = P_{p0} t_{p0}$, $W_{m0} = P_{m0} t_{m0}$ and n is defined by Equation 3.110. The normalized energy used by the system is

$$E = \frac{W - W_{p0} - W_{m0}}{W_p + W_m} = n. \tag{3.175}$$

Using Equations 3.123 and 3.120, the work and normalized energy needed to achieve a desired settling time can be estimated as

$$W \approx (W_p + W_m)\left(\frac{t_s}{D_\phi} + \frac{\phi_0}{\pi} - \theta_e\right) + W_{p0} + W_{m0} \tag{3.176}$$

and

$$E \approx \frac{t_s}{D_\phi} + \frac{\phi_0}{\pi} - \theta_e \tag{3.177}$$

where t_s is the desired settling time.

Work Out. The exact work the variable stiffness device performs on the system can be found by solving Equation 3.9 for $\ddot{x}$, multiplying through by $\dot{x}$, and then integrating from time 0 to a desired settling time. The work is

$$W_{out} = \int_0^{t_s} \ddot{x}\dot{x}dt = -2\mu \int_0^{t_s} \dot{x}^2 dt - \int_0^{t_s} (1 + \varepsilon u)\, x\dot{x}dt. \tag{3.178}$$

In theory, substituting Equations 3.17, 3.18, 3.30, and 3.87 into Equation 3.178 and then integrating determines the work the variable stiffness device performs on the system. Unfortunately, performing the integrations is very difficult and probably should only be performed numerically for a specific system. Alternatively, the approximate work done by the variable stiffness device can be computed as

$$W_{out} = \int_0^{t_s} \ddot{x}\dot{x}dt = -2\zeta\omega_n \int_0^{t_s} \dot{x}^2 dt - \omega_n^2 \int_0^{t_s} x\dot{x}dt. \tag{3.179}$$

Substituting Equations 3.126 and 3.127 into 3.179 and performing the integration provides the approximate work the variable stiffness device performs. This is much easier to do, but tedious and creates a complicated analytic expression. Once again, it is probably easier to complete the integrations numerically for a specific system.

3.17 Variable Stiffness Design Metrics

As a result of this analysis, design metrics will now be identified and summarized. Theoretically, using the previous section, $\frac{W_{out}}{W_{in}}$ can be defined, which is an efficiency factor that could be used to compare variable stiffness devices with each other. Clearly, it is preferable to make $\frac{W_{out}}{W_{in}}$ as close as possible to unity, making the variable stiffness device as efficient as possible. Another important metric is the decay factor shown graphically in Figure 3.13, which identifies performance of a variable stiffness device in this system. Here, it is preferable to make the decay coefficient as large as possible. This is accomplished by maximizing ε and μ. The parameter ε, identified in Table 2.2, roughly links real variable

stiffness devices to system performance. Since ε should be made as large as possible, Table 2.2 can be used to select an appropriate variable stiffness device. Finally, Equation 3.167 defines the period of the system, which can be used to validate the instantaneous on-off control law assumption in any particular real system. This may limit which variable stiffness device can be chosen using Table 2.2 since this analysis is only valid when the system time constant is much larger than the time required to switch the variable stiffness device from one stiffness level to another. These metrics with supporting analysis represent a set of tools for selecting and using a variable stiffness device in a real structure.

3.18 Conclusion

A SDOF variable stiffness constantly damped system using a general on-off control law has been studied. For the initial value problem, both an exact and an approximate solution were developed. The approximate solution was found to provide a good estimate for the long term behavior of the system. In the process, insight was found about how tuning the system changes the behavior of the system. It was found that the control law could be tuned to create conditions ranging from no switching to extremely rapid switching. It was also possible to make the controlled system stable, marginally stable, or unstable. The control law was optimized creating the most damping possible for any possible variable stiffness strength and for a given viscous damper. The energy use of the variable stiffness device was analytically estimated. Finally, four metrics for understanding variable stiffness systems were identified. The results provide a new set of engineering tools for selecting and designing variable stiffness compensators.

In the next Chapter, the same SDOF variable stiffness problem with the same two parameter control law will be analyzed, except a sinusoidally forced version of the problem will be considered. Because of the nonlinear nature of variable stiffness, the results found in this Chapter for the unforced problem do not apply when other forcing functions are used. It will be seen that the optimal control policy for the forced problem is quite different from that of the unforced problem.

4. Variable Stiffness SDOF Sinusoidally Forced Problem

4.1 Introduction and Problem Statement

The forced problem is significantly different from the unforced problem because the forcing function adds new complexity to the control law. The unforced problem could be solved exactly because an exact expression for the switching could be developed. Finding the switching times analytically for the forced problem proved to be very difficult. Hence, approximation approaches were used instead.

Three different approaches were tried to gain insight into the forced problem and compared to the simulated system. The first method is a direct approximation approach which compares the exact equations of motion with a viscously damped system. An equivalent stiffness and damping coefficient are calculated for the viscously damped system. The resulting linear equation is easily solved and allows generation of frequency response plots as well as phase for the system. In a second method, both the solution and switching control law were expanded in a Fourier series. The switching control law used only the first oscillatory term in the solution. The control law Fourier series coefficients were written in terms of the solution Fourier series coefficients which generated nonlinear algebraic equations. Unfortunately, these equations were so nonlinear the coefficients could not be solved for in analytic form. This method will not be presented since it became intractable. The third method tried which will be presented is to use a perturbation method. The results of the perturbation method and the direct method were very similar. Hence, the perturbation method provides insight into the region of validity for the solution and represents a systematic approach for improving the accuracy of the resulting approximate solution. On the other hand, the direct method is more physically based than the perturbation approach which clearly identifies the work the variable stiffness device performs on the system.

Both methods provide reasonable accuracy when ε is small. However, for large ε both fail to capture other nonlinear effects. The main reason for the poor performance is because the methods fail to capture harmonics associated with the true nonlinear system. Because of the type of control law being used, the harmonics change both the solution and

the switching times for the control law. In theory, the Fourier series approach could have captured these effects. However, because the nonlinear algebraic equations could not be solved analytically, the ability to develop insight with this approach was severely limited.

The forced problem will be defined as

$$m^*\ddot{x}^* + c^*\dot{x}^* + \frac{1}{2}\left[(k_1^* + k_0^*) + (k_1^* - k_0^*)\,u\right]x^* = A^*\cos\left(\omega^* t^*\right), \tag{4.1}$$

where ω^* is the forcing frequency and A^* is the amplitude of the forcing function. Similar to the discussion in Chapter 3.2, when the right control law is used, Equation 4.1 can be used to represent a variable stiffness system using a piezoelectric device. Equation 4.1 can be nondimensionalized to become

$$\ddot{x} + 2\mu\dot{x} + (1 + \varepsilon u)\,x = \cos\left(\omega t\right). \tag{4.2}$$

The nondimesionlization is accomplished using Equations 3.4, 3.7, and 3.8 while letting

$$L^* = \frac{A^*}{m^*\omega_0^{*2}} \tag{4.3}$$

and

$$\omega = \frac{\omega^*}{\omega_0^*} \tag{4.4}$$

The initial conditions for the problem will be discussed later.

4.2 Direct Approximation

To gain insight into the solution of Equation 4.2, the viscously damped system

$$\ddot{x}_e + 2\mu_e\dot{x}_e + \omega_e^2 x_e = \cos\left(\omega t\right), \tag{4.5}$$

will be defined so Equations 4.5 and 4.2 behave in a similar dynamic way by selecting an effective damping coefficient $\mu_e = \mu_e\left(\omega, \lambda_1, \lambda_2, \mu, \varepsilon\right)$ and an effective natural frequency

$\omega_e = \omega_e(\omega, \lambda_1, \lambda_2, \mu, \varepsilon)$. The frequency ω_e will be defined as

$$\omega_e^2 = 1 + \varepsilon u_e \tag{4.6}$$

where $u_e = u_e(\omega, \lambda_1, \lambda_2, \mu, \varepsilon)$ is the effective switching control law. The subscript "e" identifies the variable as the effective behavior of the true variable it represents. Subtracting Equation 4.5 from Equation 4.2 defines the comparison differential equation

$$\ddot{y} + 2\mu\dot{y} + (1 + \varepsilon u)\, y + 2(\mu - \mu_e)\, \dot{x}_e + \varepsilon (u - u_e)\, x_e = 0, \tag{4.7}$$

where

$$y = x - x_e. \tag{4.8}$$

Ideally, μ_e and u_e would be chosen such that $y = \dot{y} = \ddot{y} = 0$. In reality, Equation 4.7 only holds under this restriction when $\mu_e = \mu$ and $u_e = u$. However, because x_e and x are periodic functions, it is possible to find an averaged value for μ_e and u_e so that Equation 4.7 is true for a set of points.

Based on Meirovitch [71], the particular solution to Equation 4.5 is

$$x_e = \Psi \cos(\omega t + \theta) \tag{4.9}$$

where

$$\Psi = \Psi(\omega, \lambda_1, \lambda_2, \mu, \varepsilon) = \frac{1}{\sqrt{\left(\omega_e^2 - \omega^2\right)^2 + \left(2\mu_e\omega\right)^2}} \tag{4.10}$$

and

$$\theta = \theta(\omega, \lambda_1, \lambda_2, \mu, \varepsilon) = -\tan^{-1} \frac{2\mu_e\omega}{\omega_e^2 - \omega^2}. \tag{4.11}$$

The variable stiffness term of Equation 4.2 is simultaneously creating damping and shifting the natural frequency of the system, so the damping and frequency contributions need to be separated. The effective stiffness will be solved approximately by averaging the control u over a period. The effective damping of the system will be found by calculating the work done on the system by changing the spring stiffness.

Effective Stiffness. The averaged value for u_e can be found as

$$u_e = \frac{1}{T}\int^{T} u(\tau)\, d\tau \tag{4.12}$$

where T is the period of u. Calculating u_e requires knowing the length of time the variable stiffness device spends in each state as defined by Equation 4.2. The switching time can be approximated by substituting Equation 4.9 into Equation 3.12 and simplifying as

$$u = sgn\left[\left(\lambda_1 - \omega\tan^{-1}(\omega t + \theta)\right)\left(1 - \lambda_2\omega\tan^{-1}(\omega t + \theta)\right)\right] \tag{4.13}$$

The switching times are

$$t_1 = \frac{1}{\omega}\left(\tan^{-1}\left(\frac{\lambda_1}{\omega}\right) - \theta\right) \tag{4.14}$$

and

$$t_2 = \frac{1}{\omega}\left(\tan^{-1}\left(\frac{1}{\lambda_2\omega}\right) - \theta\right). \tag{4.15}$$

Note that θ has not yet been determined since it depends on u_e, but will be found later. Since t_1 and t_2 are defined in terms of the arctangent function, t is periodic and it has period

$$T = \frac{\pi}{\omega}. \tag{4.16}$$

Then the system switches when

$$t = t_1, t_1 + T, t_1 + 2T, ... \tag{4.17}$$

and when

$$t = t_2, t_2 + T, t_2 + 2T, ... \tag{4.18}$$

When $t_1 < t_2$, then switching events will occur in order from smallest to largest time as

$$t = t_1, t_2, t_1 + T, t_2 + T, ... \tag{4.19}$$

Table 4.1 Variable Stiffness Constant Damping Forced Problem Control Law Values for One Time Period

	$t_1 < t_2$		$t_2 < t_1$	
	$\lambda_2 \geq 0$	$\lambda_2 < 0$	$\lambda_2 \geq 0$	$\lambda_2 < 0$
$u = -1$	$t_1 < t < t_2$	$t_2 < t < t_1 + T$	$t_2 < t < t_1$	$t_1 < t < t_2 + T$
$u = 1$	$t_2 < t < t_1 + T$	$t_1 < t < t_2$	$t_1 < t < t_2 + T$	$t_2 < t < t_1$

and likewise, if $t_2 < t_1$, then switching events will occur in order from smallest to largest time as

$$t = t_2, t_1, t_2 + T, t_1 + T, ... \tag{4.20}$$

From Equation 3.12, the length of time that $u = \pm 1$ can be found by solving the inequalities

$$\left(\lambda_1 - \omega \tan^{-1}(\omega t + \theta)\right)\left(1 - \lambda_2 \omega \tan^{-1}(\omega t + \theta)\right) > 0 \tag{4.21}$$

and

$$\left(\lambda_1 - \omega \tan^{-1}(\omega t + \theta)\right)\left(1 - \lambda_2 \omega \tan^{-1}(\omega t + \theta)\right) < 0. \tag{4.22}$$

Table 4.1 identifies conditions and time intervals that $u = \pm 1$ over one period of time T.

Using Table 4.1, it is now possible to solve Equation 4.12 as

$$u_e = \frac{1}{T}\begin{cases} -\int_{t_1}^{t_2} d\tau + \int_{t_2}^{t_1+T} d\tau & \text{if } t_1 < t_2 \wedge \lambda_2 \geq 0 \\ \int_{t_1}^{t_2} d\tau - \int_{t_2}^{t_1+T} d\tau & \text{if } t_1 < t_2 \wedge \lambda_2 < 0 \\ -\int_{t_2}^{t_1} d\tau + \int_{t_1}^{t_2+T} d\tau & \text{if } t_2 < t_1 \wedge \lambda_2 \geq 0 \\ \int_{t_2}^{t_1} d\tau - \int_{t_1}^{t_2+T} d\tau & \text{if } t_2 < t_1 \wedge \lambda_2 < 0 \end{cases} \tag{4.23}$$

which simplifies to

$$u_e = \begin{cases} 1 - \frac{2\omega}{\pi}|t_1 - t_2| & \lambda_2 \geq 0 \\ -1 + \frac{2\omega}{\pi}|t_1 - t_2| & \lambda_2 < 0 \end{cases} \tag{4.24}$$

or by making use of Equations 4.14 and 4.15,

$$u_e = \begin{cases} 1 - \frac{2}{\pi}\left|\tan^{-1}\left(\frac{\lambda_1}{\omega}\right) - \tan^{-1}\left(\frac{1}{\lambda_2 \omega}\right)\right| & \lambda_2 \geq 0 \\ -1 + \frac{2}{\pi}\left|\tan^{-1}\left(\frac{\lambda_1}{\omega}\right) - \tan^{-1}\left(\frac{1}{\lambda_2 \omega}\right)\right| & \lambda_2 < 0 \end{cases}. \tag{4.25}$$

Effective Damping. Varying the stiffness in a system causes work to be performed. [4] Several authors have used work to explain how varying stiffness changes the energy of the system [17], [139] and the same approach is applied here. The equivalent viscous damping coefficient that matches the work applied by varying the spring stiffness will be developed. Multiplying Equation 4.7 by $\dot{x}_e$, assuming $y = \dot{y} = \ddot{y} = 0$, and integrating over one period results in

$$\int_0^{2T} 2\left(\mu - \mu_e\right)\dot{x}_e^2 + \varepsilon\left(u - u_e\right)x_e\dot{x}_e dt = 0 \tag{4.26}$$

where $T = \frac{\pi}{\omega}$ as before. Breaking up Equation 4.26 results in

$$2\left(\mu - \mu_e\right)\int_0^{2T} \dot{x}_e^2 dt + \varepsilon\int_0^{2T} u x_e\dot{x}_e dt - \varepsilon u_e\int_0^{2T} x_e\dot{x}_e dt = 0. \tag{4.27}$$

Substituting Equation 4.9 into Equation 4.27 and solving for μ_e results in

$$\mu_e = \mu + \frac{\varepsilon}{2\psi^2\omega\pi}\int_0^{2T} u x_e\dot{x}_e dt = \mu + \frac{\varepsilon}{8\pi}\int_0^{2T} u\sin\left[2\left(\omega t + \theta\right)\right]dt. \tag{4.28}$$

The integral of Equation 4.28 can be solved by referring to Table 4.1 to determine bounds of integration. The result is

$$\mu_e = \mu + \frac{\varepsilon}{2\omega\pi}\begin{cases} T_1 - T_2 & \text{if } \lambda_2 \geq 0 \wedge t_1 < t_2 \\ T_2 - T_1 & \text{if } \lambda_2 < 0 \wedge t_1 < t_2 \\ T_2 - T_1 & \text{if } \lambda_2 \geq 0 \wedge t_2 < t_1 \\ T_1 - T_2 & \text{if } \lambda_2 < 0 \wedge t_2 < t_1 \end{cases} \tag{4.29}$$

where

$$T_1 = \frac{\omega^2 - \lambda_1^2}{\omega^2 + \lambda_1^2} \tag{4.30}$$

and

$$T_2 = \frac{\lambda_2^2\omega^2 - 1}{\lambda_2^2\omega^2 + 1}. \tag{4.31}$$

With u_e and μ_e known, Equations 4.10 and 4.11 are now completely specified.

4.3 Perturbation Approximation

Perturbation methods for approximating solutions are well known and are often used on nonlinear problems [146]. The perturbation method used here follows similar reasoning the direct approach used. The development begins the same way as the direct approach, but diverges at Equation 4.8. It is now assumed

$$x = x_e + \varepsilon y\left(t, \varepsilon\right) \tag{4.32}$$

where x is defined using Equation 4.2, x_e is defined using Equation 4.5. The error, $x - x_e$, between the true solution and the effective approximate solution is assumed to be of order ε (where ε is also assumed to be small) and written as $\varepsilon y\left(t, \varepsilon\right)$. This is not strictly true, since it is possible for $\varepsilon \to 1$. However, for small values of ε, perturbation techniques can provide accurate analytic approximations. The effective solution, natural frequency, and damping of 4.5 are expanded in a power series as

$$x_e = x_{e_0} + \varepsilon x_{e_1} + \varepsilon^2 x_{e_2} + ..., \tag{4.33}$$

$$\omega_e = \omega_{e_0} + \varepsilon \omega_{e_1} + \varepsilon^2 \omega_{e_2} + ... \tag{4.34}$$

and

$$\mu_e = \mu_{e_0} + \varepsilon \mu_{e_1} + \varepsilon^2 \mu_{e_2} + ... \tag{4.35}$$

The error can also be expanded as

$$y = y_0 + \varepsilon y_1 + \varepsilon^2 y_2 + ... \tag{4.36}$$

Substituting 4.32 and 4.5 into Equation 4.2 results in

$$\varepsilon\left[\ddot{y} + 2\mu\dot{y} + \left(1 + \varepsilon u\right) y\right] = -2\left(\mu - \mu_e\right)\dot{x}_e - \left(1 - \omega_e^2 + \varepsilon u\right) x_e. \tag{4.37}$$

When $\varepsilon \to 0$, the order 1 solution to 4.37 becomes

$$2\left(\mu - \mu_{e_0}\right)\dot{x}_e + \left(1 - \omega_{e_0}^2\right) x_e = 0 \tag{4.38}$$

which means

$$\begin{array}{l} \mu_{e_0} = \mu \\ \omega_{e_0} = 1 \end{array} . \tag{4.39}$$

Substituting Equation 4.39 into Equation 4.37, dividing by ε and letting $\varepsilon \to 0$ results in

$$\ddot{y}_0 + 2\mu\dot{y}_0 + (1 + \varepsilon u)\, y_0 = 2\mu_{e_1}\dot{x}_{e_0} + \left[2\omega_{e_1} - u\left(x_{e_0}, \dot{x}_{e_0}\right)\right] x_{e_0}. \tag{4.40}$$

The right hand side of Equation 4.40 is a forcing function with unknown coefficients μ_{e_1} and ω_{e_1}. Equation 4.40 has a particular solution in the form

$$y_0 = A_1 \cos\left(\omega t + \theta_{e_0}\right) + A_2 \sin\left(\omega t + \theta_{e_0}\right) \tag{4.41}$$

where θ_{e_0} is the order one expansion of Equation 4.11, considering Equation 4.35. Substituting Equation 4.41 and 4.9 into Equation 4.40 results in

$$\begin{array}{c} \left[\left(1-\omega^2\right) A_1 + 2\mu\omega A_2\right] \cos\left(\omega t + \theta_{e_0}\right) + \left[\left(1-\omega^2\right) A_2 - 2\mu\omega A_1\right] \sin\left(\omega t + \theta_{e_0}\right) \\ = \Psi_0 \left[-2\mu_{e_1}\omega \sin\left(\omega t + \theta_{e_0}\right) + \left(2\omega_{e_1} - u\right) \cos\left(\omega t + \theta_{e_0}\right)\right] \end{array} . \tag{4.42}$$

Taking advantage of orthogonality, Equation 4.42 can be multiplied by $\cos\left(\omega t + \theta_{e_0}\right)$ and by $\sin\left(\omega t + \theta_{e_0}\right)$, then can be integrated over one period resulting in

$$\frac{\pi}{\omega} \begin{bmatrix} 1-\omega^2 & 2\mu\omega \\ -2\mu\omega & 1-\omega^2 \end{bmatrix} \begin{bmatrix} A_1 \\ A_2 \end{bmatrix} = \Psi_0 \left(2\pi \begin{bmatrix} \frac{1}{\omega} & 0 \\ 0 & -1 \end{bmatrix} \begin{bmatrix} \omega_{e_1} \\ \mu_{e_1} \end{bmatrix} - \begin{bmatrix} Z_c \\ Z_s \end{bmatrix} \right) \tag{4.43}$$

where

$$\begin{aligned} Z_c &= \frac{1}{2}\left[\int^{2T} u dt + \int^{2T} u \cos\left[2\left(\omega t + \theta_{e_0}\right)\right] dt\right] && \text{(4.44a)} \\ &= \int^{T} u dt + \int^{T} u \cos\left[2\left(\omega t + \theta_{e_0}\right)\right] dt, && \text{(4.44b)} \end{aligned}$$

$$Z_s = \frac{1}{2}\int^{2T} u \sin\left[2\left(\omega t + \theta_{e_0}\right)\right] dt \tag{4.45}$$

$$= \int^{T} u \sin\left[2\left(\omega t + \theta_{e_0}\right)\right] dt, \tag{4.46}$$

and

$$u = u\left(x_e, \dot{x}_e\right)\big|_{\varepsilon=0}. \tag{4.47}$$

Ideally, A_1 and A_2 in Equation 4.42 vanish since it is desired that $x_e \approx x$. Then

$$\omega_{e_1} = \frac{\omega}{2\pi} Z_c \tag{4.48}$$

and

$$\mu_{e_1} = -\frac{1}{2\pi} Z_s. \tag{4.49}$$

Then to order ε, the expressions for ω_e and μ_e are

$$\omega_e = 1 + \frac{\varepsilon\omega}{2\pi} Z_c \tag{4.50}$$

and

$$\mu_e = \mu - \frac{\varepsilon}{2\pi} Z_s. \tag{4.51}$$

All that is left is to evaluate the integrals of Equations 4.50 and 4.51. Using Table 4.1, Equation 4.50 evaluates to

$$\omega_e = 1 + \varepsilon \left[\frac{1}{2} \left\{ \begin{array}{ll} 1 - \frac{2\omega}{\pi}\left|t_1 - t_2\right| & \text{if } \lambda_2 \geq 0 \\ -1 + \frac{2\omega}{\pi}\left|t_1 - t_2\right| & \text{if } \lambda_2 < 0 \end{array} \right\} + \frac{1}{\pi} \left\{ \begin{array}{ll} \Omega_1 - \Omega_2 & \text{if } \lambda_2 \geq 0 \wedge t_1 < t_2 \\ \Omega_2 - \Omega_1 & \text{if } \lambda_2 < 0 \wedge t_1 < t_2 \\ \Omega_2 - \Omega_1 & \text{if } \lambda_2 \geq 0 \wedge t_2 < t_1 \\ \Omega_1 - \Omega_2 & \text{if } \lambda_2 < 0 \wedge t_2 < t_1 \end{array} \right\} \right] \tag{4.52}$$

where

$$\Omega_1 = \frac{\lambda_1 \omega}{\omega^2 + \lambda_1^2}, \tag{4.53}$$

$$\Omega_2 = \frac{\lambda_2 \omega}{\lambda_2^2 \omega^2 + 1}, \tag{4.54}$$

t_1 is defined by Equation 4.14, and t_2 is defined by Equation 4.15. Equation 4.50 evaluates to the same expression as Equation 4.29.

4.4 Comparisons of Approximate and Simulated Solutions

Comparison of Equation 4.52 and Equation 4.25 substituted into Equation 4.6 shows the perturbation solution adds a correction term the direct solution misses. The extra term is small as $\omega \to 0$ and $\omega \to \infty$, but does make a correction at low frequency.

Simulation Approach. To gain insight into the accuracy of the approximate solutions, Equation 4.2 was simulated at various frequencies using a fixed time step Runge-Kutta method. Since only the steady state solution was needed for comparison purposes, a procedure was needed to separate the transient response from the steady state behavior. Ideally, only the steady state response would be calculated or equivalently the transient behavior would not be excited. In a linear system, the transient response can be made zero by making the homogeneous portion of the response zero. Considering Equation 4.5, the general solution with both homogeneous and particular solutions is

$$x_e = Ae^{-\mu t}\cos\left(\omega_d t + \theta_H\right) + \Psi\cos\left(\omega t + \theta\right) \tag{4.55}$$

where ω_d is the damped natural frequency of the system [71]. The velocity of the system is

$$\dot{x}_e = -Ae^{-\mu t}\left[\mu\cos\left(\omega_d t + \theta_H\right) + \omega_d\sin\left(\omega_d t + \theta_H\right)\right] - \Psi\omega\sin\left(\omega t + \theta\right). \tag{4.56}$$

At time $t = 0$, the displacement and velocity are

$$x_e\left(0\right) = A\cos\left(\theta_H\right) + \Psi\cos\left(\theta\right) \tag{4.57}$$

and

$$\dot{x}_e\left(0\right) = -A\left[\mu\cos\left(\theta_H\right) + \omega_d\sin\left(\theta_H\right)\right] - \Psi\omega\sin\left(\theta\right). \tag{4.58}$$

It is desired to make $A = 0$ to prevent a transient response from being excited. Hence, the initial conditions should be

$$x_e(0) = \Psi \cos(\theta) \tag{4.59}$$

and

$$\dot{x}_e(0) = -\Psi\omega \sin(\theta). \tag{4.60}$$

Since the real system is nonlinear and the initial conditions were developed for the approximate solution, the time response was run for 20 periods as measured by the forcing function period to ensure steady state was found. Some time response plots were inspected to verify steady state was being achieved for the nonlinear problem with satisfactory results. It should be noted that finding steady state for the nonlinear problem using other initial conditions will likely require many more periods to be run, which increases the time needed to complete the simulations. Only the last 20% of the time response was kept to identify the amplitude of the response. Again, some time response plots were inspected and the 20% number may be overly conservative.

The amplitude of the response was determined by finding the root mean square of the response and dividing by the root mean square of the input. The root mean square is defined as

$$rms(z) = \sqrt{\frac{\sum_{i=1}^{n} z_i^2}{n}} \tag{4.61}$$

where z is a vector of time response data and n is the number of points in z. Using the rms smooths out nonlinear behavior such as harmonics that appear due to the nonlinear nature of the system. Figure 4.1 shows a steady state time response forced at a frequency of 0.1. The simulated response shows high frequency harmonics have also been excited by the forcing function, but the predominate behavior is at the forcing frequency of 0.1.

Approximate Solution Validation. The magnitude of response at various frequencies was graphed a various frequencies for the simulated system and for the two approximate systems to make comparisons using a plot like a Bode magnitude plot, shown in Figures 4.2, 4.3, and 4.4 on pages 4-14 - 4-16. Care must be used in interpreting these plots because the variable stiffness system is a nonlinear system and the superposition principle

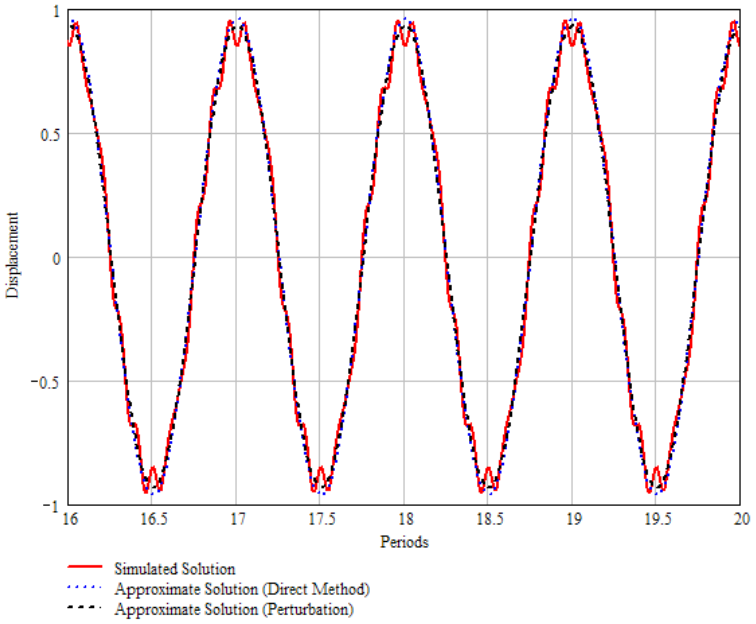

Figure 4.1 Forced Response at $\omega = 0.1$ $(\mu = 0,\ \varepsilon = 0.1,\ \lambda_1 = 0.1,\ \lambda_2 = 0)$

often associated with these types of plots in linear systems does not apply. Changes in the forcing function (such as adding a second sinusoid function) requires complete reanalysis of system behavior. With this caveat, Figures 4.2, 4.3, and 4.4 can be considered Bode magnitude plot equivalents.

Figure 4.2 shows a comparison of simulated results with approximate results for both the direct calculation method and the perturbation method. The parameters λ_1 and λ_2 were both set to 0. Additionally, it shows the effects of using variable stiffness as compared to the same system with no variable stiffness. In this case, since damping is 0, the system with no variable stiffness is a simple linear oscillator with infinitely strong resonance at its natural frequency of 1. For $\varepsilon < 0.5$, the approximate results reasonably match the simulated results. For high values of ε, however, the approximate solutions fail to capture system behavior. No difference was seen between the two approximate solutions since both solutions are the same when $\lambda_1 = 0$ and $\lambda_2 = 0$.

Figure 4.3 shows comparisons of the simulated and approximate solutions using the unforced optimal control of Figure 3.12 and sets $\mu = 0.1$. This control policy may not be optimal for this system as will be discussed later, but still provides much damping,

especially for the higher values of ε. At very low frequencies, the variable stiffness method provides significant attenuation that the standard viscously damped system does not provide, though apparently at the expense of less attenuation as resonance is approached.

To better understand where the low frequency attenuation comes from, consider Equation 4.2 and let $\omega \to 0$. In the limit, the system is being forced by a unit step function or

$$\ddot{x} + 2\mu\dot{x} + (1 + \varepsilon u)\, x = 1. \tag{4.62}$$

Assuming the control law is chosen to make the system stable, it is expected the system will settle to a constant value as time $t \to \infty$. It may be possible that certain settings of λ_1 and λ_2 could cause limit cycle or other oscillatory behavior (which has not yet been observed), but this type of behavior is undesirable for damping out vibration in the system and was not further pursued. The settling value can be found by finding the stationary point of Equation 4.62 or steady state error to a unit step function which is

$$x = \frac{1}{1 + \varepsilon u}. \tag{4.63}$$

Since $\dot{x} \to 0$ by definition of a stationary point, the control law of Equation 3.12 simplifies to

$$u = sgn\left(\lambda_1 x^2\right) = sgn\left(\lambda_1\right) \tag{4.64}$$

since $x^2 > 0$. Then as $\omega \to 0$,

$$x \to \begin{cases} \frac{1}{1+\varepsilon} & \text{if} \quad \lambda_1 > 0 \\ 1 & \text{if} \quad \lambda_1 = 0 \\ \frac{1}{1-\varepsilon} & \text{if} \quad \lambda_1 < 0 \end{cases}. \tag{4.65}$$

or the attenuation in dB is

$$x \to \begin{cases} -20\log\left(1+\varepsilon\right) & \text{if} \quad \lambda_1 > 0 \\ 0 & \text{if} \quad \lambda_1 = 0 \\ -20\log\left(1-\varepsilon\right) & \text{if} \quad \lambda_1 < 0 \end{cases} = -20\log\left[1 + \varepsilon sgn\left(\lambda_1\right)\right]. \tag{4.66}$$

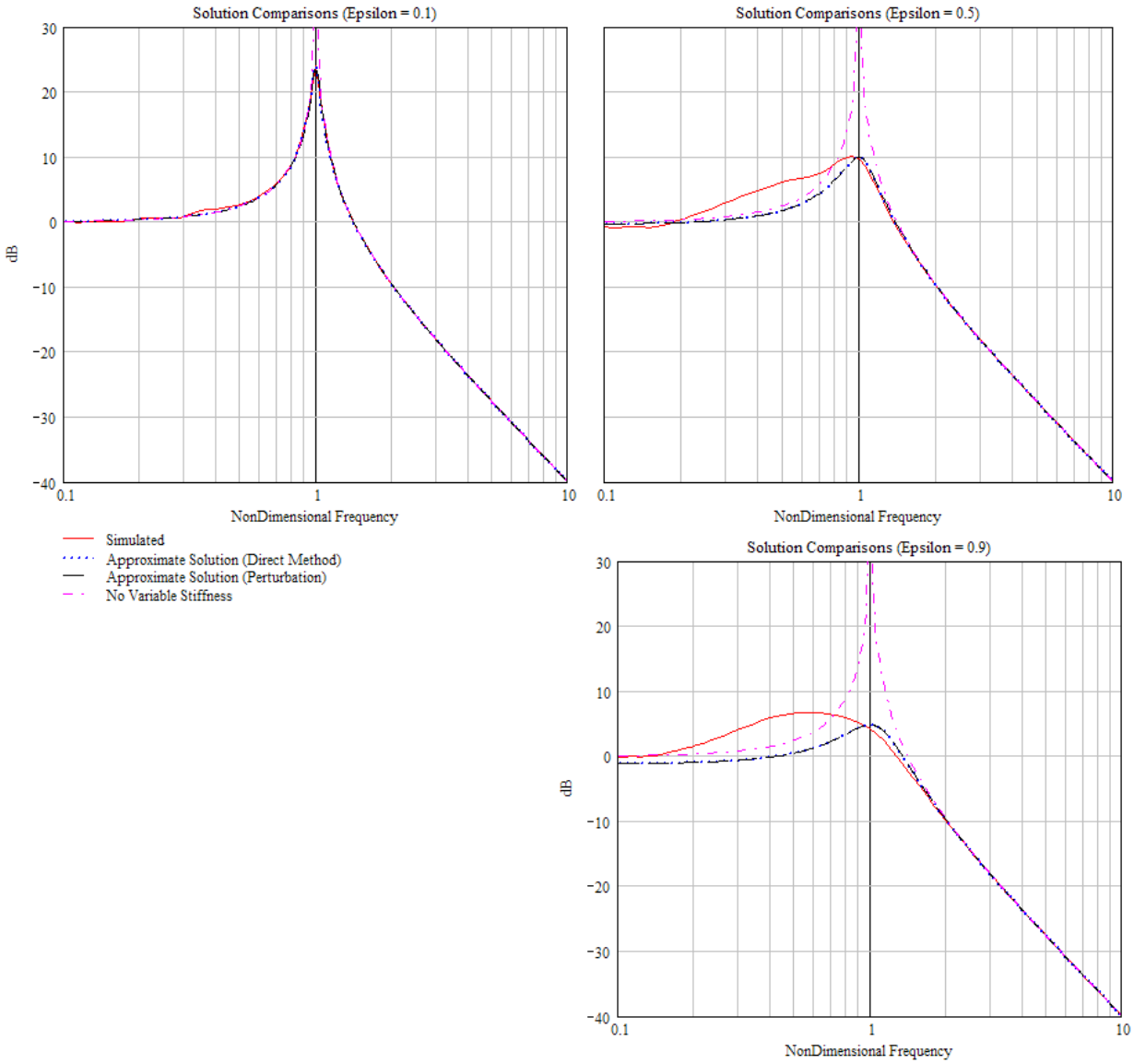

Figure 4.2 Comparison of Simulation with Approximate Solutions ($\lambda_1 = 0$, $\lambda_2 = 0$, $\mu = 0$)

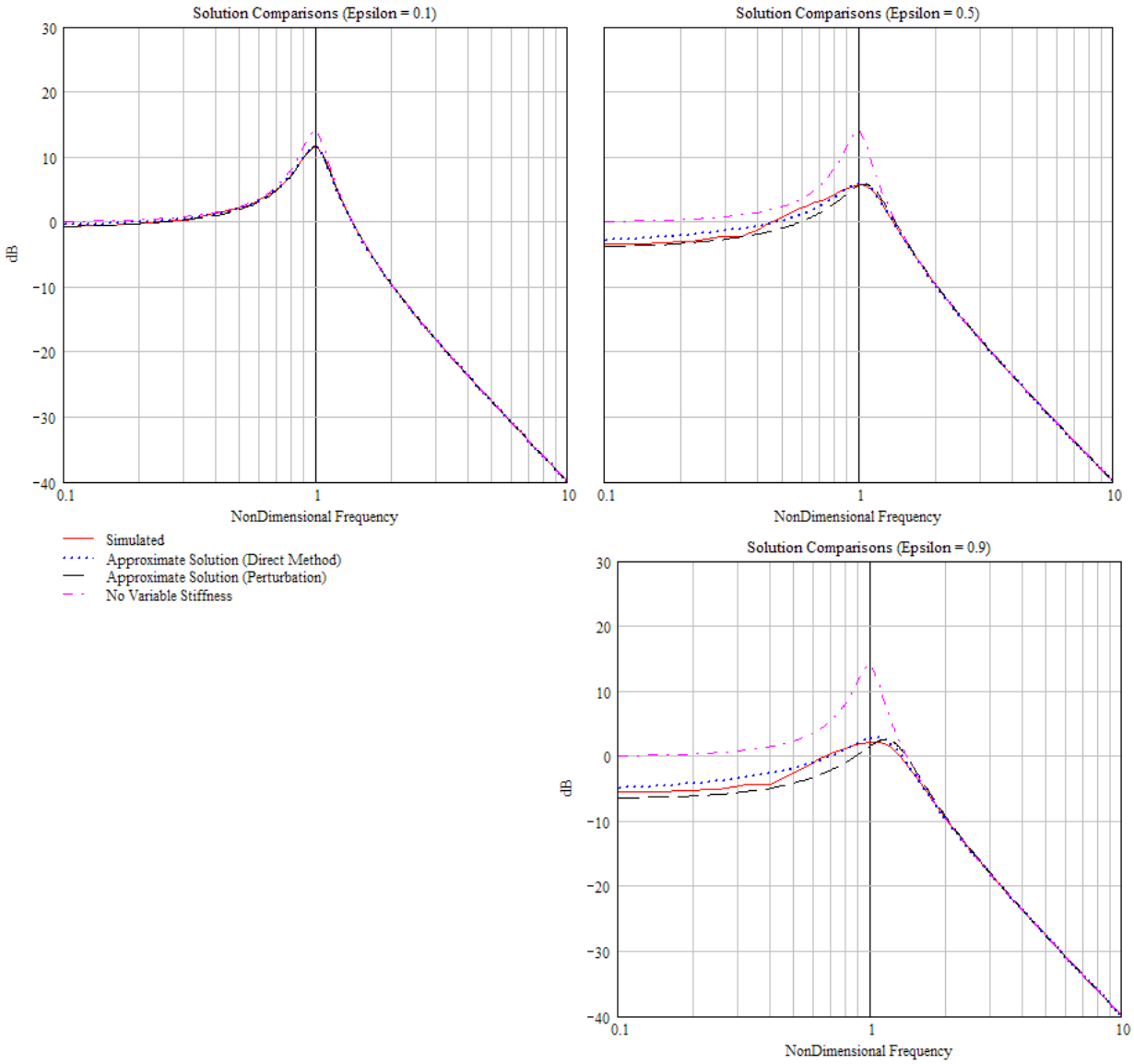

Figure 4.3 Comparison of Simulation with Approximate Solutions (λ_1 =Unforced Optimal, $\lambda_2 = 0$, $\mu = 0.1$)

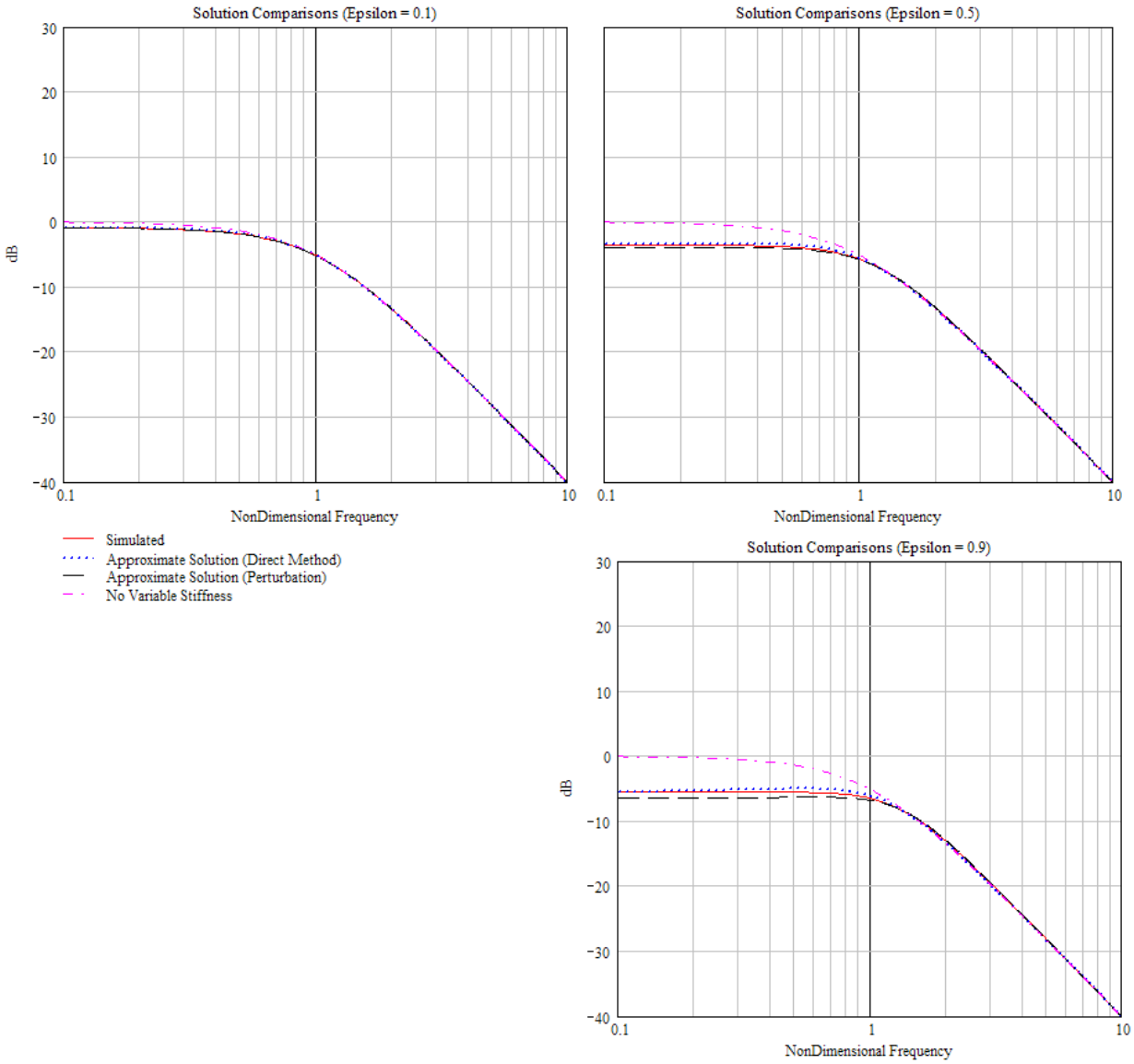

Figure 4.4 Comparison of Simulation with Approximate Solutions (λ_1 =Unforced Optimal, $\lambda_2 = 0$, $\mu = 0.9$)

Clearly, letting $\lambda_1 > 0$ provides the best low frequency attenuation.

Figure 4.4 shows that even with very high damping, variable stiffness is still valuable because of the low frequency attenuation it provides. The control law was once again set to the same settings as the unforced optimal control law of Figure 3.12, since $\lambda_1 > 0$ for this policy. In the case where $\varepsilon = 0.9$, the variable stiffness device is providing approximately 5.58 dB more attenuation than a viscously damped system with no variable stiffness.

4.5 Approximate Optimal Control Law

From the previous section, it would appear an optimal control law should have $\lambda_1 > 0$, since it provides much better low frequency behavior than other settings for λ_1. One approach that estimates an optimal control law considering the low frequency behavior is to minimize the area of the response curve over all frequencies. The results are limited to being near optimal and may only be approximate local minimums, since the approximate solutions derived earlier have limited accuracy. Numerical methods were used to solve for relevant parameters because the functions for the approximate amplitude are too complex to allow analytic methods. For the direct method, the approximate amplitude is represented by Equation 4.10 using Equations 4.6, 4.25, and 4.29. For the perturbation method, the amplitude is represented by Equation 4.10 using Equations 4.52 and 4.29.

The area under the frequency response curve can be found by solving

$$I(\lambda_1, \lambda_2, \mu, \varepsilon) = \int_0^\infty \Psi(\omega, \lambda_1, \lambda_2, \mu, \varepsilon)\, d\omega. \tag{4.67}$$

Then, the settings for λ_1 and λ_2 that minimize the peak response can be found by solving

$$\nabla I(\lambda_1, \lambda_2, \mu, \varepsilon) = \underline{0} \tag{4.68}$$

for λ_1 and λ_2. Figure 4.5 shows the near optimal values for λ_1 for various values of μ. The curves for $0.3 \leq \mu \leq 0.9$ are difficult to tell apart and range between 0.32 and 0.37 for small ε and are very close to 0.46 for large ε. The parameter λ_2 was found to be 0 while $\lambda_1 > 0$ as expected. A comparison between Figure 4.5 and Figure 3.12 shows the control

laws for the initial value and sinusoidally forced problems is radically different. However, two common results are that $\lambda_1 > 0$ and $\lambda_2 = 0$. If a suboptimal control is acceptable for one or the other disturbance types, it may be possible to use a single control law to meet two disturbance rejection criteria.

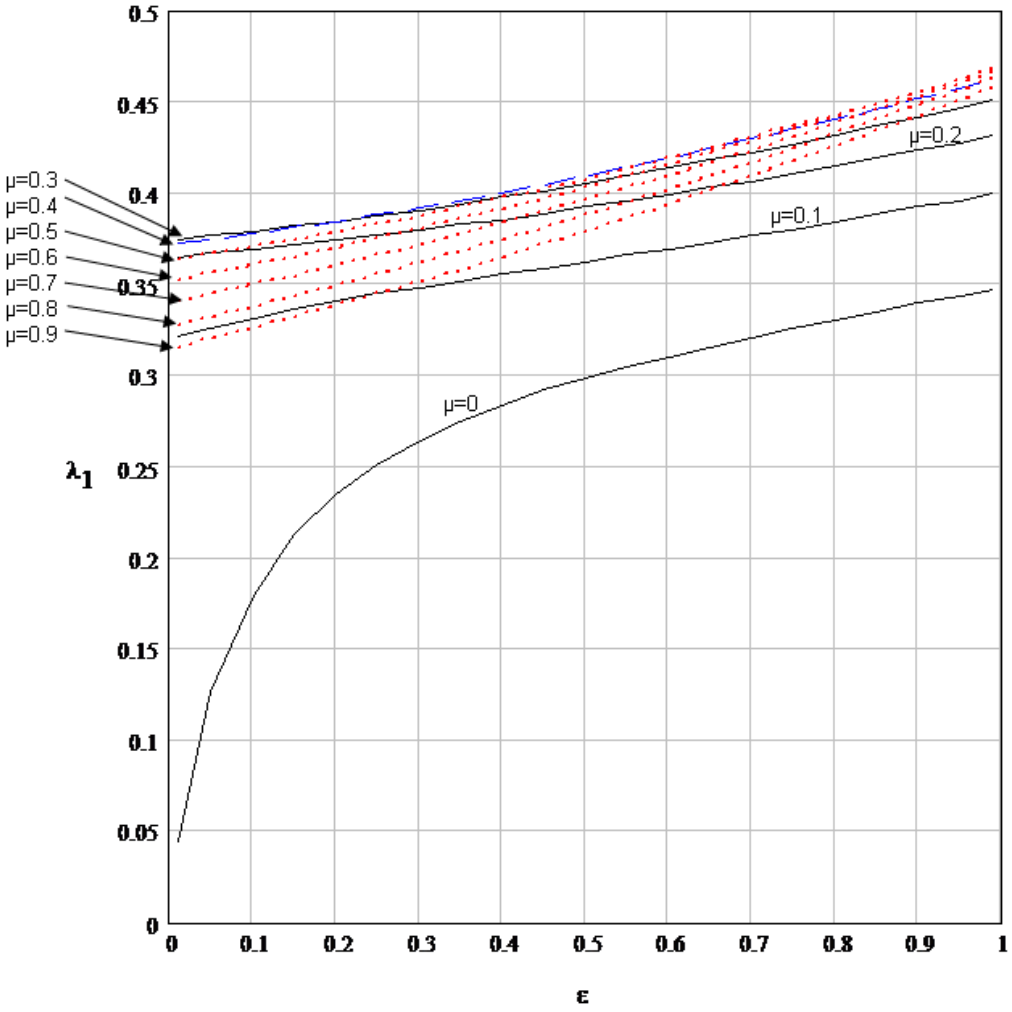

Figure 4.5 Near Optimal λ_1 for Sinusoidally Forced Problem using Perturbation Approximation ($\lambda_2 = 0$)

4.6 Equivalent Damping and Stiffness Coefficients

As was done in Chapter 3.13, an equivalent stiffness and equivalent damping coefficient can be calculated to use in the dimensioned SDOF equivalent forced system.

Comparing Equations 4.2 and 4.5 suggests

$$1 + \varepsilon u \backsim \omega_e^2 \tag{4.69}$$

and

$$\mu \backsim \mu_e \tag{4.70}$$

where " $\backsim$ " again is used to mean the quantity on the left hand side of the relationship is replaced by the quantity on the right hand side. Once again, the quantities of the relationship are not equal since μ_e is a combination of viscous damping and dissipating work done on the system due to switching the stiffness. Solving Equation 3.10 for c^* and applying the approximations of Equations 4.69 and 4.70 to Equation 4.2 suggests the original dimensional differential equation can be approximated as

$$m^*\ddot{x}_e^* + c_{eq}^*\dot{x}_e^* + k_{eq}^* x_e^* = A^* \cos\left(\omega^* t^*\right), \tag{4.71}$$

where

$$c_{eq}^* = 2\mu_e\sqrt{m^* k^*} \tag{4.72}$$

$$k_{eq}^* = k^*\omega_e^2 \tag{4.73}$$

with

$$k^* = \frac{k_1^* + k_0^*}{2}. \tag{4.74}$$

Equation 4.71 represents a well known viscously damped oscillator that can be used to approximate some behavior of Equation 4.1.

4.7 Conclusion

Two approximate methods were developed to estimate the dominant response of a SDOF sinusoidally forced system. The system can make use of both variable stiffness and viscous damping to attenuate the input. Both methods were found to provide good approximations of the response for low variation in the variable stiffness device. For high variation in the variable stiffness, the methods did not always capture all of the nonlinear

effects such as high frequency harmonics. The approximate solutions were used to develop a near optimal control law, which was only near optimal due to the limited accuracy of the approximate solutions. For certain settings of the variable stiffness control law, it is possible to substantially improve the low frequency attenuation of the response as compared to a passively damped system, even when the system has strong viscous damping.

5. *Variable Stiffness for Multi-Degree of Freedom Systems*

5.1 Introduction

The utility of the SDOF approximate solutions of Chapter 3 and Chapter 4 for multi-degree of freedom problems will be explored for the initial value problem and for the sinusoidally forced problem. Because the approximate solution is linear, linear theory was used to study the MDOF problems. A parallel mass lumped parameter system representative of a space telescope structure will be examined. Afterward, a series mass lumped parameter system that could represent the model of a continuous beam with varying stiffness will be considered. In both cases, equations of motion will be developed and nondimensionalized. Since space applications are the focus, the system examined is one floating in space, meaning it has no fixed constraints. Hence, the rigid body modes were removed from the system using a center of mass transformation. In both cases, a 3 DOF problem was selected, where one DOF is a rigid body mode. After removing the rigid body mode, a 2 DOF problem was found with acceleration coupling in both equations. In both cases, limiting assumptions had to be made about the masses and control law to allow the 2 DOF problems to be solved. For the parallel mass lumped parameter system, the assumptions were physically reasonable while the series mass lumped parameter system was restricted enough to limit the utility of the results. The coupling in the parallel mass lumped parameter system was weak while in the series mass lumped parameter system it was much stronger. Hence, the results for the parallel mass MDOF model were much more accurate than the series mass MDOF model.

5.2 Parallel Mass MDOF Model

Equations of Motion. Figure 5.1 is one type of multi-degree of freedom model (MDOF). It could represent a cross section of a space telescope where the satellite bus is m_1^* and the other masses represent mirrors. Alternatively, if there are only two masses in the system, it could represent a simple vibration isolation problem. The equations of

motion can be written as

$$m_1^*\ddot{x}_1^* + \sum_{i=2}^{p}\left[c_i^*\left(\dot{x}_1^* - \dot{x}_i^*\right) + \tilde{k}_i^*\left(x_1^* - x_i^*\right)\right] = Q_1^* \tag{5.1}$$

and

$$m_j^*\ddot{x}_j^* + c_j^*\left(\dot{x}_j^* - \dot{x}_1^*\right) + \tilde{k}_j^*\left(x_j^* - x_1^*\right) = Q_j^* \tag{5.2}$$

for $j = 2, 3, ..., p$, where p is the total number of masses in the system and $p > 1$. For the MDOF model, m_1^* is a mass allowed to vibrate while m_j^* are masses to be isolated from vibration, c_j^* is the coefficient of damping for the j^{th} viscous damper, $\tilde{k}_j^*$ is the variable stiffness function for the j^{th} variable stiffness spring, Q_j^* is the j^{th} disturbance force acting on the j^{th} mass m_j^*, and Q_1^* is the disturbance force on m_1^*. As previously used, the "*" notation defines the variable as a dimensional variable. The initial conditions are

$$x_1^*(0) = x_{10}^*,\ \dot{x}_1^*(0) = \dot{x}_{10}^* \tag{5.3}$$

and

$$x_j^*(0) = x_{j0}^*,\ \dot{x}_j^*(0) = \dot{x}_{j0}^* \tag{5.4}$$

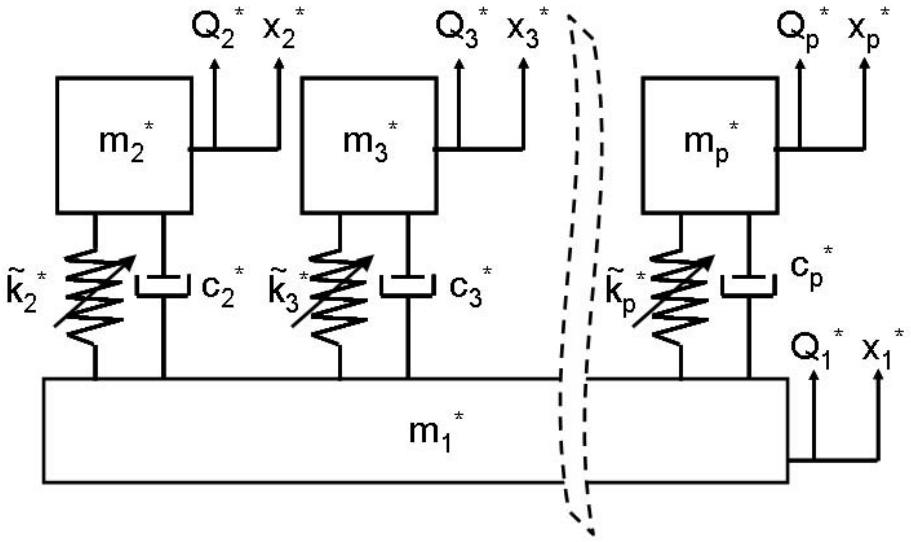

Figure 5.1 MDOF Masses in Parallel Variable Stiffness Constantly Damped Problem

Equations 5.1 and 5.2 can be transformed to separate rigid body modes by defining

$$y^* = \frac{\sum_{i=1}^{p} m_i^* x_i^*}{m_T^*} = \frac{\sum_{j=2}^{p} m_j^* x_j^* + m_1^* x_1^*}{m_T^*} \tag{5.5}$$

and

$$z_j^* = x_j^* - x_1^* \tag{5.6}$$

where

$$m_T^* = \sum_{i=1}^{p} m_i^*. \tag{5.7}$$

Solving Equation 5.6 for x_j^* and substituting into Equation 5.5 results in

$$y^* = \frac{\sum_{j=2}^{p} \left(m_j^* z_j^* + m_j^* x_1^* \right) + m_1^* x_1^*}{m_T^*} = x_1^* + \frac{\sum_{j=2}^{p} m_j^* z_j^*}{m_T^*} \tag{5.8}$$

or

$$x_1^* = y^* - \frac{\sum_{j=2}^{p} m_j^* z_j^*}{m_T^*}. \tag{5.9}$$

Substituting 5.9 into Equation 5.6 and solving for x_j^* results in

$$x_j^* = z_j^* + y^* - \frac{\sum_{j=2}^{p} m_j^* z_j^*}{m_T^*}. \tag{5.10}$$

Substituting 5.9 and 5.10 into Equations 5.1 and 5.2 results in

$$m_j^* \left(\ddot{z}_j^* + \ddot{y}^* - \frac{\sum_{j=2}^{p} m_j^* \ddot{z}_j^*}{m_T^*} \right) + c_j^* \dot{z}_j^* + \tilde{k}_j^* z_j^* = Q_j^* \tag{5.11}$$

and

$$m_1^* \left(\ddot{y}^* - \frac{\sum_{j=2}^{p} m_j^* \ddot{z}_j^*}{m_T^*} \right) - \sum_{j=2}^{p} \left[c_j^* \dot{z}_j^* + \tilde{k}_j^* z_j^* \right] = Q_1^*. \tag{5.12}$$

Adding all j equations of Equation 5.11 to Equation 5.12 and simplifying results in

$$\ddot{y}^* = \frac{\sum_{i=1}^{p} Q_i^*}{m_T^*}. \tag{5.13}$$

Equation 5.13 describes the rigid body motion of the system and can be immediately solved as

$$y^* = \frac{1}{m_T^*}\int_0^{t^*}\int_0^{\tau}\sum_{i=1}^{p} Q_i^* dT d\tau + R^*(t^*) \tag{5.14}$$

$$= \frac{1}{m_T^*}\int_0^{t^*}(t^*-\tau)\sum_{i=1}^{p} Q_i^* d\tau + R^*(t^*) \tag{5.15}$$

where

$$R(t^*)^* = \dot{y}_0^* t^* + y_0^* \tag{5.16}$$

represents rigid body modes of the system. The other term of Equation 5.14 represents forced vibration with respect to the center of mass of the system measured by the inertial coordinate y. Substituting Equation 5.13 into Equation 5.11 and simplifying results in

$$\sum_{\substack{k=1\\k\neq j}}^{p} m_k^* \frac{m_j^*}{m_T^*}\ddot{z}_j^* + c_j^*\dot{z}_j^* + \tilde{k}_j^* z_j^* = Q_j^* + \frac{m_j^*}{m_T^*}\sum_{\substack{k=2\\k\neq j}}^{p} m_k^*\ddot{z}_k^* - \frac{m_j^*}{m_T^*}\sum_{i=1}^{p} Q_i^*. \tag{5.17}$$

Now, it will be assumed that $m_j^* = m^*$, $c_j^* = c^*$, and $\tilde{k}_j^* = \tilde{k}^* = k^*(1+\varepsilon u)$, where u is a control law for the variable stiffness device, k^* is the uncontrolled stiffness of the variable stiffness device, and ε measures the range the variable stiffness device can achieve, defined by Equation 3.11. These definitions assume all of the masses, springs and dampers of Figure 5.1 are the same, except for m_1^*. This is a reasonable assumption for some systems such as a space telescope, since it assumes all masses and isolation devices were manufactured to be identical. Equation 5.17 can be simplified to be

$$\frac{m^*}{1+\gamma}\ddot{z}_j^* + c^*\dot{z}_j^* + k^*(1+\varepsilon u) z_j^* = Q_j^* + \frac{\gamma m^*}{1+\gamma}\sum_{\substack{k=2\\k\neq j}}^{p}\ddot{z}_k^* - \frac{\gamma}{1+\gamma}\sum_{i=1}^{p} Q_i^* \tag{5.18}$$

where

$$\gamma = \frac{m^*}{m_1^* + (p-2)m^*}. \tag{5.19}$$

The transformed initial conditions are found using Equations 5.3, 5.4, 5.5, and 5.6 and are

$$y_0^* = \frac{\gamma}{1+\gamma}\sum_{j=2}^{p} x_{i0}^* + \frac{1-(p-2)\,\gamma}{1+\gamma}x_{10}^*,\ \dot{y}_0^* = \frac{\gamma}{1+\gamma}\sum_{j=2}^{p} \dot{x}_{i0}^* + \frac{1-(p-2)\,\gamma}{1+\gamma}\dot{x}_{10}^* \tag{5.20}$$

and

$$z_{j0}^* = x_{j0}^* - x_{10}^*,\ \ \dot{z}_{j0}^* = \dot{x}_{j0}^* - \dot{x}_{10}^*. \tag{5.21}$$

By letting

$$w_0^* = \sqrt{\frac{k^*\,(1+\gamma)}{m^*}} \tag{5.22}$$

and defining a nonzero length (will be specified later)

$$L^* \neq 0 \tag{5.23}$$

Equation 5.18 can be nondimensionalized by letting

$$t^* = \frac{t}{w_0^*}, \tag{5.24}$$

$$z_j^* = L^* z_j, \tag{5.25}$$

and

$$Q_j^* = \frac{m^* L^* \omega_0^{*^2}}{1+\gamma} Q_j = L^* k^* Q_j. \tag{5.26}$$

Hence, Equation 5.18 becomes

$$\ddot{z}_j + 2\mu\dot{z}_j + (1+\varepsilon u)\,z_j = \frac{1}{1+\gamma}Q_j + \gamma\sum_{\substack{k=2\\k\neq j}}^{p}\ddot{z}_k - \frac{\gamma}{1+\gamma}\sum_{\substack{i=1\\k\neq j}}^{p} Q_i \tag{5.27}$$

where

$$\mu = \frac{c^* w_0^*}{2k^*}. \tag{5.28}$$

From Equation 5.27, it can now be seen that the parameter γ is a measure of the coupling between the different masses in the system. Clearly $0 < \gamma < 1$ and as $p \to \infty$ or if $m_1^* >> m^*$, $\gamma \to 0$, which means the coupling with all other masses in the system is weak.

To determine if γ will be large or small for a space telescope, Powers et. al. was consulted. Their preliminary design identifies a total mirror mass with support structure for a space telescope with six mirrors as 883. 4 kg while the mass of the rest of the satellite is 2533 kg [29]. One mirror with support structure would have a mass of about 147 kg. Considering Equation 5.19 clearly shows $m^* << m_1^*$ so it is expected that γ would typically be small.

For the special case where $p = 2$, Equation 5.27 simplifies to

$$\ddot{z}_2 + 2\mu\dot{z}_2 + (1 + \varepsilon u)\, z_2 = \frac{1}{1+\gamma} Q_2 - \frac{\gamma}{1+\gamma} Q_1 \tag{5.29}$$

which has already been solved for some cases. For example, when $Q_1 = Q_2 = 0$, Equation 5.29 becomes the constantly damped variable stiffness problem solved in Chapter 3. Similarly, if either Q_1 or Q_2 are sinusoidal forcing functions, the results of Chapter 4 can be used to estimate the response. Hence, the work of the SDOF problem directly applies to the 2DOF problem.

For $p > 2$, as $\gamma \to 0$, Equation 5.27 becomes j SDOF problems. When $\gamma \to 1$, $m_1^* \to 0$. This implies the other masses are connected to each other through their isolation devices. Equation 5.27 is very similar to Equation 3.9 found in Chapter 3. With the right forcing function, it is similar to Equation 4.2. The main difference between Equation 5.27 and the equations studied in Chapter 3 is the coupling with the other masses on the order of γ.

Based on previous work, two methods of solving Equation 5.27 are possible. One way is to consider γ to be a small parameter and treat Equation 5.27 as a perturbation problem. This is possible because the unperturbed problem has already been solved. This has the advantage of allowing any settings for μ and ε, but limits the size of the coupling of the system. The second approach is to develop an approximate solution using the equivalent linear approximate solution developed in Chapter 3. This appeals to well

known linear tools making it easier to develop, but is limited in accuracy in the short term as ε and μ become large. The second approach was used.

Initial Value Problem. The solution to Equation 5.27 can be approximated by solving the linear equation

$$\ddot{z}_j + 2\zeta\omega_n\dot{z}_j + \omega_n^2 z_j = \gamma \sum_{\substack{k=2 \\ k\neq j}}^{p} \ddot{z}_k \tag{5.30}$$

where it is assumed all external forces are 0. The parameters ζ and ω_n are defined using Equations 3.157 and 3.158 and represent the equivalent damping ratio and natural frequency, respectively, for the SDOF variable stiffness constant damping problem solved in Chapter 3.

Linear Approximate Solution. Taking the Laplace transform of 5.30 with $Z_j = \mathcal{L}(z_j)$ results in

$$Z_j s^2 - s z_{j0} - \dot{z}_{j0} + 2\zeta\omega_n Z_j s - 2\zeta\omega_n z_{j0} + \omega_n^2 Z_j = \gamma \sum_{\substack{k=2 \\ k\neq j}}^{p} \left(Z_k s^2 - s z_{k0} - \dot{z}_{k0} \right) \tag{5.31}$$

or

$$Z_j \left(s^2 + 2\zeta\omega_n s + \omega_n^2 \right) - \gamma s^2 \sum_{\substack{k=2 \\ k\neq j}}^{p} Z_k = z_{j1} s + z_{j2} \tag{5.32}$$

where

$$z_{j1} = z_{j0} - \gamma \sum_{\substack{k=2 \\ k\neq j}}^{p} z_{k0} \tag{5.33}$$

and

$$z_{j2} = \dot{z}_{j0} + 2\zeta\omega_n z_{j0} - \gamma \sum_{\substack{k=2 \\ k\neq j}}^{p} \dot{z}_{k0}. \tag{5.34}$$

The solution to Equation 5.32 can be written in matrix form as

$$z(t) = \mathcal{L}^{-1}\left(A^{-1} B \right)(t) \tag{5.35}$$

where

$$A = \begin{bmatrix} Z_D(s) & Z_N(s) & ... & Z_N(s) \\ Z_N(s) & Z_D(s) & ... & Z_N(s) \\ ... & ... & ... & ... \\ Z_N(s) & Z_N(s) & ... & Z_D(s) \end{bmatrix}, \tag{5.36}$$

$$B = \begin{bmatrix} z_{21}s + z_{22} \\ z_{31}s + z_{32} \\ ... \\ z_{p1}s + z_{p2} \end{bmatrix}, \tag{5.37}$$

and $\mathcal{L}^{-1}$ denotes the inverse Laplace transform operator. The variables Z_D and Z_N are defined as

$$Z_D(s) = s^2 + 2\zeta\omega_n s + \omega_n^2 \tag{5.38}$$

and

$$Z_N(s) = -\gamma s^2. \tag{5.39}$$

The matrix A is in a special patterned form, which is called a circulant matrix [147]. To find A^{-1}, the special form of A can be exploited. It is postulated that A^{-1} will have the form

$$A^{-1} = D(s) \begin{bmatrix} \alpha(s) & Z_N(s) & ... & Z_N(s) \\ Z_N(s) & \alpha(s) & ... & Z_N(s) \\ ... & ... & ... & ... \\ Z_N(s) & Z_N(s) & ... & \alpha(s) \end{bmatrix} \tag{5.40}$$

where $\alpha(s)$ is the diagonal of A^{-1} and $D(s)$ is the determinant of A, with $\alpha(s)$ and $D(s)$ to be found. Since $AA^{-1} = I$ where I is the identity matrix, multiplying AA^{-1} results in

$$D(s)\left[\alpha(s) Z_D(s) + Z_N(s)^2 (p-2)\right] = 1 \tag{5.41}$$

for a diagonal element and

$$Z_D(s) + \alpha(s) + Z_N(s)(p-3) = 0 \tag{5.42}$$

for an off diagonal element. Then

$$\alpha(s) = -\left[Z_D(s) + Z_N(s)(p-3)\right] \tag{5.43}$$

and

$$\begin{aligned} D(s) &= \frac{1}{\left(\alpha(s) Z_D(s) + Z_N(s)^2 (p-2)\right)} && (5.44a)\\ &= \frac{1}{-Z_D(s)\left[Z_D(s) + Z_N(s)(p-3)\right] + Z_N(s)^2 (p-2)} && (5.44b)\\ &= \frac{1}{-Z_D(s)^2 - Z_D(s) Z_N(s)(p-3) + Z_N(s)^2 (p-2)} && (5.44c)\\ &= \frac{1}{\left[Z_N(s) - Z_D(s)\right]\left[(p-2) Z_N(s) + Z_D(s)\right]}. && (5.44d) \end{aligned}$$

With a general form for A^{-1} known, it is now possible to fully specify Equation 5.35. First,

$$A^{-1}(s) B(s) = D(s) \begin{bmatrix} \alpha(s)\left[z_{21}s + z_{22}\right] + Z_N(s) \sum_{\substack{i=2 \\ i\neq 2}}^{p} \left(z_{i1}s + z_{i2}\right) \\ \alpha(s)\left[z_{31}s + z_{32}\right] + Z_N(s) \sum_{\substack{i=2 \\ i\neq 3}}^{p} \left(z_{i1}s + z_{i2}\right) \\ \cdots \\ \alpha(s)\left[z_{p1}s + z_{p2}\right] + Z_N(s) \sum_{\substack{i=2 \\ i\neq p}}^{p} \left(z_{i1}s + z_{i2}\right) \end{bmatrix} \tag{5.45}$$

or in tensor notation

$$\begin{aligned} A^{-1}(s) B(s)_j &= D(s) \left[\alpha(s)\left[z_{j1}s + z_{j2}\right] + Z_N(s) \sum_{\substack{i=2 \\ i\neq j}}^{p} \left(z_{i1}s + z_{i2}\right)\right] && (5.46a)\\ &= D(s) \begin{bmatrix} \alpha(s)\left[z_{j1}s + z_{j2}\right] - Z_N(s)\left[z_{j1}s + z_{j2}\right] \\ +Z_N(s) \sum_{i=2}^{p} \left(z_{i1}s + z_{i2}\right) \end{bmatrix} && (5.46b) \end{aligned}$$

where $j = 2, 3, ..., p$. Substituting Equations 5.44d and 5.43 into Equation 5.46b and then simplifying results in

$$A^{-1}(s)\,B(s)_j = \frac{-\left[z_{j1}s + z_{j2}\right]}{Z_N(s) - Z_D(s)} - \frac{\gamma s^2 \sum_{i=2}^{p}\left[z_{i1}s + z_{i2}\right]}{\left[Z_N(s) - Z_D(s)\right]\left[(p-2)\,Z_N(s) - Z_D(s)\right]} \tag{5.47}$$

or recalling Equations 5.38 and 5.39,

$$A^{-1}(s)\,B(s)_j = \frac{-\left[z_{j1}s + z_{j2}\right]}{\left[(1-\gamma)\,s^2 + 2\zeta\omega_n s + \omega_n^2\right]} - \frac{\gamma s^2 \sum_{i=2}^{p}\left[z_{i1}s + z_{i2}\right]}{\left[(1-\gamma)\,s^2 + 2\zeta\omega_n s + \omega_n^2\right]\left[(1-\gamma\,(p-2))\,s^2 + 2\zeta\omega_n s + \omega_n^2\right]}. \tag{5.48}$$

Equation 5.48 can be expanded into partial fractions resulting in

$$A^{-1}(s)\,B(s)_j = \frac{F_{j1}s + F_{j2}}{s^2 + \frac{2\zeta\omega_n}{1-\gamma}s + \frac{\omega_n^2}{1-\gamma}} + \frac{G_{j1}s + G_{j2}}{s^2 + \frac{2\zeta\omega_n}{1-\gamma(p-2)}s + \frac{\omega_n^2}{1-\gamma(p-2)}} \tag{5.49}$$

where

$$F_{j1} = \frac{(p-2)\,z_{j1} - \sum_{\substack{i=2 \\ i\neq j}}^{p} z_{i1}}{(p-1)\,(1+\gamma)}, \tag{5.50}$$

$$F_{j1} = \frac{(p-2)\,z_{j2} - \sum_{\substack{i=2 \\ i\neq j}}^{p} z_{i2}}{(p-1)\,(1+\gamma)}, \tag{5.51}$$

$$G_{j1} = \frac{\sum_{i=2}^{p} z_{i1}}{(p-1)\,(1-\gamma\,(p-2))}, \tag{5.52}$$

and

$$G_{j1} = \frac{\sum_{i=2}^{p} z_{i2}}{(p-1)\,(1-\gamma\,(p-2))}. \tag{5.53}$$

Using a table of Laplace transforms [145], Equation 5.49 can be transformed to the time domain allowing Equation 5.35 to be written as

$$
\begin{aligned}
z(t)_j &= \mathcal{L}^{-1}\left(A^{-1}(s)\,B(s)_j\right)(t) \\
&= \frac{1}{\omega_n\sqrt{1+\gamma-\zeta^2}}e^{-\frac{\zeta\omega_n}{1+\gamma}t}\left[\begin{array}{c} F_{j1}\omega_n\sqrt{1+\gamma-\zeta^2}\cos\left(\frac{\omega_n\sqrt{1+\gamma-\zeta^2}}{1+\gamma}t\right) \\ +\left[F_{j1}\zeta\omega_n+F_{j2}(1+\gamma)\right]\sin\left(\frac{\omega_n\sqrt{1+\gamma-\zeta^2}}{1+\gamma}t\right)\end{array}\right] \\
+\frac{1}{\omega_n\sqrt{1-\gamma(p-2)-\zeta^2}}e^{-\frac{\zeta\omega_n}{1-\gamma(p-2)}t}&\left[\begin{array}{c} G_{j1}\omega_n\sqrt{1-\gamma(p-2)-\zeta^2}\cos\left(\frac{\omega_n\sqrt{1-\gamma(p-2)-\zeta^2}}{1-\gamma(p-2)}t\right) \\ +\left[G_{j1}\zeta\omega_n+G_{j2}(1-\gamma(p-2))\right]\sin\left(\frac{\omega_n\sqrt{1-\gamma(p-2)-\zeta^2}}{1-\gamma(p-2)}t\right)\end{array}\right]
\end{aligned}
\tag{5.54}
$$

For the special case when $p=3$, the solution is

$$z_2(t) = \frac{1}{2}\left[Z_f(t,\Omega_p,C_p,D_p,\gamma)+Z_f(t,\Omega_m,C_m,D_m,-\gamma)\right] \tag{5.55}$$

and

$$z_3(t) = \frac{1}{2}\left[-Z_f(t,\Omega_p,C_p,D_p,\gamma)+Z_f(t,\Omega_m,C_m,D_m,-\gamma)\right] \tag{5.56}$$

where

$$Z_f(t,\Omega,C,D,\Gamma) = \frac{1}{(1+\Gamma)\,\Omega}e^{-\frac{\zeta\omega_n}{1+\Gamma}t}\left[\left[C(1+\Gamma)-D\zeta\omega_n\right]\sin\left(\frac{\Omega}{1+\Gamma}t\right)+D\Omega\cos\left(\frac{\Omega}{1+\Gamma}t\right)\right], \tag{5.57}$$

$$C_m = z_{32}+z_{22}, \tag{5.58}$$

$$C_p = -z_{32}+z_{22}, \tag{5.59}$$

$$D_m = z_{31}+z_{21}, \tag{5.60}$$

$$D_p = -z_{31}+z_{21}, \tag{5.61}$$

$$\Omega_m = \omega_n\sqrt{1-\gamma-\zeta^2} \tag{5.62}$$

and

$$\Omega_p = \omega_n\sqrt{1+\gamma-\zeta^2}. \tag{5.63}$$

This special case will be compared later with the true system to determine how accurate the approximation is.

Optimal Control. Determining the optimal control policy in a rigorous way for the coupled system appears daunting. One approach would be to calculate the energy of the system and then take partial derivatives with respect to λ_1 and λ_2 to identify settings that minimize energy. Another approach is to minimize the approximate equations for displacement. Both of these approaches result in time varying parameters for λ_1 and λ_2 and requires time consuming numerical study.

A second approach is to examine Equation 5.27 when γ is small and for the initial value problem (no forcing). The result if the perturbation problem was completed would be in the form of

$$z_j = z_j^{(0)} + \gamma z_j^{(1)} + ... \tag{5.64}$$

The leading order solution is known, since the problem looks exactly like the SDOF constantly damped variable stiffness initial value problem solved in Chapter 3. The 1^{st} order correction is of order γ. Hence, for small γ, the optimal control policy found for the SDOF problem will be approximately optimal for the coupled problem.

This result can also be seen by looking at the approximate solution for the coupled problem (Equation 5.54) and by assuming the goal is to maximize the decay coefficients in the exponential terms. The arguement of the exponential decay terms are nearly the same for both terms, and only differ in the arguement's denominator. As the denominator of the arguement of the exponential term is not a function of λ_1 and λ_2, it would seem desirable to maximize numerator of the arguement (i.e. maximize $\zeta\omega_n$). This is equivalent to choosing the SDOF uncoupled optimal control policy found in Chapter 3 (see Equations 3.158 and 3.159 while using Figures 3.12 and 3.13). Hence, this policy will be used.

Time Response Results. Time response plots were created for both the approximate solution and for the simulated solution of the exact equations of motion. In what follows, only the initial velocity problem is considered, since the initial displacement problem would be very similar. For the 3 DOF problem, two initial value problems are

considered. One possibility is only the base mass m_1^* has an initial velocity, resulting in

$$z_{j0}^* = 0, \quad \dot{z}_{j0}^* = -\dot{x}_{10}^* \tag{5.65}$$

and

$$y_0^* = 0, \quad \dot{y}_0^* = \frac{m_1^*}{m_T^*}\dot{x}_{10}^* \tag{5.66}$$

by applying Equation 5.21 and 5.20. Here, $j = 2, 3$ and $p = 3$. In this situation, letting

$$L^* = -\frac{\dot{x}_{10}^*}{\omega_0^*} \tag{5.67}$$

results in the nondimensional initial conditions

$$z_{j0} = 0, \quad \dot{z}_{j0} = 1 \tag{5.68}$$

and

$$y_0 = 0, \quad \dot{y}_0 = -\frac{m_1^*}{m_T^*}. \tag{5.69}$$

The other case is for one of the other masses to have an initial velocity, say m_2^*. Since $m_2^* = m_3^*$ and the isolation devices are identical, it does not matter which one is chosen. In this case applying Equation 5.21 and 5.20 results in

$$z_{j0}^* = 0, \quad \dot{z}_{20}^* = \dot{x}_{20}^*, \quad \dot{z}_{30}^* = 0 \tag{5.70}$$

and

$$y_0^* = 0, \quad \dot{y}_0^* = \gamma\xi\dot{x}_{20}^* \tag{5.71}$$

where $j = 2, 3$, again. Selecting

$$L^* = \frac{\dot{x}_{20}^*}{\omega_0^*} \tag{5.72}$$

results in the nondimensional initial conditions

$$z_{j0} = 0, \quad \dot{z}_{20} = 1, \quad \dot{z}_{30} = 0 \tag{5.73}$$

and

$$y_0 = 0, \quad \dot{y}_0 = \gamma\xi. \tag{5.74}$$

Representative results for the second case will be shown, since only one case is required to understand the basic utility of these results.

Figure 5.2 shows a time response plot for the case $\gamma = 0.2$, $\varepsilon = 0.8$, and $\mu = 0$. The SDOF uncoupled time response was plotted, showing that for small coupling, the response could be used to estimate the coupled response at least for the disturbed mass. Naturally, no information is provided for the undisturbed mass with this formulation. The simulated and estimated coupled solutions are also plotted, showing that the estimated solution is a reasonable approximation to the true system, for both the disturbed and undisturbed masses.

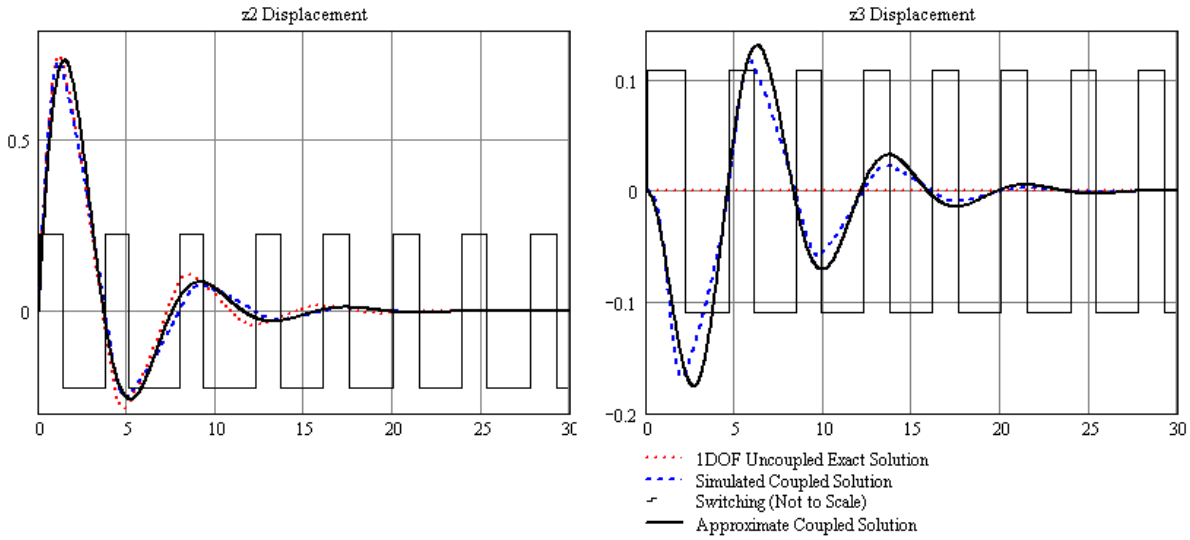

Figure 5.2 Nondimensional Relative Displacements for the 3 DOF Initial Velocity Problem ($\gamma = 0.2$, $\varepsilon = 0.8$, $\mu = 0$)

Figure 5.3 shows a time response plot for the case $\gamma = 0.2$, $\varepsilon = 0.8$, and $\mu = 0.6$. In this result, the approximate solution underpredicts the simulated displacement in the near time behavior, resulting in error. However, the error is not so large that the approximate solution cannot be used in a preliminary design. Running other simulations shows as coupling increases and ε increases, the accuracy of the approximate solution decreases.

Since the coupling is expected to be small for space telescopes, the error between actual and approximate solutions is expected to be reasonably small.

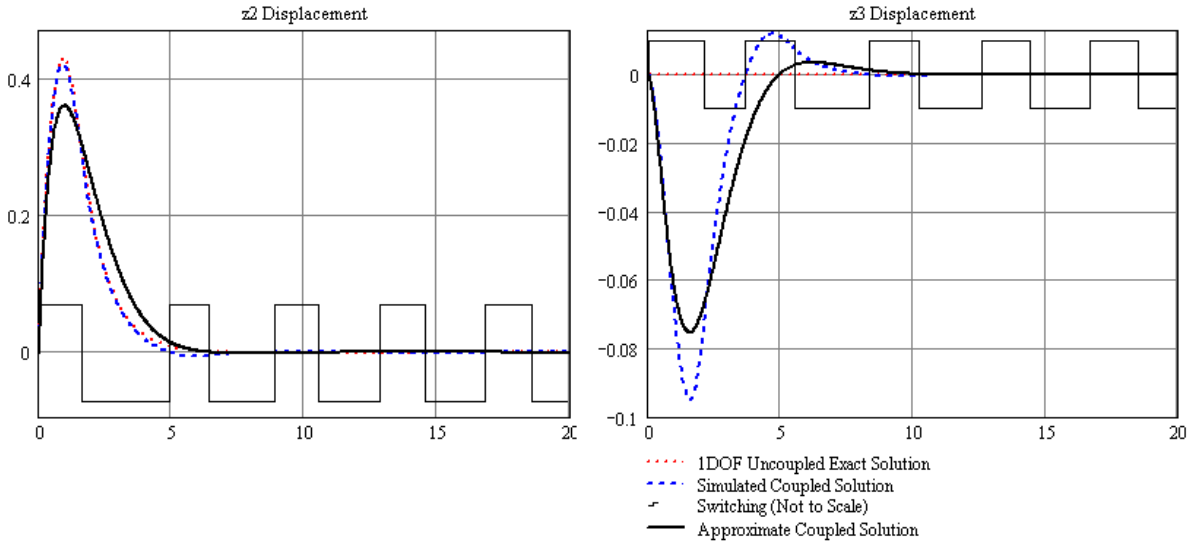

Figure 5.3 Nondimensional Relative Displacements for the 3 DOF Initial Velocity Problem ($\gamma = 0.2$, $\varepsilon = 0.8$, $\mu = 0.6$)

Sinusoidally Forced Problem. In this section, the sinusoidally forced space telescope problem was considered. It was assumed m_1 was disturbed sinusoidally and the goal was to minimize the transmission of the disturbance to two masses connected in parallel. This equates to $Q_1^* = A^* \cos \omega^* t^*$ with all other disturbances 0, and $p = 3$. Then Equation 5.27 becomes

$$\ddot{z}_j + 2\mu \dot{z}_j + (1 + \varepsilon u)\, z_j = \gamma \sum_{\substack{k=2 \\ k \neq j}}^{3} \ddot{z}_k - \frac{\gamma}{1+\gamma} \cos \omega t \tag{5.75}$$

where $j = 2, 3$ and by Equation 5.26, $L^* = \frac{A^*}{k^*}$.

Linear Approximate Solution. Another well known approach for solving linear problems is through modal analysis [71]. Essentially, a transformation matrix of eigenvectors is found that completely decouples all of the differential equations in a system of equations. It is assumed as previously done that the masses of the forced system are all equal (except the base mass m_1^*) and the isolators are all exactly the same. An estimated analytic solution can be found by applying Equations 4.69 and 4.70 to Equation

5.75 resulting in

$$\ddot{z}_j + 2\mu_e \dot{z}_j + \omega_e^2 z_j = \gamma \sum_{\substack{k=2 \\ k \neq j}}^{3} \ddot{z}_k - \frac{\gamma}{1+\gamma} \cos \omega t. \tag{5.76}$$

or in matrix form

$$\ddot{z} + \frac{2\mu_e}{1-\gamma^2} \begin{bmatrix} 1 & \gamma \\ \gamma & 1 \end{bmatrix} \dot{z} + \frac{\omega_e^2}{1-\gamma^2} \begin{bmatrix} 1 & \gamma \\ \gamma & 1 \end{bmatrix} z = -\frac{\gamma}{1-\gamma^2} \cos \omega t \begin{bmatrix} 1 \\ 1 \end{bmatrix}. \tag{5.77}$$

Letting

$$z = Pq \tag{5.78}$$

where $P = \begin{bmatrix} -1 & 1 \\ 1 & 1 \end{bmatrix}$ allows Equation 5.77 to be put in modal form resulting in

$$\ddot{q} + \frac{2\mu_e}{1-\gamma^2} \begin{bmatrix} 1-\gamma & 0 \\ 0 & 1+\gamma \end{bmatrix} \dot{q} + \frac{\omega_e^2}{1-\gamma^2} \begin{bmatrix} 1-\gamma & 0 \\ 0 & 1+\gamma \end{bmatrix} q = -\frac{\gamma}{1-\gamma^2} \cos \omega t \begin{bmatrix} 0 \\ 1 \end{bmatrix}. \tag{5.79}$$

The solution to Equation 5.79 is

$$q = \begin{bmatrix} 0 \\ \psi \cos(\omega t + \theta) \end{bmatrix} \tag{5.80}$$

where

$$\psi = \frac{\gamma}{(1+\gamma)\sqrt{\left[\omega_e^2 - \omega^2(1-\gamma)\right]^2 + (2\mu_e \omega)^2}} \tag{5.81}$$

and

$$\theta = \pi - \tan^{-1} \frac{2\mu_e \omega}{\omega_e^2 - \omega^2(1-\gamma)}. \tag{5.82}$$

Then

$$z = \psi \cos(\omega t + \theta) \begin{bmatrix} 1 \\ 1 \end{bmatrix} \tag{5.83}$$

showing both mirrors oscillate in phase and with the same displacement. This basic process could be applied to solve problems where there are more than 2 mirrors (i.e. $p > 3$).

Frequency Response Comparison. Equation 5.75 was simulated over a range of frequencies using the same method discussed in Chapter 4.4 to develop a Bode plot of the response. The simulated solution was the same for both mirrors (m_2^* and m_3^*). Both approximations developed in Chapter 4 were compared to the simulated response. Figure 5.4 shows a comparison for the frequency response of both approximate and simulated solutions for a lightly coupled system and for $\lambda_1 = 0.5$. Reasonable agreement was found for low frequency and peak response. At high frequency, the approximate solutions show a 40 dB/decade decrease while the simulated solution decreases at a more shallow rate. The reason for this is not currently known. Hence, it would appear the approximate solution provides reasonable accuracy, except at high frequency.

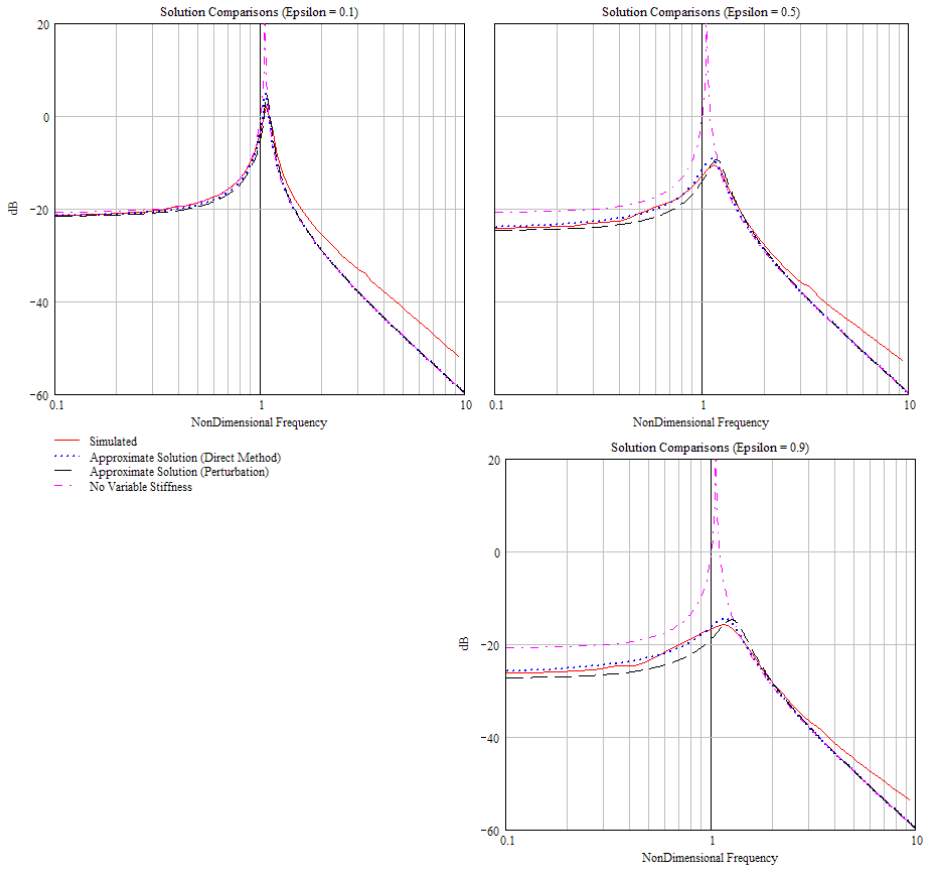

Figure 5.4 Nondimensional Relative Displacements for the 3 DOF Initial Velocity Problem ($\gamma = 0.2$, $\lambda_1 = 0.5$, $\lambda_2 = 0$, $\mu = 0$)

The setting for $\lambda_1 = 0.5$ was arbitrary. It is possible to estimate an optimal control law for the system, which might differ from the optimal control law found for the SDOF problem. The difference in control law is because of the coupling coefficient γ found in Equation 5.81 which does not appear in the SDOF approximate amplitude. For small γ, the control law will match the SDOF problem, but for large γ, there will likely be a difference.

5.3 Series Mass MDOF System

Equations of Motion. Figure 5.5 represents another type of model with all masses in series with each other. The equations of motion are

$$m_1^*\ddot{x}_1^* + \tilde{c}_2^*\left(\dot{x}_1^* - \dot{x}_2^*\right) + \tilde{k}_2^*\left(x_1^* - x_2^*\right) = Q_1^*, \tag{5.84}$$

$$m_i^*\ddot{x}_i^* + \tilde{c}_i^*\left(\dot{x}_i^* - \dot{x}_{i-1}^*\right) + \tilde{c}_{i+1}^*\left(\dot{x}_i^* - \dot{x}_{i+1}^*\right) + \tilde{k}_i^*\left(x_i^* - x_{i-1}^*\right) + \tilde{k}_{i+1}^*\left(x_i^* - x_{i+1}^*\right) = Q_i^*, \tag{5.85}$$

and

$$m_p^*\ddot{x}_p^* + \tilde{c}_p^*\left(\dot{x}_p^* - \dot{x}_{p-1}^*\right) + \tilde{k}_p^*\left(x_p^* - x_{p-1}^*\right) = Q_p^*, \tag{5.86}$$

where $p > 1$ is the number of masses in the system and $i = 2...p-1$. For the MDOF model, a particular mass or group of masses may be allowed to vibrate while another particular mass or group of masses may need to be isolated from vibration. For example, this type of model has been used to model a launch vehicle with a payload [148], [47]. Alternatively, this type of system can be used to approximate the solution to a distributed system [149]. In this case, the system might represent a variable stiffness beam in axial vibration. The parameter $\tilde{c}_i^*$ is the coefficient of damping for the i^{th} viscous damper, $\tilde{k}_i^*$ is the variable stiffness function for the i^{th} variable stiffness spring, Q_i^* is the i^{th} disturbance force acting on the i^{th} mass m_i^*, and Q_1^* is the disturbance force on m_1^*.

The initial conditions can be defined in the same way as the parallel mass MDOF system using Equations 5.3 and 5.4 by defining $j = 2, 3, ..., p$. The rigid body modes for

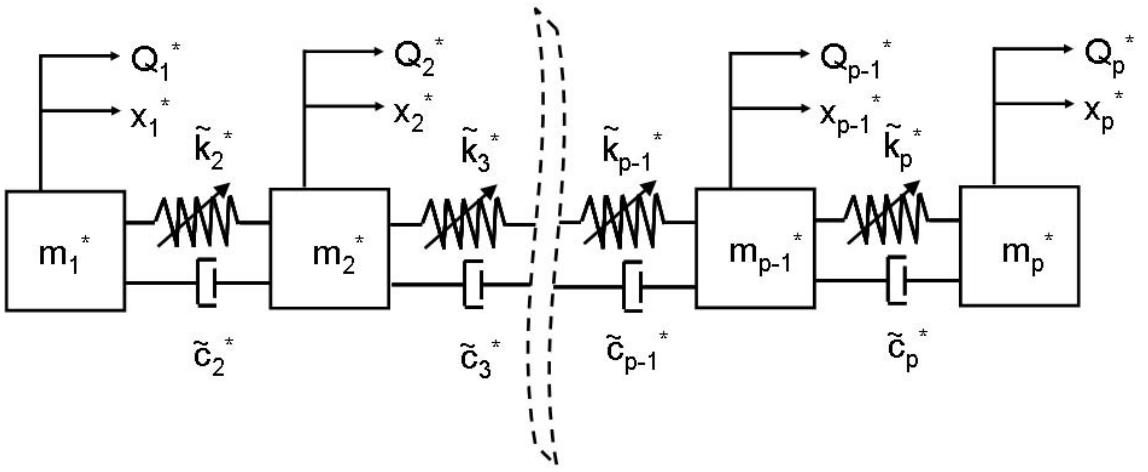

Figure 5.5 MDOF Masses in Series Variable Stiffness Constantly Damped Problem

Equations 5.84, 5.85, and 5.86 can be separated out by defining

$$z_j^* = x_j^* - x_{j-1}^* \tag{5.87}$$

and using Equations 5.5 and 5.7. Solving Equation 5.87 for x_j^* and recognizing it is a recursive relationship results in

$$x_j^* = x_1^* + \sum_{n=2}^{j} z_n^*. \tag{5.88}$$

Solving for x_1^* and x_j^* results in

$$x_1^* = y^* - Z_p^*, \tag{5.89}$$

$$x_j^* = y^* - Z_p^* + \sum_{i=2}^{j} z_j^*. \tag{5.90}$$

where

$$Z_p^* = \frac{\sum_{i=2}^{p} m_i^* \sum_{j=2}^{i} z_j^*}{m_T^*} = \frac{\sum_{j=2}^{p} z_j^* \sum_{i=j}^{p} m_i^*}{m_T^*}. \tag{5.91}$$

Substituting Equations 5.87, 5.89 and 5.90 into Equations 5.84, 5.85, and 5.86 results in

$$m_1^* \left(\ddot{y}^* - \ddot{Z}_p^* \right) - \tilde{c}_2^* \dot{z}_2^* - \tilde{k}_2^* z_2^* = Q_1^*, \tag{5.92}$$

$$m_i^* \left(\ddot{y}^* - \ddot{Z}_p^* + \sum_{n=2}^{i} \ddot{z}_n^* \right) + \tilde{c}_i^* \dot{z}_i^* - \tilde{c}_{i+1}^* \dot{z}_{i+1}^* + \tilde{k}_i^* z_i^* - \tilde{k}_{i+1}^* z_{i+1}^* = Q_i^*, \tag{5.93}$$

and

$$m_p^* \left(\ddot{y}^* - \ddot{Z}_p^* + \sum_{n=2}^{p} \ddot{z}_j^* \right) + \tilde{c}_p^* \dot{z}_p^* + \tilde{k}_p^* z_p^* = Q_p^*. \tag{5.94}$$

Adding all i equations of Equation 5.93 to Equations 5.92 and 5.94 results in

$$\ddot{y}^* = \frac{\sum_{i=1}^{p} Q_i^*}{m_T^*} \tag{5.95}$$

which is the same as Equation 5.13 and represents rigid body motion. Substituting Equation 5.95 into Equations 5.93, 5.92, and 5.94 results in

$$\frac{m_1^* \sum_{i=2}^{p} m_i^*}{m_T^*} \ddot{z}_2^* + \tilde{c}_2^* \dot{z}_2^* + \tilde{k}_2^* z_2^* = \frac{m_1^*}{m_T^*} \sum_{i=1}^{p} Q_i^* - Q_1^* - \frac{m_1^*}{m_T^*} \sum_{j=3}^{p} \ddot{z}_j^* \sum_{i=j}^{p} m_i^*, \tag{5.96}$$

$$m_i^* \left(-\ddot{Z}_p^* + \sum_{n=2}^{i} \ddot{z}_n^* \right) + \tilde{c}_i^* \dot{z}_i^* - \tilde{c}_{i+1}^* \dot{z}_{i+1}^* + \tilde{k}_i^* z_i^* - \tilde{k}_{i+1}^* z_{i+1}^* = Q_i^* - \frac{m_i^*}{m_T^*} \sum_{i=1}^{p} Q_i^* \tag{5.97}$$

$$m_p^* \left(-\ddot{Z}_p^* + \sum_{n=2}^{p} \ddot{z}_j^* \right) + \tilde{c}_p^* \dot{z}_p^* + \tilde{k}_p^* z_p^* = Q_p^* - \frac{m_i^*}{m_T^*} \sum_{i=1}^{p} Q_i^*. \tag{5.98}$$

The transformed initial conditions are found by applying Equations 5.5 and 5.87.

3 DOF Problem. Next, a 3 DOF problem is considered, by letting $p = 3$. The simplified equations of motion are

$$\frac{m_1^* \left(m_2^* + m_3^* \right)}{m_T^*} \ddot{z}_2^* + \tilde{c}_2^* \dot{z}_2^* + \tilde{k}_2^* z_2^* = \frac{m_1^*}{m_T^*} \sum_{i=1}^{3} Q_i^* - Q_1^* - \frac{m_1^* m_3^*}{m_T^*} \ddot{z}_3^* \tag{5.99}$$

and

$$\frac{m_3^* \left(m_1^* + m_2^* \right)}{m_T^*} \ddot{z}_3^* + \tilde{c}_3^* \dot{z}_3^* + \tilde{k}_3^* z_3^* = \frac{m_1^* + m_2^*}{m_T^*} Q_3^* - \frac{m_3^*}{m_T^*} \left(Q_1^* + Q_2^* \right) - \frac{m_1^* m_3^*}{m_T^*} \ddot{z}_2^*. \tag{5.100}$$

Next, the damping and variable stiffness functions are specified as

$$\begin{aligned}\tilde{c}_2^* &= c_2^* \\ \tilde{c}_3^* &= c_3^* \\ \tilde{k}_2^* &= k_2^* \left(1 + \varepsilon_2 u_2\right) \\ \tilde{k}_3^* &= k_3^* \left(1 + \varepsilon_3 u_3\right)\end{aligned} \tag{5.101}$$

where c_2^*, c_3^*, k_2^*, and k_3^* are constants. The parameters ε_2 and ε_3 are the total variation in variable stiffness while the functions u_2 and u_3 are defined as

$$\begin{aligned}u_2 &= sgn[(\lambda_1 z_2 + \dot{z}_2)(\lambda_2 \dot{z}_2 + z_2)] \\ u_3 &= sgn[(\lambda_1 z_3 + \dot{z}_3)(\lambda_2 \dot{z}_3 + z_3)]\end{aligned} \tag{5.102}$$

which are control laws. This represents the 3 DOF equation of motion in exact form. However, the exact form is difficult to solve, so the coefficients will be replaced with an approximate form based on the approximate equivalent damping and stiffness coefficients defined by Equations 3.163 and 3.164. The damping and stiffness functions are replaced as

$$\begin{aligned}\tilde{c}_2^* &= 2\zeta_2 \omega_{n_2} \sqrt{\frac{m_1^*\left(m_2^*+m_3^*\right)k_2^*}{m_T^*}} \\ \tilde{c}_3^* &= 2\zeta_3 \omega_{n_3} \sqrt{\frac{m_3^*\left(m_1^*+m_2^*\right)k_3^*}{m_T^*}} \\ \tilde{k}_2^* &= k_2^* \omega_{n_2}^{*^2} \\ \tilde{k}_3^* &= k_3^* \omega_{n_3}^{*^2}\end{aligned} \quad . \tag{5.103}$$

Next, the equations of motion will be nondimsionalized. To begin, define

$$w_0^* = \sqrt{\frac{k_2^* m_T^*}{m_1^*\left(m_2^* + m_3^*\right)}} \tag{5.104}$$

which is the uncontrolled natural frequency for Equation 5.99 and will be used to scale time for the system. By selecting a nonzero length $L^* \neq 0$ which will be selected later, Equations 5.99 and 5.100 can be nondimensionalized by letting

$$t^* = \frac{t}{w_0^*}, \tag{5.105}$$

$$z_i^* = L^* z_i, \tag{5.106}$$

and

$$Q_i^* = \frac{m^* L^* {\omega_0^*}^2}{1+\gamma} = L^* k^* Q_i. \tag{5.107}$$

The nondimensional equations become

$$\ddot{z}_2 + 2\zeta_2 \omega_{n_2} \dot{z}_2 + \omega_{n_2}^2 z_2 = -\gamma_2 \ddot{z}_3 + \frac{m_1^*}{m_T^* k_2^* L^*} \left(Q_2^* + Q_3^*\right) - \frac{m_2^* + m_3^*}{m_T^* k_2^* L^*} Q_1^* \tag{5.108}$$

and

$$\ddot{z}_3 + 2\zeta_3 \omega_{n_3} \sqrt{\frac{\gamma_3}{\gamma_2}} \xi \dot{z}_3 + \omega_{n_3}^2 z_3 = -\gamma_3 \ddot{z}_2 + \frac{m_1^*}{m_T^* \gamma_2 k_2^* L^*} Q_3^* - \frac{\gamma_3 \left(m_2^* + m_3^*\right)}{m_T^* k_2^* L^*} \left(Q_1^* + Q_2^*\right) \tag{5.109}$$

where

$$\gamma_2 = \frac{m_3^*}{m_2^* + m_3^*}, \tag{5.110}$$

$$\gamma_3 = \frac{m_1^*}{m_1^* + m_2^*}, \tag{5.111}$$

and

$$\xi = \sqrt{\frac{k_3^*}{k_2^*}}. \tag{5.112}$$

The parameters γ_2 and γ_3 are measures of the coupling of the system which are bounded between 0 and 1.

Considering Equations 5.108 and 5.109, an appropriate length scale can now be chosen. For an unforced problem a length scale can be created by defining a nonzero length such as

$$L^* = \max\left(x_{10}^*, x_{20}^*, x_{30}^*\right) \tag{5.113}$$

for the initial displacement problem or

$$L^* = \frac{\max\left(\dot{x}_{10}^*, \dot{x}_{20}^*, \dot{x}_{30}^*\right)}{w_0^*} \tag{5.114}$$

for the initial velocity problem. For the forced problem with no initial conditions, it is convenient to choose L^* such that the amplitude of at least one of the forcing functions is unity.

3 DOF Initial Value Problem. For the initial value problem when $Q_i^* = 0$, Equations 5.108 and 5.109 become

$$\begin{bmatrix} 1 & \gamma_2 \\ \gamma_3 & 1 \end{bmatrix} \begin{Bmatrix} \ddot{z}_2 \\ \ddot{z}_3 \end{Bmatrix} + \begin{bmatrix} 2\zeta_2\omega_{n_2} & 0 \\ 0 & 2\zeta_3\omega_{n_3}\sqrt{\frac{\gamma_3}{\gamma_2}\xi} \end{bmatrix} \begin{Bmatrix} \dot{z}_2 \\ \dot{z}_3 \end{Bmatrix} + \begin{bmatrix} \omega_{n_2}^2 & 0 \\ 0 & \omega_{n_3}^2 \end{bmatrix} \begin{Bmatrix} z_2 \\ z_3 \end{Bmatrix} = 0 \tag{5.115}$$

or

$$\begin{Bmatrix} \ddot{z}_2 \\ \ddot{z}_3 \end{Bmatrix} + 2A \begin{Bmatrix} \dot{z}_2 \\ \dot{z}_3 \end{Bmatrix} + B \begin{Bmatrix} z_2 \\ z_3 \end{Bmatrix} = 0 \tag{5.116}$$

where

$$A = \frac{1}{1-\gamma_2\gamma_3} \begin{bmatrix} 1 & -\gamma_2 \\ -\gamma_3 & 1 \end{bmatrix} \begin{bmatrix} \zeta_2\omega_{n_2} & 0 \\ 0 & \zeta_3\omega_{n_3}\sqrt{\frac{\gamma_3}{\gamma_2}\xi} \end{bmatrix} \tag{5.117}$$

and

$$B = \frac{1}{1-\gamma_2\gamma_3} \begin{bmatrix} 1 & -\gamma_2 \\ -\gamma_3 & 1 \end{bmatrix} \begin{bmatrix} \omega_{n_2}^2 & 0 \\ 0 & \omega_{n_3}^2\sqrt{\frac{\gamma_3}{\gamma_2}\xi} \end{bmatrix}. \tag{5.118}$$

Equation 5.116 can be solved analytically if A and B are simultaneously diagonalizable. This occurs if and only if $AB = BA$ [74], [75], [76]. Using symbolic software, $AB = BA$ when

$$\frac{\zeta_2\omega_{n_2}}{\zeta_3\omega_{n_3}} = \sqrt{\frac{\gamma_2}{\gamma_3\xi}}. \tag{5.119}$$

Equation 5.119 can also be derived by examining what is different between A and B and requiring

$$\zeta_2 = C\omega_{n_2} \tag{5.120}$$

and

$$\zeta_3 = C\omega_{n_3}\sqrt{\frac{\gamma_3}{\gamma_2}\xi} \tag{5.121}$$

where C is an arbitrary constant. Then solving one equation for C and substituting it into the other results in Equation 5.119. This method of diagonalizing the matrices is

called proportional damping where C is the proportional damping coefficient [71]. The restriction of Equation 5.119 prevents analytic solutions to a rocket problem, and limits approximations to a beam problem.

When Equation 5.119 is true, Equation 5.116 can be solved using classical modal analysis methods. Equation 5.116 can be rewritten as

$$\{\ddot{z}\} + 2C_D [K] \{\dot{z}\} + C_S [K] \{z\} = 0 \tag{5.122}$$

where C_D and C_S are constants. A transformation P can defined such that

$$[P]^{-1} [K] [P] = [D] \tag{5.123}$$

where $[D]$ is a diagonal matrix. Defining a new coordinate vector $\{q\}$ using the relationship

$$\{z\} = [P] \{q\}, \tag{5.124}$$

substituting into Equation 5.122, then premultiplying Equation 5.122 by $[P]^{-1}$ results in

$$\{\ddot{q}\} + 2C_D [D] \{\dot{q}\} + C_S [D] \{q\} = 0. \tag{5.125}$$

Solving for q_n where $n = 2, 3$ results in

$$q_n = a_n e^{-C_D D_n t} \cos\left(\sqrt{C_S D_n - C_D^2 D_n^2}\, t + \theta_n\right) \tag{5.126}$$

where

$$a_n = \frac{\sqrt{q_{n0}^2 \left(C_S D_n - C_D^2 D_n^2\right) + \left(\dot{q}_{n0} + C_D D_n q_{n0}\right)^2}}{\sqrt{C_S D_n - C_D^2 D_n^2}} \tag{5.127}$$

and

$$\theta_n = -\tan^{-1}\left(\frac{\dot{q}_{n0} + C_D D_n q_{n0}}{q_{n0}\sqrt{C_S D_n - C_D^2 D_n^2}}\right). \tag{5.128}$$

The variables q_{n0} and $\dot{q}_{n0}$ are the initial conditions for Equation 5.122 and can be found by applying Equation 5.124.

Time Response Results. The 3 DOF problem was simulated using the nonlinear system and was approximated. The values

$$\begin{aligned} m_1^* &= m_2^* = m_3^* = 20 \\ c_1^* &= c_2^* = 0 \\ k_1^* &= k_2^* = 10^4 \end{aligned} \tag{5.129}$$

were selected to compare the approximate solution with the simulated exact solution. Results are shown in dimensional form and using the original inertial references. The initial conditions were all assumed to be 0, except for the initial velocity on m_1^* which was set to 1. By applying the solution to Equation 5.95, the rigid body motion of the system was subtracted out of the response leaving just the vibrational motion for examination.

The control law was set to match the optimal SDOF unforced problem. While this control law is optimal for the SDOF problem, it is uncertain whether it is optimal for the 3 DOF system. It was found that the approximate solution becomes increasingly less accurate as the control law is changed from the SDOF optimal control law. The inaccuracy due to changing the control law means that the real 3DOF system is switching differently than the SDOF problem. The difference in switching is because coupling between the masses is strong. Recalling Equations 5.110 and 5.111, the coupling coefficients γ_2 and γ_3 are both $\frac{1}{2}$. Further, as ε is increased, the approximate solution was found to become less accurate. Increasing ε strengthens the nonlinear behavior of the variable stiffness device, which then increases any switching errors. Hence, for sufficiently small values of ε, the approximate solution works well. For large values of ε, however, the approximate solution is not valid.

Figure 5.6 shows a time displacement history when $\varepsilon = 0.1$ and there is no viscous damping. The results show the approximate solution slightly overpredicts the amplitude of the real system, but otherwise is providing a good estimate of the behavior of the real system.

Next, the response when $\varepsilon = 0.9$ was examined, shown in Figure 5.7. The response has about the right order of magnitude, but the frequency of the approximate solution

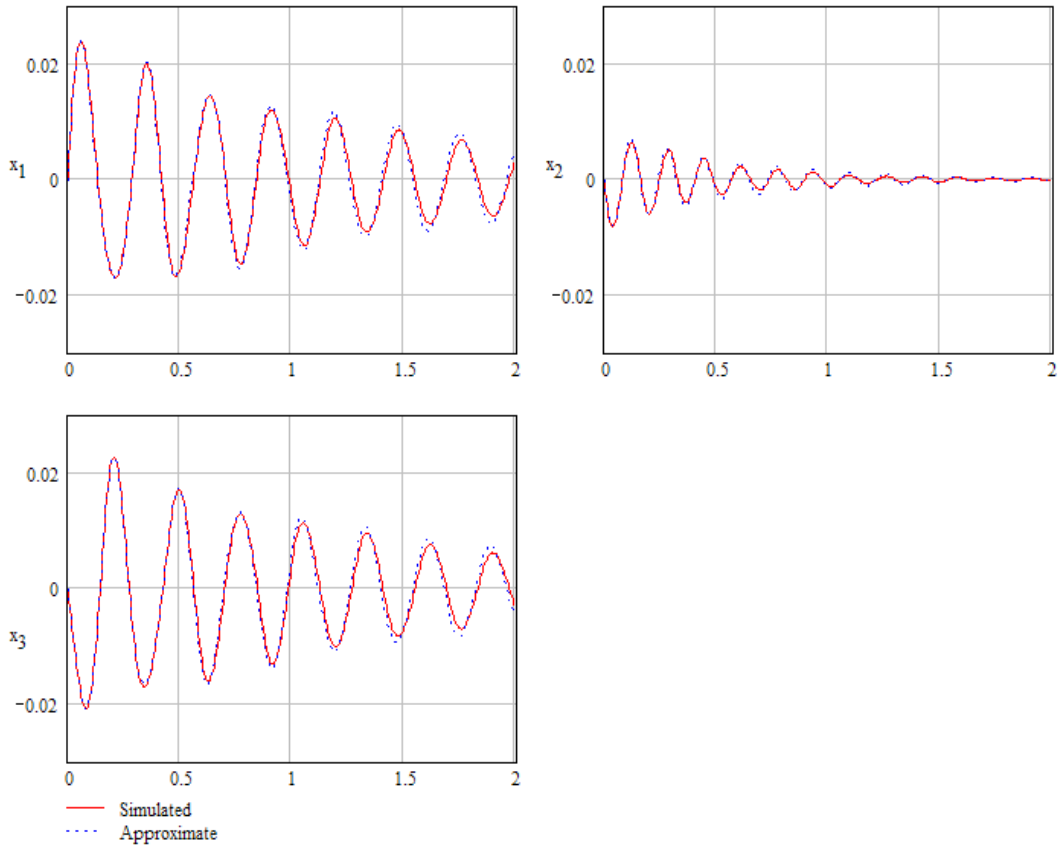

Figure 5.6 Dimensional 3 DOF Series Model Vibrational Displacement History ($\varepsilon = 0.1$, $\mu = 0$)

is too fast and out of phase with the clearly nonlinear simulated response. This shows the switching time has been poorly estimated and the high value of ε has exacerbated the situation.

Next, a viscous damping of $c_1^* = c_2^* = 365$ was selected, making $\mu = 0.5$. Figure 5.8 shows the response for the system when $\varepsilon = 0.1$. Good agreement was found for both the simulated and approximate solutions. Though not shown, for values of $\varepsilon < 0.4$, the approximate solution appears to reasonably agree with the simulated solution. For higher values of ε, the approximate solution fails to predict the system behavior. For high values of μ, the approximate solution becomes inaccurate for lower values of ε, though values of ε as high as 0.1 seem reasonable as $\mu \to 1$. Since real devices operate for these settings of

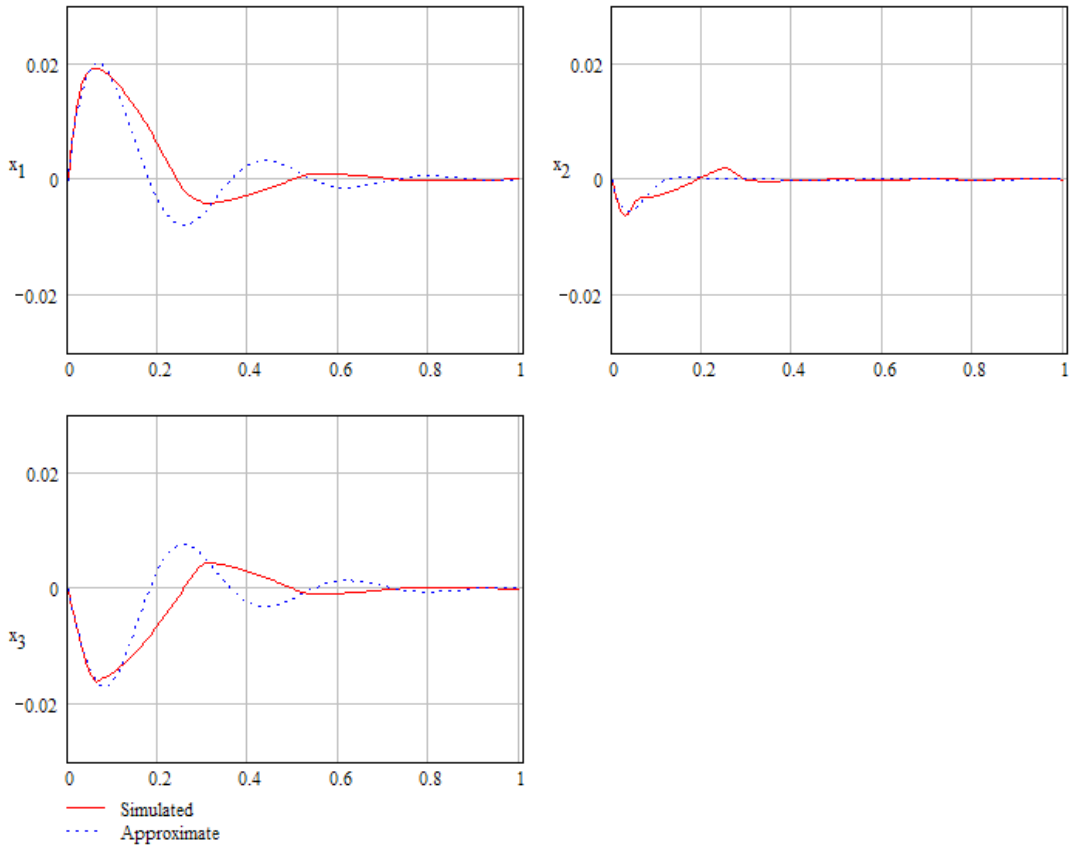

Figure 5.7 Dimensional 3 DOF Series Model Vibrational Displacement History ($\varepsilon = 0.9$, $\mu = 0$)

ε as seen in Table 2.2, this method can be used to approximate the system behavior of a system when ε is small.

5.4 Conclusions

Two types of variable stiffness MDOF problems were examined using the approximate solutions developed in Chapters 3 and 4. One MDOF problem can be used for preliminary design in a space telescope problem while the other MDOF problem can be used to approximate a variable stiffness continuous beam. In both cases, the approximate solution provided a good estimate of the simulated solution for small ε and small coupling between the masses in the system. For higher values of ε but with small coupling, the approximate solution was reasonable, but contained error. For higher coupling and higher

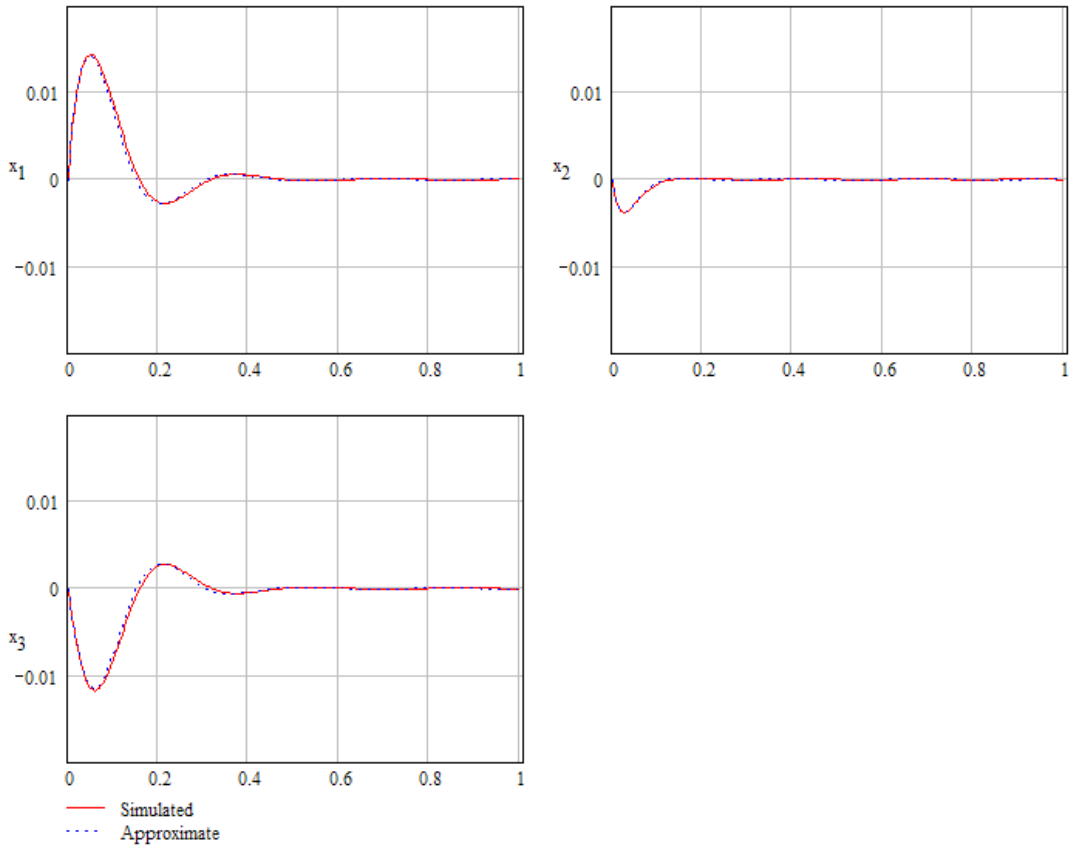

Figure 5.8 Dimensional 3 DOF Series Model Vibrational Displacement History ($\varepsilon = 0.1$, $\mu = 0.5$)

ε values, the error became rather large, making the approximate solution a poor estimate of the system.

6. Conclusions and Recommendations

Semi-active vibration control or the ability to dynamically change damping and/or stiffness of a structure to reduce vibration is a rich area for investigation. It has the potential to be used in many space applications because it can provide almost the same capabilities as combined passive and active control (often called hybrid control), but uses much less power. Semi-active systems (like hybrid systems) can also fail gracefully in that they can still provide a passive control capability if the powered portion of a device were to fail. A great deal of research is being done on smart materials that are capable of changing both damping and stiffness. These smart materials include electrorheological dampers, magnetorhelogical dampers, shunted piezoelectric crystals, shape memory alloys, magnetorheological elastomers, and mechanical devices. The difficulty with the control concepts and the devices considered is that they are all nonlinear making engineering design difficult [1].

In this work, a simple analytic variable stiffness device using a general on-off control law was analyzed using several models. All models combined the variable stiffness device with a constant viscous damper. In all cases, the initial value problem was examined, while the sinusoidally forced problem was examined for the single degree of freedom problem and one version of a multi-degree of freedom model. These disturbances are representative of shocks and rotating machinery, respectively. Analysis started with a single degree of freedom model and worked up to multi-degree of freedom models making use of the insight gained from the smaller problems. Various methods were applied to gain insight into the problems to include exact analytic solutions, ad hoc approximations, perturbation methods, nonlinear analysis, and linear approximate methods. In the next sections, important results will be summarized. Next, developed engineering tools will be identified. Finally, follow on research is extensively outlined to include extensions to this work and an approach for analyzing variable mass systems.

6.1 Executive Summary of Research Results and Conclusions

For the first time, the damped single degree of freedom variable stiffness initial value problem using a general on-off control law was solved. The author and others also recently solved the undamped single degree of freedom problem using a less general on-off control law [144]. The reason this was possible was because an exact representation of the switching was found. The exact solution was used to develop an approximate viscously damped system, which can reasonably reproduce the true system. From the exact solution, behavior of the system was explained for changes in the control law, for variations in variable stiffness strength, and for changes in the viscous damping. The variable stiffness strength was linked to real variable stiffness devices, developing a rough performance metric. Further, the guaranteed stability region taking all parameters into account was found. Using the approximate solution, the optimal control law that causes the system to settle the fastest was determined. While the optimal control law has been found previously for a system with no viscous damping, these results include viscous damping effects. It was discovered that it is possible to switch the system between underdamped and overdamped states, removing significantly more energy from the system than a viscously damped system could by itself. This is because the variable stiffness device does work on the system to remove energy and also changes the equivalent natural frequency of the system, which is impossible for a viscously damped system. Finally, the work required to achieve a desired settling time was found and a method for finding the work the variable stiffness does on the system was explained. Dividing the work in by the work out creates an efficiency factor. This result can be used to measure efficiency of real devices.

After analyzing the unforced problem, the sinusoidally forced single degree of freedom problem was examined, using the same parameters as the unforced problem. Three approximate methods were considered to develop insight and only two were viable. An ad hoc approach and a perturbation approach were found to provide a reasonable estimate for system behavior when the variable stiffness strength was small. A Fourier series approach was attempted, but the method resulted in analytically unsolvable nonlinear algebraic equations and provided no insight. The other approaches provided reasonable solutions as compared to simulated solutions of the true system. Regions for the control

law were identified that provide low frequency attenuation that a viscously damped system cannot provide. The perturbation solution was then minimized over all frequency to find a near optimal control law policy. Comparing the near optimal control policy of the forced problem to the optimal control of the unforced problem shows the policies were quite different. However, it appears possible to accept suboptimal performance for one type of disturbance and optimal performance in the other disturbance type, allowing the same control law to be used in both situations. This would, of course, be dependent on the particular application the variable stiffness is used on.

Having analyzed the single degree of freedom problem, two multi-degree of freedom problems were analyzed, where each controller has the same parameters as the single degree of freedom system. In both cases, the control laws for all of the variable stiffness devices was made the same to allow the problems to be solved analytically and restrictions on the masses were made. This made it impossible to determine if the optimal control law should vary for each mass, which seriously limited insight. The purpose of this analysis was to extend the single degree of freedom results to larger models more representative of real systems.

A system representing the cross section of a simple space telescope was examined, first. To represent the variable stiffness, the single degree of freedom equivalent viscous damping model was used. Examining the solution for the 3 degree of freedom system, it was determined that the optimal control law found from the single degree of freedom problem would still be optimal. Comparing the approximate solution to simulations using an exact model showed the approximate solution reasonably approximated the exact solution and should be usable for design purposes.

The same process was applied to a multi degree of freedom system with all masses in series. In this case, the system could represent a variable stiffness beam. This problem was much more difficult because it lacked symmetries the space telescope problem had. As a result, it required solving a more difficult eigenvalue problem, which is difficult to solve as the number of degrees of freedom in the system increase. For a 3 degree of freedom problem, it can be solved. Comparisons were made once again between the approximate and exact simulated solutions. In this case, if the variable stiffness strength was not too

strong, approximate solution provided reasonable results. For larger variable stiffness strength, the approach failed. A major difference between the space telescope problem and the beam problem was the coupling between masses in the space telescope was much smaller than in the beam problem.

6.2 Developed Engineering Tools Summary

Important new engineering tools will be summarized. The most important results of this research will be repeated here and reference to applicable discussion will be provided.

In Chapter 2, the literature was searched to gain understanding of variable damping and variable stiffness systems. As this work focused on variable stiffness, only these results are summarized. In searching the literature, an important parameter ε representing the total variation in variable stiffness was identified as a way of comparing variable stiffness devices. It is defined as

$$\varepsilon = \frac{k_1^* - k_0^*}{k_1^* + k_0^*} \tag{6.1}$$

where k_0^* is the smallest variable stiffness and k_1^* is the largest stiffness a device can be controlled to create. The "*" notation defines the variable as a dimensional quantity. Many variable stiffness devices exist in the literature which nearly span the possible range of ε between 0 and 1, as can be seen in Table 6.1.

An obvious question is which variable stiffness device should be used to minimize vibration in a system? Answering the question requires knowing what the performance of a system might be given a particular selection for ε. To help answer this question, the single degree of freedom vibration suppression problem

$$m^*\ddot{x}^* + c^*\dot{x}^* + \frac{(k_1^* + k_0^*)}{2}\left[1 + \varepsilon u\right] x^* = A^* \cos \omega^* t^* \tag{6.2}$$

was analyzed where m^* is a vibrating mass, c^* is the damping coefficient, A^* is the amplitude of the forcing function, w^* is the forcing frequency of a forcing function, x^* is the displacement of the vibrating mass, u is a control law, and t^* is time. In Chapter 3, the initial value problem ($A^* = 0$) was solved exactly and approximately while in Chapter 4

Table 6.1 Parameter Values for Proposed Variable Stiffness Devices in the Literature

Source	Year	Device	ε
Albanese and Cuefare [122]	2003	MRE 30% Fe	0.98
Walsh and Lamancusa [129]	1992	Leaf Spring	0.96
Albanese and Cuefare [121], [122]	2003	MRE 35% Fe	0.91
Albanese and Cuefare [121], [122]	2003	MRE 25% Fe	0.80
Albanese and Cuefare [121], [122]	2003	MRE 40% Fe	0.68
Albanese and Cuefare [121], [122]	2003	MRE 10% Fe	0.53
Williams, Chiu, and Bernhard [109]	2002	SMA	0.50
Albanese and Cuefare [121], [122]	2003	MRE 50% Fe	0.49
Clark [125]	2000	Piezoelectric Patch on Cantilever (On-Off)	0.33
Zhou [120]	2003	MRE 27% Fe	0.23
Albanese and Cuefare [121], [122]	2003	MRE 0% Fe	0.10
Ramaratnam, Jalili, and Grier [127]	2003	Piezoelectric (Capactive Shunt)	0.05
Davis and Lesieutre [126]	2000	Piezoelectric (Capactive Shunt)	0.04

the forced problem was approximated. The control law chosen in both cases was

$$u\left(x^*, \dot{x}^*\right) = sgn\left[\left(\lambda_1^* x^* + \dot{x}^*\right)\left(\lambda_2^* \dot{x}^* + x^*\right)\right] \tag{6.3}$$

where λ_1^* and λ_2^* are arbitrary real constants that tune the controller. When λ_1^* and λ_2^* are both 0, Equation 6.2 can represent a single degree of freedom system with a piezoelectric element. Equation 6.2 was nondimensionalized to generalize its use for any dimensional problem resulting in

$$\ddot{x} + 2\mu\dot{x} + (1 + \varepsilon u)\, x = 0 \tag{6.4}$$

for the unforced problem or

$$\ddot{x} + 2\mu\dot{x} + (1 + \varepsilon u)\, x = \cos\omega t \tag{6.5}$$

for the forced problem where

$$\mu = \frac{c^*}{\sqrt{2m^*\left(k_0^* + k_1^*\right)}}, \tag{6.6}$$

$$t = t^* \omega_0^*, \tag{6.7}$$

$$\lambda_1^* = \lambda_1 \omega_0^*, \tag{6.8}$$

$$\lambda_2^* = \frac{\lambda_2}{\omega_0^*}, \tag{6.9}$$

and

$$\omega_0^* = \sqrt{\frac{k_0^* + k_1^*}{2m^*}}. \tag{6.10}$$

Initial Value Problem. Equations 6.4 and 6.5 are four parameter (λ_1, λ_2, μ, ε) nonlinear problems. The exact solution, switching times, and approximate solutions for the initial value problem in terms of the four parameters can be found in Chapter 3. In the analysis process, depending on the settings of μ and ε, it was discovered switching could occur between two underdamped systems, an underdamped and a critically damped system, or an underdamped and an overdamped system. For convenience, a system switching between two underdamped systems will simply be called an underdamped system, while a system switching between underdamped and overdamped systems will be called an overdamped system. The relationship determining when the system will operate as an underdamped or overdamped system is

$$\mu_{crit} = \sqrt{1 - \varepsilon} \tag{6.11}$$

and the settings for μ and ε resulting in a particular system behavior can be found in Figure 6.1. It was found that an underdamped system displayed stable and unstable behavior depending on the settings for the control law as shown in Figure 6.2. For the overdamped system, regions where switching stopped, where switching occurred extremely rapidly, where switching caused unstable system behavior, and where switching caused stable system behavior were found as shown in Figure 6.3.

Using the approximate solution, the optimal control law that maximizes energy dispersion was identified. It was found that $\lambda_2 = 0$ and λ_1 can be set using Figure 6.4. Figure 6.4 extends results found in the literature because it allows viscous damping to be added to the system.The approximate solution was used to develop an equivalent viscously damped system, and the average natural frequency (Figure 6.6) and average damping ratio (Figure 6.5) of the system was found for the optimal control policy. Hence, using stan-

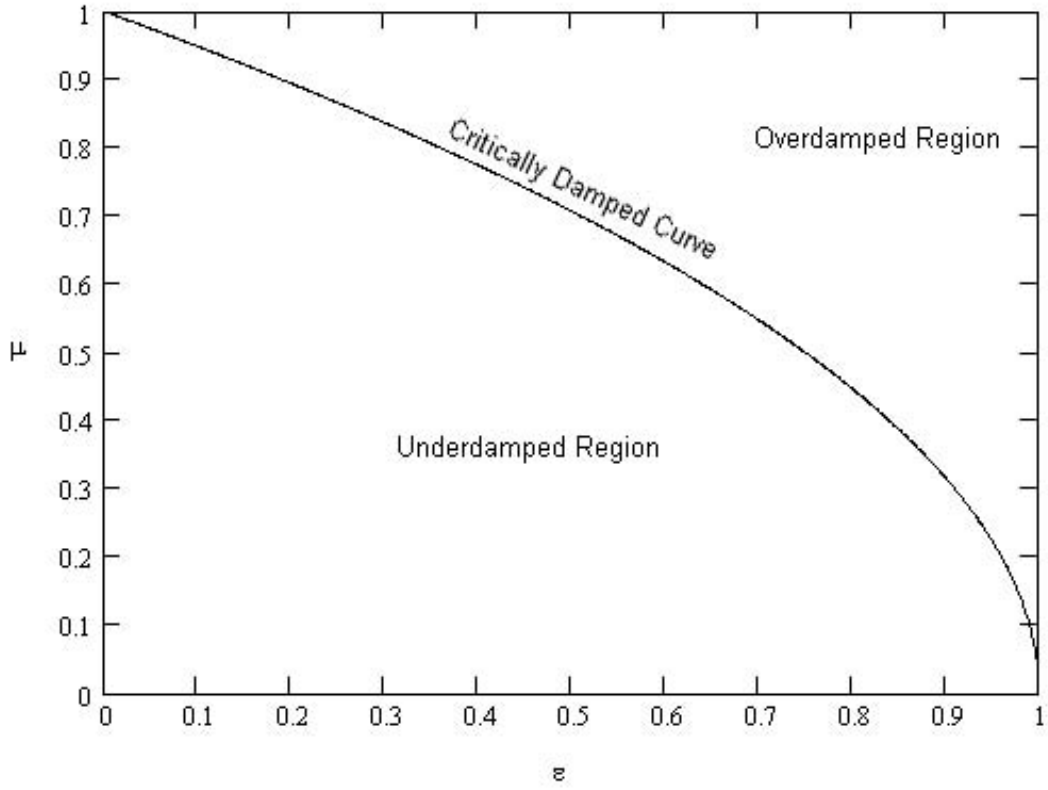

Figure 6.1 Overdamped and Underdamped Regions

dard linear control concepts (settling time, overshoot, etc.), it is now possible to classically design a single degree of freedom control system to meet a desired performance. Once the classically designed system is identified, it is now possible to select a desired variable stiffness device that will roughly provide the desired performance. The analogy is rough because real variable stiffness devices display more nonlinearity than was assumed for this analysis.

Forced Problem. An approximate solution related to a viscously damped system was developed and used to estimate the long term behavior of a sinusoidally forced system (Equation 6.5). The approximate solution is able to approximate the primary behavior of the system, but fails to take into account harmonics excited by the forcing function. The approximation works reasonably well when ε is small, but as ε increases, the error between simulated and approximate results increases at low frequency. It was discovered

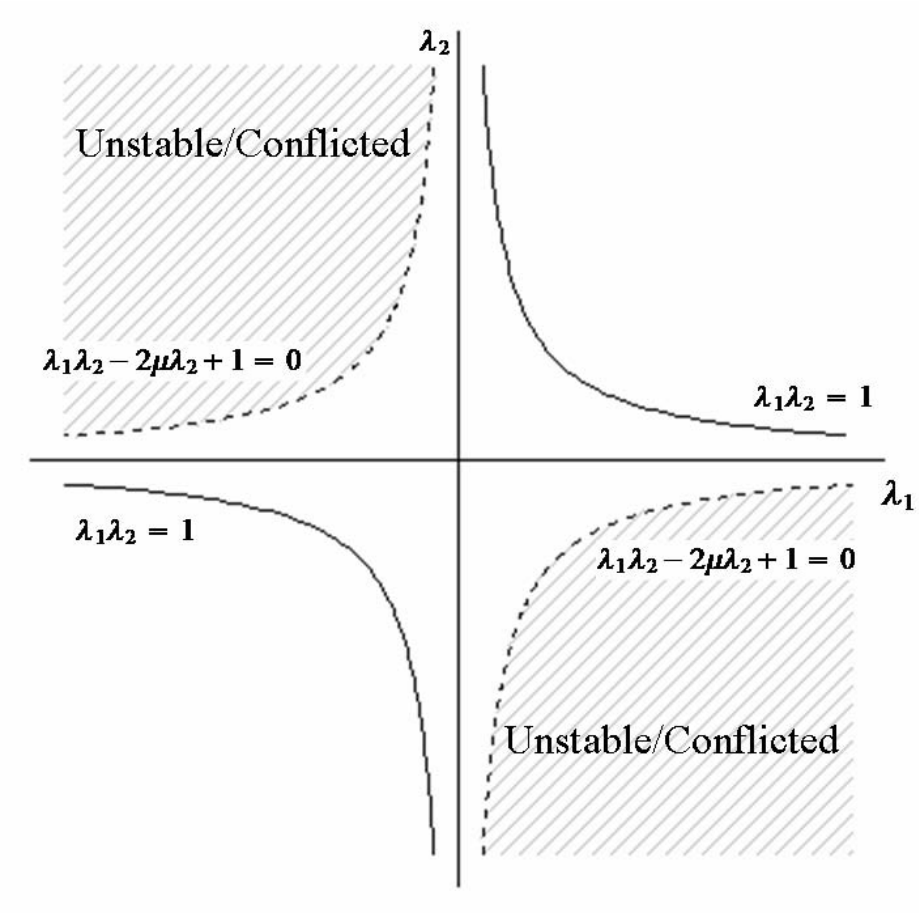

Figure 6.2 Regions where the Variable Stiffness Device Controller is Guarranteed Stable

that making $\lambda_1 > 0$ caused improved attenuation of the system, impossible for a passive system to duplicate. When $\lambda_1 = 0$, the system attenuation was similar to what a passive system could create, and setting $\lambda_1 < 0$ resulted in attenuation worse than a passive system might create. However, letting $\lambda_1 > 0$ causes a DC displacement, which may not be acceptable in all systems. The optimal control law that minimizes the system attenuation for all frequency was estimated using the approximate solutions, resulting in a near optimal control law of Figure 6.7. Once again, $\lambda_2 = 0$ for all optimal settings. Hence, the question of how to select ε has been answered for the forced system.

Multi-Degree of Freedom Problems. The approximate solutions were used to estimate the behavior of two systems with multi-degrees of freedom. For a 2 degree of freedom

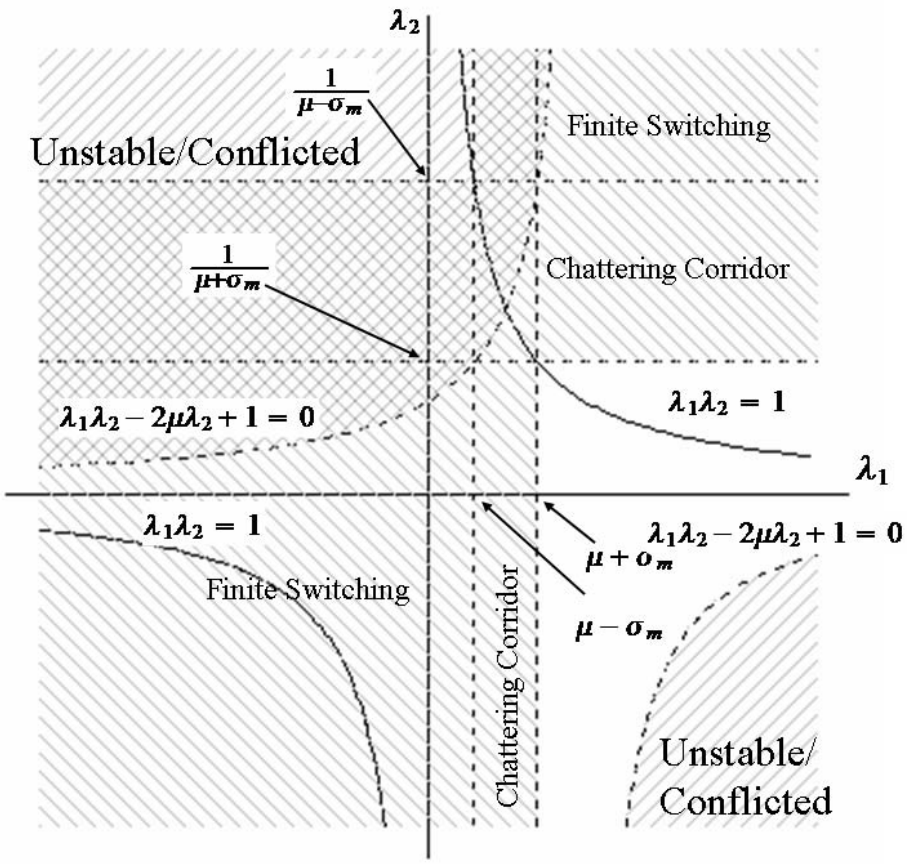

Figure 6.3 Variable Stiffness Constant Damping Overlaid Unstable Controller and Non-Switching Regions for Overdamped or Critically Damped System

problem, the equations of motion could be transformed to a single degree of freedom problem making all single degree of freedom problem results directly applicable. Higher degree of freedom problems were also examined, such as a system representative of a cross section of a space telescope. The unforced problem and the forced problem were estimated for a 3 degree of freedom problem and it was found the estimate reasonably agreed with simulated results. A problem possibly representative of a beam was also examined for the unforced problem, only. In this case, for small ε and μ, the estimated solution reasonably approximated the simulated solution. For larger values of ε and μ, the approximate solution was off, significantly. The reason for the error was because the coupling between masses in the system was fairly high. Overall, it was concluded that the single degree of freedom

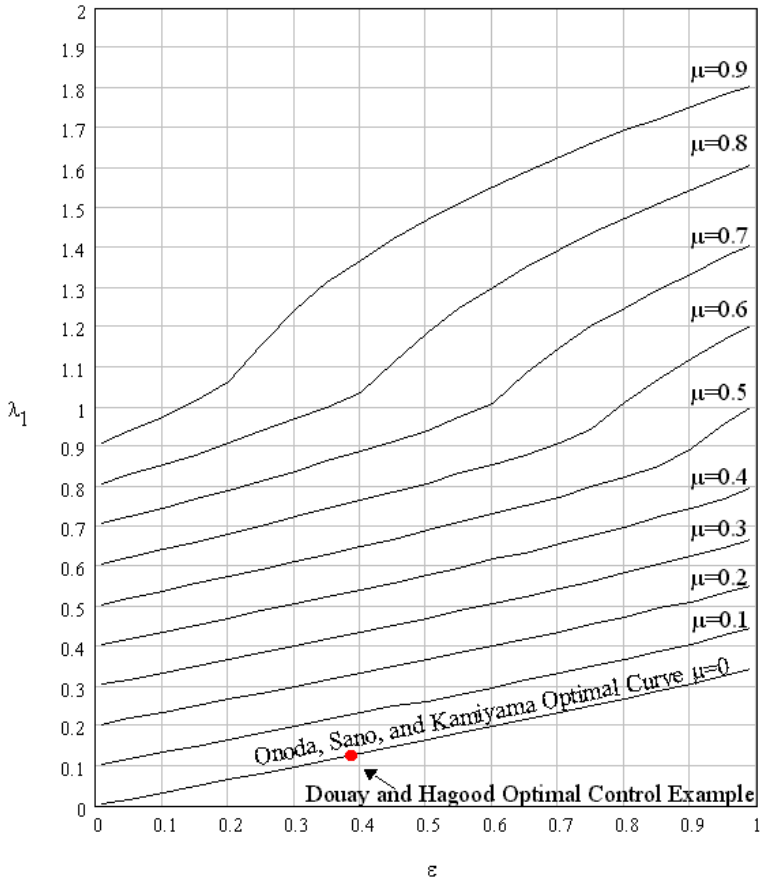

Figure 6.4 Variable Stiffness Constant Damping Optimal Control Policy ($\lambda_2 = 0$)

approximations could be used in some multi-degree of freedom problems to provide design insight.

6.3 Recommendations for Additional Research

As this research was carried out, many new questions and ideas were identified for future research. There are two directions that eventually merge to a single body of work. First, more research can be accomplished on constant mass systems. This type of research would extend the work discussed in this dissertation. Second, variable mass systems could be examined. Variable mass research could be considered with passive isolation to begin with, and then could add the complexity of variable stiffness and/or variable damping, later.

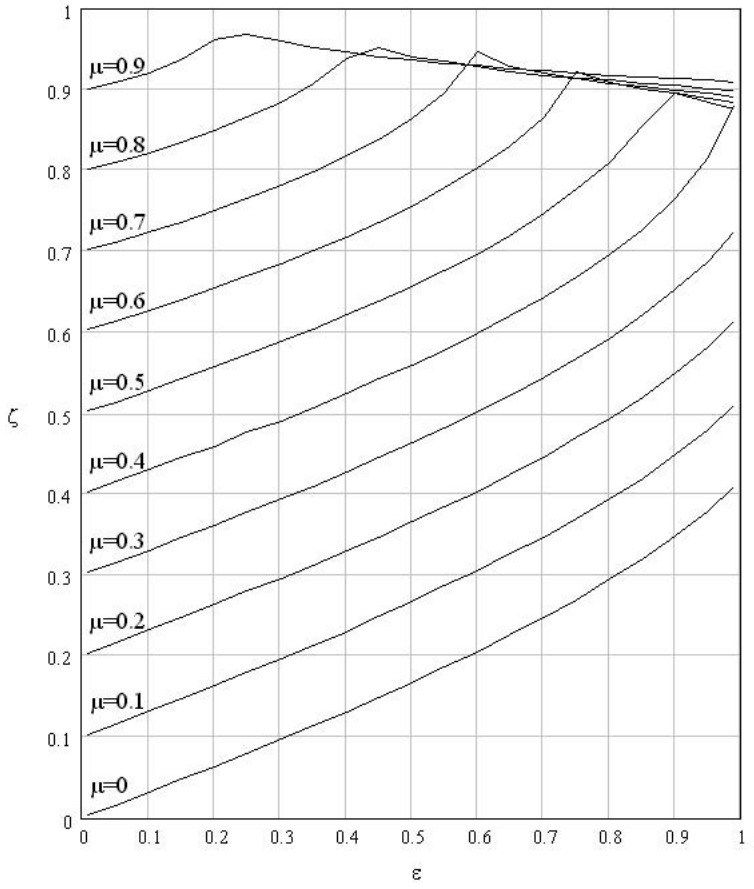

Figure 6.5 Variable Stiffness Constant Damping Optimal Equivalent Damping Ratio

Constant Mass Semi-Active Control Problems. To begin, much more work can be accomplished with the single degree of freedom problem. Using the methods in Chapter 3, it should now be possible to solve an initial value problem in the form

$$\ddot{x} + 2\mu\left(1 + \varepsilon_c u\right)\dot{x} + \left(1 + \varepsilon_k u\right)x = 0 \tag{6.12}$$

where $0 \leq \varepsilon_c < 1$ is a change in damping, ε_k is defined as ε in Equation 3.11, and u is defined using Equation 3.12. Real variable stiffness devices have been seen to create a small change in viscous damping of the system, also. For example, magnetorheological dampers are known to behave this way [121], [122].

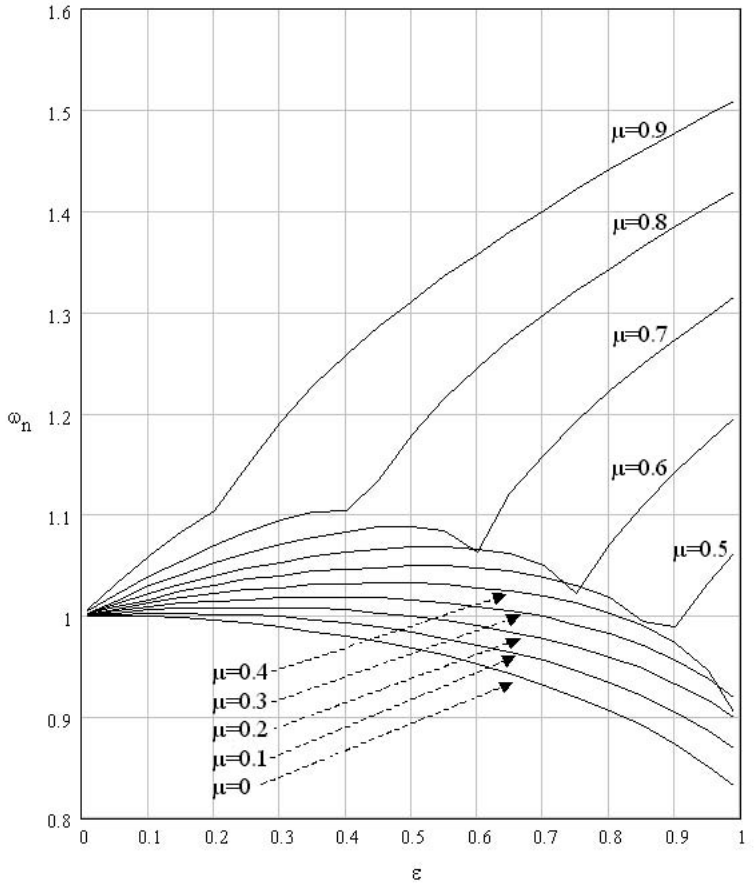

Figure 6.6 Variable Stiffness Constant Damping Optimal Equivalent Natural Frequency

Another single degree of freedom problem it may be possible to solve using the Chapter 3 approach is the three parameter problem. As discussed in Chapter 2, the approach is to place a variable damper in series with a spring, which is then placed in parallel with another spring, creating a three parameter isolator. Varying the damping then changes the apparent stiffness of the isolator [128], [7].

Assuming these problems can be solved, the next problem to attempt would be to change the variable stiffness device from the abstract device used to a real one, based on experimental results. This may require solving a nonlinear problem with hysteresis. Analytic models using real devices may not exhibit analytic solutions, since the equations of motion become considerably more nonlinear. In this case, analysis would have to be done numerically and would focus on developing good models that could be simulated. If

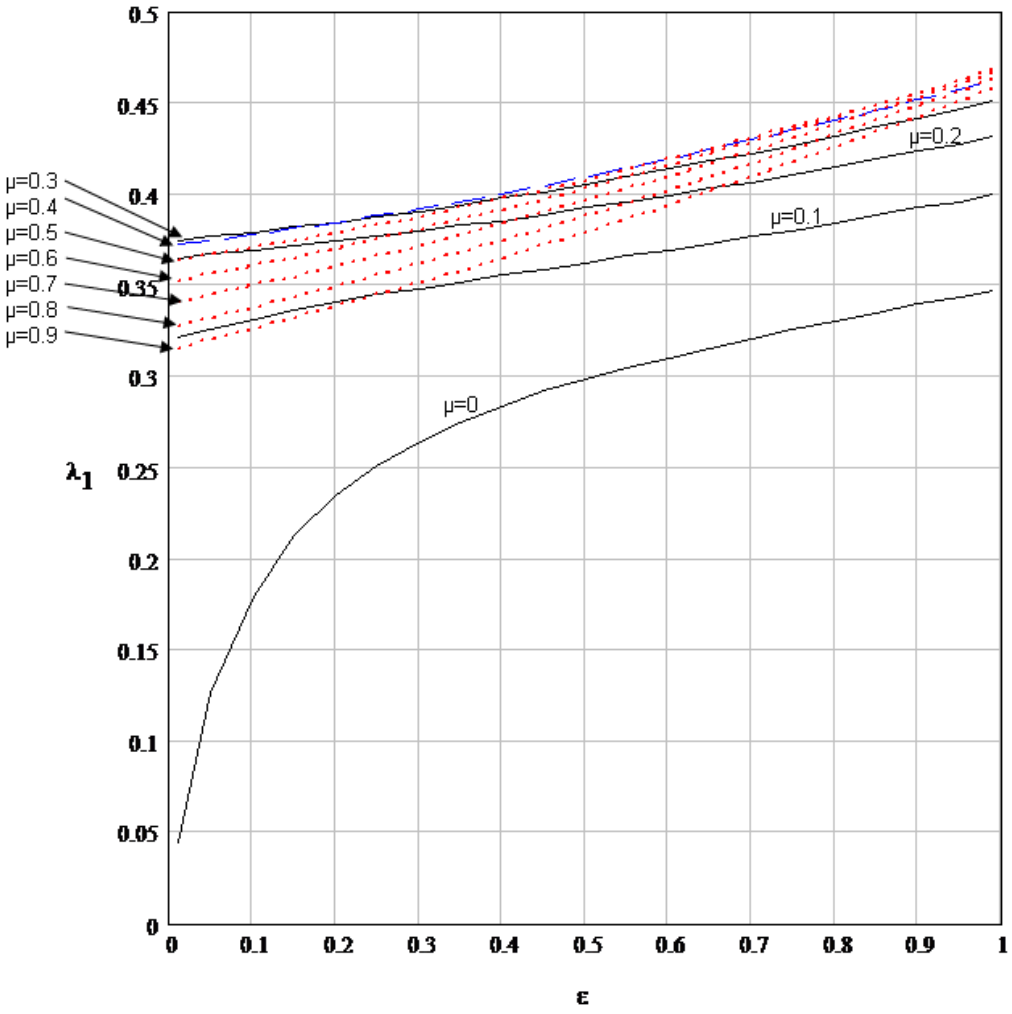

Figure 6.7 Near Optimal λ_1 for Sinusoidally Forced Problem using Perturbation Approximation ($\lambda_2 = 0$)

the problem were solvable using a nonlinear device or even if unsolvable, the next step would be to experimentally verify results. In this situation, the analytic results (as far as possible) would be linked to real experimental evidence, building confidence in the created design tools.

For the sinusoidally forced problem, it would be desirable to find an improved approximate solution. The main limitation of the current approximate solution is it fails to account for harmonics excited in the system. The attempt to account for this using the Fourier series approach could not be solved. Hence, some other method is needed to

account for this. At the same time, this method must allow the control law to be solved or closely approximated. Adding terms of the Fourier series to the assumed solution of the problem will not allow the problem to be solved if the switching times cannot be found because the switching equation is a transcendental equation.

Regardless of whether or not the sinusoidally forced problem of Chapter 4 can be more accurately approximated, the same systems identified for the unforced problem could also be approximated for the forced problem. Further, a problem where variable damping and variable stiffness are controlled independently could also be examined. The problem has the form

$$\ddot{x} + 2\mu\left(1 + \varepsilon_c u_c\right)\dot{x} + \left(1 + \varepsilon_k u_k\right)x = \cos\left(\omega t\right) \tag{6.13}$$

where u_k is defined using Equation 3.12 and u_c is defined using the 2 degree of freedom skyhook control law introduced by Karnopp [80]. In this case, the 2 degree of freedom problem would be transformed to the single degree of freedom problem using the transformations of Chapter 5. This would transform the skyhook control law, also, creating a system to be approximated. The payoff here is that a combination of variable stiffness and variable damping with the right control law will create even more attenuation than either variable damping or variable stiffness alone. This can be validated using simulation.

As previously discussed with the unforced single degree of freedom problem, the forced problem should be experimentally verified. If real devices can be used in the analytic problems, it would be useful to solve these nonlinear problems and then experimentally verify results. If not, it would be useful to determine how close to reality the problems that have been solved compare with real systems.

With more insight into the single degree of freedom problems, the multi-degree of freedom problems can be considered. The current method would be to use linear approximations of the nonlinear behavior and verify their usefulness in multi-degree of freedom problems. This could be accomplished for a myriad of such problems or at least for those that can be analytically solved. For those that cannot be analytically solved due to coupling in the linear equations, methods of approximating the coupling through perturbation approaches or removing the coupling could be explored. Further, it may be possible to

increase the solvability of coupled linear equations using Lie algebra methods [76]. With this research, the restrictions on the multi-degree of freedom problems noted earlier might be relaxed. Finally, just like the single degree of freedom problems, the multi-degree of freedom problems should be verified experimentally. This would increase confidence in the analytic tools being developed by validating them.

Another research possibility is to determine how well variable stiffness and variable damping devices can be calibrated and to determine if they can be qualified for use in space. It is possible to change the maximum variation in stiffness and/or damping created by the devices by simply increasing or decreasing the power supplied to the device. Since the control law can also be changed easily using computers, this has the effect of providing tremendous flexibility to change both the control law and the behavior of the structure, possibly even remotely. For space systems, this could be a great advantage, since it might allow vibration control to be optimized while a satellite is in orbit, using much less power than an active system might require.

Variable Mass Semi-Active Control Problems. The variable mass problem has not been considered in this dissertation, except initially in the literature review of Chapter 2. In this section, a simplified variable mass problem representative of vibration isolation for a launch vehicle with a payload is considered. After formulating the problem, future research that could be accomplished is identified.

2 DOF Variable Mass Formulation. Recalling Figure 2.8, the equations of motion are

$$m_1^* \ddot{x}_1^* + \dot{m}_1^* \dot{x}_1^* + \tilde{c}^* \dot{z}^* + \tilde{k}^* z^* = Q_1^* \tag{6.14}$$

and

$$m_2^* \ddot{x}_2^* - \tilde{c}^* \dot{z}^* - \tilde{k}^* z^* = Q_2^* \tag{6.15}$$

where $m_1 = m_1(t)$ represents the total mass of the rocket at any time, m_2^* represents a payload to be isolated, $\tilde{c}^* = \tilde{c}^*(z^*, \dot{z}^*)$ is a damping function, $\tilde{k}^* = \tilde{k}^*(z^*, \dot{z}^*)$ is a stiffness function,

$$z^* = x_2^* - x_1^*, \tag{6.16}$$

$Q_1^* = Q_1^*(t)$ is the thrust of the rocket engine, and $Q_2^* = Q_2^*(t)$ is a disturbance forced applied directly to the payload, such as acoustical noise generated by the rocket engine. Equations 6.14 and 6.15 could also be representative of an SBL (briefly reviewed in Chapter 2). Similar to Chapter 5, Equations 6.14 and 6.15 can be transformed to a center of mass coordinate system using

$$y^* = \frac{m_1^* x_1^* + m_2^* x_2^*}{m_1^* + m_2^*}. \tag{6.17}$$

Equations 6.16 and 6.17 look the same as center of mass transformation equations used in Chapter 5, but have one important difference in that m_1^* of Equation 6.17 is a function of time. Solving Equations 6.16 and 6.17 for x_1^* and x_2^* results in

$$x_1^* = y^* - \frac{m_2^* z^*}{m_1^* + m_2^*} \tag{6.18}$$

and

$$x_2^* = y^* + \frac{m_1^* z^*}{m_1^* + m_2^*}. \tag{6.19}$$

For this simplified problem, it will be assumed that

$$m_1^*(t) = \begin{cases} m_{10}^* - \rho^* t^* & \text{if } t^* < T_B^* \\ m_{10}^* - \rho^* T_b^* & \text{if } t^* \geq T_B^* \end{cases} \tag{6.20}$$

where $m_{10}^* = m_1^0(0)$, ρ^* is a constant mass flow rate out of the system, and T_b^* is the length of time mass is being removed from the system (burn time for a rocket). Substituting Equations 6.18 and 6.19 into Equations 6.14 and 6.15 and then simplifying results in

$$\ddot{y}^* - \frac{\rho^*}{q^*}\dot{y}^* = \frac{Q_1^*}{q^*} + \frac{{\rho^*}^2 m_2^*}{{q^*}^2} z^* + \frac{\rho^* m_2^*}{q^*}\dot{z}^* \tag{6.21}$$

and

$$\frac{m_2^*(m_{10}^* - \rho^* t^*)}{q^*}\ddot{z}^* + \left(\tilde{c}^* - \frac{2{\rho^*}^2 {m_2^*}^2}{{q^*}^2}\right)\dot{z}^* + \left(\tilde{k}^* - \frac{2{\rho^*}^2 {m_2^*}^2}{{q^*}^3}\right) z^* = Q_2^* - m_2^* \ddot{y}^* \tag{6.22}$$

where

$$q^* = q^*(t) = m_T^* - \rho^* t^* \tag{6.23}$$

and $m_T^* = m_{10}^* + m_2^*$.

Next, Equations 6.21, 6.22, and 6.23 will be nondimensionalized. To nondimensionalize, first define

$$t = \omega_0^* t^*, \tag{6.24}$$

$$L^* \neq 0, \tag{6.25}$$

$$m_p = \frac{m_2^*}{m_T^*}, \tag{6.26}$$

$$m_f = 1 - m_p = \frac{m_{10}^*}{m_T^*}, \tag{6.27}$$

$$\tilde{c}^* = c^* \tilde{c}, \tag{6.28}$$

and

$$\tilde{k}^* = k^* \tilde{k}. \tag{6.29}$$

The time scaling factor ω_0^* and the length scale L^* will be defined after the nondimensional form of Equations 6.21, 6.22, and 6.23 are examined. The variables m_p and m_f represent the mass fraction of the payload and mass fraction of the fully fueled launch vehicle, respectively. These quantities have physical meaning as identified in Table 2.1 and Appendix A. The quantities c^* and k^* represent a convenient scaling factor for the damping and stiffness functions, respectively.

After some algebraic manipulation, the nondimensional forms of Equations 6.21, 6.22, and 6.23 are

$$\ddot{y} - \rho \dot{y} = Q_1 + \frac{\rho^2 m_p}{q^2} z + \frac{\rho m_p}{1 - \rho t} \dot{z}, \tag{6.30}$$

$$\ddot{z} + \left(\frac{c^* \tilde{c} q}{m_2^* w_0^* \left(m_f - \rho t \right)} - \frac{2 \rho m_p}{\left(m_f - \rho t \right) q} \right) \dot{z} + \left(\frac{k^* \tilde{k} q}{m_2^* {\omega_0^*}^2 \left(m_f - \rho t \right)} - \frac{2 \rho^2 m_p}{\left(m_f - \rho t \right) q^2} \right) z = \frac{q}{m_f - \rho t} \left(Q_2 - \ddot{y} \right), \tag{6.31}$$

and

$$q = q\left(t\right) = 1 - \rho t \tag{6.32}$$

where

$$\rho = \frac{\rho^*}{\omega_0^* m_T^*}, \tag{6.33}$$

$$Q_1 = \frac{Q_1^*}{m_T^* L^* \omega_0^{*^2}}, \tag{6.34}$$

and

$$Q_2 = \frac{Q_2^*}{m_T^* L^* \omega_0^{*^2}} \tag{6.35}$$

Now, it is possible to select ω_0^* and L^*. A good way of selecting L^* is

$$L^* = \frac{\max\left(Q_j^*\right)}{m_T^* \omega_0^{*^2}} \tag{6.36}$$

where $j = 1, 2$ making $Q_j \leq 1$. There are several time scales that could be used for this problem. These time scales include T_b^* or the total time mass is flowing out of the system, a time based on mass flow rate such as $T_\rho^* = \frac{\rho^*}{M_T^*}$, and a scaling related to the natural frequency of the structure such as

$$\frac{1}{T_S^*} = \omega_0^* = \sqrt{\frac{k^*}{m_2^* m_f}} = \sqrt{\frac{k^* m_T^*}{m_2^* m_{10}^*}}. \tag{6.37}$$

There are other valid ways of defining T_ρ^* and T_S^* since different masses could be used in the definitions than those chosen such as the mass at burn out time, the mass at the start time, the total mass of the system at the starting time, and so on.

A valuable way of choosing a time scale would be one that makes ρ a small parameter. If this occurs, it then might be possible to implement perturbation methods to find out how the system behaves. Selecting the time scale of Equation 6.37 appears to meet this criteria. Additionally, this selection is consistent with the time scaling used in the constant mass problems analyzed in earlier chapters. Using Equation 6.37, Equation 6.31 simplifies slightly to

$$\ddot{z} + \left(\frac{2\mu m_f \tilde{c} q}{(m_f - \rho t)} - \frac{2\rho m_p}{(m_f - \rho t)\, q}\right) \dot{z} + \left(\frac{m_f \tilde{k} q}{(m_f - \rho t)} - \frac{2\rho^2 m_p}{(m_f - \rho t)\, q^2}\right) z = \frac{q}{m_f - \rho t} \left(Q_2 - \ddot{y}\right), \tag{6.38}$$

which is basically the same as Equation 5.29 when $\rho = 0$.

To understand why Equation 6.37 makes ρ a small parameter requires substituting Equation 6.37 into Equation 6.33. Then

$$\rho = \frac{\rho^* \sqrt{m_2^* m_{10}^*}}{m_T^* \sqrt{k^* m_T^*}} = \frac{\rho^* \sqrt{m_p m_f}}{\sqrt{k^* m_T^*}}. \tag{6.39}$$

Referring to Table 2.1 or Appendix A and recalling Equations 6.26 and 6.27 shows $0 < m_p < 0.153$ and $0.847 < m_f < 1$. In a worst case scenario, $\sqrt{m_p m_f} < 0.36$, which was determined by finding $\max\left(\sqrt{m_p m_f}\right)$ using the data in Appendix A. Further, $\sqrt{k^* m_T^*}$ is likely to be large.

Using the Taurus launch vehicle, a sample ρ can be found. Stage 0 of the Taurus launch vehicle has an average vacuum thrust of $363,087$ lbf and a specific impulse of 277.9 seconds. The mass flowrate ρ^* can be calculated to be about 1306.5 lb/sec [150]. Using Appendix A, $\sqrt{m_p m_f} = 0.14$ and $m_T^* = 160,000$ lb. Hence, $\rho = \frac{0.457}{\sqrt{k^*}}$ lb/sec where k^* is still to be determined. For a launch vehicle, k^* cannot be made small or the payload will have too much vibration displacement and will impact the payload fairing. It is more likely that k^* will be a large stiffness value, so it appears ρ is in fact a small parameter. More research could be done to verify ρ is a small parameter for the different launch vehicles identified in Appendix A.

Since ρ is a small parameter, perturbation methods should be applicable to approximate a solution to Equation 6.38. Equation 6.30, which represents rigid body motion coupled with the vibrational motion, may be directly solvable, in which case the solution could be substituted into Equation 6.38.

The rocket engine creates both random vibrations and sustained oscillations at specific frequencies. These disturbances manifest as vibration transmitted mechanically to the payload and as acoustical induced vibration [21]. As a first cut analysis, $Q_1(t)$ and $Q_2(t)$ could be modeled as white noise or sinusoidal forcing frequencies to determine isolator performance. Afterward, a more representative colored noise disturbance would need to be modeled and perhaps combined with specific narrow band resonances that real rockets create. Ultimately, real test data might be used as the disturbance force.

Future Research. Having formulated and nondimensionalized a simple 2 DOF variable mass problem, a research direction can be formulated. Moving from simpler problems to the more complex, it would be best to analyze Equation 6.38 assuming a passive isolation system. The results of the analysis could be linked to real data to validate the results. Next, either variable stiffness and/or variable damping could be added to the system. In might be better to understand variable stiffness and variable damping with a constant mass problem, since this problem does not appear to have been analyzed before with random noise disturbances. Whether or not this step would be needed would depend on how easily the passive isolation problem could be solved.

Finally, before attempting semi-active control on a launch vehicle, simpler laboratory work could be accomplished. In two recent articles, Flores et. al. created two simple experiments demonstrating the effects of variable mass in a single degree of freedom problem. In one experiment, they filled a bottle with sand and suspended it from a spring attached to a fixed support. The sand was allowed to drain from the bottle through an orifice and was found to drain at a constant rate, even when the bottle of sand was oscillating [151], [152]. Extending this experiment to a two degree of freedom problem and forcing the system with white noise, colored noise, and/or other forcing functions could simulate a system similar to a launch problem. Comparing analysis using a passive isolation system linked to existing launch results with an experimental laboratory device would gauge the accuracy of the laboratory experiment. If successful, it would constitute a cost effective experiment with semi-active control for launch vehicles.

Appendix A. Launch Vehicle Performance

Table A.1 provides calculated mass and payload fractions for various launch vehicles. [153]

Table A.1 Payload and Mass Fractions for Various Launch Vehicles

Launch Vehicle	**Country**	**Launch Weight (lb)**	**Payload (lb)**	**Orbit**	**Mass Frac**	**Payload Frac**
Arian 4	France	1,090,000	10,900	GTO	0.990	0.010
Arian 4	France	545,000	4,800	GTO	0.991	0.009
Arian 5	France	1,650,000	15,000	GTO	0.991	0.009
Athena 1	USA	146,000	1,805	LEO	0.988	0.012
Athena 2	USA	266,000	4,520	LEO	0.983	0.017
Atlas 2A	USA	413,000	6,760	GTO	0.984	0.016
Atlas 2AS	USA	522,000	8,202	GTO	0.984	0.016
Atlas 3	USA	496,900	9,920	GTO	0.980	0.020
Atlas 5 (400 series)	USA	734,800	16,843	GTO	0.977	0.023
Atlas 5 (500 series)	USA	1,191,200	19,110	GTO	0.984	0.016
Cosmos 3M	Russia	240,000	3,100		0.987	0.013
Cyclone 2	Ukraine	404,000	7,900	LEO	0.980	0.020
Cyclone 3	Ukraine	417,000	7,900	LEO	0.981	0.019
Delta 2 (7326)	USA	333,000	2,040	GTO	0.994	0.006
Delta 2 (7425)	USA	364,000	2,510	GTO	0.993	0.007
Delta 2 (7925)	USA	511,000	4,060	GTO	0.992	0.008
Delta 2 (7925H)	USA	665,000	4,815	GTO	0.993	0.007
Delta 3	USA	660,000	8,400	Not Listed	0.987	0.013
Delta 4 Heavy	USA	1,617,000	28,950	GTO	0.982	0.018
Delta 4 Medium	USA	565,000	9,285	GTO	0.984	0.016
Delta 4 Medium + (4,2)	USA	723,000	12,890	GTO	0.982	0.018
Delta 4 Medium + (5,2)	USA	736,000	10,230	GTO	0.986	0.014
Delta 4 Medium + (5,4)	USA	892,000	14,475	GTO	0.984	0.016
Dnepr-1	Ukraine	464,377	8,377	LEO	0.982	0.018
GSLV	India	888,000	3,520	GTO	0.996	0.004
H-2A (H2A202)	Japan	642,400	9,000	GTO	0.986	0.014
H-2A (H2A2022)	Japan	708,400	9,900	GTO	0.986	0.014
H-2A (H2A2024)	Japan	774,400	11,000	GTO	0.986	0.014
J-1	Japan	201,000	2,540	LEO	0.987	0.013

Launch Vehicle	Country	Launch Weight (lb)	Payload (lb)	Orbit	Mass Frac	Payload Frac
K-1	USA	290,000	10,000	LEO	0.966	0.034
LK-1	Israel	Not Listed	720	LEO	N/A	N/A
Long March LM-2C	China	422,400	2,200	GTO	0.995	0.005
Long March LM-2E	China	1,012,000	7,430	GTO	0.993	0.007
Long March LM-3A	China	708,400	5,720	GTO	0.992	0.008
Long March LM-3B	China	936,760	9,900	GTO	0.989	0.011
Long March LM-4	China	712,800	2,430	GTO	0.997	0.003
M-5	Japan	302,000	4,000	LEO	0.987	0.013
Minotaur	USA	80,340	1,400	LEO	0.983	0.017
Moniya M	Russia	672,000	4,400	GEO	0.993	0.007
Pegasus XL	USA	51,000	7,800		0.847	0.153
Proton K	Russia	1,547,000	45,747	GTO	0.970	0.030
Proton K/Block DM	Russia	1,547,000	46,189	GTO	0.970	0.030
Proton M/Breeze M	Russia	1,595,996	7,072	GTO	0.996	0.004
PSLV	India	644,600	2,640	Sun Synch	0.996	0.004
Rockot	Russia	237,575	4,044	LEO	0.983	0.017
Shavit	Israel	66,000	352	LEO	0.995	0.005
Shtil	Russia	88,000	195	LEO	0.998	0.002
Shtil 2.1	Russia	88,000	488	LEO	0.994	0.006
Soyuz TM/TMA	Russia	15,700	Not Listed	Not Listed	N/A	N/A
Soyuz U	Russia	683,000	16,100	LEO	0.976	0.024
Space Shuttle	USA	4,500,000	54,000		0.988	0.012
Start	Russia	132,275	1,401	LEO	0.989	0.011
Start	Russia	132,275	481		0.996	0.004
Start-1	Russia	103,400	1,077	LEO	0.990	0.010
Start-1	Russia	103,400	232		0.998	0.002
Taurus	USA	160,000	3,300		0.979	0.021
Titan 2	USA	340,000	4,200	LEO	0.988	0.012
Titan 4	USA	2,100,000	47,000	LEO	0.978	0.022
Titan 4	USA	2,100,000	39,000	LEO	0.981	0.019
Titan 4	USA	2,100,000	12,700	GEO	0.994	0.006
Vega	Italy	286,650	3,300	Polar	0.988	0.012
VLS-1	Brazil	110,000	275	LEO	0.998	0.002
Volna	Russia	77,000	244		0.997	0.003
Zenit 2	Ukraine	1,012,620	29,980	LEO	0.970	0.030
Zenit 3SL	Ukraine	1,042,785	13,228	LEO	0.987	0.013

Appendix B. Variation of Parameters for the Initial Value Variable Stiffness Constant Damping Problem

The method of variation of parameters [154] will be applied to solve Equation 3.9 using the control law defined by Equation 3.12. The following discussion is very similar to a derivation developed by Nayfeh [146] in the preliminaries of using the averaging perturbation method and uses his reasoning. Rather than continuing by using the method of averaging like Nayfeh uses on other nonlinear equations, the resulting first order differential equations were solved exactly in Chapter 3. The reason for not using perturbation methods is these methods assume a small parameter exists in the equations of motion, which is not strictly true in Equation 3.9. Specifically, the parameter of interest in Equation 3.9 is ε which represents the variation of stiffness in the system and $0 \leq \varepsilon < 1$. If a perturbation method was used, the analytic approximation would likely fail as $\varepsilon \to 1$, which would have limited insight into this problem. Table 2.2 shows that real variable stiffness devices can be selected that have large values for ε.

When $\varepsilon = 0$, the solution to Equation 3.9 is

$$x = ae^{-\mu t}\cos\phi \tag{B.1}$$

where

$$\phi = \psi t + \beta, \tag{B.2}$$

$$\psi = \sqrt{1-\mu^2} \tag{B.3}$$

and a and β are constants determined by the initial conditions. Then

$$\dot{x} = -ae^{-\mu t}\left[\mu\cos\phi + \psi\sin\phi\right]. \tag{B.4}$$

When $\varepsilon \neq 0$, the parameters a and β in Equation B.1 are considered to be functions that vary in time, which is where the name variation of parameters comes from. Equation B.1 can be thought of as a transformation that relates $x(t)$ to $a(t)$ and $\phi(t)$. Equations 3.9 and B.1 define two equations with three unknowns. One way to choose a third independent equation to uniquely define the transformation is to consider the derivatives of Equation

B.1 when $\varepsilon \neq 0$ and force the first derivative to have the same form as Equation B.4. The first and second derivatives when $\varepsilon \neq 0$ are

$$\dot{x} = e^{-\mu t}\left[(\dot{a} - a\mu)\cos\phi + \left(-a\psi - a\dot{\beta}\right)\sin\phi\right] \tag{B.5}$$

and

$$\ddot{x} = e^{-\mu t}\left[\left(a - \dot{a}\mu - a\dot{\beta}\psi\right)\cos\phi + \left(2a\psi\mu + a\dot{\beta}\mu - \dot{a}\psi\right)\sin\phi\right]. \tag{B.6}$$

Hence, to make Equation B.5 have the same form as Equation B.4 requires

$$\dot{a}\cos(\phi) - a\dot{\beta}\sin(\phi) = 0 \tag{B.7}$$

or by solving for $\dot{\beta}$ and recalling Equation B.2

$$\dot{\beta} = \frac{\dot{a}\cos(\phi)}{a\sin(\phi)} = \dot{\phi} - \psi. \tag{B.8}$$

Note that $a(t) \neq 0$, since this can only occur when $x(t) = 0$ by Equation B.1, which only occurs when Equation 3.9 has 0 initial conditions and represents the trivial solution to Equation 3.9. Substituting Equations B.1, B.4, and B.6 into Equation 3.9 results in

$$\left(-\dot{a}\mu - a\dot{\beta}\psi + a\varepsilon u\right)\cos\phi + \left(a\dot{\beta}\mu - \dot{a}\psi\right)\sin\phi = 0. \tag{B.9}$$

Substituting Equation B.8 into B.9 and simplifying results in

$$\frac{\dot{a}}{a} = \frac{\varepsilon u\sin(2\phi)}{2\psi}. \tag{B.10}$$

Substituting B.10 into B.8 and solving for $\dot{\phi}$ results in

$$\dot{\phi} = \frac{\varepsilon u\left[1 + \cos(2\phi)\right] + 2\psi^2}{2\psi} = \frac{\varepsilon u\cos^2\phi + \psi^2}{\psi}. \tag{B.11}$$

Equations B.10 and B.11 can be simplified somewhat by using Equations 3.23 and 3.24, resulting in Equations 3.21 and 3.22.

Next, the initial conditions for Equations B.10 and B.11 will be found for the case

$$x(0) = 1,\ \dot{x}(0) = 0 \tag{B.12}$$

and for the case

$$x(0) = 0,\ \dot{x}(0) = 1. \tag{B.13}$$

Substituting Equation B.12 into Equations B.1 and B.4 followed by solving them for a_0 and ϕ_0 results in

$$a_0 = a(0) = \frac{1}{\psi} \tag{B.14}$$

and

$$\phi_0 = \phi(0) = -\tan^{-1}\frac{\mu}{\psi}. \tag{B.15}$$

Since $0 \leq \mu < 1$ and $0 < \psi \leq 1$, then $\frac{\mu}{\psi} \geq 0$ which means $-\frac{\pi}{2} < \phi_0 \leq 0$ for the initial displacement problem. Similarly, substituting Equation B.13 into Equations B.1 and B.4 results in Equation B.14 and

$$\phi_0 = \phi(0) = -\frac{\pi}{2} \tag{B.16}$$

for the initial velocity problem.

Bibliography

1. M. Winthrop and R. Cobb. "Survey of State-of-the-Art Vibration Isolation Research and Technology for Space Applications." *Proc. SPIE Vol. 5052, Smart Structures and Materials 2003: Damping and Isolation*. 13–26. 2003.

2. F. Nelson. "Shock and Vibration Isolation: Breaking the Academic Paradigm." *ASME PVP*. 1–6. 1991.

3. N. Jalili. "A Comparative Study and Analysis of Semi-Active Vibration-Control Systems," *Journal of Vibration and Acoustics*, *124*(4):593–605 (2002).

4. J. Sun, M. Jolly, and M. Norris. "Passive, Adaptive and Active Tuned Vibration Absorbers-A Survey," *50th Anniversary of the Design Engineering Division; A Special Combined Issue of the Journal of Mechanical Design and the Journal of Vibration and Acoustics*, *117*(3B):234–242 (1995).

5. M. Brennan and J. Dayou. "Global Control of Vibration using a Tunable Vibration Neutralizer," *Journal of Sound and Vibration*, *232*(3):585–600 (2000).

6. D. Inman. *Engineering Vibration*. Prentice-Hall, Inc., 1996.

7. S. Kelso, R. Blankinship, and B. Henderson. "Precision Controlled Actuation and Vibration Isolation Utilizing Magnetorheological (MR) Fluid Technology." *IAA Space 2001 Conference*. 2001.

8. M. Franchek, M. Ryan, and R. Bernhard. "Adaptive Passive Vibration Control," *Journal of Sound and Vibration*, *189*(5):565–585 (1995).

9. F. Nelson. "Vibration Isolation: A Review, I. Sinusoidal and Random Excitations," *Shock and Vibration*, *1*(5):485–493 (1994).

10. C. Grodsinsky and M. Whorton. "Survey of Active Vibration Isolation Systems for Microgravity Applications," *Journal of Spacecraft and Rockets*, *37*(5):586–596 (2000).

11. J. Tang, Y. Liu, and K. Wang. "Semiactive and Active-Passive Hybrid Structural Damping Treatments via Piezoelectric Materials," *Shock and Vibration Digest*, *32*(3):189–200 (2000).

12. L. Sullivan, R. Erwin, and K. Denoyer. "Experiences with Smart Structures for On-Orbit Vibration Isolation." *Proc. SPIE Vol. 3991, Smart Structures and Materials 2000: Industrial and Commercial Applications of Smart Structures Technologies*, edited by J. Jacobs. 122– 130. SPIE–International Society for Optical Engineering, 2000.

13. F. Khorrami, J. Rastegar, and R. Erwin. "A Three Degrees-of-Freedom Adaptive-Passive Isolator for Launch Vehicle Payloads." *Proc. SPIE Vol. 3991, Smart Structures and Materials 2000: Industrial and Commercial Applications of Smart Structures Technologies*, edited by J. Jacobs. 164– 175. SPIE–International Society for Optical Engineering, 2000.

14. G. Yao, F. Yap, G. Chen, W. Li, and S. Yeo. "MR Damper and Its Application for Semi-Active Control of Vehicle Suspension System," *Mechatronics*, *12*(7):963–973 (2002).

15. D. Karnopp. "Active and Semi-Active Vibration Isolation," *50th Anniversary of the Design Engineering Division; A Special Combined Issue of the Journal of Mechanical Design and the Journal of Vibration and Acoustics*, *117*(3B):177–185 (1995).

16. M. Corless and G. Leitmann. "Destabilization via Active Stiffness," *Dynamics and Control*, *7*(3):263–268 (1997).

17. L. Corr and W. Clark. "Energy Dissipation Analysis of Piezoceramic Semi-Active Vibration Control," *Journal of Intelligent Material Systems and Structures*, *12*(11):729–736 (2001).

18. V. Skormin, M. Tascillo, and D. Nicholson. "Jitter Rejection Technique in a Satellite-Based Laser Communication System," *Optical Engineering*, *32*(11):2764–2769 (1993).

19. K. Denoyer and C. Johnson. "Recent Achievements in Vibration Isolation Systems for Space Launch and On-Orbit Applications." *52nd International Astronautical Congress*. 1–11. 2001.

20. D. Quenon, J. Boyd, P. Buchele, R. Self, T. Davis, T. Hintz, and J. Jacobs. "Miniature Vibration Isolation System for Space Applications." *Proc. SPIE Vol. 4332, Smart Structures and Materials 2001: Industrial and Commercial Applications of Smart Structures Technologies*, edited by A. McGowan. 159– 170. SPIE–International Society for Optical Engineering, 2001.

21. B. Keegan. *Dynamic Environmental Criteria*. Technical Report, NASA, 2001.

22. R. Masterson, D. Miller, and R. Grogan. "Development and Validation of Reaction Wheel Disturbance Models: Empirical Model," *Journal of Sound and Vibration*, *249*(3):575–598 (2002).

23. R. Ross. "Vibration Suppression of Advanced Space Cryocoolers - An Overview." *Proc. SPIE Vol. 5052, Smart Structures and Materials 2003: Smart Structures and Materials*. 2003.

24. C. Baugher, N. Ramachandran, and R. Delombard. "An Overview of the Space Shuttle Acceleration Environment." *Sensing, Imaging, and Vision for Control and Guidance of Aerospace Vehicles*. 90–101. 1994.

25. R. Erwin, K. Schrader, R. Moser, and S. Griffin. "Experimental Demonstation of Precision Control of a Deployable Optics Structure," *Journal of Vibration and Acoustics*, *124*(3):441–450 (2002).

26. M. Lake, L. Peterson, and M. Levine. "A Rationale for Defining Structural Requirements for Large Space Telescopes." *42nd AIAA/ASME/ASCE/AHS/ASC Structures, Structural Dynamics, and Materials Conference and Exhibit*. 2001.

27. R. Grogan and R. Laskin. "On Multidisciplinary Modeling of the Space Interferometry Mission." *Proceedings of the 1998 American Control Conference*. 1558–1562. 1998.

28. G. Neat, J. Melody, and B. Lurie. "Vibration Attenuation Approach for Spaceborne Optical Interferometers," *IEEE Transactions on Control Systems Technology* (1998).

29. M. Powers, J. Leitner, E. Hackney, K. Bell, R. Boucher, I. Robertson, L., and K. Schrader. "Assessment of a Large Aperture Telescope Trade Space and Active Opto-Mechanical Control Architecture." *1997 IEEE Aerospace Conference*. 197–229. 1997.

30. K. Schrader, R. Fetner, S. Griffin, and R. Erwin. "Integrated Control System Development for Phasing and Vibration Suppression for a Sparse-Array Telescope." *Proc. SPIE Vol. 4849, Highly Innovative Space Telescope Concepts*, edited by H. MacEwen. 134–145. SPIE–International Society for Optical Engineering, 2002.

31. P. Bely, C. Perrygo, and R. Burg. *NGST Monograph No. 1 NGST 'Yardstick' Mission*. Technical Report, Next Generation Space Telescope Project Office, NASA Goddard Space Flight Center, 1999.

32. K. Schrader, R. Fetner, S. Griffin, and R. Erwin. "Development of a Sparse-Aperature Testbed for Optomechanical Control of Space-Deployable Structures." *Proc. SPIE Vol. 4849, Highly Innovative Space Telescope Concepts*, edited by H. MacEwen. 384–395. SPIE–International Society for Optical Engineering, 2002.

33. S. Huybrechts, P. Wegner, A. Maji, B. Kozola, S. Griffin, and T. Meink. "Structural Design for Deployable Optical Telescopes." *2000 IEEE Aerospace Conference Proceedings*. 367–372. 2000.

34. M. Lake, L. Peterson, M. Mikulas, J. Hinkle, L. Hardaway, and J. Heald. "Structural Concepts and Mechanics Issues for Ultra-Large Optical Systems." *Ultra-Lightweight Space Optics Workshop*. 1999.

35. J. Domber, J. Hinkle, L. Peterson, and P. A. Warren. "The Deployment Repeatability of a High Stiffness Folded Composite Hinge." *Proceedings of the 42nd Structures, Structural Dynamics and Materials Conference*. 2001.

36. N. Pedreiro. "Spacecraft Architecture for Disturbance-Free Payload." *AIAA Guidance, Navigation, and Control Conference and Exhibit*. 2002.

37. National Research Council of the National Academies. *The Mission of Microgravity and Physical Sciences Research at NASA*. Technical Report, National Academy of Science, 2001.

38. G. Bushnell and M. Becraft. "Flight Test of an International Space Station Active Rack Isolation Prototype System," *Smart Materials and Structures*, *8*(6):791– 797 (1999).

39. C. Casgrain, J. Marrone, R. Herring, and S. Tetreault. "Microgravity Sciences in the ISS Era." *40th Aerospace Sciences Meeting and Exhibit*. 2002.

40. D. Putnam, J. Eraker, and J. Mohl. "Vibration Isolation Module for Exposed Facility Payloads." *Conference and Exhibit on International Space Station Utilization*. 2001.

41. P. Calhoun and D. Hampton. "Optimal Control Design using an H2 Method for the Glovebox Integrated Microgravity Isolation Technology (G-LIMIT)." *AIAA Guidance, Navigation, and Control Conference and Exhibit*. 2002.

42. L. Peterson, M. Lake, and L. Hardaway. "Micron Accuracy Deployment Experiments (MADE): A Space Station Laboratory for Actively Controlled Precision Deployable Structures Technology." *Proceedings of the Space Technology and Applications International Forum*. 1999.

43. S. Arnon and N. Kopeika. "Laser Satellite Communication Network–Vibration Effect and Possible Solutions," *Proceedings of the IEEE*, *85*(10):1646–1661 (1997).

44. R. Ninneman, M. Vigil, and D. Founds. "Projected Technology Needs for an Operational Space-Based Laser." *32nd AIAA Plasmadynamics and Lasers Conference*. 2001.

45. E. Zimet. "High-Energy Lasers: Technical, Operational, and Policy Issues," *Defense Horizons*, *18*:1–8 (2002).

46. J. Riker. "Overview of the Space-Based Laser (SBL) Program." *Proc. SPIE Vol. 4632, Laser and Beam Control Technologies*. 181–186. SPIE–International Society for Optical Engineering, 2002.

47. G. Karahalis. *Whole Spacecraft Vibration Isolation*. Masters, Air Force Inst of Tech Wright-Patterson AFB OH School of Engineering, 1999.

48. B. Henderson, S. Lane, J. Gussy, S. Griffin, and K. Farinholt. "Development of an Acoustic Actuator for Launch Vehicle Noise Reduction," *Journal of the Acoustical Society of America*, *111*(1):174–179 (2000).

49. K. Denoyer, S. Griffin, and D. Sciulli. "Hybrid Structural/acoustic Control of a Sub-Scale Payload Fairing." *Proc. SPIE Vol. 3329, Smart Structures and Materials 1998: Smart Structures and Integrated Systems*, edited by M. Regelbrugge. 237–243. SPIE–International Society for Optical Engineering, 1998.

50. C. Johnson, P. Wilke, and K. Darling. "Multi-Axis Whole-Spacecraft Vibration Isolation for Small Launch Vehicles." *Proc. SPIE Vol. 4331, Smart Structures and Materials 2001: Damping and Isolation*, edited by D. Inman. 153– 161. Proceedings of the SPIE - The International Society for Optical Engineering, 2001.

51. L. Davis, T. Allen, and J. Vise. "A Launch Isolation System for the Shuttle Resupplied Hubble Space Telescope Solar Array." *Proc. of The International Conference DAMPING'93*. 1992.

52. N. Jedrich and S. Pendleton. "Isolation Systems for Electronic Black-Box Transportation to Orbit." *Proc. SPIE Vol. 3327, Smart Structures and Materials 1998: Passive Damping and Isolation*, edited by L. Davis. 423–430. SPIE–International Society for Optical Engineering, 1998.

53. G. Lee-Glauser, G. Ahmadi, and J. Layton. "Satellite Active and Passive Vibration Control During Liftoff," *Journal of Spacecraft and Rockets*, *33*(3):428–432 (1996).

54. P. Wilke, C. Johnson, and K. Darling. "Whole-Spacecraft Vibration Isolation Flown on the Minotaur Launch Vehicle." *Fifteenth Annual AIAA/USU Conference on Small Satellites*. 1–9. 2001.

55. C. Johnson and P. Wilke. "Whole-Spacecraft Shock Isolation System." *Proc. SPIE Vol. 4697, Smart Structures and Materials 2002: Damping and Isolation*, edited by G. Agnes. 1–8. Proceedings of the SPIE - The International Society for Optical Engineering, 2002.

56. J. Maly, P. Wilke, P. Wegner, L. Berenberg, and G. Sanford. "ESPA from Concept to Flight Hardware." *AIAA Space 2003 Conference and Exposition*. AIAA, 2003.

57. G. Sanford. "Development and Structural Qualification of the EELV Secondary Payload Adaptor (ESPA)." *43rd AIAA/ASME/ASCE/AHS/ASC Structures, Structural Dynamics, and Materials Conference*. 2002.

58. J. Maly, S. Haskett, P. Wilke, E. Fowler, D. Sciulli, and T. Meink. "ESPA: EELV Secondary Payload Adapter with Whole-Spacecraft Isolation for Primary and Secondary Payloads." *Proc. SPIE Vol. 3989, Smart Structures and Materials 2000: Damping and Isolation*, edited by T. Hyde. 430– 439. SPIE–International Society for Optical Engineering, 2000.

59. E. Fosness, P. Wegner, B. Arritt, and S. Buckley. "Multiple Payload Adaptors for Low Cost Access to Space." *AIAA Space 2001 - Conference and Exposition*. 2001.

60. D. Cunningham. "Active vs Passive Launch Isolation." *Proc. of The International Conference DAMPING'93*. 1993.

61. D. Edberg, B. Bartos, J. Goodding, P. Wilke, and T. Davis. "Passive and Active Launch Vibration Studies in the LVIS Program." *Proc. SPIE Vol. 3327, Smart Structures and Materials 1998: Passive Damping and Isolation*, edited by L. Davis. 411–422. SPIE–International Society for Optical Engineering, 1998.

62. D. Sciulli and S. Griffin. "Hybrid Launch Isolation System." *Proc. SPIE Vol. 3674, Smart Structures and Materials 1999: Industrial and Commercial Applications of Smart Structures Technologies*, edited by J. Jacobs. 352– 359. SPIE–International Society for Optical Engineering, 1999.

63. M. Evert, P. Janzen, E. Anderson, C. Gerhart, and B. Henderson. "Active Vibration Isolation System for Launch Load Alleviation." *Proc. SPIE Vol. 5388, Smart Structures and Materials 2004: Industrial and Commercial Applications of Smart Structures Technologies*. 62–77. AIAA, 2003.

64. J. Jarosh, G. Agnes, and G. Karahalis. "Adaptive Control for Payload Launch Vibration Isolation." *Proc. SPIE Vol. 4331, Smart Structures and Materials 2001: Damping and Isolation*, edited by D. Inman. 162–174. SPIE–International Society for Optical Engineering, 2001.

65. J. Boyd, T. Hyde, D. Osterberg, and T. Davis. "Performance of a Launch and On-Orbit Isolator." *Proc. SPIE Vol. 4327, Smart Structures and Materials 2001: Smart Structures and Integrated Systems*, edited by L. Davis. 433–440. SPIE–International Society for Optical Engineering, 2001.

66. S. Isakowitz, J. Hopkins, and J. Hopkins. *International Reference Guide to Space Launch Systems*. American Institute of Aeronautics and Astronautics, 1999.

67. D. Thayer, M. Campbell, J. Vagners, and A. von Flotow. "Six-Axis Vibration Isolation System using Soft Actuators and Multiple Sensors," *Journal of Spacecraft and Rockets*, *39*(2):206–212 (2002).

68. R. Cobb, J. Sullivan, A. Das, L. Davis, T. Hyde, T. Davis, Z. Rahman, and J. Spanos. "Vibration Isolation and Suppression System for Precision Payloads in Space," *Smart Materials and Structures*, *8*(6):798–812 (1999).

69. Z. Geng and L. Haynes. "Six Degree-of-Freedom Active Vibration Control using the Stewart Platforms," *IEEE Transactions on Control Systems Technology*, *2*(1):45–53 (1994).

70. G. Lang. "What Herman Tried to Tell Ya'... [Vibration Isolation]," *Sound and Vibration*, *36*(1):74–76 (2002).

71. L. Meirovitch. *Elements of Vibration Analysis* (2nd Edition). McGraw-Hill, 1986.

72. D. Sciulli. *Dynamics and Control for Vibration Isolation Design*. PhD, Virginia Polytechnic Institute and State University, 1997.

73. D. Sciulli. "Comparison of Single- and Two-Degree-of-Freedom Models for Passive and Active Vibration Isolation Design." *Proc. SPIE Vol. 2720, Smart Structures and Materials 1996: Passive Damping and Isolation*, edited by C. Johnson. 293–304. 1996.

74. T. Caughey. "Classical Normal Modes in Damped Linear Dynamic Systems," *Journal of Applied Mechanics*, *27*:269–271 (1960).

75. T. Caughey and M. O'Kelly. "Classical Normal Modes in Damped Linear Dynamic Systems," *Journal of Applied Mechanics*, 583–588 (1965).

76. T. Caughey and F. Ma. "Complex Modes and Solvability of Nonclassical Linear Systems," *Journal of Applied Mechanics*, *60*:26–28 (1993).

77. G. Leitmann. "Semiactive Control for Vibration Attenuation," *Journal of Intelligent Material Systems and Structures*, *5*:841–846 (1994).

78. J. Onoda, T. Sano, and K. Kamiyama. "Vibration Suppression by Variable-Stiffness Members," *AIAA Journal*, *29*(6):977–983 (1991).

79. W. Clark. "Vibration Control with State-Switched Piezoelectric Materials," *Journal of Intelligent Material Systems and Structures*, *11*(4):263–271 (2000).

80. D. Karnopp, M. Crosby, and R. Harwood. "Vibration Control using Semi-Active Force Generators," *Journal of Engineering for Industry*, *96*(2):619–626 (1974).

81. T. Butz and O. von Stryk. "Modelling and Simulation of Electro- and Magnetorheological Fluid Dampers," *Zamm-Z. Angew. Math. Mech.*, *82*(1):3–20 (2002).

82. R. Hoppe, G. Mazurkevitch, O. von Stryk, and U. Rettig. "Modeling, Simulation, and Control of Electrorheological Fluid Devices." *Lectures on Applied Mathematics*, edited by Bungartz, Hoppe, and Zenger. 251–276. Springer-Verlag, 2000.

83. H. Lam and W. Liao. "Semi-Active Control of Automotive Suspension Systems with Magnetorheological Dampers." *Proc. SPIE Vol. 4327, Smart Structures and Materials 2001: Smart Structures and Integrated Systems*, edited by L. Davis. 125–136. SPIE–International Society for Optical Engineering, 2001.

84. D. Balandin, N. Bolotnik, and P. D. "Review: Optimal Shock and Vibration Isolation," *Shock and Vibration*, *5*(2):73–87 (1998).

85. D. Balandin, N. Bolotnik, and W. Pilkey. *Optimal Protection from Impact, Shock, and Vibration*. Gordon and Breach Science Publishers, 2001.

86. L. Davis, B. Workman, C.-C. Chu, and E. Anderson. "Design of a D-Strut and Its Application Results in the JPL, MIT, and LARC Test Beds." *American Institute of Aeronautics and Astronautics Structural Dynamics Meeting*. 1992.

87. C. Johnson. "Design of Passive Damping Systems," *50th Anniversary of the Design Engineering Division; A Special Combined Issue of the Journal of Mechanical Design and the Journal of Vibration and Acoustics*, *117*(3B) (1995).

88. D. Karnopp. "Design Principles for Vibration Control Systems using Sem-Active Dampers," *Journal of Dynamic Systems, Measurement and Control*, *112*:448–445 (1990).

89. Lord Corporation. "Rheonetic MR Technology from Lord Corporation in Cadillac Suspension Takes Prestigious Award from Popular Science Magazine at http://www.rheonetic.com/," (2002).

90. R. Stanway, J. Sproston, and A. El-Wahed. "Applications of Electro-Rheological Fluids in Vibration Control: A Survey," *Smart Materials and Structures*, *5*(4):464–482 (1996).

91. N. Sims, R. Stanway, D. Peel, W. Bullough, and A. Johnson. "Controllable Viscous Damping - An Experimental Study of an Electrorheological Long-Stroke Damper Under Proportional Feedback Control," *Smart Materials and Structures*, *8*(5):601–615 (1999).

92. M. Jolly, J. Carlson, and B. Munoz. "A Model of the Behavior of Magnetorheological Materials," *Smart Materials and Structures*, *5*(5):607–614 (1996).

93. Y. Kim, K. Wang, and H. Lee. "Feedback Control of ER-Fluid-Based Structures for Vibration Suppression," *Smart Materials and Structures*, *1*(2):139–145 (1992).

94. B. Spencer, S. Dyke, M. Sain, and J. Carlson. "Phenomenological Model of a Magnetorheological Damper," *Journal of Engineering Mechanics*, *123*(3):230–238 (1997).

95. L. Pang, G. Kamath, and N. Wereley. "Dynamic Characterization and Analysis of Magnetorheological Damper Behavior." *Proc. SPIE Vol. 3327, Smart Structures and Materials 1998: Passive Damping and Isolation*, edited by L. Davis. 284–302. SPIE–International Society for Optical Engineering, 1998.

96. N. Wereley, L. Pang, and G. Kamath. "Idealized Hysteresis Modeling of Electrorheological and Magnetorheological Dampers," *Journal of Intelligent Material Systems and Structures*, *9*(8):642–649 (1998).

97. A. Preumont. *Vibration Control of Active Structures: An Introduction* (2nd ed Edition). Solid mechanics and its applications, Kluwer Academic Publishers, 2002.

98. G. Pan, H. Matsuhisa, and Y. Honda. "Analytical Model of a Magnetorheological Damper and Its Application to the Vibration Control." *Proceedings of 2000 IEEE International Conference on Industrial Electronics, Control and Instrumentation*. 1850–5 vol. 2000.

99. P. Sain, M. Sain, J. Spencer, B., and J. Sain. "The Bouc Hysteresis Model: An Initial Study of Qualitative Characteristics." *Proceedings of the 1998 American Control Conference (ACC)*. 2559–63 vol. 1998.

100. N. Hagood and A. von Flotow. "Damping of Structural Vibrations with Piezoelectric Materials and Passive Electrical Networks," *Journal of Sound and Vibration*, *146*(2):243–268 (1991).

101. G. Lesieutre. "Vibration Damping and Control using Shunted Piezoelectric Materials," *Shock and Vibration Digest*, *30*(3):187–195 (1998).

102. L. Corr and W. Clark. "Comparison of Low-Frequency Piezoelectric Switching Shunt Techniques for Structural Damping," *Smart Materials and Structures*, *11*(3):370–376 (2002).

103. IEEE-STD-176-1987. "IEEE Standard on Piezoelectricity," *ANSI/IEEE STD 176-1987* (1987).

104. K. Uchino and T. Ishii. "Mechanical Damper using Piezoelectric Ceramics," *Journal of the Ceramic Society of Japan International Edition*, *96*:843–847 (1988).

105. K. Wang, J. Lai, and W. Yu. "An Energy-Based Parametric Control Approach for Structural Vibration Suppression via Semi-Active Piezoelectric Networks," *Journal of Vibration and Acoustics*, *118*(3):505–509 (1996).

106. Texas A and M SmartLab. "Introduction to Shape Memory Alloys at http://smart.tamu.edu/overview/overview.html.". 2003.

107. K. Otsuka and C. Wayman. "Shape Memory Materials.". Cambridge University Press, 1998.

108. S. Saadat, J. Salichs, M. Noori, Z. Hou, H. Davoodi, I. Bar-On, Y. Suzuki, and A. Masuda. "An Overview of Vibration and Seismic Applications of NiTi Shape Memory Alloy," *Smart Materials and Structures*, *11*(2):218–229 (2002).

109. K. Williams, G. Chiu, and R. Bernhard. "Adaptive-Passive Absorbers using Shape-Memory Alloys," *Journal of Sound and Vibration*, *249*(5):835–848 (2002).

110. D. Grant and V. Hayward. "Design of Shape Memory Alloy Actuator with High Strain and Variable Structure Control." *Proceedings of 1995 IEEE International Conference on Robotics and Automation*. 2305–2312. 1995.

111. D. Grant and V. Hayward. "Vibration Isolation with High Strain Shape Memory Alloy Actuators." *International Mechanical Engineering Congress and Exposition*. 1998.

112. D. Siler and K. Demoret. "Variable Stiffness Mechanisms with SMA Actuators." *Proc. SPIE Vol. 2721, Smart Structures and Materials 1996: Industrial and Commercial Applications of Smart Structures Technologies*, edited by C. Crowe. 427–435. SPIE–International Society for Optical Engineering, 1996.

113. D. Lagoudas, J. Mayes, and M. Khan. "Simplified Shape Memory Alloy (SMA) Material Model for Vibration Isolation." *Proc. SPIE Vol. 4326, Smart Structures and Materials 2001: Modeling, Signal Processing, and Control in Smart Structures*, edited by V. Rao. 452–461. 2001.

114. M. Khan and D. Lagoudas. "Modeling of Shape Memory Alloy Pseudoelastic Spring Elements using Preisach Model for Passive Vibration Isolation." *Proc. SPIE Vol. 4693, Smart Structures and Materials 2002: Modeling, Signal Processing, and Control*, edited by V. Rao. 336–347. 2002.

115. J. Ginder, M. Nichols, L. Elie, and J. Tardiff. "Magnetorheological Elastomers: Properties and Applications." *Proc. SPIE Vol. 3675, Smart Structures and Materials 1999: Smart Materials Technologies*, edited by M. Wuttig. 131–138. SPIE–International Society for Optical Engineering, 1999.

116. W. Schlotter, C. Cionca, S. Paruchuri, J. Cunningham, E. Dufresne, S. Dierker, D. Arms, R. Clarke, J. Ginder, and M. Nichols. "The Dynamics of Magnetorheological Elastomers Studied by Synchrotron Speckle Analysis," *International Journal of Modern Physics B*, *16*(17-18):2426–2432 (2002).

117. L. Davis. "Model of Magnetorheological Elastomers," *Journal of Applied Physics*, *85*(6):3348–3351 (1999).

118. J. Ginder, M. Nichols, L. Elie, and S. Clark. "Controllable-Stiffness Components Based on Magnetorheological Elastomers." *Proc. SPIE Vol. 3985, Smart Structures and Materials 2000: Smart Structures and Integrated Systems*, edited by N. Wereley. 418–425. SPIE–International Society for Optical Engineering, 2000.

119. J. Ginder, W. Schlotter, and M. Nichols. "Magnetorheological Elastomers in Tunable Vibration Absorbers." *Proc. SPIE Vol. 4331, Smart Structures and Materials 2001: Damping and Isolation*, edited by D. Inman. 103–110. SPIE–International Society for Optical Engineering, 2001.

120. G. Zhou. "Shear Properties of a Magnetorheological Elastomer," *Smart Materials and Structures*, *12*:139–146 (2003).

121. A.-M. Albanese and K. Cunefare. "Properties of a Magnetorheological Semiactive Vibration Absorber." *Proc. SPIE Vol. 5052, Smart Structures and Materials 2003: Damping and Isolation*, edited by G. Agnes and K.-W. Wang. 36–43. 2003.

122. A.-M. Albanese and K. Cunefare. "Properties of a Magnetorheological Semiactive Vibration Absorber.". 2003.

123. A. Kurdila, W. Clark, W. Wang, and D. McDaniel. "Stability of a Class of Real-Time Switched Piezoelectric Shunts," *Journal of Intelligent Material Systems and Structures*, *13*(2-3):107–116 (2002).

124. C. Richard, D. Guyomar, D. Audigier, and G. Ching. "Semi-Passive Damping using Continuous Switching of a Piezoelectric Device." *Smart Structures and Materials 1999: Passive Damping and Isolation*. 104–111. SPIE-Int. Soc. Opt. Eng Place of Publication: USA, 1999.

125. W. Clark. "Vibration Control with State-Switched Piezoelectric Materials," *Journal of Intelligent Material Systems and Structures*, *11*(4):263–271 (1999).

126. C. Davis and G. Lesieutre. "An Actively Tuned Solid-State Vibration Absorber using Capacitive Shunting of Piezoelectric Stiffness," *Journal of Sound and Vibration*, *232*(3):601–617 (2000).

127. A. Ramaratnam, N. Jalili, and M. Grier. "Piezoelectric Vibration Suppression of Translational Flexible Beams using Switched Stiffness." *Proc. of 2003 IMECE, ASME, Washington D.C.*. 2003.

128. J. Onoda and K. Minesugi. "Semiactive Vibration Suppression by Variable-Damping Members," *AIAA Journal*, *34*(2):340–347 (1996).

129. P. Walsh and J. Lamancusa. "A Variable Stiffness Vibration Absorber for Minimization of Transient Vibrations," *Journal of Sound and Vibration*, *158*(2):195–211 (1992).

130. A. Flatau, M. Dapino, and F. Calkins. "High Bandwidth Tunability in a Smart Vibration Absorber." *Proc. SPIE Vol. 3327, Smart Structures and Materials 1998: Passive Damping and Isolation*, edited by L. Davis. 463–473. SPIE–International Society for Optical Engineering, 1998.

131. H.-U. Oh and K. Minesugi. "Semiactive ER Isolator for Momentum-Wheel Vibration Isolation." *42nd AIAA/ASME/ASCE/AHS/ASC Structures, Structural Dynamics, and Materials Conference and Exhibit*. 2001.

132. H.-U. Oh, J. Onoda, and K. Minesugi. "Semiactive Isolator with Liquid-Crystal Type ER Fluid for Momentum-Wheel Vibration Isolation," *Journal of Vibration and Acoustics*, *126*(2):272–277 (2004).

133. K. Wang and Y. Kim. "Semi-Active Vibration Control of Structures via Variable Damping Elements," *Mechanical Systems and Signal Processing*, *5*:421–430 (1991).

134. Y. Kim and K. Wang. "On the Sliding Mode Control of Structural Vibrations via Variable Damping," *Mechanical Systems and Signal Processing*, *7*(4):335–347 (1993).

135. M. Kidner and M. Brennan. "Real-Time Control of Both Stiffness and Damping in an Active Vibration Neutralizer," *Smart Materials and Structures*, *10*(4):758–769 (2001).

136. S. Kimbrough. "Bilinear Modelling and Regulations of Variable Component Suspensions." *Symposium on Simulation and Control of Ground Vehicles and Transportation Systems*, edited by L. Segel, J. Wong, E. Law, and D. Hrovat. 235–255. The American Society of Mechanical Engineers, 1986.

137. N. Jalili. "A New Perspective for Semi-Automated Structural Vibration Control," *Journal of Sound and Vibration*, *238*(3):481–494 (2001).

138. E. Esmailzadeh. "Vibration Isolation System with Variable Natural Frequency," *International Journal of Mechanical Engineering Education*, *6*(3):125–129 (1977).

139. A. Douay and N. Hagood. "Evaluation of Optimal Variable Stiffness Feedback Control Authority, Stability, Feasibility and Implementation." *Proceedings of the Fourth International Conference on Adaptive Structures*. 388–404. 1993.

140. T. Kobs and J. Sun. "A Non-Linear Variable Stiffness Feedback Control with Tuning Range and Rate Saturation," *Journal of Sound and Vibration*, *205*(2):243–249 (1997).

141. J. Onoda, T. Sano, and K. Kamiyama. "Active, Passive and Semi-Active Vibration Suppression by Stiffness Variation," *AIAA Journal*, *30*(12):2922–2929 (1992).

142. L. Crespo and J. Sun. "Solution of Fixed Final State Optimal Control Problems via Simple Cell Mapping," *Nonlinear Dynamics*, *23*(4):391–403 (2000).

143. L. Crespo and J. Sun. "Fixed Final Time Optimal Control via Simple Cell Mapping," *Nonlinear Dynamics*, *31*(2):119–131 (2003).

144. M. Winthrop, W. Baker, and R. Cobb. "A Variable Stiffness Device Selection and Design Tool for Lightly Damped Structures," *Accepted for Publication in Journal of Sound and Vibration* (2004).

145. D. Zwillinger. *CRC Standard Mathematical Tables and Formulae*, *31*. Chapman and Hall/CRC, 2003.

146. A. Nayfeh. *Introduction to Perturbation Techniques*. John Wiley and Sons, 1981.

147. P. Davis. *Circulant Matrices*. Wiley, 1979.

148. G. Karahalis and G. Agnes. "Preliminary Analysis of Hybrid Launch Isolation for Spacecraft." *Proc. SPIE Vol. 3674, Smart Structures and Materials 1999: Industrial and Commercial Applications of Smart Structures Technologies*, edited by J. Jacobs. 360– 370. SPIE–International Society for Optical Engineering, 1999.

149. L. Meirovitch. *Principles and Techniques of Vibrations*. Prentice-Hall, Inc., 1997.

150. Orbital-Sciences. "Taurus Launch System Payload Users Guide," (1999).

151. J. Flores, G. Solovey, and S. Gil. "Variable mass oscillator," *American Journal of Physics*, *71*(7):721–725 (2003).

152. J. Flores, G. Solovey, and S. Gil. "Flow of sand and a variable mass Atwood machine," *American Journal of Physics*, *71*(7):715–720 (2003).

153. M. Caceres. "Reusable Launch Vehicles: And Then There Were . . .," *Aviation Week and Space Technology*, *158*(2):138–149 (2003).

154. R. Wylie and L. Barrett. *Advanced Engineering Mathematics* (6th ed Edition). McGraw-Hill, 1995.

Vita

Major Winthrop was born at Tinker AFB, Oklahoma. He earned a Bachelor of Science in Astronautical Engineering from the USAF Academy in Colorado Springs, CO in 1989. On 23 Mar 1999, he earned a Masters of Science in Operations Research from the Air Force Institute of Technology. He is currently studying for his PhD in Astronautical Engineering, at the Air Force Institute of Technology.

From 1989-1993, he serve as an Astronautical Engineer at Phillips Lab, Edwards AFB. He worked three major programs: the XLR-132 (an experimental upperstage rocket engine), lead development of a new test facility for testing hydrostatic bearings in rocket engine turbopumps, and worked to find new less toxic propellants for existing rockets.

In March 1994, he began working as Wing Future Systems Planning Manager for 30th Space Wing, Program Requirements group at Vandenberg AFB, CA. The branch is responsible for working with new programs and marketing capabilities of Vandenberg AFB. Major programs he was in charge of planning included the Airborne Laser Program and Evolved Expendable Launch Vehicle.

After competing his Master's Degree, Major Winthrop worked for Air Force Studies and Analyses at the Pentagon. He supported decision-makers in Low Density/High Demand (LD/HD) Aircraft operations tempo, future military space plane, and Quadrennial Defense Review Space superiority force structure analyses. He developed a concept for analysis of Air Force force structure. LD/HD results were directly linked to AF Chief of Staff and SECDEF decisions and presented at NATO Partnership for Peace conference.

REPORT DOCUMENTATION PAGE

Form Approved
OMB No. 0704–0188

1. REPORT DATE *(DD–MM–YYYY)*	2. REPORT TYPE	3. DATES COVERED *(From — To)*
13-12-2004	Doctoral Dissertation	September 2001 — December 2004

4. TITLE AND SUBTITLE

ENGINEERING TOOLS FOR VARIABLE STIFFNESS VIBRATION SUPPRESSION AND ISOLATION

5a. CONTRACT NUMBER

5b. GRANT NUMBER

5c. PROGRAM ELEMENT NUMBER

6. AUTHOR(S)

Winthrop, Michael F., Major, USAF

5d. PROJECT NUMBER

03-299

5e. TASK NUMBER

5f. WORK UNIT NUMBER

7. PERFORMING ORGANIZATION NAME(S) AND ADDRESS(ES)

Air Force Institute of Technology
Graduate School of Engineering and Management
2950 Hobson Way
WPAFB OH 45433-7765

8. PERFORMING ORGANIZATION REPORT NUMBER

AFIT/DS/ENY/05-02

9. SPONSORING / MONITORING AGENCY NAME(S) AND ADDRESS(ES)

IMINT/RNTS
Attn: Lt. Col. David Lee
14675 Lee Road — DSN 898-3084
Chantilly, VA 20151 — e-mail: David.Lee@nro.mil

10. SPONSOR/MONITOR'S ACRONYM(S)

11. SPONSOR/MONITOR'S REPORT NUMBER(S)

12. DISTRIBUTION / AVAILABILITY STATEMENT

Approval for public release; distribution is unlimited.

13. SUPPLEMENTARY NOTES

14. ABSTRACT

With the advent of smart materials, the concept of semi-active control or dynamic control of stiffness and/or damping for vibration control of structures has become practical and has seen limited use. Semi-active control has advantages over active and passive control methods, since it provides almost as much capability as active control while requiring much less power. Its main disadvantage is its inherent nonlinearity, greatly complicating engineering design. The purpose of this research is to extend semi-active control vibration isolation tools and methods considering space launch and on-orbit systems.

15. SUBJECT TERMS

semiactive systems; stiffness; vibration isolators; nonlinear analysis; nonlinear differential equations; semiactive control; variable stiffness; vibration suppression

16. SECURITY CLASSIFICATION OF:			17. LIMITATION OF ABSTRACT	18. NUMBER OF PAGES	19a. NAME OF RESPONSIBLE PERSON
a. REPORT	b. ABSTRACT	c. THIS PAGE			Richard G. Cobb, PhD, (ENY)
U	U	U	UU	211	19b. TELEPHONE NUMBER *(include area code)* (937) 255–3636 x4559; Richard.Cobb@afit.edu